NOTE TO USERS

This reproduction is the best copy available.

Proteomic analysis of clathrin-coated vesicles and functional characterization of the mammalian DnaJ domain-containing protein receptor-mediated endocytosis 8

Martine Girard

Department of Neurology and Neurosurgery
Montreal Neurological Institute
McGill University

Montréal, January 26th, 2009

A thesis submitted to McGill University in
partial fulfillment of the requirements for the degree of
Doctor of Philosophy in Neurological Sciences

Your file Votre référence
ISBN: 978-0-494-66306-6
Our file Notre référence
ISBN: 978-0-494-66306-6

ABSTRACT

Clathrin-mediated endocytosis (CME) plays a central role in the regulation of multiple cellular processes such as uptake of nutrients, recycling of housekeeping receptors and transporters, as well as for cell surface removal and downregulation of signaling receptors. Once endocytosed, cargo passes through early endosomes where sorting mechanisms traffic the cargo to the recycling pathway or to degradation in the lysosome. The general objectives of this doctoral research were to identify and characterize new players of the clathrin-mediated trafficking pathway to reveal differences between the abundant components of the trafficking machinery in two tissues, and to examine the mechanisms of endosomal sorting.

We used subcellular proteomics to reveal the differences in components of clathrin-coated vesicles (CCVs) isolated from brain and liver and to identify new molecules participating in clathrin trafficking. We demonstrated that the ratio between the clathrin adaptor proteins AP-1 and AP-2 is different in brain and liver, which indicates differential functions between the two tissues. We also discovered that clathrin-light chains, which have been proposed for many years to be regulatory proteins in the assembly of CCVs, were less abundant relative to clathrin-heavy chain in liver and in non-brain tissues compared to brain.

We identified a new DnaJ domain-containing protein, receptor-mediated endocytosis protein 8 (RME-8) that was detected in liver CCVs specifically. Further characterization revealed that the RME-8 DnaJ domain binds to the chaperone heat-shock cognate 70 (Hsc70) in an ATP-dependent manner. RME-8 is a ubiquitously expressed protein that tightly associates with endosomes, and its depletion causes intracellular trafficking defects. Moreover, we demonstrated that RME-8 depletion also leads to a decrease in levels of epidermal growth factor receptor (EGFR), as a result of an increase in EGFR degradation. RME-8 knock-down causes decreased EGFR levels even in cancer cells lines where EGFR is generally protected from degradation.

Globally this doctoral project revealed new insights on specialized functions for clathrin-mediated trafficking in different tissues and allowed the identification and characterization of a novel protein implicated in sorting decisions occurring on endosomes.

RÉSUMÉ

L'endocytose tributaire de la clathrine exerce un rôle primordial dans différents processus comme l'entrée de nutriments, le recyclage des récepteurs et des transporteurs, de même que dans la régulation de la quantité des récepteurs de la signalisation. Après son entrée dans la cellule par endocytose, le cargo rejoint les endosomes précoces où des mécanismes de triage le dirigent vers le processus de recyclage ou vers le processus de dégradation par le lysosome. Les objectifs généraux de cette thèse de doctorat étaient d'identifier et de caractériser de nouvelles protéines impliquées dans le trafic cellulaire tributaire de la clathrine, afin de révéler les différences entre les composantes abondantes de la machinerie responsable du trafic intracellulaire au sein de deux tissues, et d'examiner les mécanismes impliqués dans le triage qui se déroule au niveau du compartiment endosomal.

Nous avons utilisé la protéomique subcellulaire afin de découvrir les différences dans la composition des vésicules tapissées de clathrine isolées à partir du cerveau et du foie et d'identifier des nouvelles molécules qui participent au trafic cellulaire tributaire de la clathrine. Nous avons démontré que le ratio entre les adaptateurs de la clathrine AP-1 et AP-2 est différent selon qu'il s'agit du foie ou du cerveau, ce qui est indicatif d'une différence au niveau de la fonction entre les deux tissus. Nous avons également découvert que les chaines légères de la clathrine, qui avaient été proposées pendant de nombreuses années comme étant des protéines régulatrices de l'assemblage des vésicules tapissées de clathrine, étaient présentes en moindre abondance dans le foie et les tissus dits non-cérébraux comparativement au cerveau.

Nous avons également identifié une nouvelle protéine, RME-8 (de l'anglais receptor-mediated endocytosis protein 8), qui contient un domain DnaJ et qui a été détectée spécifiquement dans les vésicules tapissées de clathrine isolées à partir du foie. La caractérisation de RME-8 nous a appris que RME-8 se lie à la protéine chaperone Hsc70 (de l'anglais heat shock cognate Hsc-70) et que cette interaction est tributaire de l'ATP. RME-8 est une protéine ubiquitaire associée aux endosomes et sa déplétion

engendre des perturbations au niveau du trafic intracellulaire. Nous avons aussi démontré que la déplétion de RME-8 cause une diminution des niveaux d'expression du récepteur de l'EGF (EGFR) et que cette diminution est due à une augmentation de sa dégradation. L'absence de RME-8 cause également une diminution des niveaux d'expression de EGFR et ce, même dans des lignées de cellules cancéreuses chez lesquelles EGFR est normalement protégé contre la dégradation.

Globalement, ce projet de doctorat a permis de mettre en lumière les différentes fonctions de spécialisation du trafic cellulaire tributaire de la clathrine entre les différents tissus et nous a également permis d'identifier et de caractériser une nouvelle protéine impliquée dans les mécanismes de triage qui se déroulent dans le compartiment endosomal.

TABLE OF CONTENTS

LIST OF FIGURES

LIST OF TABLES

LIST OF ABBREVIATIONS

AAK1	adaptor-associated kinase 1
ADP	adenosine diphosphate
AP-1/AP-2	adaptor protein 1/adaptor protein 2
APEX	absolute protein expression
AQUA	absolute quantification of proteins
Arf	ADP-ribosylation factor
ATP	adenosine triphosphate
ATPase	adenosine triphosphatase
CCP	clathrin-coated pit
CCV	clathrin-coated vesicle
CHC	clathrin heavy chain
CLC	clathrin-light chain
CME	clathrin-mediated endocytosis
COP1/COPII	coat protein I/coat protein II
CTB	cholera toxin B
CVAK104	coated-vesicle-associated kinase of 104 kDa
DIGE	differential gel electrophoresis
EEA1	early endosomal antigen 1
EGF	epidermal growth factor
EGFR	epidermal growth factor receptor
Eps15	EGF pathway substrate clone 15
Epsin	Eps15-interacting protein
ER	endoplasmic reticulum
ERK	extracellular signal-regulated kinase
ESCRT	endosomal sorting complexes required for transport
ESI	electrospray ionization
FENS-1	FYVE domain containing protein localized to endosomes 1
FGFR	fibroblast growth factor receptor
FYVE	Fab1, YOTB, Vac1, and EEA1
GAK	Cyclin G-associated kinase
GDP	guanosine diphosphate
GFP	green fluorescent protein
GGA	Golgi-localized, γ-ear-containing, Arf-binding
GST	glutathione S-transferase
GTP	guanosine triphosphate
GTPase	guanosine triphosphatase
HB-EGF	heparin-binding EGF-like growth factor (HB-EGF)
HGFR	hepatocyte growth factor receptor
HIP1R	Huntingtin interacting protein 1 related
Hrs	hepatocyte growth factor-regulated tyrosine kinase substrate
Hsp40	heat shock protein 40
Hsp70	heat shock protein 70
Hsp73	heat shock protein 73
Hsc70	heat shock cognate protein 70 kDa

ICAT	isotope-coded affinity tag
ICR	ion cyclotron resonance
InsR	insulin receptor
JAK/STAT	janus kinases /signal transducer and activators of transcription
KD	knock-down
kDa	kilodalton
LAMP1	Lysosomal-associated membrane protein 1
LBPA	lysobiphosphatidic acid
LC-Q-ToF MS/MS	liquid chromatography quadrupole time-of-flight tandem MS
LDL	low density lipoprotein
LDLR	low density lipoprotein receptor
MALDI	matrix-assisted laser desorption/ionization
MAPK	mitogen-activated protein kinase
MPR	mannose phosphate receptor
MS	mass spectrometry
mSos	mammalian Son-of-sevenless
MVB	multivesicular body
NECAP	adaptin-ear-binding coat-associated protein
NGFR	nerve growth factor receptor
NSF	*N*-ethylmaleimide-sensitive factor
PACS1	phosphofurin acidic cluster sorting protein 1
PDGFR	platelet-derived growth factor receptor
PI3K	phosphatidylinositol-3 kinase
PTB	phosphotyrosine binding
RME-1	receptor-mediated endocytosis protein 1
RME-8	receptor-mediated endocytosis protein 8
RTK	receptor tyrosine kinase
SDS-PAGE	sodium dodecyl sulfate polyacrylamide gel electrophoresis
SH2/SH3	Src homology 2/Src homology 3
Shc	SH2 domain-containing transforming protein
SILAC	stable isotope labeling by amino acids in cell culture
SNARE	soluble *N*-ethylmaleimide-sensitive factor attachment protein receptor
STAM	SH3 domain and ITAM motif
SV	synaptic vesicle
Tf	transferrin
TfR	transferrin receptor
TGFα	transforming growth factor alpha
TGFβ	transforming growth factor alpha
TGN	*trans*-Golgi network
ToF	time of flight
TSG101	tumor susceptibility gene 101
VAMP4	vesicle-associated membrane protein 4
VEGFR	vascular endothelial growth factor receptor
VPS	vacuolar protein sorting

CONTRIBUTIONS OF AUTHORS

CHAPTER 2

NON-STOICHIOMETRIC RELATIONSHIP BETWEEN CLATHRIN HEAVY AND LIGHT CHAINS REVEALED BY QUANTITATIVE PROTEOMICS OF CLATHRIN-COATED VESICLES FROM BRAIN AND LIVER

Martine Girard, Patrick D. Allaire, Peter S. McPherson, and Francois Blondeau.
Molecular and Cellular Proteomics, 4, 1145-1154 (2005).

M. Girard, F. Blondeau and P. McPherson first observed that CCVs derived from liver had fewer clathrin-light chains relative to clathrin-heavy chain than CCVs from brain. Experiments were performed by M. Girard, F. Blondeau and P. Allaire. Data analysis was done by M. Girard, F. Blondeau and P. McPherson. The article was written by M. Girard, F. Blondeau and P. McPherson.

Contribution to figures:

Martine Girard	Figures 1, 2, 3, 4 and 5. Supplemental Figures 1, 2 and 3. Table I and Supplemental Table
Francois Blondeau	Figures 1, 2, 3, 4 and 5. Supplemental Figures 1, 2 and 3. Table I and Supplemental Table
Patrick Allaire	Figure 1C

CHAPTER 3

THE DNAJ-DOMAIN PROTEIN RME-8 FUNCTIONS IN ENDOSOMAL TRAFFICKING

Martine Girard, Viviane Poupon, Francois Blondeau and Peter S. McPherson.
Journal of Biological Chemistry, 280, 40135-40143 (2005).

M. Girard, F. Blondeau and P. McPherson analyzed the proteomics table of novel proteins in which RME-8 was previously identified (see chapter 2). F. Blondeau, M. Girard and P. McPherson did the protein alignment and the bioinformatic searches. Experiments were performed by M. Girard and V. Poupon. Data analysis was done by M. Girard, V. Poupon and P. McPherson. The article was written by M. Girard, V. Poupon and P. McPherson.

Contribution to figures:

Martine Girard	Figures 1, 2, 3, 4, 5, 6B, 7B and 7D, 8C, 9C and 9D
Viviane Poupon	Figures 6A, 7A and 7C, 8, 9A and 9B, Supplemental Figures 1 and 2
Francois Blondeau	Figure 1

CHAPTER 4

RME-8 REGULATES TRAFFICKING OF THE EPIDERMAL GROWTH FACTOR RECEPTOR

Martine Girard and Peter S. McPherson.
FEBS Letters, 582, 961-966 (2008).

M. Girard and P. McPherson noticed that EGFR expression levels were decreased upon RME-8 depletion (see chapter 3). Experiments were performed by M. Girard. Data analysis was done by M. Girard and P. McPherson. The article was written by M. Girard and P. McPherson

Contribution to figures:

Martine Girard	Figures 1, 2, 3, 4, and 5

ACKNOWLEDGEMENTS

My first thanks are for my supervisor, Dr. Peter McPherson, who shared with me his scientific knowledge and taught me how important being passionate about your work is. During the last years you guided me through the tortuous road of the doctorate and you helped me become a better scientist and more importantly, a better person too. Thanks for your patience; I am so grateful you believed in me. Thanks to the members of my committee, Dr. Wayne Sossin and Dr. Morag Park for advice, guidance and helpful discussions.

All that work would not have been possible without the technical, scientific and moral support provided by past and present lab members. Thanks to Elaine, Lyne and Jacynthe who spoiled me with their excellent technical assistance, and also to Linda for taking care of all the administrative and bureaucratic issues. To my graduate student colleagues, Patrick, Jonathon and Andrea, to the incomparable postdoctoral fellows, Brigitte, Viviane, Sébastien and Yohei, to former lab members François, Natasha, Sylwia, Valerie and Annie, my most sincere gratitude. Knowing you and working with you was a pleasure and an honour.

Je tiens tout particulièrement à remercier ma famille d'avoir toujours cru en mes rêves et de m'avoir appuyée durant toutes ces années. Mille mercis à toi Jean-François d'être à mes côtés et d'avoir vécu avec moi les moments de joie et les tempêtes qui ont accompagnés ce doctorat et la rédaction de cette thèse.

CHAPTER 1
INTRODUCTION

1.1 INTRODUCTION TO MASS SPECTROMETRY AND PROTEOMICS

1.1.1 TECHNICAL ASPECTS OF MASS SPECTROMETRY

Genomics can be defined as the study of the global genome of an organism; similarly, proteomics refers to the analysis of its gene expression at the protein level. Despite many proteomic studies, proteomic analysis remains a challenge. Whereas the human genome comprises 25 000 genes, those genes encode as many as one million proteins that could be differentially expressed in different cell types and at different cellular states. Proteomic analysis has been facilitated by the development of sophisticated mass spectrometry (MS) techniques (Aebersold and Mann, 2003; Dreger, 2003; Cravatt et al., 2007). MS allows the identification of proteins based on the precise mass of peptides that are generated upon enzymatic or chemical cleavage. There are several enzymes available for cleavage but the most popular is trypsin, which cuts after arginine and lysine residues. The information obtained from that cleavage and mass analysis is then used to search protein databases or genomic databases following *in silico* translation. The typical experimental approach for analysis of a complex protein sample by MS includes a fractionation and proteolysis of the sample, followed by the analysis of the digested fractions in the MS apparatus. The design of a mass spectrometer has three essential modules: an ionization source, where the digested peptides are vaporized and ionized; a mass analyzer, which sorts the ions by their masses by applying electromagnetic fields; and a detector to record mass spectra. Mass spectrometers operate under vacuum conditions in order to avoid collisions with other ions or with air molecules. The two main techniques used for ionization are the electrospray ionization (ESI) and the matrix-assisted laser desorption/ionization (MALDI). In ESI, the analyte is mixed with an organic solvent (usually methanol, isopropanol or acetonitrile) and pushed through a capillary so it forms an aerosol when it exits. The solvent will evaporate and leaving only the ion. It is now common to add a chromatography step to allow a better separation of the peptides before the ionization procedure with ESI. In MALDI, the peptides are mixed with a solvent, dried on a plate, and the sample is then hit with a laser, which causes the peptide to be ejected from the plate as an ion. The

main types of analyzers are the quadrupoles, the time of flight (ToF), and the trap instruments. In quadrupole instruments, parallel rods create oscillatory electrical fields and only ions with stable trajectories reach the detector. The ToF analyzer is basically a flight tube that uses electric fields to accelerate the ions with equal energy. The ions fly within the tube and the time they need to reach the detector depends on their mass. Lighter ions fly faster and reach the detector before heavier ones. Trap instruments include ion traps and ion cyclotron resonance (ICR) mass spectrometers. In the trap instruments, the ions are retained in the analyzer during the entire MS process. It is possible to do multiple steps of mass spectrometry with fragmentation procedures in between the steps which refers to tandem mass spectrometry (MS/MS). For example, quadrupole ToF tandem MS (QToF-MS/MS) is a hybrid tandem MS technique that combines a quadrupole analyzer with a ToF analyzer. In this case, the ionized peptides are first analyzed in the quadrupole. The most charged ionized peptides are then presented to the collision chamber for further fragmentation and from there they reach the ToF analyzer. The masses of the fragmented ions are recorded by the detector.

1.1.2 PRINCIPAL QUANTIFICATION METHODS IN MS AND PROTEOMICS

Once mass spectra have been assigned to corresponding peptides and proteins, it is crucial to quantify the proteins in order to gain insights into biological systems, and many groups have worked on developing quantitative approaches. Many quantification methods are based on the use of stable isotopes (SILAC, ICAT, and AQUA), some are gel-bases approaches (DIGE) and others are label-free methods (peptide/spectral counts). In the stable isotope labeling by amino acids in cell culture (SILAC), a given amino acid labeled with stable, heavy isotope is included in the cell culture media of one set of cells, while the other set is grown in normal media (Ong et al., 2002). As the cells grow and divide, they incorporate the heavy amino acid in all of their proteins. Therefore cell populations are mixed and analyzed together in the mass spectrometer, which recognizes that a given pair of peptides is chemically identical, but have a

different mass. The ratio of the two peptides allows relative quantification. ICAT refers to isotope-coded affinity tag, and was developed by Aebersold's group (Smolka et al., 2001). In ICAT, side chains of cysteine residues of protein samples are labeled with a reagent that contains either zero (light isotope) or eight deuterium (heavy isotope) atoms, together with a biotin group for affinity purification. The samples are then pooled, digested, enriched on an avidin column, and processed in the mass spectrometer, which will recognize the difference in mass of a chemically identical peptide. The AQUA (absolute quantification of proteins) strategy is based on the addition in the protein digestion mixture of known quantities of standard peptide(s), which is (are) stably labeled with an isotope (Gerber et al., 2003). This latest technique can not be applied for peptide and protein identification but only for quantification, since the peptide sequence needs to be known before "*in silico*" synthesis with the required modification (Gerber et al., 2003). Differential gel electrophoresis (DIGE) allows the analysis on a single two-dimensional gel of up to three samples, each of them being labeled with a different fluorescent dye (Wang et al., 2003; Orenes-Pinero et al., 2007). Label-free quantification is aimed to count and compare the number of spectra/peptides of a given protein, and is based on the principle that the more abundant is a protein in a sample, the more peptides it will generate upon trypsin digest (Liu et al., 2004; Blondeau et al., 2004; Gilchrist et al., 2006). This peptide accounting approach also takes into consideration the fact that larger proteins generate more peptides per mol. Therefore, the number of accounted peptides is normalized for the size of the protein it belongs to by dividing the number of specific peptides identified for the protein by its mass in kilo Dalton (kDa) thus generating a peptide to mass ratio. Moreover, the peptide accounting approach has been refined. The absolute protein expression (APEX) profiling method introduces correction factors that allow to correct for the differences between the number of tryptic peptides that are theoretically expected for a given protein and the ones that are practically observed by MS (Lu et al., 2007) A computational approach recently developed is based on the prediction of proteotypic peptides and could be used as "standards" in MS experiments where absence or presence of a given protein has to be assessed (Mallick et al., 2007).

1.2 VESICULAR CARRIERS AND TRAFFICKING

Eukaryotic cells are divided into elaborated functionally distinct membrane-enclosed compartments. Each compartment is defined as an organelle and possesses its own specialized set of proteins. The cell is a highly dynamic structure and its different membrane-bound organelles such as endoplasmic reticulum (ER), Golgi apparatus, mitochondria and the endosomal/lysosomal system are in constant communication. One key aspect of intracellular communication relies on the transport of vesicular carriers between the compartments. The donor compartment generates a transport vesicle that is received exclusively by the appropriate acceptor compartment. This process is tightly regulated since both carriers and organelles need to maintain their cellular identity. Characterizing the mechanisms that regulate this transport, as well as the carriers and proteins implicated in such trafficking events, are crucial for understanding cellular homeostasis.

1.2.1 OVERVIEW OF VESICULAR TRAFFICKING

Following their insertion into the lumen of the ER, newly synthesized proteins are transported to the *cis* face of the Golgi apparatus, and then to the Golgi cisternae where they undergo post-translational modifications. The modified proteins then move to the *trans*-Golgi network (TGN), which acts as a sorting center for the proteins. Within the Golgi apparatus, the cargoes are transported in small coated vesicles named COPI and COPII vesicles (Orci et al., 1986; Kirchhausen, 2007). From the TGN, proteins are directed to their appropriate cellular destination that could be endosomes, the plasma membrane, or the cell exterior (for review see van Vliet et al., 2003). The different cargoes destined for different compartments will be packaged into different types of carriers and the size of the carriers will depend on their content and their final destination. For example, in the formation of dense core secretory granules in endocrine cells, the cargo is concentrated into aggregates that can not fit into small vesicles and therefore requires a relatively large secretory vesicle (Thiele et al., 1997). In contrast,

hydrolases that need to get to lysosomes exit the TGN, together with their receptors, in CCVs that are approximately 100 nm in diameter (Ghosh et al., 2003b). Carriers arising from TGN are therefore variable in size and shape.

Fusion of TGN-derived vesicles with the plasma membrane is the end point of the secretory pathway and it needs to be compensated with endocytosis in order to maintain plasma membrane homeostasis. Endocytosis allows large extracellular molecules, nutrients, plasma membrane components, and receptors to enter the cell. In mammalian cells, endocytosis can occur via five different pathways: pinocytosis, phagocytosis, caveolar pathway, clathrin-dependent pathway and clathrin- and caveolae-independent pathway (for review, see Connor and Schmid, 2003). The clathrin-dependent pathway is certainly the best understood of the endocytosis pathways and has been the focus of many studies over the last 30 years.

Clathrin-mediated endocytosis (CME) has several important cellular functions including the uptake of nutrients, such as cholesterol-bound low-density lipoprotein and iron-bound transferrin, as well as the recapture of proteins such as albumin after their filtration by kidneys (Royle and Murrell-Lagnado, 2003; Maxfield and McGraw, 2004). CME also downregulates several signaling receptors by regulating their levels at the cell surface (Di Fiore and De Camilli, 2001; Seto et al., 2002). Moreover, since signaling receptors can also signal along the endocytic pathway, including the endosomes, CME also has a positive role in the regulation of signaling activity (Miaczynska et al., 2004). CME is also crucial in neuronal cells where it is responsible for the internalization of ion channels and neurotransmitter receptors, including glutamatergic receptors, thus allowing control of synaptic transmission and molecular foundations of learning and memory (Carroll et al., 2001). Finally, synapses need to retrieve and reform an enormous amount of synaptic vesicles (SVs) following neuronal stimulation and CME is the preferred mechanism to fulfill this role (for a review see Murthy and De Camilli, 2003).

Following endocytosis of SVs, the vesicles lose their clathrin coat, refill with

neurotransmitter and re-enter the functional SV pool (for review see Murthy and De Camilli, 2003). However, in most non-synaptic examples, the endocytic vesicles fuse with early endosomes that constitute a sorting station in the endocytic trafficking pathway (Maxfield and McGraw, 2004). From there, cargoes either recycle back to the plasma membrane, or are directed further down the late endosomal pathway. Transferrin receptor (TfR) is one receptor that constitutively recycles back to the plasma membrane. Receptors that continue to travel along the endosomal pathway are usually destined for degradation in lysosomes (Gruenberg and Stenmark, 2004). The receptors that are targeted for degradation are often conjugated to a small molecule called ubiquitin at the plasma membrane. Once internalized, ubiquitinated receptors will reach the early endosomes, will be delivered to late endosomes, and then to lysosomes to be degraded (Gruenberg and Stenmark, 2004).

1.3 CCVs

The first observation of coated vesicles was by EM in 1964 by Roth and Porter who reported their presence close to the plasma membrane and TGN areas (Roth and Porter, 1964). In 1975, Barbara Pearse showed that the main constituent of vesicle coats was clathrin (Pearse, 1975), and it is now clear that clathrin provides the scaffold necessary for protein sorting and membrane budding (Kirchhausen, 1993; Smith and Pearse). The clathrin coat of a vesicle has a basket-like shape composed of hexagons and pentagons (Ungewickell and Branton, 1981; Kirchhausen and Harrison, 1981) (Figure 1.1A). Clathrin itself is composed of heavy chains (CHCs) and light chains (CLCs) that form a triskelion, which consists of three CHCs connected through their C-terminal region in a central hub region (Ungewickell and Branton, 1981; Kirchhausen and Harrison, 1981). Each CHC contains a proximal and distal leg segment and ends in an N-terminal globular domain (Figure 1.2B). The proximal leg segment comprises sequences mediating CHC trimerization and binding sites for CLCs. Seven CHC repeat motifs are distributed within the proximal and distal segments of CHC (Brodsky et al., 1991; Liu et al., 1995; Ybe et al., 1999). The N-terminal globular domain include

binding sites for different clathrin-interacting proteins (ter Haar et al., 1998)

CLCs bind to the hub region of the triskelion and it has been traditionally thought that one CLC associates with each CHC leg (Brodsky et al., 2001). Vertebrates have two forms of CLCs (CLCa and CLCb) and each form has a neuronal splice variant (Brodsky et al., 1991). Clathrin triskelia have a random distribution of either CLCa or CLCb isoforms, which are competing with each other for CHC binding (Brodsky, 1988). CLCa and CLCb are differently expressed in tissues and cell lines, but attempts to identify differences in their functions have not been conclusive (Acton and Brodsky, 1990). Both CLCs have a calcium binding site at their N-termini and a central clathrin binding domain (Brodsky et al. 1991). When expressed together with CHC in a 1:1 molar ratio, CLC inhibits clathrin polymerization into cages (Ungewickell and Ungewickell, 1991). Assembly proteins such as HIP1 and HIP1R are required to overcome this inhibitory effect of CLCs (Chen and Brodsky, 2005; Legendre-Guillemin et al., 2005). Thus, the model is that CLCs function as a negative regulator of clathrin assembly. Most of the experiments were done using CHC and CLCs purified from brain. We compared stoichiometric ratio of CLCs to CHCs by proteomics and found differences in CLCs to CHC ratio between brain and liver. In brain, the ratio was 1:1 but in liver the CLCs to CHC ratio was 0.2:1 (Blondeau et al., 2004; Girard et al., 2005b), and at this ratio, CLCs inhibitory effect on clathrin assembly should be minimal (Ungewickell and Ungewickell, 1991). Those findings led to questioning the model that has been accepted for years, and it is now clear that CLCs are not universal regulators of clathrin assembly. In fact, the regulatory role of CLCs and the 1:1 CLCs to CHCs ratio may be unique to brain and its specialized synaptic vesicle retrieval functions. Indeed, it has been shown that CHC and CLCs were not forming in a 1:1 ratio when coproduced in bacteria (Liu et al., 1995), and loss-of-function experiments also contributed to the elucidation of the role of CLCs in non-neuronal cells. In *Dictyostelium*, loss of CLC has no effect on CHC steady state levels and no effect on triskelia formation (Wang et al., 2003). In non-neuronal mammalian cells, CLC depletion does not affect clathrin-mediated endocytosis (Yang et al., 2002; Huang et al, 2004) but does perturb actin organization and protein trafficking at the TGN (Poupon et al., 2008). We now know

that CLCs role in non-neuronal cell is to provide the recruitment platform necessary for actin assembly and clathrin-mediated trafficking of the TGN-derived CCVs (Poupon et al., 2008)

FIGURE 1.1 *Structure of clathrin and the AP-2 complex*

A) EM from the inside of the PM of a skin cell. The image shows CCPs and CCVs forming on the inner surface of the PM. © 1998 Garland Publishing.

B) Clathrin triskelion. Proximal and distal segments of CHC are identified. The N-terminal of CHC forms the terminal globular domain. The C-terminal of CHC is found in the central hub region. Positions of CLCs are shown schematically. Adapted by permission from Macmillan Publishers Ltd:, Nature, Volume 432, © 2004.

C) Schematic representation of the AP-2 complex composed of the α, β-2, μ-2 and σ-2 subunits. Structurally, the AP-2 complex comprises the ear domain, the hinge and the core (also referred as the trunk). Reprinted by permission from Macmillan Publishers Ltd., EMBO Reports, Volume 5, © 2004.

A

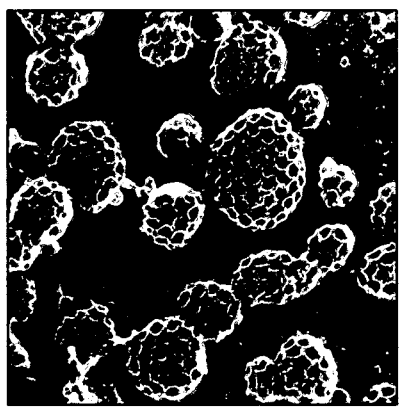

B

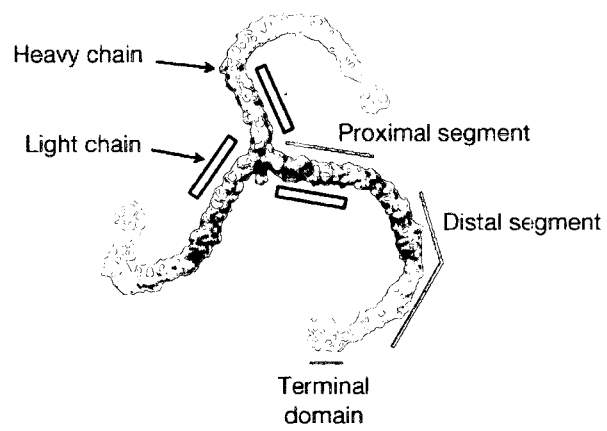

C

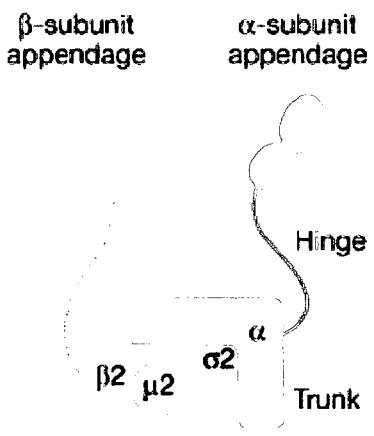

FIGURE 1.1

1.4. CME

At the plasma membrane, CME is responsible for the uptake of nutrients and internalization of different classes of receptors such as TfR, epidermal growth factor receptor (EGFR) and low-density lipoprotein receptors (LDLR). Clathrin-mediated vesicle formation can be subdivided into 4 main steps : 1) the beginning of coat assembly and cargo recruitment (initiation); 2) further coat assembly and cargo recruitment accompanied by membrane deformation (propagation); 3) completion of the coat and vesicle fission (budding); and 4) disassembly of the clathrin coat (uncoating) (Kirchhausen, 2000). Clathrin-mediated events involve many accessory proteins in order to regulate and coordinate all the various steps from cargo recruitment to vesicle uncoating.

1.4.1 INITIATION STEP

In the initiation step, the assembly of clathrin triskelia into a coat and cargo recruitment is beginning. Clathrin recruitment from the cytosol to the plasma membrane, as well as recruitment of cargo proteins, is orchestrated by the adaptor protein AP-2 (Zaremba and Keen, 1983; Keen, 1987; Blondeau et al., 2004). AP-2 is a heterotetrameric protein complex composed of two large α and β-2 subunits (~100 kDa), one μ-2 subunit (~50 kDa), and one σ-2 subunit (~17 kDa) (for review see Brodsky et al., 2001). Morphologically, AP-2 resembles a head with ears (Heuser and Keen, 1988). The head (or the core domain), contains the N-terminal two thirds of the α and β-2 subunits, as well as the μ-2 and σ-2 subunits (Figure 1.1C). The ears are formed by the C-termini of the α and β-2 subunits linked to the core by hinges (Figure 1.1C). The factors responsible for the recruitment of AP-2 itself to the plasma membrane are still not fully understood, but *in vitro* experiments demonstrated that AP-2 recruitment to the membrane is dependent on cytosolic factors that require ATP and GTP (Seaman et al., 1993; Traub et al., 1996). Among potential factors responsible for AP-2 targeting to the plasma membrane are protein kinases and small GTPases such as ARF6 (Krauss et al.,

2003; Paleotti et al., 2005), the lipid phosphatidylinositol 4,5-biphosphate ($PI(4,5)P_2$) (Beck and Keen, 1991; Gaidarov et al., 1996; Collins et al., 2002), as well as the protein synaptotagmins (Haucke et al., 2000; Marqueze et al., 2000). Together with the hinge domain, the β-2 ear binds to the CHC terminal domain and promotes assembly (Shih et al., 1995). Moreover, the globular α and β-2 ears are platforms for interactions with clathrin accessory proteins that contain motifs such as DPF, DPW, FXDXF and WXXF (Owen et al., 1999; Traub et al., 1999; Brett et al., 2002; Ritter et al., 2003). The μ-2 interacts and recruits cargo molecules that contain signal motifs in their cytoplasmic tails (Owen and Evans, 198). YXXϕ (tyrosine-based), NPXY, and [DE]XXXL[LI] (dileucine-based), where ϕ is a bulky hydrophobic residue and X any amino acid, are well known binding motifs for AP-2 (Bonifacino and Traub, 2003; McNiven and Thompson, 2006). NPXY motif is found in the insulin receptor (InsR), EGFR and LDLR cytoplasmic tails, YXXϕ is found in TfR and mannose-6-phosphate receptor (MPR), and the dileucine-based motif is found in proteins that are targeted to the endosomal/lysosomal compartment (McNiven and Thompson, 2006).

1.4.2 PROPAGATION AND BUDDING STEPS

During the propagation step, clathrin assembly and cargo recruitment continue and the membrane gradually deforms and invaginates to form a clathrin-coated pit (CCP), in a process that is tightly regulated by accessory proteins. For example, the accessory proteins epsin, endophilin A1 and amphiphysin I, co-operate with AP-2 to promote the membrane curvature necessary for vesicle budding (Schmidt et al., 1999; Farsad et al., 2001; Ford et al., 2002).

Once the clathrin lattice is completed and the cargo recruited, the deeply invaginated CCP, which is connected to the plasma membrane by a tubular neck, is ready to detach from the plasma membrane and to become a mature vesicle. Fission of the CCP is done by the GTPase protein dynamin that is massively and rapidly recruited to the CCP just before fission and that self-assembles in a spiral around the neck

(Hinshaw and Schmid, 1995; Merrifield et al., 2002; Praefcke and McMahon, 2004). Although the constriction of the vesicle neck created by the twisted dynamin and its GTPase activity is important for fission, it may not be sufficient (Roux et al., 2006). Efficient fission of the vesicle needs additional longitudinal tension that might be provided by actin motor proteins such as myosin 1E and myosin VI (Krendel et al., 2007; Spudich et al., 2007). However, dynamin's role might not be restricted to the fission reaction as electron microscopy studies showed dynamin was found in all stages of CCV formation (Damke et al., 1994; Evergren et al., 2004) and other groups demonstrated a gradual increase of clathrin and dynamin association before endocytosis (Rappoport and Simon, 2003; Ehrlich et al., 2004).

1.4.3 UNCOATING STEP

The chaperone Hsc70

Once the vesicle has pinched off the plasma membrane, it needs to lose its clathrin coat to allow fusion of the vesicle with the appropriate intracellular compartment, and recycling of the coat components for other rounds of endocytosis. The uncoating process involves two molecules: the ATPase Hsc70 (heat shock cognate protein of 70 kDa) and the cofactor auxilin (Lemmon, 2001). The cytosolic chaperone Hsc70 (also known as Hsp73) is probably the best known member of the heat shock protein 70 family (Hsp70). Hsp70 family proteins function as molecular chaperones by binding to other proteins and even though their interactions were first thought to be specific to certain cellular processes, it is now clear that Hsp70 proteins are functioning in various aspects of protein dynamics (Flynn et al., 1991). Hsc70 contributes to folding and refolding of newly synthesized and denatured proteins, respectively (Hartl and Hayer-Hartl, 2002), and does conformational work at different subcellular compartments, and in a vast array of cellular processes such as exocytosis, endocytosis, protein transport and trafficking, assembly and disassembly of protein complexes (Young et al., 2003). Hsc70 contains an ATPase domain in its N-terminus, and a

polypeptide binding domain in its C-terminus (for review see Hartl et al., 1992; Young et al., 2004). Hsc70 recognizes short hydrophobic stretches, and its regulation depends on the nucleotide-bound state that creates binding and release cycles for substrates (for review see Hartl et al., 1992; Hartl and Hayer-Hartl, 2002; Young et al., 2004). Recruitment of Hsc70 to specific sites of action is necessary for its activities and co-chaperones are responsible of such recruitment (Young et al., 2003; Kelley, 1999). Hsc70 interacts with co-chaperone proteins that contain a DnaJ domain (also referred to as heat shock protein 40s, Hsp40s) (Kelley, 1999).

DnaJ-domain containing proteins

Originally, the DnaJ domain was known to stimulate the ATPase activity of DnaK, which is the bacterial homolog of Hsc70, and help replicate the λ phage DNA in host cells (Liberek et al., 1988; Yochem et al., 1978). Since then, a large number of DnaJ homologs have been identified in both prokaryotes and eukaryotes, and in mammals more than 20 DnaJ homologues with diverse functions have been reported (for review see Qiu et al., 2006); which functions will depend on their localization. The DnaJ domain proteins are found in diverse cellular compartments including the cytosol, nucleus, mitochondria, ER, ribosomes and the endosomal/lysosomal system (for review see Qiu et al., 2006). Moreover, DnaJ domain proteins can be either ubiquitously expressed, or expressed in a specific tissue (Hu et al., 2004; Terada et al., 2005). The DnaJ domain itself is a 70 amino acids α-helical structure composed of four helices (helices I-IV) (Cheetham and Caplan, 1998). In addition to the DnaJ domain, many DnaJ-domain containing proteins contain other conserved regions critical for their functions (Cajo et al., 2006). Based on the DnaJ domain and the differences in the presence of these other regions, DnaJ domain containing proteins can be categorized into three groups (Cheetham and Caplan, 1998). Type I proteins contain the DnaJ domain in N-terminus, followed by a Gly/Phe-rich region and cysteine repeats. Type II proteins have the DnaJ domain in their N-terminus and the Gly/Phe-rich region but no cysteine repeats. Type III proteins have the DnaJ domain only, and although for most of the type

III proteins the DnaJ domain is present in the N-terminal region, there are some exceptions (for review, see Qiu et al., 2006). For example, auxilins and RME-8 are type III DnaJ-domain containing proteins that do not have their DnaJ domain in the N-terminus. In auxilins, the DnaJ domain is found in the C-terminal region, and the protein RME-8, which will be extensively discussed later in this thesis, has an internal DnaJ domain (Lemmon, 2001; Girard et al., 2005c). The DnaJ domain binds directly to Hsc70 ATPase domain, and stimulates its ATPase hydrolysis activity (Kelley, 1999; Cheetham and Caplan, 1998). Within the DnaJ domain, three highly conserved residues, HPD (the so called HPD motif), which are located between the helices II and III are essential for the interaction of DnaJ domain and Hsc70, as mutating these residues completely abolishes the DnaJ stimulated ATP hydrolysis activity of Hsc70 (Genevaux et al., 2002; Tsai and Douglas, 1996).

Auxilins are well characterized DnaJ-domain containing proteins (Lemmon, 2001). Auxilin-1 was originally identified as a neuron-specific component of CCVs (Ahle and Ungewickell, 1990) and auxilin-2 (also known as cyclin G-associated kinase or GAK) was later found to be a ubiquitously expressed isoform (Umeda et al., 2000). Auxilins are the co-chaperones for Hsc70 in clathrin coat disassembly, and they bind and interact with both clathrin (through their clathrin binding region) and AP-2 (through DPF motifs) (Lemmon, 2001). Auxilins bound to clathrin baskets recruit ATP-activated Hsc70 and stimulate the ATPase activity of Hsc70 (Ungewickell et al., 1995; Jiang et al., 1997), which causes disruption of clathrin-clathrin interactions, and release of the coat (Holstein et al., 1996). The importance of Hsc70 and auxilin interactions in the endocytic cycle has been demonstrated in many organisms. In yeast, deletion of the auxilin gene causes multiples defects: CCV accumulation, impaired cargo delivery to the vacuole, increased clathrin association with vesicles at the expense of cytosolic clathrin, and global slowdown of cell growth (Pishvaee et al., 2000; Gall et al., 2000). In the nematode *C. elegans*, inhibition of auxilin expression by RNA interference (RNAi) reduces receptor-mediated endocytosis of yolk protein in oocytes, and changes the dynamic of clathrin exchange in coelomocytes (Greener et al., 2001). In *Drosophila* deletion of auxilin is lethal (Hagedorn et al., 2006). Injection of peptides that inhibit the

uncoating action driven by Hsc70 and auxilin in the squid presynaptic terminal inhibits CCV uncoating, as well as presynaptic transmission (Morgan et al., 2001). More recently, it was shown that deletion of the GAK (auxilin-2) gene in mice causes embryonic lethality (Lee et al., 2008). Auxilin and Hsc70 roles were also extensively studied in mammalian cells. In 2001, Newmyer and Schmid showed that overexpression of the dominant-negative Hsc70 mutant inhibits CCV uncoating and impairs TfR internalization recycling (Newmyer and Schmid, 2001). Depletion of GAK (auxilin-2) causes inhibition of transferrin (Tf) uptake and partial inhibition of the trafficking from the TGN to lysosomes (Zhang et al., 2005). Moreover, Lee et al. (2005) observed a stronger phenotype, similar to the one observed by Newmyer and Schmid with their Hsc70 dominant negative construct. Indeed, they found that GAK (auxilin-2) depletion causes a) a decrease in CME, b) an impairment in TGN to lysosome trafficking, c) a significant depletion of clathrin at the plasma membrane and d) a reduction in AP-2 and AP-1 at the plasma membrane and TGN, respectively (Lee et al., 2005). From these studies it is clear that the interaction between auxilin and Hsc70 is crucial for clathrin-mediated trafficking.

1.5 CLATHRIN-MEDIATED MEMBRANE BUDDING AT THE TGN

As stated above, the TGN is the exit station of the biosynthetic pathway from where newly synthesized proteins leave for other cellular destinations. CCVs are one type of carrier that arise from TGN membranes and are involved in TGN to endosome trafficking. The same main sequential steps (initiation, propagation, budding and uncoating) occur at the TGN, although there are some major differences between the formation of CCVs at the plasma membrane and at the TGN with respect to the nature of the donor membrane and the adaptor responsible for clathrin and cargo recruitment. The donor plasma membrane is flat and cholesterol rich whereas the TGN donor membrane is tubulated (for review see Brodsky et al., 2001). Moreover, CCVs arising from the TGN are less stable than CCVs arising from the plasma membrane. AP-1 is the adaptor responsible for the recruitment of clathrin coats at the TGN and, as is the case for AP-2,

AP-1 also binds to clathrin and to peptide motifs within the cytoplasmic tail of cargoes (for review see Hinners and Tooze, 2003; Bonifacino and Traub, 2003). Similar to AP-2, AP-1 is a heterotetrameric complex composed of two large γ and β-1 subunits (~100 kDa), one μ-1 subunit (~47 kDa), and one σ-1 subunit (~19 kDa) (for review see Brodsky et al., 2001). AP-1 recruitment to the TGN membranes, however, depends on the small G protein Arf1, which cycles between the cytoplasm (when bound to GDP) and membranes (when bound to GTP) (Zhu et al., 1998; Donaldson and Jackson, 2000). Other adaptors and accessory proteins also function in clathrin-mediated trafficking at the TGN, such as the Golgi-localized, γ-ear-containing, Arf-binding (GGA) proteins 1, 2 and 3 (Bonifacino, 2004), HIP1R (Carreno et al., 2004), dynamin 2 (Cao et al., 2000), and enthoprotin (Wasiak et al., 2002). Cargo recognition by CCVs in the TGN can occur directly via the interaction of the μ-1 subunit with cytoplasmic domains bearing the YXXϕ motif (for review see Bonifacino and Traub, 2003), or indirectly through proteins such as PACS1 (Wan et al., 1998).

The mechanism for vesicle scission is less well understood than the one at the plasma membrane, although dynamin clearly appears to have a role at the TGN in addition to the plasma membrane (McNiven et al., 2000). Moreover, CCVs that budded from the TGN also need to uncoat in order to be able to deliver their cargo to the appropriate compartment. Uncoating of the TGN-derived CCVs is thought to occur by the same process as for the CCVs from the plasma membrane, i.e. through Hsc70 and auxilin interaction. In the case of the TGN CCVs, the cochaperone working with Hsc70 is probably GAK (auxilin-2) due to the fact that it was predominantly found at the perinuclear area (Greener et al., 2000). However, since less is known about the CCV uncoating arising from the TGN, it leaves open the possibility that other protein(s) could contribute to the process.

1.6. INTRACELLULAR AND ENDOSOMAL TRAFFICKING

1.6.1. MECHANISTIC OF FUSION EVENTS

What's the fate of a CCV once it loses its coat? After budding from the TGN and the plasma membrane, the vesicle fuses with components of the highly dynamic endosomal/lysosomal system, in order to deliver its cargo. Fusion with these compartments is a tightly regulated process that involves a vast array of proteins including SNAREs (soluble *N*-ethylmaleimide-sensitive factor attachment protein receptor) and Rab proteins (for review see Hong, 2005 as well as Jahn and Scheller, 2006). Fusion events involve tethering of the transport vesicle to the specific target membrane followed by docking and the fusion of the vesicle and its content to its target compartment (for review see Hong, 2005). SNAREs play a central role by catalyzing the fusion reaction and Rabs and their effector proteins regulate the tethering and docking of vesicles with the acceptor compartment (for review see Hong, 2005 as well as Jahn and Scheller, 2006).

In mammalian cells at least 30 different SNAREs are found, each of them being associated with a particular organelle of the secretory or endocytic pathway, where they orchestrate the orderly transport of cargo molecules (or review see Hong, 2005). SNAREs present in opposing membranes associate in a complex that can be dissociated by *N*-ethylmaleimide-sensitive factor (NSF) (Söllner et al., 1993). Based on that observation, SNAREs were divided into v-SNAREs (vesicle-membrane SNAREs) and t-SNAREs (target-membrane SNAREs) (Söllner et al., 1993). The mode of action of SNAREs in transport can be divided into four stages. In the first stage, the v-SNARE is packaged into budding vesicles, together with cargo proteins, thus generating a transport intermediate competent for fusion with the acceptor compartment. V-SNAREs usually consist of a complex of two or three polypeptides (Fukuda et al., 2000). In the second stage, tethering factors, such as Rab proteins and their effectors, position the vesicle at the target compartment containing the appropriate t-SNARE. In the third stage, v-SNARE and t-SNARE on the opposing membranes interact to form a *trans*-SNARE

complex, which then becomes a *cis*-SNARE complex as the vesicles fuse. In the fourth stage, the *cis*-SNARE complex on the target membrane is disassembled by the ATPases NSF and VPS4, thus leaving the SNAREs ready for other fusion and docking events (for review see Hong, 2005). Many SNARE proteins are members of the syntaxin and VAMP (vesicle-associated membrane protein also known as synaptobrevin) families. Different members of syntaxin and VAMP families are found in different subcellular compartments. For example, the majority of VAMP4 is located at the TGN where it colocalizes with syntaxin 6, and coimmunoprecipitation studies showed that VAMP4 and syntaxin 6 exit as a complex, thus indicating that VAMP4 and syntaxin 6 are involved in TGN to endosomes trafficking (Steegmaier et al., 1999). It has been demonstrated that MPR and syntaxin 6 exit the TGN in AP-1-positive CCVs and are then delivered to endosomes (Klumperman et al., 1998). Moreover, a mutant syntaxin 6 that is cytosolic instead of membrane anchored perturbs transport to lysosomes and delays endosomal maturation (Kuliawat et al., 2004).

As stated previously, the ATPase NSF ensures that uncomplexed SNAREs are always available for fusion, and these "free" SNAREs are not only capable of interacting with each other, but they are also capable of interacting with other proteins (for review see Jahn and Scheller, 2006). For example, VAMP4 interacts with AP-1 at the TGN and this interaction is necessary for VAMP-4 recruitment into trafficking vesicles at the TGN, since when using a VAMP4 construct unable to bind to AP-1, VAMP4 failed to localize correctly at the TGN, and instead was redistributed in peripheral structures (Peden et al., 2001). Although syntaxin 6 is predominantly localized at the TGN, a pool of syntaxin 6 is located at the early endosome compartment where it can bind directly to the tethering factor EEA1 (early endosomal antigen 1), and facilitate the formation of docking and fusion complexes (Simonsen et al., 1999). So SNARE proteins including VAMP4 and syntaxin 6 are implicated in many trafficking events including the transport arising from the TGN.

1.6.2 TRANSPORT OF VESICLES AND CARGOES FROM THE TGN AS ILLUSTRATED BY MPR TRAFFICKING ROUTE

One of the major destinations for TGN-derived CCVs is the endosomal/lysosomal system, and in fact, CCVs are responsible for the transport of lysosomal hydrolases, thereby contributing to biogenesis of the system (Klumperman et al., 1993). MPR is responsible for transporting the hydrolases out of the TGN. Lysosomal hydrolases are tagged with a mannose-6 phosphate group as they are passing through the lumen of the *cis* Golgi and this group will be recognized by the transmembrane MPR which is present at the TGN. MPR binds to the immature enzymes within the lumen of the TGN, and to clathrin adaptors on the cytosolic side, and together they exit the TGN in CCVs. The vesicles uncoat and fuse with late endosomes and the acidic pH of that organelle causes the enzymes and the receptor to dissociate. From there the enzymes reach the lysosome, where they are cleaved into their mature form and the MPR recycles back to the TGN, ready for another round of packaging and sorting. Not all the hydrolases tagged with mannose-6 phosphate are delivered to lysosomes, and some are instead transported to the cell surface and secreted into the extracellular fluid as immature enzyme. However, since a portion of the MPR proteins are also routed to the plasma membrane, they will act to recapture the escaped enzymes by CME and will return them to lysosomes via early and late endosomes (for review see Ghosh et al., 2003a). AP-1 interacts with the cytoplasmic tail of MPR and clearly has a role in the transport of the hydrolases between the TGN and the endosomal/lysosomal system (Le Borgne et al., 1996; Le Borgne and Hoflack, 1998). AP-1 was first thought to be implicated in the anterograde (TGN to endosome) transport of hydrolases (Le Borgne et al., 1996; Le Borgne and Hoflack, 1998; Ghosh et al., 2003a). However, analysis of MPR trafficking in μ1A-adaptin knockout mice revealed that MPR accumulates in endosomes and does not recycle back to the TGN, thus indicating that AP-1 is required for retrograde (endosome to TGN) transport (Meyer et al., 2000; Robinson and Bonifacino, 2001). Anterograde cargo transport would be mediated by the interaction of AP-1 and GGA adaptor proteins (Puertollano et al., 2001; Doray et al., 2002a; Doray et al., 2002b; Bai et al., 2004). Indeed, overexpression of mutated GGAs traps MPR

within the TGN (Puertollano et al., 2001), downregulation of GGAs expression impairs incorporation of MPR into AP-1-positive CCVs (Ghosh et al., 2003b), and mutated MPR that are unable to bind to GGAs are not packaged into CCVs (Doray et al., 2002). Therefore, efficient transport of cargo such as MPR between the TGN and endosomes is mediated by the GGA and AP-1 adaptor proteins.

1.6.3 TRANSPORT OF VESICLES AND CARGOES ARISING FROM CME

Newly formed endosomes arising from CME at the plasma membrane can fuse with each other or with pre-existing early endosomes (for review see Maxfield and McGraw, 2004). The early endosomes are the first arrest following endocytosis, and act as a relay to sort the molecules to their appropriate destinations (Gruenberg, 2001). Three destinations are possible after the molecules have passed through early endosomes (also known as sorting endosomes): the plasma membrane, recycling endosomes, or late endosomes/lysosomes. Early, recycling, late endosomes/lysosomes are morphologically and functionally distinct compartments, and as different entities, they possess their own sets of proteins that have important function for cargo sorting and organelle biogenesis.

Recycling pathway

Early/sorting endosomes are located at the periphery, have a tubulo-vesicular morphology, and a lumenal pH of ~6.0 (Mayor et al., 1993). Early endosomes accept incoming material for about 5-10 minutes and then they translocate along microtubules, stop fusing, become more acidic and start to acquire acid hydrolases that are characteristic features of the late endosomes as part as their maturation process (Dunn et al., 1989). Before the maturation process starts, some constitutively recycling molecules will return back to the plasma membrane, either directly or indirectly via the recycling endosome compartment. Many receptors are constitutively recycling back to the plasma

membrane from the early endosomal compartment, and among those are TfR (Hopkins, 1983), InsR (Knutson, 1991), and LDLR (Brown and Goldstein, 1979). TfR are removed rapidly from early/sorting endosomes and, in less than 5 minutes, more than 95% of endocytosed TfR is removed from the early endosomes before their maturation (Dunn et al., 1989; Mayor et al., 1993). Many proteins contribute to the organization of early endosomes and to the regulation of the protein transport occurring through this compartment and can therefore be considered as markers for the organelle. Rab proteins are small GTPases that oscillate between GDP (inactive) and GTP (active) bound states. Rab proteins function in the fusion process of vesicles to their proper targeted compartment, as well as in vesicle budding and in vesicle interactions with cytoskeleton components. Early endosomes are mainly composed of Rab5 and Rab4 together with a small portion of Rab11, although all these three Rab proteins have also been found to be localized to other compartments, thus indicating that they are probably involved in many trafficking pathways (for review see Zerial and McBride, 2001). Rab5 regulates transport of clathrin-derived endosomes from the plasma membrane to the early endosomes and homotypic fusion of early endosomes (for review see Zerial and McBride, 2001). Rab5 also interacts with its effector protein EEA1 and with the SNARE protein syntaxin 6 to regulate docking and fusion of CCP- derived vesicle with early endosomes (Simonsen et al., 1999; Woodman, 2005). Early endosomes are thus very dynamic structures which constitute the first delivery site proteins that have undergone CME.

As stated previously, there are two main routes back to the plasma membrane from sorting endosomes. Some molecules will return directly to the cell surface, others will transit through the recycling endosomes, also called the endocytic recycling compartment. Recycling endosomes are mainly composed of thin tubules of ~60 nm diameter that are associated with microtubules (Hopkins, 1983; Yamashiro et al., 1984). Most molecules that transit through the recycling endosomes will be returned back to the plasma membrane, although recycling endosomes can also sort molecules to the TGN (as it is the case for the protein TGN38 and shiga toxin), and back to the early/sorting endosomes (Maxfield and McGraw, 2004). The carriers used by the constitutively

recycling molecules arise from the budding of the narrow-diameter recycling tubule system (Dunn et al., 1989; Mayor et al., 1993). The majority of LDLR and TfR transit via the recycling endosomes (Maxfield and McGraw, 2004) and the regulation of transport from the recycling endosomes is ensured, among others, by the proteins Rab11 (Zerial and McBride, 2001) and RME-1 (Lin et al., 2001).

Degradation pathway

As constitutively recycling cargoes bud off early and/or recycling endosomes (Gruenberg, 2001), cargoes destined for degradation, such as EGFR, reside in the remaining early endosomes that will mature into late endosomes (Rink et al., 2005). Maturation of early endosomes to late endosomes occurs through sequential fusion and fission events that are coupled to loss of early endosome resident proteins, such as Rab5, and acquisition of late endosome resident proteins, such as Rab7 (Rink et al., 2005). As part of the endosomal maturation process, the cargoes destined for degradation undergo inward invagination into the lumen of the early endosomes, to form endosomal intermediates, the multivesicular bodies (MVB), that will detached from early/sorting endosomes, fuse with late endosomes, and eventually with lysosomes, to allow degradation of the cargoes by lysosomal hydrolases (Gruenberg, 2001). MVBs are large ~300-400 nm structures that have small vesicles contained in their lumen and that are distinct from early and late endosomes. Indeed, MVBs do not contain any of the specific proteins or recycling receptors of early endosomes, nor do they contain the characteristic lipids and proteins of the late endosomes (Gruenberg, 2001). But how are the proteins that are destined for degradation and the ones that are recycled to the cell surface sorted? Many factors can influence the sorting decision at early/sorting endosomes. For example, the acidic pH of ~6.0 that characterizes this compartment will cause dissociation of the LDL from LDLR; LDLR will recycle back to the surface and LDL will be sent for degradation (Maxfield and McGraw, 2004). Moreover, the presence of sorting signals such as YXXϕ and [DE]XXXL[LI] can also influence the destination of receptors (Bonifacino and Traub, 2003; McNiven and Thompson, 2006).

In addition to the above motifs, the targeting from the early endosomes to the late endosomes/lysosomes is often achieved by ubiquitination of the endocytosed cargo within its cytoplasmic domain (for review see Hicke and Dunn, 2003).

Ubiquitin is a 76 amino-acid protein that forms stable chemical bonds with other proteins by linking to their lysine residues (Hicke and Dunn, 2003; Clague and Urbé, 2006). Ubiquitination is a powerful mechanism that can regulate stability, activity and even location of proteins (Hicke and Dunn, 2003). Proteins can be monoubiquitinated (only one single ubiquitin moiety is attached to a single lysine within the protein), multimonoubiquitinated (single ubiquitin moieties are attached to multiple lysines within the protein), or polyubiquitinated (chain(s) containing multiple ubiquitin molecules linked to each other are attached to lysine(s) within the protein), and the type of ubiquitination will influence the protein fate (Pickart and Eddins, 2004). For example, proteins targeted for degradation within the proteasome are polyubiquitinated and proteins destined for lysosomal degradation are monoubiquitinated or multimonoubiquitinated (Pickart and Eddins, 2004). Indeed, endocytosed cargoes that are destined for lysosomal degradation are mono- or multimonoubiquitinated (Williams and Urbé, 2007). As mentioned above, the early/sorting endosome is organized in microdomains (Gruenberg, 2001). Non-ubiquitinated, recycling cargoes will transit through early/sorting endosome microdomains enriched with Rab5 and EEA1 proteins (Pfeffer, 2003; Maxfield and McGraw, 2004). In contrast, ubiquitinated cargoes will transit through early/sorting endosome microdomains enriched with Hrs (hepatocyte growth factor (HGF)-regulated tyrosine kinase substrate) and clathrin proteins (Raiborg et al., 2001; Pfeffer, 2003) and then will transfer to the ESCRT (endosomal sorting complexes required for transport) machinery for inward budding (Williams and Urbé, 2007). There are four ESCRT complexes that are known as ESCRT-0, -I, -II, and -III. ESCRT complexes are recruited to endosomes through protein and lipid interactions and they are essential for sorting of ubiquitinated cargoes and for the formation of MVBs (Russell et al., 2006; Hurley and Emr, 2006; Slagsvold et al., 2006; van der Goot and Gruenberg; 2006; Williams and Urbé, 2007).

ESCRT-0 is probably the best known of the four ESCRT complexes and is composed, in mammalian cells, of the proteins Hrs and STAM (signal transducing adaptor molecule). Hrs recruitment to endosomes is driven by the binding of the Hrs FYVE (Fab1, YOTB, Vac1 and EEA1) domain to the membrane lipid phosphatidylinositol-3-phosphate (PI3P). Hrs also recruits clathrin and organizes it into a poorly defined flat lattice that appears as a bilayer by electron microscopy (Raiborg et al., 2001; Sachse et al., 2002) and, in turn, the bilayer endosomal clathrin coat is responsible of segregating Hrs to sites of inward invagination (Qualmann et al., 2000; Sachse et al., 2002). Hrs binding to clathrin has been mapped to the LISFD clathrin-box motif located in its C-terminus (Raiborg et al., 2001). STAM also binds to clathrin but the binding site has not been mapped yet (McCullough et al. 2006). Through its ubiquitin-interacting motif, Hrs recruits and sorts ubiquitinated cargoes to the clathrin lattices (Raiborg et al., 2002; Urbé et al., 2003). STAM also possess an ubiquitin-interacting motif and has been shown to be involved in sorting the ubiquitinated cargoes (Bache et al., 2003). By providing the scaffold for proper localization of Hrs, clathrin would act as the organizer of the ESCRT pathway to ensure efficient sorting of ubiquitinated cargoes into ESCRT-0, and subsequent ESCRT complexes, and ultimately efficient degradation of cargoes in lysosomes. Indeed, Raiborg et al. demonstrated that clathrin recruitment to endosomes by Hrs, as well as the ability of clathrin to scaffold Hrs in endosomal microdomains, were essential for EGFR efficient degradation (Raiborg et al., 2006). Hrs function is also crucial in development since Hrs-deficient mice die at the embryonic stage (Komada and Soriano, 1999). The Hrs- and clathrin-containing endosomal microdomains are very dynamic structures that are constantly exchanging the Hrs and clathrin present within these microdomains with cytosolic pools of clathrin and Hrs, with a similar kinetic for both proteins (Raiborg et al., 2006). Despite the advance in the characterization of ESCRT complexes, the exact molecular composition of the Hrs-clathrin coats is still unclear, as is the factor that regulates their exchange between the microdomains and the cytosol. However, it has been proposed that the mammalian ATPase hVPS4, which is responsible of dissociating the SNAREs and the ESCRT complexes, may also participate in disassembly of the endosomal clathrin lattice, since overexpression of an ATPase-deficient mutant increases the

association of clathrin coats with endosomal membrane (Sachse et al., 2004).

Within the ESCRT-0 complex, Hrs and STAM are responsible for recruiting the ESCRT-I complex which sorts the ubiquitinated cargo into the lumen of the vesicles initiating the formation of MVBs (Babst, 2005). In mammalian cells, the ESCRT-I complex is composed of the proteins TGS101 (tumor susceptibility gene-101), VPS28 and one of the four isoforms of the protein VPS37 (VPS37A-D) (for review see Williams and Urbé, 2007). Binding of ESCRT-I complex to ubiquitinated cargo is ensured by TSG101 ubiquitin-binding domain (Sundquist et al., 2004). Interestingly, depletion of TSG101 causes a stronger inhibitory effect on EGFR degradation than does Hrs depletion. Moreover, the absence of TSG101 impedes MVB formation, thus indicating the importance of the ESCRT-I complex in the maintenance of this endosomal carrier (Doyotte et al., 2005; Razi and Futter, 2006). ESCRT-I recruits the ESCRT-II complex and then the ubiquitinated cargo is recognized by the ESCRT-II complex and transferred to it (Williams and Urbé, 2007). ESCRT-II complex recruits the ESCRT-III complex that contains the machinery for inward budding and that is the final relay for the cargo within the ESCRT pathway (Williams and Urbé, 2007). Within the ESCRT-III complex, the cargo will be deubiquitinated and the ESCRT components will be disassembled, probably by the ATPase VPS4 (Williams and Urbé, 2007). It is clear that all four ESCRT complexes are involved in sorting of proteins destined for degradation. However, recent studies have raised the possibility that they might play diverse roles in the different endocytic pathways, thus reflecting the complexity of cellular trafficking (Raiborg et al., 2008).

The next steps for MVBs are the late endosomes and the lysosomes. In mammalian cells, late endosomes constitute a very dynamic compartment organized in a pleiomorphic network of tubules, cisternae, vesicles and membrane invaginations that by EM can appear as multivesicular or multilammelar structure (Griffiths et al., 1988; Bomsel et al., 1990; Aniento et al., 1993). Late endosomes contain high amounts of LAMP1 (lysosomal-associated membrane protein 1) and LBPA (lysobiphosphatidic acid), and are characterized by the presence of MPR in their internal membranes, as well

as the proteins Rab7 and Rab9 (Griffiths et al., 1988; Gruenberg and Maxfield, 1995; Kobayashi et al., 1998). For many reasons, it is difficult to draw a line between late endosomes and lysosomes. Both compartments have a very similar acidic pH of ~5.5, contain LAMP1 protein, share the same machinery for fusion and docking and have the same limiting membrane composition (Gruenberg and Maxfield 1995; Gruenberg, 2001). Lysosomes can be distinguished from late endosomes by their properties on gradients, by their electron-dense appearance by EM, and by the absence of the above mentioned proteins that are characterizing late endosomes (Gruenberg and Maxfield, 1995; Gruenberg, 2001). Late endosomes and lysosomes can exchange proteins very rapidly and they are probably forming a hybrid intermediate organelle (Jahraus et al., 1994; Mullock et al. 1998).

1.7 SIGNALING ALONG THE ENDOCYTIC PATHWAY AS ILLUSTRATED BY THE ITINERARY OF EGFR

The endocytic pathway allows molecules to enter and to travel inside the cell, but it also provides a platform for signaling events. Over the last few years, much progress has been made regarding the partnership between endocytosis and signaling, and most of the insights came from the study of EGFR trafficking and signaling pathways, which constitute the best characterized example of these links. It is now appreciated that not only endocytic events can regulate signaling, but that signaling can also influence the endocytic, trafficking and sorting processes.

1.7.1 EGFR

EGFR is a member of the receptor tyrosine kinase (RTK) family. RTK family members, including EGFR, are responsible for many biological functions such as proliferation, differentiation, cell survival, migration and adhesion (Ullrich and Schlessinger, 1990). The RTK family also contains other well studied members such as

InsR, platelet-derived growth factor receptor (PDGFR), fibroblast growth factor receptor (FGFR), hepatocyte growth factor receptor (HGFR or Met), vascular endothelial growth factor receptor (VEGFR), and nerve growth factor receptor (NGFR or TrkA-C) (Ullrich and Schlessinger, 1990).

EGFR, also known as ErbB1, is a member of the ErbB family of RTKs that also comprises three other members, ErbB2, ErbB3 and ErbB4 (Pinkas-Kramarski et al., 1998). The structure of EGFR comprises an extracellular domain, a short transmembrane alpha-helical region and a large intracellular cytoplasmic domain (Carpenter, 1987; Ullrich and Schlessinger, 1990). The intracellular domain comprises internalization motifs and also exhibits a tyrosine kinase domain and multiple sites for tyrosine, threonine and serine phosphorylation. These sites, in particular the phosphorylated tyrosine residues, serve to recruit and activate components of the EGFR signaling pathways (Sorkin and Waters, 1993). The cysteine-rich extracellular domain contains the binding site for EGF and transforming growth factor alpha (TGFα), as well as other ligands, such as amphiregulin, betacellulin and heparin-binding EGF-like growth factor (HB-EGF) (Michalopoulos and Khan, 2005).

EGF binding to EGFR activates a vast array of signaling pathways that are involved in crucial biological processes such as cell division, differentiation and survival (Citri and Yarden, 2006). EGFR signaling cascades triggered by EGF stimulation comprises the JAK/STAT, the PI3kinase/AKT, and the well characterized ERK/MAP kinase (ERK/MAPK) pathways (Ulrich and Schlessinger, 1990). The tyrosine residues that autophosphorylate upon EGF stimulation within the cytoplasmic tail of EGFR serve as binding sites for signaling proteins containing SH2 (Src homology) and/or PTB (phosphotyrosine binding) domains. The recruitment of the above mentioned signaling molecules allows the formation of signaling complexes on the receptor, and thus provides the connection between activated EGFR and downstream signaling pathways (Pawson and Gish, 1992; van der Geer and Pawson, 1995). Specifically, activated EGFR binds to the SH2 domain of Grb2 which, through its SH3 domain, recruits the guanine nucleotide exchange factor son of sevenless (mSos) to the plasma membrane,

where it activates Ras by converting the small GTPase from its GDP-bound form to its GTP-bound form (Bar-Sagi and Hall, 2000; Schlessinger, 2000). Ras activation is the starting point of sequential phosphorylation events within the signaling cascade. In the case of the ERK/MAPK pathway, Ras-GTP binds to and activates its effector, the kinase Raf, which is thus recruited to the plasma membrane where it activates the kinase MEK. MEK phosphorylates and activates the kinase ERK/MAPK, which in turn elicits phosphorylation of a vast array of membrane and cytoplasmic targets. For example, ERK/MAPK will dissociate from MEK and translocate to the nucleus, where it will activate transcription factors that stimulate cell proliferation (for review see Kolch, 2000 and Scott and Pawson, 2000).

At the plasma membrane, EGFR is present as a monomer. Upon binding of extracellular ligand, EGFR dimerizes, which causes autophosphorylation of the tyrosine residues located in its cytoplasmic domain (Schlessinger, 1988; Schlessinger, 2002). Ligand stimulation of EGFR causes rapid clustering into CCPs and translocation into CCVs (Carpentier et al., 1982; Hanover et al., 1984). The tyrosine kinase activity of EGFR is necessary for proper phosphorylation by Src of CHC, for the rapid recruitment and assembly of clathrin at the plasma membrane, and for the increased endocytosis rate seen upon EGF stimulation. Indeed, cells treated with inhibitors of the tyrosine kinase Src have delayed EGFR internalization, and tyrosine kinase deficient EGFRs failed to localize to CCPs and have impaired internalization (Prywes et al., 1986; Lamaze and Schmid, 1995; Wilde, 1999; Sorkina, 2002). Whether or not the increase in clathrin machinery recruitment and internalization rate observed upon EGF stimulation may also accommodate and increase the endocytosis rate of constitutively recycling cargoes such as TfR is still unsolved (Wiley, 1988; Warren et al., 1998). Activation and dimerization of EGFR also allow the interaction of the endocytic sorting motif YXXϕ with the μ2 subunit of AP-2 and AP-2 recruits of accessory proteins such as dynamin and Eps15 (for review see Marsh and McMahon, 1999; McPherson et al., 2001). Eps15 was first identified as a major cytoplasmic substrate of activated EGFR; it is now clear that Eps15 is more than a substrate and has important regulatory functions in EGFR endocytosis. Upon stimulation with EGF, Eps15 is phosphorylated and translocated to the plasma

membrane where it interacts with AP-2 and clathrin (Benmerah et al., 1995; van Delft et al., 1997; Stang et al., 2004). Eps15, in turn, interacts with other accessory proteins such as epsin and synaptojanin and together they contribute to the formation of the CCVs necessary for EGFR endocytosis (Salcini et al., 1997). EGFR activation also causes elevation in phosphatidylinositol 3,4,5-triphosphate ($PI(3,4,5)P_3$) and phosphatidylinositol 4,5-bisphosphate ($PI(4,5)P_2$) lipids which are both known to bind to many endocytic accessory proteins (Honda et al., 1999; Heath et al., 2003). Moreover, activation of EGFR also triggers phosphorylation of the ubiquitin ligase c-Cbl, which will then ubiquitinate the receptor itself, and also possibly other accessory proteins implicated in its endocytosis, such as Eps15 (van Delft et al., 1997; Levkowitz et al., 1999). The importance of cargo ubiquitination in endocytosis was first demonstrated in the yeast G-protein coupled plasma membrane receptor Ste2p (Hicke and Riezman, 1996). These studies were followed by others in both vertebrates and invertebrates confirming the importance of ubiquination in endocytosis and also throughout the endocytic process (for reviews see LeBorgne et al., 2005 and Miranda and Sorkin, 2007). However, there is still some debate as to whether it is ubiquitination of EGFR that is crucial for its internalization, or ubiquitination of other accessory proteins and that, because of the fact that an EGFR construct mutated on several lysine residues is still able to endocytose normally (Huang et al., 2007).

As internalization is the first key step of EGFR endocytic transport, its sorting in endosomes is surely the second one, and this endosomal sorting is a crucial step for EGFR fate, as is the activated state of EGFR (Figure 1.2 for EGFR endocytosis and trafficking). Inactive EGFR is recycled back to the plasma membrane and activated EGFR is sorted for the degradation pathway (Felder et al., 1990; Futter et al., 1993). Endocytosis and degradation of EGFR reduces the number of receptors present at the surface and inside the cells, and is therefore a powerful mechanism to attenuate and terminate cell signaling (Beguinot et al., 1984; Stoscheck and Carpenter, 1984). In the degradative pathway, EGFR sorting is sequentially accomplished through ubiquitination of EGFR, recognition of ubiquitinated EGFR, and sequestration in MVBs. Perturbation of these sorting steps causes aberrant morphology of MVBs and impaired signaling (Di

Fiore and Gill, 1999; Di Fiore and De Camilli, 2001; Waterman and Yarden, 2001; Wiley and Burkey, 2001). EGFR interacts with many proteins of the internalization and endosomal sorting machineries encountered along the degradation route. Activated EGFR is a continuous substrate for ubiquitination by c-Cbl in endosomes, and this additional ubiquitination is crucial for EGFR sorting into the lumen of MVBs (Longva et al., 2002). Ubiquitinated EGFR is recognized by the protein Hrs within the ESCRT-0 complex (Bache et al., 2003). From ESCRT-0, ubiquitinated EGFR is probably transferred to the ESCRT-I complex where it is recognized by the protein TSG101. EGFR is then transferred to the ESCRT-II and ESCRT-III complexes to finally bud inward into the lumen of MVBs (for review see Miranda and Sorkin, 2007). The sequential passage from ESCRT-I, -II, and -III complexes is still hypothetical since direct binding of EGFR to these complexes has not been demonstrated yet (Slagsvold et al., 2006). Based on yeast studies, it is also proposed that EGFR gets deubiquitinated by enzymes of the ESCRT machinery but again this has not been directly demonstrated yet (Slagsvold et al., 2006). Sequestration of EGFR into MVBs, and further degradation into lysosomes, terminates signaling since once inward budding has occurred, EGFR is no longer in contact with cytoplasmic signaling molecules. Even if some of the molecular mechanisms residing behind EGFR sorting in the endosomal pathway have not been elucidated yet, it is clear that the endosomal sorting of EGFR receptor is crucial for its degradation and the termination of its signaling, as mutations in either c-Cbl, Hrs or TSG101 impair degradation and increase signaling (for review see Babst, 2005)

FIGURE 1.2 *EGFR endocytosis and intracellular trafficking*

EGFR bound to EGF enters the cell through CME. Activated EGFR recruits Cbl which ubiquitinates EGFR. Cbl associates with CIN85 and endophilins, as EGFR phosphorylates and induces the ubiquitnation of Eps15 and epsin. In early endosomes, HRS binds to PI3P through its FYVE domain, and forms a complex with the signal transduction adaptor molecule STAM and Eps15 that interacts with EGFR. Non-ubiquitinated EGFR recycles back to the cell surface and ubiquitinated EGFR is sorted towards the MVB. At MVB, HRS interacts with TSG101 within the ESCRT-I. EGFR is then transferred to ESCRT-II and -III and to the intralumenal vesicles of MVB from where it reaches late/lysosome for degradation. Adapted by permission from Macmillan Publishers Ltd:, Nature Reviews Molecular Cell Biology, Volume 6, © 2005.

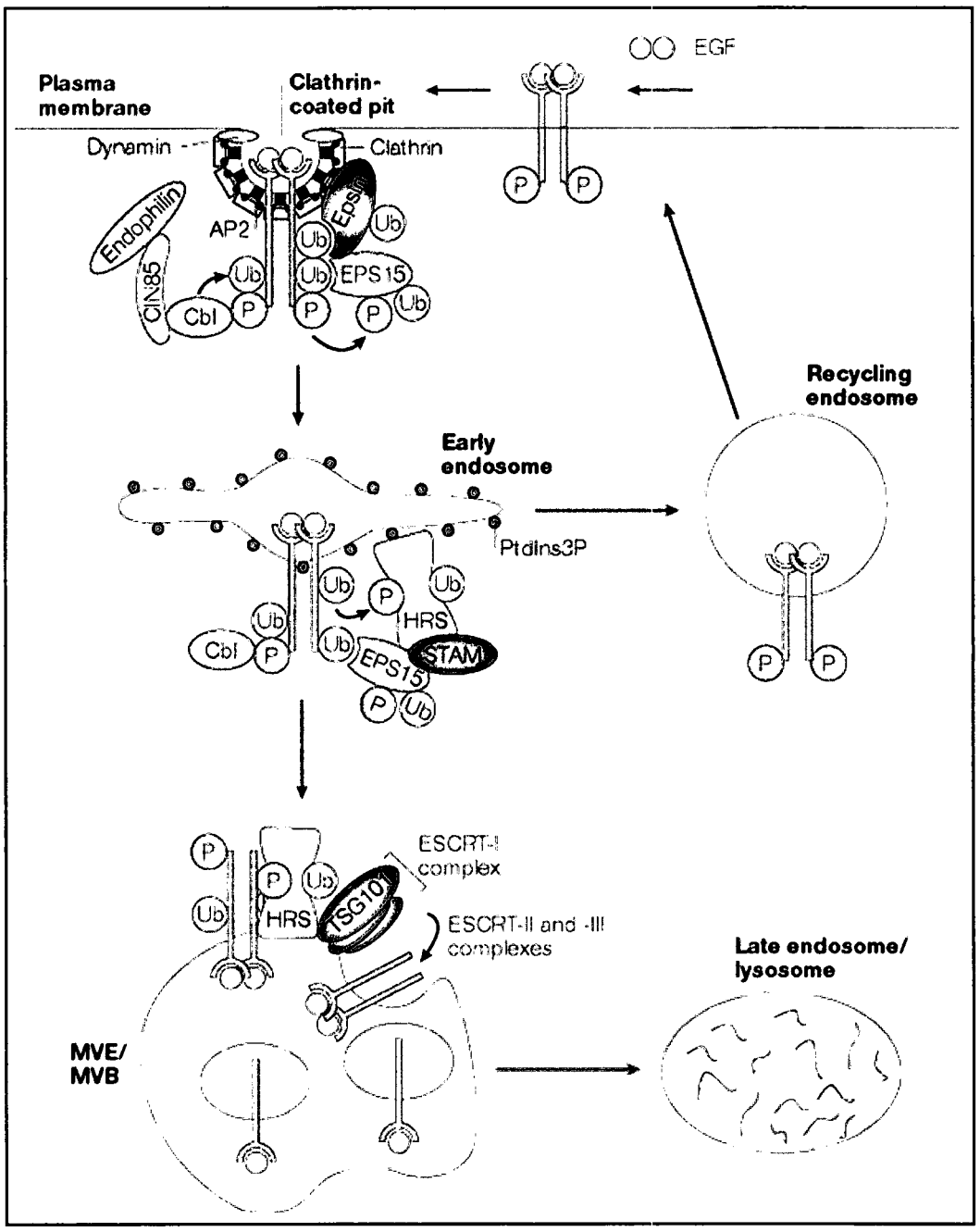
EGF
Plasma membrane
Clathrin-coated pit
Dynamin
Clathrin
Endophilin
AP2
Eps15
Ub
CIN85
Cbl
P
EPS15
Recycling endosome
Early endosome
PtdIns3P
HRS
STAM
ESCRT-I complex
TSG101
ESCRT-II and -III complexes
Late endosome/ lysosome
MVE/ MVB

FIGURE 1.2

As activated EGFR travels along the endosomal pathway, it continues to signal. That concept of signaling endosomes was first proposed by John Bergeron who observed that, shortly after EGF stimulation, the majority of activated EGFRs remains associated with signaling molecules such as Grb2, Shc and mSos in endosomes (Di Guglielmo et al., 1994). Since then, the concept has been refined and supported by other studies (for reviews see Sorkin and von Zastrow; von Zastrow and Sorkin, 2007). As examples, EGFR has been shown to interact with Grb2 in endosomes in living cells (Sorkin et al., 2000), a computational modeling of the EGF signal transduction via the MAPK cascade predicts that, even at low EGF concentrations, endocytosed EGF continues to signal (Schoeberl et al., 2002), and TGFβ may scaffold specific interactions in endosomes that would produce distinct signaling responses from those elicited at the plasma membrane (Di Guglielmo et al., 2003; Chen et al., 2007). From a physiological point of view, signaling from endosomes may provide temporal regulation as different receptors may have different fates upon endocytosis, and given receptors may be targeted differentially depending on which ligand is bound to it (Wiley, 2003). The EGFR family provides a nice example of this temporal regulation and will be discussed later. They may also provide spatial regulation by restricting the signaling events to specific compartments and/or specific subdomains within organelles (Miaczynska et al., 2004). Another function of signaling via endosomes might be the targeting of signaling complexes to their site of actions. For example, in neurons, NGF and its receptor, TrkA, must travel long distances from axon terminals to the cell body to reach their effectors, and endosomes may serve as transport intermediates. Indeed, activated TrkA was found in endosomes, together with activated effectors such as ERK and AKT, in both axons and cell bodies (Delcroix et al., 2003).

Mechanisms other than CME have been proposed for EGFR internalization and downregulation, especially in the context of EGFR stimulation with high concentrations of EGF ligand (Sigismund et al., 2005). Physiologically, EGF concentrations can vary from 1-2 ng/ml (in tissue fluid), to up to 100 ng/ml (in duct lumens of tissues such as the mammary gland) (Carpenter and Cohen, 1979; Hayashi and Sakamoto, 1988). In normal cells, EGFR is never in contact with high concentrations of EGF, but in cancer

cells the compartmentalization of EGFR is impaired and the receptor can access the high concentrations of ligand (Mullin, 2004). It was demonstrated that, upon stimulation with EGF at 20 ng/ml and 30 ng/ml concentrations, EGFR internalization occurs through caveolae (Sigismund et al., 2005; Orlichenko et al., 2006). It was also observed that concentrations of 30 ng/ml and 100 ng/ml EGF can induce formation of dorsal waves, which progress inward and sequester about 50% of the EGFR from the plasma membrane, but the mechanism underlying this process has yet to be elucidated (Orth et al., 2006; Roepstorff et al., 2008). However, other studies have shown that an EGF concentration of 100 ng/ml did not result in any EGFR internalization via caveolae, and that CHC depletion strongly inhibits EGF endocytosis at both 1 ng/ml and 60 ng/ml EGF, and therefore CME is still considered as the predominant mechanism for EGFR downregulation (Kazazic et al., 2006).

1.7.2 OTHER DOWNREGULATED RTKs

Most of the current knowledge about CME and signaling along the endocytic pathway, as well as receptor downregulation, is based on the behavior of EGFR upon EGF stimulation (for reviews see Dikic, 2003; von Zastrow and Sorkin, 2007). Within the RTK family other receptors have been proposed to be degraded and downregulated using similar sorting mechanisms as EGFR including PDGFR (Mori et al., 1992), ErbB3 and ErbB4 (Cao et al., 2007), stem cell factor receptor or c-kit (Masson et al. 2006), NGFR or TrkA (Geetha et al., 2005; Arévalo et al., 2006; Geetha and Wooden, 2008), HGFR or Met (Peschard et al., 2001), VEGFR (Duval et al., 2003), colony stimulating factor receptor 1 (CSFR-1) (Lee et al., 1999), insulin-like growth factor I receptor (IGF-IR) (Vecchione et al., 2003) and FGFR1-3 (Lax et al., 2002; Wong et al., 2002; Cho et al., 2004).

1.7.3 OTHER MEMBERS OF THE EGFR FAMILY

As stated previously, different receptors may have different fates upon endocytosis, and a given receptor may be targeted differentially depending on which ligand is bound to it (Wiley et al., 2003). Since endocytic events and signaling of EGFR are intimately linked, these differences in sorting will be reflected in the biological outcome of signaling. EGFR, also known as ErbB1, dimerizes upon ligand stimulation and this dimerization can occur with itself (homodimerization), or with the other members of the family known as ErbB2, ErbB3 and ErbB4 (heterodimerization) (Citri and Yarden, 2006). ErbB2, ErbB3 and ErbB4 have a similar structure as EGFR, with an extracellular domain, a short transmembrane alpha-helical region and a large intracellular cytoplasmic domain, and they can all homo- or heterodimerize (Citri and Yarden, 2006). However, only EGFR appears able to undergo ligand-induced endocytosis, and the internalization rate of the other ErbB receptors appears to be independent of ligand presence (Waterman et al., 1998; Worthylake et al., 1999). ErbB2 and ErbB3 present characteristic features that render them non-autonomous. Indeed, ErbB2 does not bind to any ligand (Klapper et al., 1999) and ErbB3 has no kinase activity (Guy et al., 1994). ErbB2 is the preferred dimerization partner for the other ErbB receptors (Garret et al., 2003; Graus-Porta, 1997), and it binds to a broader range of PTB-proteins than do the other ErbBs (Jones et al., 2006). Moreover, the heterodimers that contain ErbB2 bind to ligand with more affinity than the non-ErbB2 heterodimers, which results in a slower rate of ligand dissociation in the ErbB2-containing complexes (Jones et al., 2006). The behavior of ErbB2 regarding endocytosis is also different than EGFR. The endocytic rate of ErbB2 and ErbB2-containing heterodimers is slower than EGFR homodimers, and recycling to the plasma membrane is frequent (Baulida et al., 1996; Lenferink et al., 1998; Worthylake et al., 1999). ErbB2-containing heterodimers are therefore capable of escaping endocytic downregulation and recruiting more signaling molecules, which will consequently amplify and prolong the signaling (Pinkas-Kramarski et al., 1996). What is causing this difference in the endocytic behavior for ErbB2-containing heterodimers, and especially the ones formed by ErbB2 and EGFR, is still unknown and several studies have tried to

understand the underlying mechanisms. Among proposed models are reduced targeting to lysosomes (Worthylake et al., 1999), inhibited formation of CCPs after ligand stimulation (Haslekas et al., 2005), and lack of recruitment of the ubiquitin ligase Cbl to the activated heterodimer (Muthuswamy et al., 1999). ErbB3 and ErbB4 were first proposed to also have impaired endocytosis (Baulida et al., 1996) but there is now evidence that it may not be the case, as both receptors can be ubiquitinated and efficiently degraded in pathways involving both the proteasome and the lysosome (Qiu and Goldberg, 2002; Cao et al., 2007; Omerovic et al., 2007).

1.7.4 EGFR FATE UPON BINDING TO A DIFFERENT LIGAND

EGFR receptor can bind to EGF as well as to several other ligands, and its fate upon binding to most of these other ligands has not been extensively characterized, except for TGFα, which has received more attention with respect to EGFR trafficking. Upon EGF stimulation, EGFR is efficiently targeted for degradation and its signaling is eventually attenuated. In contrast, stimulation of EGFR with TGFα promotes its recycling to the plasma membrane (Decker, 1990). This difference in intracellular sorting is due to the different sensitivities of both ligands to acidic pH. The first relay compartment upon endocytosis of EGFR is the early endosome which has an acidic pH of ~6.0, and although EGF binding to EGFR is relatively stable at the acidic pH found in the different compartments of the sorting process, TGFα binding is sensitive to this acidic pH and therefore, dissociates from EGFR (Ebner and Derynck, 1991). This dissociation of TGFα from EGFR in the early/sorting endosome causes receptor dephosphorylation and deubiquitation, and therefore recycling back at the plasma membrane (Longva et al., 2002). TGFα potential to induce EGFR degradation is weaker than EGF, and this is probably why TGFα induces prolonged signaling (Waterman, 1998). Regarding the other ligands, only the effect of amphiregulin have been investigated and the study showed that stimulation of EGFR with amphiregulin does not induce its degradation, even in a context where EGFR was highly ubiquitinated due the overexpression of Cbl, thus suggesting that ubiquitination may not be sufficient

to target EGFR for lysosomal degradation (Stern et al., 2008).

1.7.5 EGFR FAMILY IN CANCER

ErbB receptors and the signaling cascades they trigger are important for many cellular processes and dysregulation in these pathways, or in their associated cellular events, can have dramatic effects on homeostasis. ErbB receptors are involved in pathogenesis of cancer and are attractive targets in the development of anti-cancer therapies (Hynes and Lane, 2005). Several mechanisms can lead to the aberrant signaling seen in cancer cells, including increased ErbB receptor expression, mutations within the receptors, and escape of endocytic regulation by the receptors (Bache et al., 2004; Normanno, 2005; Citri and Yarden, 2006; Warren and Landgraf, 2006). EGFR overexpression has been reported, among others, in lung, pancreas, head and neck, brain gliomas, and breast tumors (Nicholson et al., 2001; Ford and Grandis, 2003). ErbB2 overexpression was observed in many kind of cancers as well, including lung, pancreas, endometrium, ovarian, and breast cancers, where it also correlates with poor prognosis for the patients, especially in the case of breast and ovarian cancers (Slamon et al., 1989; Ross et al., 2003). ErbB3 and ErbB4 overexpression have been reported in colorectal cancer (Lee et al., 2001) and in breast cancer (Kraus et al., 1989; Plowman et al., 1993). In cells overexpressing ErbB receptors, ligand-induced degradation is delayed because of the limited capacity of the CME machinery, which is causing, at least in part, the aberrant mitogenic signaling (Citra and Yarden, 2006). Several EGFR mutations have been identified in many type of tumors and the increased signaling they are causing can be due to a constitutive activation of the mutated receptor and/or a decrease in its downregulation rate, as it the case for EGFR that have mutations affecting the binding with the ubiquitin ligase c-Cbl (Frederick et al., 2000; Peschard and Park, 2003; Zandi et al., 2007). Since impaired downregulation is an important feature in cancer biogenesis, stimulating the endocytosis and lysosomal degradation of ErbB receptors presents an attractive therapeutic avenue in treatment tumors. Indeed, some approaches are promising. One of the approaches is based on the use of antibody-mediated

crosslinking, and two monoclonal antibodies have been used either alone or in combination to promote endocytic downregulation of EGFR and/or ErbB2 receptors (Roepstorff et al., 2008). One approach that has been explored is the use of inhibitors against the chaperone Hsp90, since it has been shown that inhibition of Hsp90 leads to ubiquitination and subsequent degradation of ErbB2 (Xu et al., 2002; Zhou et al., 2003). However, due to the differences in the expression of ErbB receptors in the different types of cancers, it is likely that a successful approach for a given type of tumor will fail in another type of neoplastic cells and, therefore, more specific therapeutic approaches will have to be developed.

1.8 PROJECT RATIONALE AND RESEARCH OBJECTIVES

Intracellular trafficking is a complex process that implicates a vast array of proteins that ensure transport, proper targeting, adequate signaling and efficient downregulation of the cargoes that are traveling inside the cell. The key to a better understanding of the trafficking process lies in the characterization of the proteins that are regulating this cellular function. Many efforts have been made over the last decades to study the different molecules implicated in intracellular trafficking and also to discover and characterize novel proteins. The general objective of my doctoral project was to provide new information on the understanding of the regulatory mechanisms that govern the endocytic trafficking. This was achieved by 1) the study the CCVs and the differences in their composition between tissues that have different trafficking needs and 2) the study of a novel protein implicated in intracellular trafficking.

The specific research objectives described in this thesis were:

I. Having previously developed a spectral/peptide accounting approach that was applied in characterizing the proteome of brain CCVs (Blondeau et al., 2004), we decided to characterize the proteome of liver CCVs and to quantify abundant CCV

components using this new label-free quantitative approach. We hypothesized that different tissues would have different trafficking needs that will be reflected in the composition and properties of their CCVs. Therefore, upon identification and quantification of the abundant components of liver CCVs, we sought to compare these data with those obtained from their brain counterparts to examine for indications of different functioning of the same organelle in the different tissues.

II. Since CCVs are key players in the trafficking process, we also performed a proteomic study of liver CCVs in order to discover new proteins that could be implicated in intracellular trafficking and were successful in identifying new, uncharacterized, proteins. We hypothesized that the newly identified molecules would likely function in trafficking events. From the list of novel proteins provided by our subcellular proteomic approach, we chose the mammalian homolog of the protein RME-8, and characterized its biochemical properties and its function(s) in order to confirm our hypothesis.

III. Having characterized the biochemical properties of RME-8 and demonstrated that RME-8 functions in intracellular trafficking within the endosomal compartments, we sought to examine an intriguing observation we made during the RME-8 characterization process and to investigate the causes of a decrease in EGFR expression levels that occurs upon RME-8 depletion from cells. Finding the mechanisms underlying this decrease was crucial since it would indicate that RME-8 plays a central role in sorting decisions along the trafficking pathway.

PREFACE TO CHAPTER 2

CME is the major entry pathway for nutrients, signalling receptors and viruses. The clathrin budding machinery is complex and is regulated by various cofactors. New players implicated in clathrin-mediated vesicle formation process are still being discovered. Protein identification through MS is a powerful approach that has been used to identify protein components of cellular compartments and protein complexes. The approach involves purification/enrichment of the organelle to be studied followed by identification by MS of its protein contents. Since the complexity of the protein mixture is simpler than would be seen in a crude cell or tissue extract, the chance of detecting low abundance proteins is increased. Moreover, it allows the assignment of protein to particular organelles in the cell. Several groups have used subcellular proteomics to determine the composition of different organelles and protein complexes, including phagosomes (Garin et al., 2001), the mitochondria (Lopez et al., 2000; Taylor et al., 2003), the Golgi apparatus (Bell et al., 2001; Wu et al., 2000; Gilchrist et al., 2006), the nuclear pore (Rout et al., 2000; Cronshaw et al., 2002), the spliceosome (Zhou et al., 2002), and many others, including CCVs (Wasiak et al., 2002; Blondeau et al., 2004). Not only did the proteomic study of brain CCVs lead to the identification of new components of the clathrin machinery, it also has introduced peptide accounting as an efficient quantitative way to determine molar ratios of abundant CCV components (Blondeau et al., 2004).

In this chapter, highly purified CCVs from rat liver were isolated using differential centrifugation (Pilch et al., 1983) and the relative expression levels of abundant protein components were compared to those from brain CCVs using the previously developed peptide accounting approach (Blondeau et al., 2004). This comparative study provided us with new insights regarding CCV formation and allowed the identification of new CCV-associated proteins.

CHAPTER 2

NON-STOICHIOMETRIC RELATIONSHIP BETWEEN CLATHRIN HEAVY AND LIGHT CHAINS REVEALED BY QUANTITATIVE COMPARATIVE PROTEOMICS OF CLATHRIN-COATED VESICLES FROM BRAIN AND LIVER

Martine Girard, Patrick D. Allaire, Peter S. McPherson and Francois Blondeau

From the Department of Neurology and Neurosurgery, Montreal Neurological Institute, McGill University, Montreal, QC H3A 2B4, Canada

Reproduced from *Molecular and Cellular Proteomics* 4, 1145-1154 (2005) by copyright permission of the American Society for Biochemistry and Molecular Biology

SUMMARY

We used tandem mass spectrometry with peptide counts to identify and to determine the relative levels of expression of abundant protein components of highly enriched clathrin-coated vesicles (CCVs) from rat liver. The stoichiometry of stable protein complexes including clathrin heavy chain and clathrin light chain dimers and adaptor protein (AP) heterotetramers was assessed. We detected a deficit of clathrin light chain compared to clathrin heavy chain in non-brain tissues, suggesting a level of regulation of clathrin cage formation specific to brain. The high ratio of AP-1 to AP-2 in liver CCVs is reversed compared to brain where there is more AP-2 than AP-1. Despite this, general endocytic cargo proteins were readily detected in liver but not in brain CCVs, consistent with the previous demonstration that a major function for brain CCVs is recycling synaptic vesicles. Finally we identified 21 CCV-associated proteins in liver not yet characterized in mammals. Our results further validate the peptide accounting approach, reveal new information on the properties of CCVs, and allow for the use of quantitative proteomics to compare abundant components of organelles under different experimental and pathological conditions.

INTRODUCTION

Vesicle budding and trafficking via clathrin-coated pits (CCPs) and vesicles (CCVs) provides a major route by which proteins are transported out of the trans-Golgi network (TGN) and by which receptors, transporters, and nutrients are endocytosed at the plasma membrane (1-3). Many clathrin-dependent trafficking events mediate cargo transport that is needed in all cell types. These "housekeeping" forms of clathrin trafficking include the turnover of plasma membrane proteins and lipids, endocytic uptake of nutrients such as iron saturated transferrin and low-density lipoproteins, and endocytosis of a diverse range of activated growth factor receptors (1-3). Moreover, all cells have housekeeping trafficking at the TGN. An important example is the delivery of mannose-6-phosphate tagged lysosomal hydrolases from the TGN to endosomes/lysosomes via the mannose-6-phosphate receptor (MPR) (4).

In addition to these housekeeping activities of CCVs, some tissues have specialized trafficking needs. For example, in secretory cells, clathrin coats are involved in the formation of secretory granules at the TGN (5), and polarized cells utilize CCVs for the trafficking of certain receptors from the TGN to the basolateral membrane, necessary for the maintenance of polarity (2). At the plasma membrane, intestinal epithelial cells in rat or placental cells in humans use CCVs for the uptake of maternal immunoglobulins, a necessary aspect of maternal derived immunity (6). A striking example of specialized CCV function is seen in neurons, which communicate by releasing neurotransmitters through fusion of synaptic vesicles with the plasma membrane following transient increases in Ca^{2+} concentration (7). These vesicles are then retrieved through CCVs (8-10). Thus, neurons need CCVs not only for housekeeping forms of clathrin-mediated endocytosis but also to retrieve synaptic vesicle membranes. It has been unclear whether or not the mechanisms mediating these two related but distinct events taking place at the plasma membrane could be distinguished. Moreover the relative amount of brain CCVs specialized for synaptic function has never been assessed.

The presence of clathrin adaptor proteins (APs) can provide one level of discrimination of vesicle type as CCVs arising from the TGN contain AP-1 and CCVs derived from the plasma membrane contain AP-2. AP-1 and AP-2 are heterotetramers composed of four subunits each, namely γ–, β_1-, μ_1- and σ_1-adaptin for AP-1 and α-, β_2-, μ_2- and σ_2-adaptin for AP-2 (11). Two genes code for α-adaptin giving rise to αA and αC variants, with an alternative brain-specific splice form for αA (12). AP-1 and AP-2 provide a link between membranes and clathrin, the major component of CCVs (13). In addition, AP-2 stimulates clathrin assembly, whereas this assembly activity is significantly reduced for AP-1 (14). The reduced clathrin assembly activity of AP-1 at the TGN may be taken up by other proteins such as enthoprotin (15). Clathrin itself is composed of heterodimers of clathrin-heavy chain (CHC) and one of two clathrin-light chains (CLCs), CLCa and CLCb. CHC/CLC dimers form a structure referred to as a triskelia that has been shown in CCVs derived from brain to be composed of three CHCs and three CLCs (16,17). The 1:1 stoichiometry of CHC to CLC in brain CCVs has been confirmed by quantitative proteomics (18). This notion regarding the structure of clathrin triskelia has been extended to all tissues without further testing and has gradually become dogmatic.

To better understand the structure and function of CCVs, we have taken advantage of an approach that we recently developed to determine the relative levels of proteins within complex mixtures using tandem mass spectrometry (MS) (18). The approach works on the principle that the more abundant a protein is, the more peptides it will generate upon trypsin digest. These peptides will be sampled more often in the mass spectrometer, thus giving more spectra. Of course this will depend on the length of the protein as longer proteins will generate more peptides and also on the amino acid composition of the protein as certain peptides will be more readily resolved and detected than others. Regardless, differences in peptide numbers between proteins within a sample should provide a reflection of their relative ratios. Indeed we have been able to demonstrate the molar ratios of abundant components of CCVs from rat brain (18). The approach was independently demonstrated by Liu et al. (19) who spiked complex protein mixtures with known concentrations of test proteins. They determined that changes in

the number of MS/MS spectra identified for a given protein correlated directly to changes in its concentration over several orders of magnitude (19). In this study, we performed a proteomic analysis of highly purified CCVs from rat liver. Application of the peptide accounting approach, when compared with similar analysis on brain CCVs, allowed us to reveal new information regarding the machinery for CCV formation.

EXPERIMENTAL PROCEDURES

Antibodies - Monoclonal antibodies for CHC, AP-1 (γ-adaptin) and AP-2 (α-adaptin) were from BD Biosciences. Monoclonal antibody CON.1, which recognizes CLCa and CLCb, was from Santa Cruz Biotechnology. Monoclonal antibody X16 against CLCa (20) was a generous gift of Dr. Frances Brodsky.

Preparation and analysis of liver CCVs - Liver CCVs were isolated using previously described procedures (21,22) from adult rats that had been starved overnight. Suspensions of liver CCVs were deposited on 0.22 μm nitrocellulose filters to ensure random sampling (23) and were then processed for electron microscopy (EM) using an osmium tetroxide and tannic acid double fixation procedure (24). The purity of liver CCVs was assessed by counting the number of coated vesicles and contaminants in pictures taken from randomly selected fields from six independent preparations.

Liver CCV proteins were separated by SDS-PAGE and each lane was cut into 66 slices (Supplemental Fig. 1). Each slice was individually processed for tandem MS as previously described (18). Spectra were analyzed by MASCOT software to identify tryptic peptide sequences matched to the National Center for Biotechnology Information (NCBI) non-redundant protein database with a confidence level of 95% or greater (25). Specific and shared peptides with an equal or greater score than the identity score were kept and recorded for each band. Peptides from the entire lane were then grouped based on their GI number and thus defined as specific peptides for their cognate protein. To add another level of confidence, only proteins found in two out of three preparations and with five or more peptides were retained (26).

Other subcellular fractionation procedures - CCVs were isolated from adult rat brains as described previously (15,22). For specific experiments, CCVs were isolated from the livers of starved adult rats using the same protocol. For analysis on velocity gradients, ~1 mg of liver or brain CCVs isolated using this protocol was layered on linear 20-50% sucrose gradients prepared in buffer A (100 mM MES, pH 6.5, 1 mM

EGTA, 0.5 mM $MgCl_2$) and centrifuged in a Sorvall AH629 rotor at 145,000 x g for 1.5 h. The gradients were fractionated from the bottom, and proteins from equal volume aliquots of each fraction were analyzed by SDS-PAGE and Western blot. To prepare P2 microsomes, various tissues and cell lines were homogenized in buffer A as described (22). The samples were centrifuged at 17,000 x g for 20 min, and the supernatant was further spun at 56,000 x g for 1 h. Variable amounts of protein from the resulting microsomal (P2) fractions from each tissue were analyzed by SDS-PAGE and Western blot in order to generate an equivalent signal for the CHC. The supernatant (cytosolic fraction, S2) was also analyzed by Western blot. In other cases, microsomal fractions were prepared from 1 g each of two different tissues mixed together prior to homogenization or from 2 g of a single tissue. For these samples, gels were loaded with 100 μg of microsomes prepared from a single tissue and 200 μg of mixed tissues in order to account for the dilution of the tissues when mixed together.

RESULTS

Isolation of CCVs - CCVs were isolated from the livers of starved, adult rats using a well establish protocol (21, 22). Enrichment for protein bands corresponding to the molecular masses of CHC, CLCs and the α-, β-, γ- and μ-adaptin subunits of the AP-1 and AP-2 complexes was observed in the consecutive fractions of the CCV preparation (Fig. 2.1A). The enrichment of CHC, CLCs and γ-adaptin was demonstrated by Western blot (Fig. 2.1B). Transmission EM on six independent preparations using filtration methods to ensure a random sampling of the material (22, 23) revealed the presence of CCVs recognizable based on their basket-like shape (Fig. 2.1C). Uncoated and partially coated vesicles, heterogeneous in shape and size were also seen. Quantitation of the number of CCVs compared to various contaminants in 95 randomly selected fields from six independent preparations demonstrated that the CCVs were 89.3% pure (see Fig. 2.1C for a typical view of a randomly sampled EM field).

Protein identification by tandem MS - The proteins from three independent CCV preparations were separated on 5 -16% gradient SDS-PAGE gels and cut into 66 even, horizontal slices (Supplemental Fig. 2.S1). Each slice was processed for trypsin in-gel digest followed by LC Q-ToF MS/MS. To minimize the number of false positives, only proteins in which MS/MS spectra (identified with a 95% or greater confidence, see "Experimental Procedures") were found in at least two of the three replicates with at least five peptides in total were retained. All identified proteins were searched against each other by BLAST to ensure that all redundant identifications were collapsed into a single entry. Because of the high degree of homology between different tubulin isoforms, all tubulins were placed into one of two groups, tubulin α and β. With these criteria, we reproducibly identified 346 proteins in the liver CCV preparations including 21 novel proteins (Table 2.1 and supplemental table 2.S1). As expected, all known CCV coat proteins were identified with multiple peptides (supplemental table 2.S1). Interestingly the total number of peptides for CHC and CLCs and the sum of the total number of peptides for the subunits of AP-1 and AP-2 from liver (Fig. 2.1D, right) showed a distinct pattern from that seen in brain (Fig. 2.1D, left). Specifically for a

comparable portion of CHC, the level of CLCs was reduced in liver compared with brain (Fig. 2.1D). Also the ratio of AP-1 to AP-2 was distinct in the two tissues with a high AP-1 to AP-2 ratio in liver and a much lower ratio in brain (Fig. 2.1D).

Ratio of CHC to CLC - When adjusted for protein size, peptide counts provide a very good measure of the relative abundance of proteins in complex mixtures (18). When applied to CHC and the total amount of both CLCa and CLCb, the peptide:mass ratio revealed that there are fewer CLCs than CHC in liver CCVs (3.13 peptides/kDa for CHC and 0.65 peptides/kDa for CLCs; Fig. 2.2A). This is surprising because it is generally thought that CHC and CLCs form as stable heterodimers leading to a 1:1 ratio in all tissues, and peptide accounting on brain CCVs did indeed reveal a 1:1 molar ratio for the proteins (Fig. 2.2A) (18). Consistent with peptide counts, Western blot analysis with a pan-CLC antibody showed that for a comparable CHC signal there is less CLCs in CCVs from liver than CCVs from brain (Fig. 2.2B). CLCs from brain possess additional exons making them migrate more slowly on SDS-PAGE gels (27, 28). However, the CLC antibody recognizes an epitope that is conserved between the different splice forms of both CLCa and CLCb that are found in different tissues. Moreover because we apportioned the number of peptides to the size of the protein, differences in size would not affect the comparison between CHC and CLCs by peptide counts.

The protocol used to isolate liver CCVs for MS analysis, based on that of Pilch et al. (21), was different from that used for isolation of CCVs from brain, which was based on the protocol of Maycox et al. (29). This was due to the fact that the later protocol yielded CCVs that were ~50% pure when applied to liver tissue (data not shown). However, the deficit in the ratio of CLCs to CHC determined by Western blot in liver CCVs compared with brain CCVs was comparable when the CCVs were prepared in parallel using the Maycox et al. protocol (29) for each tissue (Fig. 3 and data not shown). Thus, the change in the ratio of CHC to CLCs was not due to different isolation procedures.

We next examined the relative ratio of CHC to CLCs in microsomal

preparations. This allowed us to compare multiple tissues and to minimize sample handling times to reduce any potential influence of tissue-specific proteolysis of CLCs. For a comparable signal of CHC, normalized to that found in the brain, each tissue examined exhibited a deficit of CLCs compared with brain (Fig. 2.2C). Moreover for a comparable signal of CHC, CLCs were variably less abundant in five separate cell lines with the ratio in COS-7 cells closest to that seen in the brain (Fig. 2.2D). A deficit in CLCs relative to CHC was also seen in crude lysates prepared from the cell lines compared with crude brain homogenate (Supplemental Fig. 2.S2). To further rule out a potential influence of proteolysis, we performed Western blots with monoclonal antibody X16, which is specific to CLCa but is strong on Western blot and is thus capable of detecting CLCa fragments. Even on long exposures, no lower molecular weight fragments were seen in microsomes prepared from multiple tissues with the exception of those from kidney, which demonstrated extensive proteolysis (Supplemental Fig. 2.S3). Interestingly proteolysis of CLCa was also seen in liver and brain when those tissues were mixed with kidney tissue prior to preparation of microsomes but was not observed upon mixing liver and brain with any other tissues (Supplemental Fig. 2.S3). Thus, the seeming lack of CLCs in kidney microsomes (Fig. 2.2C) appears to result from proteolysis, although proteolysis appears unlikely to account for the reduction of CLCs seen in other non-brain tissues. Our results support the notion that CLCs and CHC are not obligate heterodimers in liver and other non-brain tissues.

It is possible that the deficit in CLCs relative to CHC in liver CCVs occurs specifically on a single population of CCVs, that is, AP-1-positive CCVs from TGN/endosomes or AP-2- positive CCVs from the plasma membrane. Alternatively the deficit may be seen on both CCV populations. To examine this issue, we isolated liver and brain CCVs and subjected them to sedimentation on linear sucrose velocity gradients. In liver, AP-2 (α-adaptin)-containing CCVs peak one fraction closer to the bottom of the gradient than AP-1 (γ-adaptin)-containing CCVs, suggesting that, in this tissue, AP-2-positive CCVs are slightly larger (Fig. 2.3). CHC and CLCs appear to co-distribute throughout the gradient, suggesting that the ratio of the two proteins is

equivalent at both the AP-1 and AP-2 vesicle peaks (Fig. 2.3). Thus, there does not appear to be a selective enrichment of CHC relative to CLCs on a specific population of CCVs. Notably the clathrin proteins peak with the AP-1-positive CCVs, which represent the major population of CCVs in liver (see below). In brain, AP-1-positive CCVs migrate deeper into the gradients than AP-2-positive CCVs (Fig. 2.3, note that the AP-2 blot was deliberately underexposed to emphasize the distribution of the protein on the gradient). CHC and CLCs co-migrate on the gradient as expected given that the ratio of the proteins is 1:1 in brain (Fig. 2.3).

Ratio of AP-1 to AP-2 - AP-2 is a marker of plasma membrane-derived CCVs and in brain was found in a 5:1 molar excess to the TGN/endosome adaptor AP-1 (18). In contrast, by averaging the subunit counts for each adaptor complex as was done for brain (18), we demonstrated an overall 2:1 excess of AP-1 to AP-2 in liver CCVs (Fig. 2.4A). This inversion of the AP-1 to AP-2 ratio was due to both an increase in the relative amount of AP-1 and a decrease in the relative amount of AP-2 in liver compared with brain (Fig. 2.4A). Interestingly the decrease in AP-2 in liver appears to be accounted for primarily by a decrease in the αA isoform, whereas the αC isoform is present in liver and brain at comparable levels (Fig. 2.4B). The ratio of total AP complexes to total CHC from liver is the same as in brain; namely CCVs from both tissues exhibit the same deficit of APs to CHC (Fig. 2.4A).

The observations on the ratios of the AP complexes between CCVs from brain and liver determined by peptide counts were supported by Western blot. Indeed the γ-adaptin signal is stronger for CCVs from liver than for CCVs from brain, whereas an α-adaptin antibody specific for the αA isoform reveals the opposite pattern (Fig. 2.4A, inset). αA from brain and muscle contains an additional 21-amino acid insert that is responsible for the apparent size change of αA between brain and liver (12), although the epitope for the antibody is conserved between the splice variants. A stronger signal for AP-1 γ-adaptin in liver than brain relative to a comparable amount of CHC is also seen when CCVs were generated from the two tissues using the same protocol (Fig. 2.3). The seeming decrease in AP-2 α-adaptin in brain relative to liver CCVs in Fig. 3 was

due to the low exposure of the blot, and in fact when the α-adaptin blots from the two tissue samples were exposed for the same time, the AP-2 signal was stronger in the brain than the liver samples (data not shown). The bias toward AP-1-positive CCVs in liver is also in agreement with the detection of a larger amount of TGN cargo such as the cation-independent and cation-dependent MPRs in liver than in brain CCVs (Fig. 2.4C).

Determination of the percentage of CCVs in brain specialized for synaptic vesicle recycling - The relative ratio of CCVs between the TGN/endosome and the plasma membrane that is used for generalized housekeeping forms of membrane trafficking should be similar in most tissues. We thus calculated the number of AP-2-positive CCVs in brain that would come from non-specialized forms of CCV traffic based on the ratio between AP-1 and AP-2 found in liver. In liver, AP-1- and AP-2-positive CCVs represent 65.4 and 34.6%, respectively, of the total number of CCVs (Fig. 2.5). This is equivalent to an AP-1:AP-2 ratio of 1.9:1. In brain, AP-1- positive CCVs represent 16.9% of the total leaving 83.1% accounted for by AP-2-positive CCVs. If the 1.9:1 ratio of AP-1:AP-2 is applied to brain, one would expect that 8.9% (16.9 divided by 1.9) of AP-2 positive CCVs in brain are involved in general endocytic housekeeping functions common to all tissues. The remaining 74.2% (83.1 minus 8.9) is thus anticipated to have a specialized function (Fig. 2.5). Comparing the CCVs that are derived from the plasma membrane (8.9% housekeeping and 74.2% specialized), we can calculate that 89% of the AP-2-positive CCVs are specialized for neuron-specific functions, most likely synaptic vesicle recycling.

Proteins found and novel proteins - In total, 346 proteins were reproducibly identified in the liver CCV preparations that were placed into 18 groups (supplemental table 2.S1). Abundant Golgi proteins such as GM130, GRASP (Golgi peripheral membrane protein p65), or giantin, which are all found with high abundance in the Golgi proteome (26), were not detected in the CCV preparations. We did not detect abundant endoplasmic reticulum proteins such as calreticulin or ERp99 that Wu et al. (26) found in their Golgi proteome. Potential contaminants of the CCV preparations include abundant liver soluble enzymes and ribosomal proteins (supplemental table 2.S1).

Among the proteins identified, 21 are novel (Table 2.1 and supplemental table 2.S1). We kept enthoprotin, NECAP 1, and FENS-1 (bold in Table 2.1) in this group as they were referred to as novel when they were originally identified in the brain CCV proteome (18). Interestingly, two of the novel proteins, RME-8 and Vac14, have been shown to be involved in endocytosis and vesicle trafficking in non-mammalian species (30-32). Two additional proteins can be associated with membrane trafficking by homology (70% identity to ADP-ribosylation factor (ARF)-like- 6-interacting protein and EH domain-containing protein). None of the novel proteins were detected in brain CCVs with the exception of NECAP 1, enthoprotin, and FENS-1. This may reflect their involvement in more general, housekeeping clathrin-mediated trafficking at the plasma membrane or TGN.

DISCUSSION

The sequencing of animal genomes and the large-scale sequencing of expressed genes coupled with advances in protein and peptide separation technologies and innovations in MS have led to an explosion in the use of proteomic approaches in biology. However, due to the complexity and dynamic range of protein expression, it is currently difficult to perform a satisfactory proteomic analysis of whole cells or tissues (33). Isolated organelles present an attractive target for proteomics as their protein complexity is reduced, and lower abundance proteins that are specific to the compartment are enriched relative to whole cell lysates (34-36). Numerous organelles and suborganellar compartments have now been analyzed by subcellular proteomics, and in almost all cases, novel proteins have been identified, and the global analysis of the organelle has provided insights into organelle function that may not have been possible from the analysis of a smaller subset of the proteins (34-36).

An important next step in subcellular proteomics is the development of approaches that allow for the quantitative comparison of organelle proteomes under different experimental paradigms. Several approaches have been tested so far for their relative quantitative nature. Among them are stable isotope labeling by amino acid in cell culture (SILAC) (37), DIGE (38), ICAT (39), absolute quantification (AQUA) (40), protein correlation profiling (41), protein abundance index (42), and peptide/spectral counts (18,19). Although no extended comparative studies of all of these approaches have been performed, one can predict that each will have advantages and disadvantages and that their applicability will be influenced by the sample processing and MS apparatus available. The peptide accounting approach described here is extremely versatile and is applicable to the analysis of data generated from a wide variety of MS/MS configurations. Moreover the peptide accounting approach first analyzes the relative amounts of proteins within a sample and then compares the ratios between samples. This helps to alleviate changes due to differences in quantity and contamination of samples prepared at different time points and under different experimental conditions. In this study we applied the peptide counting approach in comparing the relative ratios

of CHC and CLCs as well as APs from liver and brain CCVs and have further verified the results by Western blot.

One of the conclusions of our study is that the APs are expressed at lower levels than clathrin in different tissues and at both the TGN and the plasma membrane. Thus, it is likely that at all sites of clathrin-mediated membrane budding there is sufficient CHC to interact simultaneously with AP-1, AP-2, and a variety of other clathrin-binding partners even when each of these proteins utilize the same binding sites on the terminal domain of the CHC (43-45). As such, there is no need for the sequential interaction of these proteins even when they interact with the CHC using the same motif. Thus, alternative cargo adaptors that bind to clathrin (43) could be found simultaneously in complexes with clathrin in a CCP that also utilizes classical APs. Another important finding of our study relates to the ratio of AP-1 and AP-2 in CCVs from brain and liver. The high ratio of AP-1 to AP-2 in liver CCVs is opposite to that found in brain, further emphasizing that the brain is specialized for endocytosis, likely due to the demand for synaptic vesicle recycling. We suggest that in brain, nine of 10 CCVs budding from the plasma membrane participate in the recycling of synaptic vesicles. Moreover from our calculations, we hypothesize that for a given number of CCVs the percentage that is involved in general housekeeping endocytosis in brain will be ~4-fold less than in liver (34.6% of total in liver, 8.9% of total in brain). Consistent with this idea, we were readily able to identify several endocytic cargo proteins in liver CCVs (supplemental table 2.S1) that despite the fact they are known to be present in brain were not detected in brain CCVs. Examples include transferrin and transferrin receptor (46), mannose receptor C type 1 (47), low density lipoprotein related-protein (48), asialoglycoprotein and asialoglycoprotein receptor (49), hyaluronan receptor (50), and ferritin (51). In contrast, in brain we identified many of the known components of synaptic vesicles (18) in agreement with 74% of brain CCVs functioning in synaptic vesicles recycling. Thus, our quantitative organelle proteomic approach allowed us to determine the relative abundance of functionally specialized classes of CCVs within tissues.

It is generally thought that CHC and CLCs are obligate heterodimers with a 1:1 stoichiometry, and this has been demonstrated in brain (16-18). However, one study that may contradict this notion is from Liu et al. (52) who determined that CLCs and the hub domain of CHC co-produced in bacteria do not form in a 1:1 ratio. Moreover loss of CLC in Dictyostelium has no effect on CHC steady state levels or triskelia formation (53), and knock-down of CLCs in non-neuronal mammalian cells does not affect clathrin-mediated endocytosis, further questioning an obligatory role for CLCs in CCV formation (54,55). As determined by peptide counts and confirmed by Western blots, we now demonstrate that there is a deficit of CLCs in CCVs from liver. Moreover this is likely to extend to all non-brain tissues and commonly used laboratory cell lines. The inability to detect fragments CLCa with the X16 antibody in microsome fractions shows that for all non-brain tissues and cell lines tested, with the exception of kidney, the deficit in CLCs relative to CHC can not be simply explained by proteolytic degradation. Moreover, the deficit in CLCs seen in crude cell lysates and the inability to detect the proteins in soluble fractions of any of the fractionation protocols utilized (data not shown) suggests that the deficit is likely due to the levels of CHC and CLCs stably expressed and is not due to a selective incorporation of CHC into CCVs. Previously, Steven et al. (56) demonstrated a 1:1 stoichiometry between CHC and CLCs in liver CCVs. This ratio was determined by densitometric scanning of bands that were thought to correspond to CHC and CLCs in Coomassie Blue-stained CCV preparations. We detected CLC peptides from gel slices 16-21 containing bands assumed to correspond to CLCs (Supplemental Fig. 2.S1), but we also detect peptides from other proteins identified in the proteomic analysis. In fact, CLCs represent ~12% of the peptides present in this region. Thus, it is not necessarily accurate to assign proteins to a specific band based on Coomassie Blue staining. However, proteomic analysis can provide a means to determine protein ratios within complex mixtures even in the face of heterogeneity within gel bands.

CLCs are clearly present and co-localized with CHC at CCPs at both the plasma membrane and the TGN (57,58), and they are likely to function at both sites even if they function in a substoichiometric manner. One function for CLCs is to inhibit clathrin

assembly (59), and assembly proteins are thus required to overcome this inhibition (60,61). A lower ratio of CLCs to CHC may be necessary to ensure that assembly proteins alone are able to stimulate clathrin assembly in non-brain tissues. Since the ratio of CHC to CLCs in brain is 1:1, this would suggest that CCV formation in brain requires an additional level of regulation of CLCs. We demonstrated that the majority of brain CCVs function in synaptic vesicle recycling, and thus the additional level of CLC regulation may in fact be specific to synaptic vesicle endocytosis. Ca^{2+} is known to alleviate the inhibitory effect of CLCs on clathrin assembly in vitro (2,62,63). However, the physiological significance of this phenomenon has remained unclear given that CLCs bind to Ca^{2+} with a K_d of 25-50 μM (64). During synaptic vesicle exocytosis, there are bursts of Ca^{2+} at the active zone that can reach 100 μM or greater (65,66). The bursts are local and transient, and Ca^{2+} concentrations decrease quickly around the active zone. Because the K_d for Ca^{2+} binding on CLCs is low, it would favor cage formation close to the active zone as proposed previously (67). The CCVs that begin to assemble close to the active zone will continue to mature as they move away from the active zone to finally pinch off at much lower Ca^{2+} concentrations (68). In this model, synaptic vesicle endocytosis requires assembly proteins working in conjunction with high Ca^{2+} concentrations. Consistent with this model, Sankaranarayanan and Ryan (69) have demonstrated that increases in intracellular Ca^{2+} concentration cause an acceleration of endocytosis of synaptic vesicles. In non-brain tissue where the Ca^{2+} concentration is low and yet the ratio of APs to CHC is similar, a decrease in the total amount of CLCs on triskelia could reduce the threshold for clathrin assembly.

Thus, through quantitative comparative proteomics, we are able to provide a model of the specialized role for CLCs in the regulation of synaptic vesicle endocytosis. Overall our study has revealed new insights into the composition of coats and specializations of CCVs for trafficking.

ACKNOWLEDGEMENTS

We are particularly grateful to Frances M. Brodsky for discussions and for the generous gift of the X16 antibody. We thank Dr. Amanda Parmar, Pascal Lejeune and Pierre-Emmanuel Foulon for help with ERACP, a multiple sequence comparison tool. We also thank all of the members of the laboratory, especially Valérie Legendre-Guillemin and Sébastien Thomas for discussions. This work was supported by Canadian Institutes of Health Research (CIHR) grant MOP-15396 to PSM. Operating grants from the Genome Quebec/Genome Canada project: Réseau Protéomique de Montréal, Montreal Proteomics Network (RPMPN) financially supported this work. M.G. is supported by studentships from the CIHR. PSM is a CIHR Investigator, a Killam Scholar, and a McGill University William Dawson Scholar.

REFERENCES

1. McPherson, P.S., Kay, B.K., and Hussain, N.K. (2001) Signaling on the endocytic pathway. Traffic **2,** 375-384
2. Brodsky, F.M., Chen, C.Y., Knuehl, C., Towler, M.C., and Wakeham, D.E. (2001) Biological basket weaving: formation and function of clathrin-coated vesicles. Annu Rev Cell Dev. Biol. **17,** 517-568
3. Conner, S.D., and Schmid, S.L. (2003) Regulated portals of entry into the cell. Nature **422,** 37-44
4. Le Borgne, R., and Hoflack, B. (1998) Protein transport from the secretory to the endocytic pathway in mammalian cells. Biochim. Biophys. Acta. **1404,** 195-209
5. Austin, C., Hinners, I., and Tooze, S.A. (2000) Direct and GTP-dependent interaction of ADP-ribosylation factor 1 with clathrin adaptor protein AP-1 on immature secretory granules. J. Biol. Chem. **275,** 21862-21869
6. Pearse, B.M., and Bretscher, M.S. (1981) Membrane recycling by coated vesicles. Annu. Rev. Biochem. **50,** 85-101
7. Sudhof, T.C. (2004) The synaptic vesicle cycle. Annu. Rev. Neurosci. **27,** 509-547
8. Murthy, V.N., and De Camilli, P. (2003) Cell biology of the presynaptic terminal. Annu. Rev. Neurosci. **26,** 701-728
9. Bauerfeind, R., David, C., Grabs, D., McPherson, P.S., Nemoto, Y., Slepnev, V.I., Takei, K., and De Camilli, P. (1998) Recycling of synaptic vesicles. Adv. Pharmacol. **42,** 253-257
10. Bauerfeind, R., David, C., Galli, T., McPherson, P.S., Takei, K., and De Camilli, P. (1995) Molecular mechanisms in synaptic vesicle endocytosis. Cold Spring Harb. Symp. Quant. Biol **60,** 397-404
11. Boehm, M., and Bonifacino, J.S. (2001) Adaptins: the final recount. Mol. Biol. Cell, **12,** 2907-2920
12. Ball, C.L., Hunt, S.P., and Robinson, M.S. (1995) Expression and localization of alpha-adaptin isoforms. J. Cell. Sci. **108,** 2865-2875
13. Ritter, B., and McPherson, P.S. (2004) Molecular mechanisms in clathrin-

mediated membrane budding. Topics in current genetics, vol 10, pp9-37. S. Keranen, J. Jantti (Eds): Regulatory Mechanisms of Intracellular Membrane Transport, Springer-Verlag Berlin. Heidelberg.

14. Lindner, R., and Ungewickell, E. (1992) Clathrin-associated proteins of bovine brain coated vesicles. An analysis of their number and assembly-promoting activity. J. Biol. Chem. **267,** 16567-16573

15. Wasiak, S., Legendre-Guillemin, V., Puertollano, R., Blondeau, F., Girard, M., de Heuvel, E., Boismenu, D., Bell, A.W., Bonifacino, J.S., and McPherson, P.S. (2002) Enthoprotin: a novel clathrin-associated protein identified through subcellular proteomics. J. Cell. Biol. **158,** 855-862

16. Ungewickell, E., and Branton, D. (1981) Assembly units of clathrin coats. Nature **289,** 420-422

17. Kirchhausen, T., and Harrison, S.C. (1981) Protein organization in clathrin trimers. Cell **23,** 755-761

18. Blondeau, F., Ritter, B., Allaire, P.D., Wasiak, S., Girard, M., Hussain, N.K., Angers, A., Legendre-Guillemin, V., Roy, L., Boismenu, D., Kearney, R.E., Bell, A.W., Bergeron, J.J.M., and McPherson, P.S. (2004) Tandem MS analysis of brain clathrin-coated vesicles reveals their critical involvement in synaptic vesicle recycling. Proc. Natl. Acad. Sci.
U S A **101,** 3833-3838

19. Liu, H., Sadygov, R.G., and Yates, J.R., 3rd (2004) A model for random sampling and estimation of relative protein abundance in shotgun proteomics. Anal. Chem. **76,** 4193-4201

20. Brodsky, F.M. (1985) Clathrin structure characterized with monoclonal antibodies. II. Identification of in vivo forms of clathrin. J. Cell Biol. **101,** 2055-2062

21. Pilch, P.F., Shia, M.A., Benson, R.J., and Fine, R.E. (1983) Coated vesicles participate in the receptor-mediated endocytosis of insulin. J. Cell Biol. **96,** 133-138

22. Girard, M., Allaire, P.D., Blondeau, F., and McPherson, P.S. (2004) Isolation of clathrin-coated vesicles by differential and density gradient centrifugation. In

Current Protocols in Cell Biology. Unit 3.13 Subcellular Fractionation and Isolation of Organelles. Juan Bonifacino, Jennifer Lippincott-Schwartz, Mary Dasso, Joe Harford and Ken Yamada (Eds): pp 3.13.1-3.13.20. John Wiley and sons, Inc.

23. Baudhuin, P., Evrard, P., and Berthet, J. (1967) Electron microscopic examination of subcellular fractions. I. The preparation of representative samples from suspensions of particles. J. Cell Biol. **32,** 181-191

24. Simionescu, N., and Simionescu, M. (1976) Galloylglucoses of low molecular weight as mordant in electron microscopy. II. The moiety and functional groups possibly involved in the mordanting effect. J. Cell Biol. **70,** 622-633

25. Perkins, D.N., Pappin, D.J., Creasy, D.M., and Cottrell, J.S. (1999) Probability-based protein identification by searching sequence databases using mass spectrometry data. Electrophoresis, **20,** 3551-3567

26. Wu, C.C., MacCoss, M.J., Mardones, G., Finnigan, C., Mogelsvang, S., Yates, J.R., 3rd, and Howell, K.E. (2004) Organellar proteomics reveals Golgi arginine dimethylation. Mol. Biol. Cell **15,** 2907-2919

27. Jackson, A.P., and Parham, P. (1988) Structure of human clathrin light chains. Conservation of light chain polymorphism in three mammalian species. J. Biol. Chem. **263,** 16688-16695

28. Wong, D.H., Ignatius, M.J., Parosky, G., Parham, P., Trojanowski, J.Q., and Brodsky, F.M. (1990) Neuron-specific expression of high-molecular-weight clathrin light chain. J. Neurosci. **10,** 3025-3031

29. Maycox, P.R., Link, E., Reetz, A., Morris, S.A., and Jahn, R. (1992) Clathrin-coated vesicles in nervous tissue are involved primarily in synaptic vesicle recycling. J. Cell. Biol. **118,** 1379-1388

30. Chang, H.C., Hull, M., and Mellman, I. (2004) The J-domain protein Rme-8 interacts with Hsc70 to control clathrin-dependent endocytosis in Drosophila. J. Cell Biol. **164,** 1055-1064

31. Zhang, Y., Grant, B., and Hirsh, D. (2001) RME-8, a conserved J-domain protein, is required for endocytosis in Caenorhabditis elegans. Mol. Biol. Cell **12,** 2011-2021

32. Dove, S.K., McEwen, R.K., Mayes, A., Hughes, D.C., Beggs, J.D., and Michell, R.H. (2002) Vac14 controls PtdIns(3,5)P(2) synthesis and Fab1-dependent protein trafficking to the multivesicular body. Curr. Biol. **12,** 885-893

33. Huber, L.A. (2003) Is proteomics heading in the wrong direction? Nat. Rev. Mol. Cell. Biol. **4,** 74-80

34. Taylor, S.W., Fahy, E., and Ghosh, S.S. (2003) Global organellar proteomics. Trends Biotechnol. **21,** 82-88

35. Brunet, S., Thibault, P., Gagnon, E., Kearney, P., Bergeron, J.J., and Desjardins, M. (2003) Organelle proteomics: looking at less to see more. Trends Cell Biol. **13,** 629-638

36. Ritter, B., Blondeau, F., Denisov, A.Y., Gehring, K., and McPherson, P.S. (2004) Molecular mechanisms in clathrin-mediated membrane budding revealed through subcellular proteomics. Biochem. Soc. Trans. **32,** 769-773

37. de Hoog, C.L., Foster, L.J., and Mann, M. (2004) RNA and RNA binding proteins participate in early stages of cell spreading through spreading initiation centers. Cell **117,** 649-662

38. Ornstein, D.K., and Petricoin, E.F., 3rd (2004) Proteomics to diagnose human tumors and provide prognostic information. Oncology **18,** 521-529

39. MacCoss, M.J., Wu, C.C., Liu, H., Sadygov, R., and Yates, J.R., 3rd (2003) A correlation algorithm for the automated quantitative analysis of shotgun proteomics data. Anal, Chem, **75,** 6912-6921

40. Gerber, S.A., Rush, J., Stemman, O., Kirschner, M.W., and Gygi, S.P. (2003) Absolute quantification of proteins and phosphoproteins from cell lysates by tandem MS. Proc. Natl. Acad. Sci. U S A. **100,** 6940-6945

41. Andersen, J.S., Wilkinson, C.J., Mayor, T., Mortensen, P., Nigg, E.A., and Mann, M. (2003) Proteomic characterization of the human centrosome by protein correlation profiling. Nature **426,** 570-574

42. Rappsilber, J., Ryder, U., Lamond, A.I., and Mann, M. (2002) Large-scale proteomic analysis of the human spliceosome. Genome Res. **12,** 1231-1245

43. Traub, L.M. (2003) Sorting it out: AP-2 and alternate clathrin adaptors in endocytic cargo selection. J. Cell Biol. **163,** 203-208

44. Ritter, B., Denisov, A.Y., Philie, J., Deprez, C., Tung, E.C., Gehring, K., and McPherson, P.S. (2004) Two WXXF-based motifs in NECAPs define the specificity of accessory protein binding to AP-1 and AP-2. Embo J. **23,** 3701-3710

45. Miele, A.E., Watson, P.J., Evans, P.R., Traub, L.M., and Owen, D.J. (2004) Two distinct interaction motifs in amphiphysin bind two independent sites on the clathrin terminal domain beta-propeller. Nat. Struct. Mol. Biol. **11,** 242-248

46. Pearse, B.M. (1982) Coated vesicles from human placenta carry ferritin, transferrin, and immunoglobulin G. Proc. Natl. Acad. Sci. U S A. **79,** 451-455

47. Harris, N., Super, M., Rits, M., Chang, G., and Ezekowitz, R.A. (1992) Characterization of the murine macrophage mannose receptor: demonstration that the downregulation of receptor expression mediated by interferon-gamma occurs at the level of transcription. Blood **80,** 2363-2373

48. Orr, A.W., Pedraza, C.E., Pallero, M.A., Elzie, C.A., Goicoechea, S., Strickland, D.K., and Murphy-Ullrich, J.E. (2003) Low density lipoprotein receptor-related protein is a calreticulin coreceptor that signals focal adhesion disassembly. J. Cell Biol. **161,** 1179-1189

49. Ciechanover, A., Schwartz, A.L., and Lodish, H.F. (1983) Sorting and recycling of cell surface receptors and endocytosed ligands: the asialoglycoprotein and transferrin receptors. J. Cell Biochem. **23,** 107-130

50. Weigel, J.A., and Weigel, P.H. (2003) Characterization of the recombinant rat 175-kDa hyaluronan receptor for endocytosis (HARE). J. Biol. Chem. **278,** 42802-42811

51. Hulet, S.W., Heyliger, S.O., Powers, S., and Connor, J.R. (2000) Oligodendrocyte progenitor cells internalize ferritin via clathrin-dependent receptor mediated endocytosis. J. Neurosci. Res. **61,** 52-60

52. Liu, S.H., Wong, M.L., Craik, C.S., and Brodsky, F.M. (1995) Regulation of clathrin assembly and trimerization defined using recombinant triskelion hubs. Cell **83,** 257-267

53. Wang, J., Virta, V.C., Riddelle-Spencer, K., and O'Halloran, T.J. (2003) Compromise of clathrin function and membrane association by clathrin light

chain deletion. Traffic **4,** 891-901

54. Huang, F., Khvorova, A., Marshall, W., and Sorkin, A. (2004) Analysis of clathrin-mediated endocytosis of epidermal growth factor receptor by RNA interference. J. Biol. Chem. **279,** 16657-16661

55. Yang, D., Buchholz, F., Huang, Z., Goga, A., Chen, C.Y., Brodsky, F.M., and Bishop, J.M. (2002) Short RNA duplexes produced by hydrolysis with Escherichia coli RNase III mediate effective RNA interference in mammalian cells. Proc. Natl. Acad. Sci. U S A. **99,** 9942-9947

56. Steven, A.C., Hainfeld, J.F., Wall, J.S., and Steer, C.J. (1983) Mass distributions of coated vesicles isolated from liver and brain: analysis by scanning transmission electron microscopy. J. Cell Biol. **97,** 1714-1723

57. Gaidarov, I., Santini, F., Warren, R.A., and Keen, J.H. (1999) Spatial control of coated-pit dynamics in living cells. Nat. Cell Biol. **1,** 1-7

58. Ehrlich, M., Boll, W., Van Oijen, A., Hariharan, R., Chandran, K., Nibert, M.L., and Kirchhausen, T. (2004) Endocytosis by random initiation and stabilization of clathrin-coated pits. Cell **118,** 591-605

59. Ungewickell, E., and Ungewickell, H. (1991) Bovine brain clathrin light chains impede heavy chain assembly in vitro. J. Biol. Chem. **266,** 12710-12714

60. Legendre-Guillemin, V., Metzler, M., Lemaire, J.F., Philie, J., Gan, L., Hayden, M.R., and McPherson, P.S. (2004) HIP1 (huntingtin interacting protein 1) regulates clathrin assembly through direct binding to the regulatory region of the clathrin light chain. J. Biol. Chem. **280,** 6101-6108

61. Chen, C.Y. and Brodsky, F.M. (2004) Huntingtin-interacting protein 1 (Hip1) and Hip1-related protein (Hip1R) bind the conserved sequences of clathrin light chains and thereby influence clathrin assembly in vitro and actin distribution in vivo. J. Biol. Chem. **280,** 6109-6117

62. Keen, J.H., Willingham, M.C., and Pastan, I.H. (1979) Clathrin-coated vesicles: isolation, dissociation and factor-dependent reassociation of clathrin baskets. Cell **16,** 303-312

63. Brodsky, F.M., Hill, B.L., Acton, S.L., Nathke, I., Wong, D.H., Ponnambalam, S., and Parham, P. (1991) Clathrin light chains: arrays of protein motifs that regulate

coated-vesicle dynamics. Trends Biochem. Sci. **16,** 208-213

64. Mooibroek, M.J., Michiel, D.F., and Wang, J.H. (1987) Clathrin light chains are calcium-binding proteins. J. Biol. Chem. **262,** 25-28
65. Matthews, G. (1996) Neurotransmitter release. Annu. Rev. Neurosci. **19,** 219-233
66. Augustine, G.J., Santamaria, F., and Tanaka, K. (2003) Local calcium signaling in neurons. Neuron **40,** 331-346
67. Heuser, J.E., and Reese, T.S. (1973) Evidence for recycling of synaptic vesicle membrane during transmitter release at the frog neuromuscular junction. J. Cell Biol. **57,** 315-344
68. Cousin, M.A., and Robinson, P.J. (2000) Ca(2+) influx inhibits dynamin and arrests synaptic vesicle endocytosis at the active zone. J. Neurosci. **20,** 949-957
69. Sankaranarayanan, S., and Ryan, T.A. (2001) Calcium accelerates endocytosis of vSNAREs at hippocampal synapses. Nat. Neurosci. **4,** 129-136

FIGURE LEGENDS

Figure 2.1: Isolation and characterization of liver CCVs. A, Coomassie blue staining of proteins separated by SDS-PAGE from each step of the enrichment protocol for CCVs. Aliquots of 40 μg of protein were loaded on each lane. H, homogenate; P, pellet; S, supernatant. The predicted migratory positions of CHC, CLCs, and α-, β-, γ- and μ-adaptins are indicated. B, protein fractions from each step of the enrichment protocol for CCVs were processed for Western blot with CHC, CLC, and γ-adaptin (AP-1) antibodies. C, CCV fractions were evaluated by random sampling EM. A representative field is shown and reveals examples of coated, uncoated and partially coated CCVs. Bar, 200 nm. D, pie chart representation of the proteomics results showing total number of peptides from all three preparations of liver CCVs and previously analyzed brain CCVs (18) for CHC, CLCs, and all of the subunits of the AP-1 and AP-2 complexes.

Figure 2.2: Ratio of CHC to CLCs. A, the total number of peptides found in each preparation of liver and brain CCVs for CHC, CLCa and CLCb was divided by the calculated mass of each protein (in kilodaltons) giving a peptide:mass ratio. The bars and error bars represent the mean and S.E. of the mean between the three preparations for each tissue. B, aliquots of liver and brain CCVs (20 μg for each) were processed for Western blot with antibodies against CHC and CLCs. C, crude microsomal fractions were prepared from different tissues and processed for Western blot with antibodies against CHC and CLCs. Variable amounts of protein were loaded to obtain an equal signal for the CHC. D, crude microsomal fractions were prepared from different cell lines and processed for Western blot with antibodies against CHC and CLCs. Variable amounts of protein from each cell line were loaded in to obtain an equal signal for the CHC. Different concentrations of brain microsomes were loaded as indicated. HEK, human embryonic kidney.

Figure 2.3: Differential migration profiles of CCV components. CCVs from liver and brain were processed by velocity sedimentation analysis on linear sucrose gradients. Equal volume aliquots of the gradient, fractionated from the bottom, were processed for

Western blot with AP-1 (γ-adaptin), AP-2 (α-adaptin), CHC, and CLC antibodies. The bands in which each antibody shows the strongest signal are indicated by the black bar underneath.

Figure 2.4: Ratios of AP complexes in liver and brain CCVs. A, comparison of the total amount of normalized APs (mean of all 4 subunits) and CHC in brain and liver CCVs. For the inset, aliquots of liver and brain CCVs (20 μg for each) were processed for Western blot with antibodies against γ-adaptin and the αA isoform of α-adaptin. B, the total number of peptides for the αA and αC isoforms of α-adaptin from all three preparations of liver or brain CCVs, divided by the calculated mass of each protein, were apportioned to the total number of CHC peptides normalized for the molecular mass of the protein to yield a peptide/clathrin peptide index. C, the total number of peptides for the cation independent (CI-MPR) and cation dependent MPRs (CD-MPR) from all three preparations of liver or brain CCVs was used to calculate an MPR peptide to clathrin peptide index as described for the α-adaptin isoforms.

Figure 2.5: Percentage of AP-2 positive CCVs involved in synaptic vesicle recycling. The black section of the bars represent the percentage of AP-1 relative to total APs found in liver and brain CCVs. The gray section in the liver bar represents the percentage of AP-2 relative to total APs in liver CCVs. The gray section in the brain bar represents the amount of AP-2 in brain that would be expected according to the ratio of AP-2 to AP-1 from liver. In white is the remaining AP-2, which is specialized for recycling synaptic vesicles. The percentages are based on the mean number of all four subunits for each adaptor from each tissue as for Fig. 4B.

TABLE 2.1

Novel proteins found in liver CCV

NECAP 1, enthoprotin, and FENS-1 are in bold to indicate their previous identification as novel proteins in the proteome of brain CCVs (15). ARF, ADP-ribosylation factor.

	Protein name	Mass Da	Total peptides	NCBI GI nos.				
1	**NECAP 1**	**37,228**	**8**	**37945074**	**27229051**	**27713302**	**15079260**	
2	**Enthoprotin; epsin 4**	**68,273**	**319**	**7661968**	**13278582**	**20345123**	**21751443**	
3	RIKEN cDNA 6030446I19 gene	112,066	7	31542027	13449265	24980923		
4	RIKEN cDNA 5730596K20, homology to ARF-like 6 interacting protein 2	60,993	12	16877810	26326645	31559920	10435296	13477255
5	Similar to hypothetical protein MGC12103 (Homo sapiens)	46,194	5	27679620	27532965			
6	Similar to hypothetical protein KIAA0678 (RME-8)	306,705	59	27721389	26006199	28546047	26328693	26350527
7	KIAA0255 gene product	73,235	6	7662028	26352305	31542095	26339180	
8	KIAA0183	116,963	8	1136426	3005744	8922114	16307515	28524994
9	Similar to KIAA1414 protein	226,839	16	27478091	26348058			
10	Similar to mKIAA0219 protein	316,133	6	27666086				
11	**FENS-1**	**47,904**	**5**	**18482373**	**7243268**	**19484187**	**30795186**	
12	Unknown (H. sapiens)	24,209	17	3005742	12857585	12857927	18490304	20531765
13	Hypothetical protein D10Wsu52e	55,631	15	21703842	6841456	7657015	7688673 2	1703842
14	Similar to protein transport protein Sec24C (SEC24-related protein C)	112,455	6	27673609	20072091	27722283	28477301	28916673
15	EH domain-containing 4	60,888	16	10181214	7212811	7657056	10181214	20302075
16	Similar to Vault poly(ADP-ribose) polymerase (VPARP)	126,096	28	2847954				
17	Similar to ATP-binding cassette, subfamily A (ABC1), member 6	65,888	18	27690422	34875258			
18	Dendritic cell protein GA17	42,946	21	21703762	23397429	27702767	3152660	12751096
19	Similar to deleted in polyposis 1-like 1	39,229	7	27717621				
20	Macrophage expressed gene 1	74,478	5	12018298	2137564	18676680	20482397	
21	Vacuole 14 protein; Vac14 protein; hydin	89,095	5	29293817	26327751	26338430	315424	

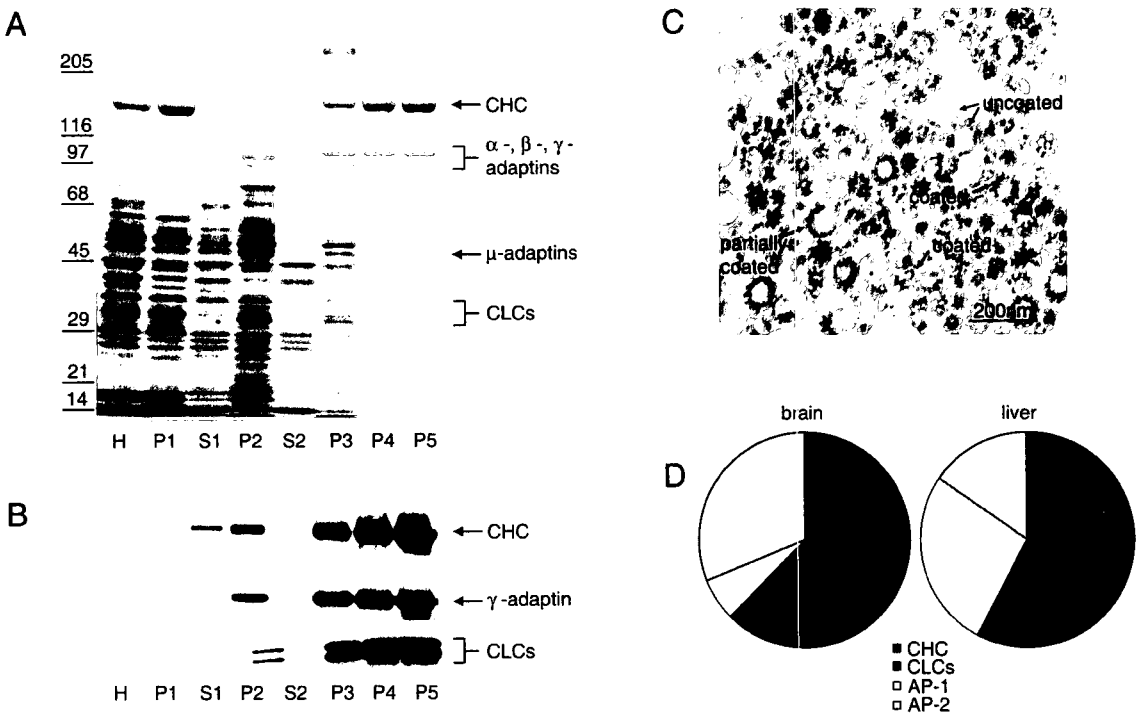
A
205
116
97
68
45
29
21
14
H P1 S1 P2 S2 P3 P4 P5
CHC
α -, β -, γ - adaptins
μ-adaptins
CLCs
B
CHC
γ-adaptin
CLCs
C
uncoated
coated
partially coated
coated
200 nm
D
brain
liver
CHC
CLCs
AP-1
AP-2

FIGURE 2.1

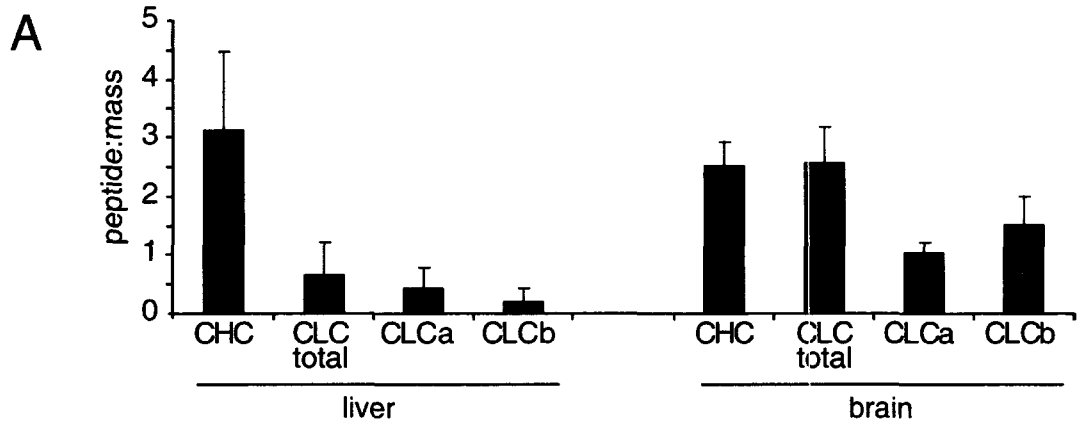
A
peptide:mass
5
4
3
2
1
0
CHC
CLC total
CLCa
CLCb
CHC
CLC total
CLCa
CLCb
liver
brain

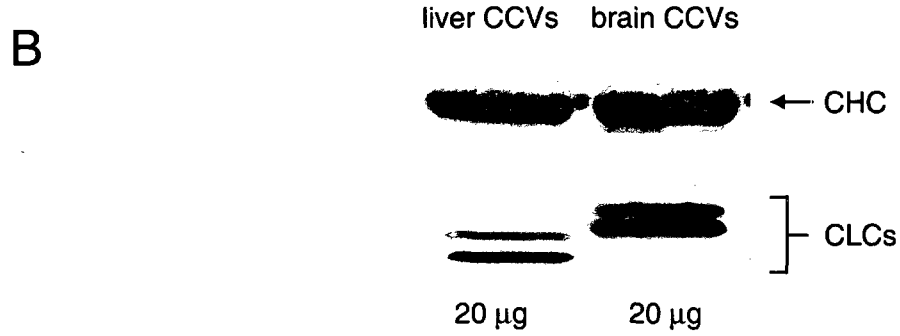
B
liver CCVs
brain CCVs
CHC
CLCs
20 µg
20 µg

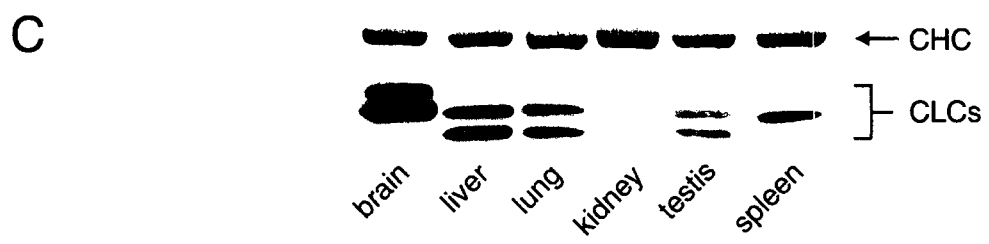
C
CHC
CLCs
brain
liver
lung
kidney
testis
spleen

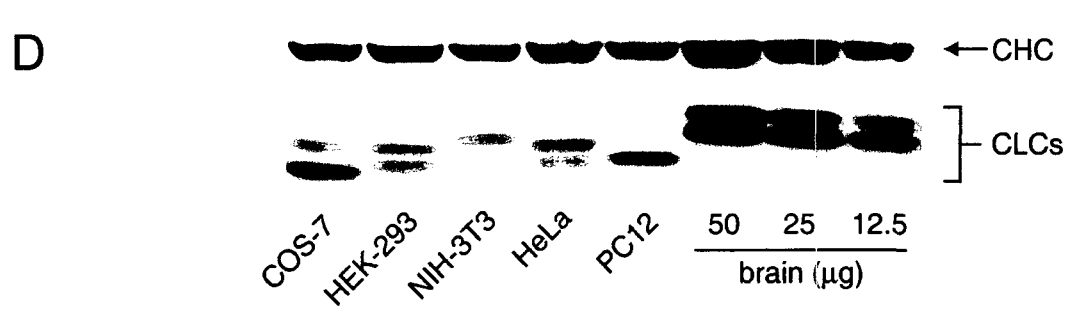
D
CHC
CLCs
COS-7
HEK-293
NIH-3T3
HeLa
PC12
50
25
12.5
brain (µg)

FIGURE 2.2

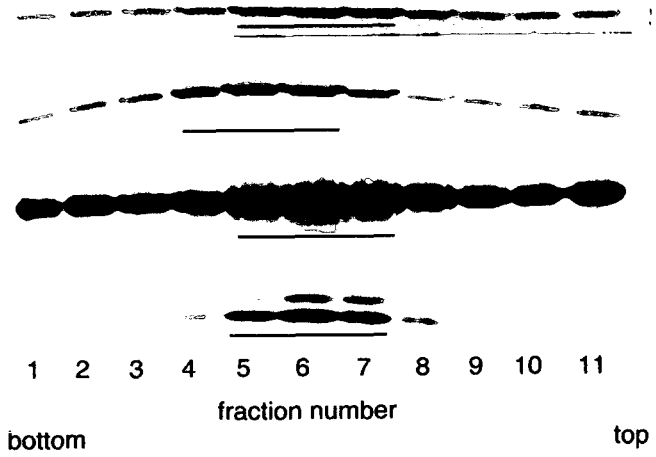

FIGURE 2.3

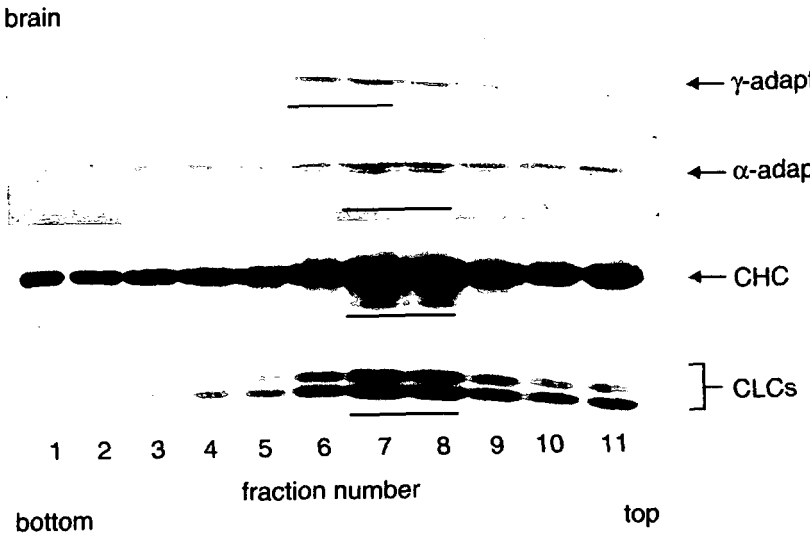
brain
γ-adaptin
α-adaptin
CHC
CLCs
1 2 3 4 5 6 7 8 9 10 11
fraction number
bottom
top

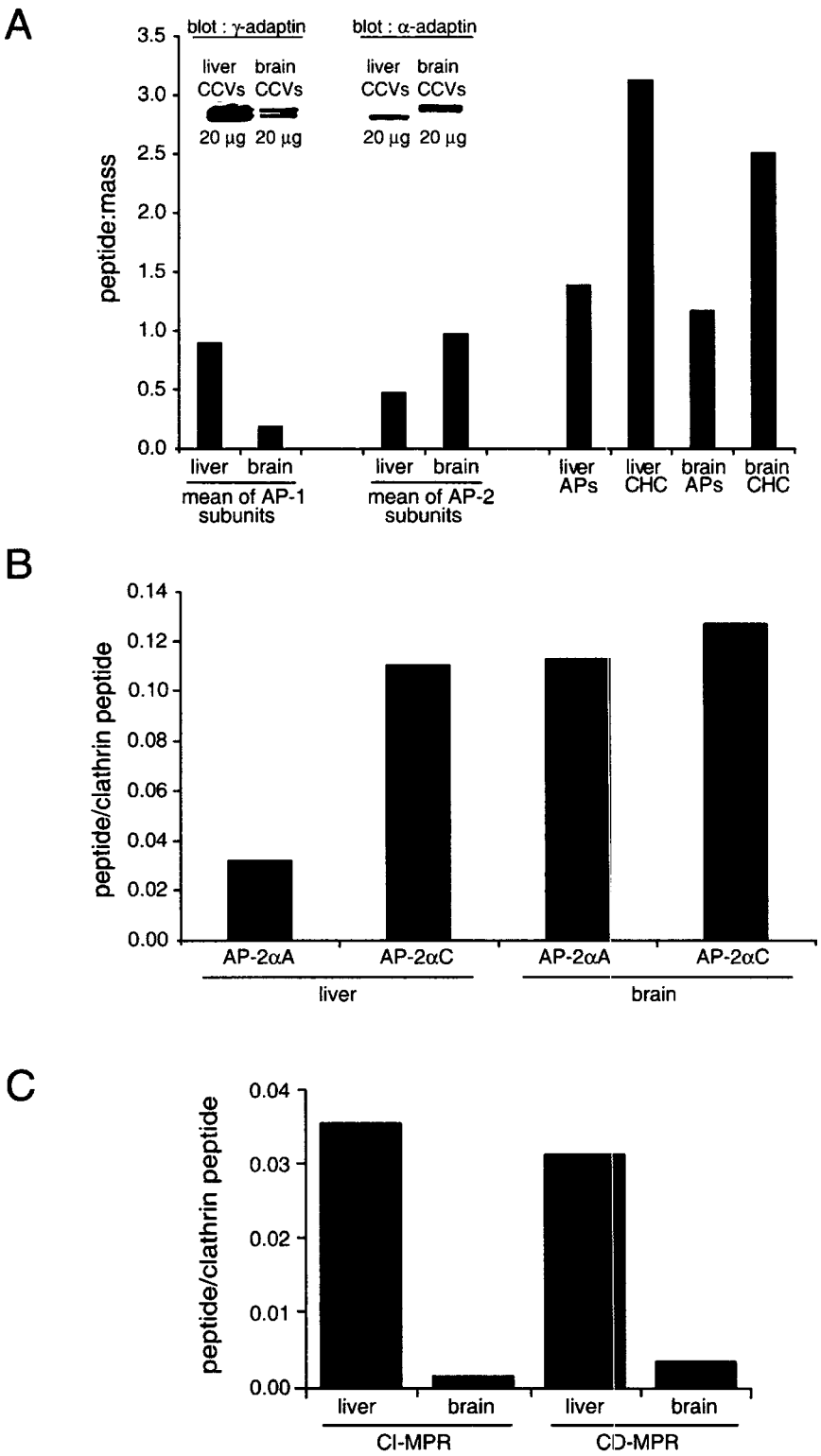
A
blot : γ-adaptin
blot : α-adaptin
liver CCVs
brain CCVs
20 µg
20 µg
peptide:mass
3.5
3.0
2.5
2.0
1.5
1.0
0.5
0.0
liver
brain
mean of AP-1 subunits
mean of AP-2 subunits
liver APs
liver CHC
brain APs
brain CHC
B
peptide/clathrin peptide
0.14
0.12
0.10
0.08
0.06
0.04
0.02
0.00
AP-2αA
AP-2αC
liver
brain
C
peptide/clathrin peptide
0.04
0.03
0.02
0.01
0.00
CI-MPR
CD-MPR

FIGURE 2.4

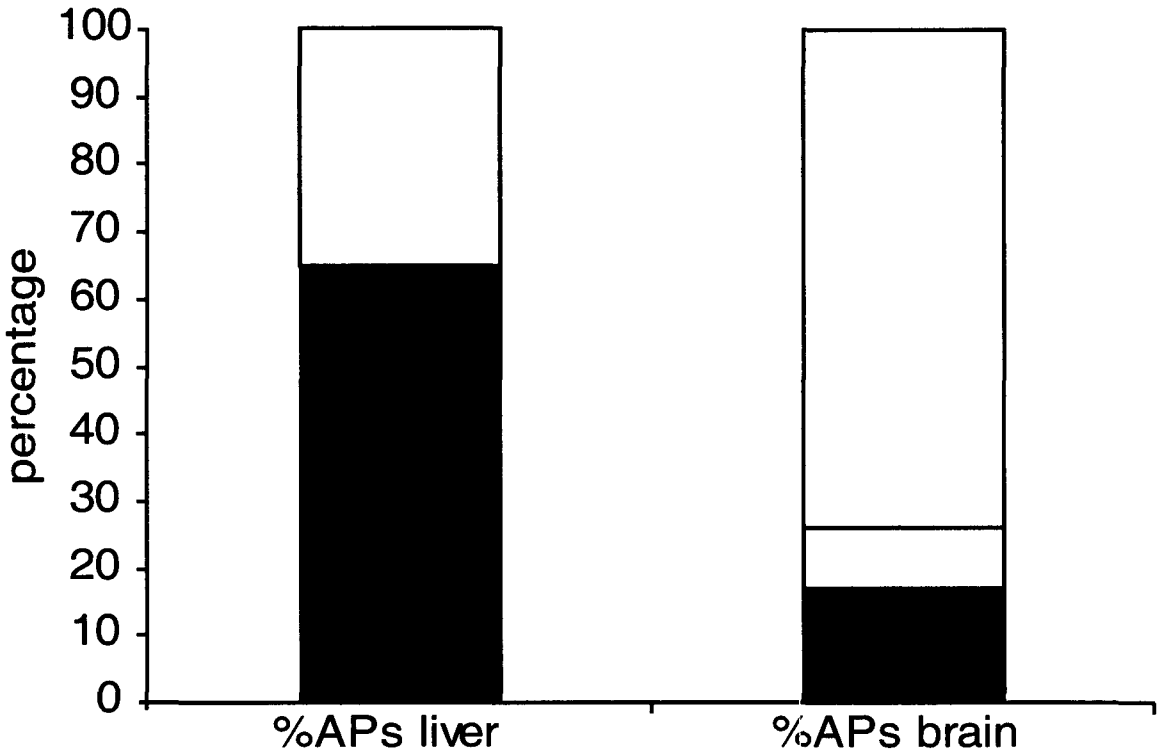
100
90
80
70
60
50
40
30
20
10
0
percentage
%APs liver
%APs brain
%brain AP-2 involved in recycling synaptic vesicles
%AP-2 according to ratio of AP-2 to AP-1 from liver
%AP-1/APs

FIGURE 2.5

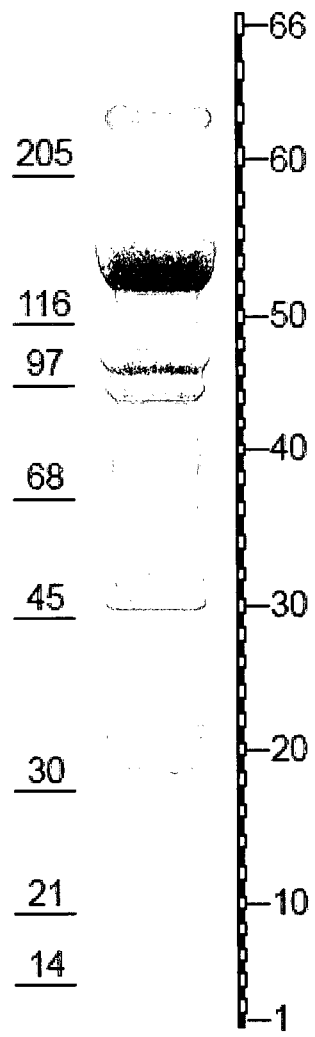

SUPPLEMENTAL FIGURE 2.S1

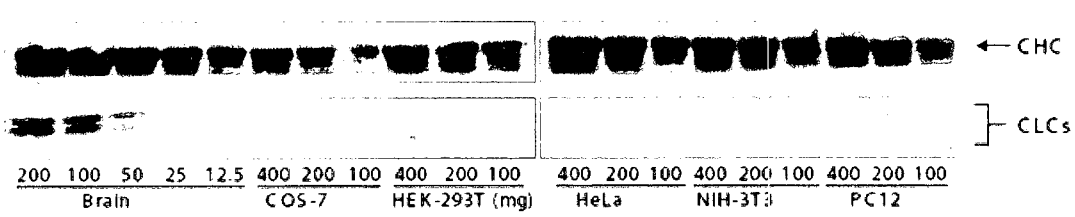

SUPPLEMENTAL FIGURE 2.S2

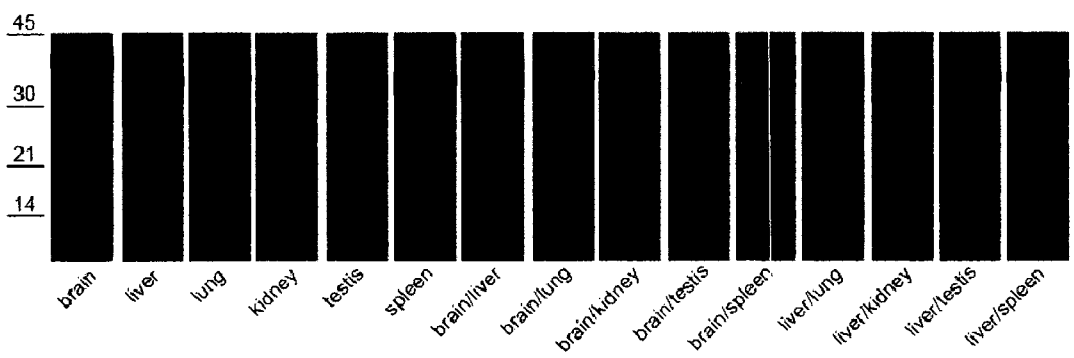

SUPPLEMENTAL FIGURE 2.S3

PREFACE TO CHAPTER 3

As introduced in chapter 2, subcellular proteomics is a useful tool to assign proteins to different cellular compartments and also to identify new components of these compartments. Proteomics of CCVs isolated from rat liver revealed 21 novel CCV-associated proteins. Several of these proteins have been studied, including NECAP1 (Ritter et al., 2003), enthoprotin (Wasiak et al., 2002), connecden (Allaire et al., 2006), Vac14 (Lemaire and McPherson, 2006), FENS-1 (Ridley et al., 2001), and p200 (Lui et al., 2003).

Among the novel proteins, we also identified the mammalian homolog of receptor-mediated endocytosis protein 8 (RME-8), which was first identified in *C.elegans*. At that time, RME-8 was partially characterized in *C. elegans* (Zhang et al., 2001) and *Drosophila* (Chang et al., 2004) and, in both organisms, RME-8 was shown to be required for endocytosis. RME-8 was later shown to cause gravitropism defects in *Arabidopsis* when defective (Silady et al., 2004). Despite the progress made in invertebrates and plants, mammalian RME-8 was yet to be characterized and its function identified.

Using biochemical and cellular biology techniques combined with an siRNA-mediated loss-of-function approach, we demonstrated that RME-8 localizes to endosomes, binds to Hsc70 and causes trafficking defects when depleted from the cells. We thus provided the first characterization of vertebrate RME-8, as well as the first evidence of its implication in intracellular trafficking.

CHAPTER 3

THE DnaJ-DOMAIN PROTEIN RME-8 FUNCTIONS IN ENDOSOMAL TRAFFICKING

Martine Girard*, Viviane Poupon*, Francois Blondeau, and Peter S. McPherson

**Equal contribution*

From the Department of Neurology and Neurosurgery, Montreal Neurological Institute, McGill University, Montreal, QC H3A 2B4, Canada

Reproduced from *Journal of Biological Chemistry* 280, 40135-40143 (2005) by copyright permission of the American Society for Biochemistry and Molecular Biology

ABSTRACT

Through a proteomic analysis of clathrin-coated vesicles from rat liver we identified the mammalian homolog of receptor-mediated endocytosis 8 (RME-8), a DnaJ domain-containing protein originally identified in a screen for endocytic defects in *Caenorhabditis elegans*. Mammalian RME-8 has a broad tissue distribution, and affinity selection assays reveal the ubiquitous chaperone Hsc70, which regulates protein conformation at diverse membrane sites as the major binding partner for its DnaJ domain. RME-8 is tightly associated with microsomal membranes and co-localizes with markers of the endosomal system. Small interfering RNA-mediated knock down of RME-8 has no influence on transferrin endocytosis but causes a reduction in epidermal growth factor internalization. Interestingly, and consistent with a localization to endosomes, knock down of RME-8 also leads to alterations in the trafficking of the cation-independent mannose 6-phosphate receptor and improper sorting of the lysosomal hydrolase cathepsin D. Our data demonstrate that RME-8 functions in intracellular trafficking and provides the first evidence of a functional role for a DnaJ domain-bearing cochaperone on endosome

INTRODUCTION

Molecular chaperones of the heat shock protein 70 family including the heat shock cognate 70 (Hsc70) function in the cytosol of eukaryotic cells to contribute generally to the folding of newly synthesized proteins and to refold proteins following stress denaturation (1). The actions of these chaperones result from cycles of substrate binding and release governed by ATP binding and hydrolysis (2). In addition, the ATPase activity of these proteins can be harnessed to do conformational work on specific proteins within a variety of functional contexts, including exocytosis, endocytosis, protein transport, and assembly or disassembly of protein complexes (2). These activities are accomplished through the actions of co-chaperones that bind to heat shock protein 70 family members and recruit them to specific membrane systems (2,3).

Co-chaperones for heat shock protein 70 family members are defined by the presence of a protein module, the DnaJ domain, which mediates chaperone binding (3). The auxilins, which are specialized for the uncoating of clathrin-coated vesicles (CCVs), provide a well characterized example of co-chaperone function (4). CCVs are evolutionary conserved carriers that transport proteins and lipids from the plasma membrane and the trans-Golgi network (TGN) to components of the endosomal system (5). CCVs pinch off the donor membrane encased in a coat; they must be uncoated for vesicle transport and fusion with the acceptor compartment (5,6). Auxilin 1 and its homolog, auxilin 2 (also known as cyclin-G-associated kinase), function to uncoat CCVs of both plasma membrane and TGN origin (7,8). Auxilins bind to the clathrin coat through interactions with the terminal domain (TD) of the clathrin heavy chain (CHC) (9) and interact in an ATP-dependent manner via their DnaJ domain with Hsc70, thus recruiting the chaperone to CCVs (10). Through its ATPase activity, Hsc70 mediates the release of clathrin triskelia by disrupting CHC/CHC interactions (10,11).

When ATPase-deficient forms of Hsc70 are expressed in mammalian cells, they function in a dominant-negative manner to block clathrin-mediated endocytosis (12), and in *Drosophila*, Hsc70 mutants have defects in the internalization of Bride of

sevenless (Boss), the ligand for the sevenless receptor tyrosine kinase (13). Interestingly, in addition to endocytic defects, Hsc70 mutant Garland cells in *Drosophila* display disruptions in the organization of endosomes (13), and dominant-negative Hsc70 constructs cause endosomal sorting defects in mammalian cells (12). Thus, Hsc70 has multiple roles on the endocytic pathway including regulation of endosomal trafficking and morphology.

In a screen for endocytic defects in *Caenorhabditis elegans*, Zhang *et al.* (14) identified a novel DnaJ domain-bearing protein that they named receptor-mediated endocytosis 8 (RME-8). RME-8 was subsequently identified in *Drosophila* where its disruption causes defects in fluid phase endocytosis and receptor-mediated endocytosis of Boss. Genetic interactions between RME-8 and Hsc70 in *Drosophila* suggested that RME-8 functions as a co-chaperone for Hsc70 in endocytosis (15). More recently, RME-8 was identified as the product of a gene that when defective causes gravitropism defects in *Arabidopsis* (16). Thus, RME-8 represents an evolutionarily conserved gene family thought to function widely in endocytosis, and yet there is currently no evidence regarding the protein expression or properties of a vertebrate isoform. We have now identified and functionally characterized mammalian RME-8. Consistent with its localization to endosomal membranes, loss of RME-8 function causes prominent defects in trafficking of the cation-independent mannose 6-phosphate receptor (CI-MPR) between the TGN and membranes of the endosomal system. These results provide the first characterization of vertebrate RME-8 revealing an important role in intracellular membrane traffic.

EXPERIMENTAL PROCEDURES

Antibodies and Fluorescent Probes - A rabbit polyclonal RME-8 serum was raised against a synthetic peptide, SNLPPPVDHEAGDLGYQT, containing amino acids 2226-2243 at the C-terminus of human RME-8 coupled to keyhole limpet hemocyanin through an added N-terminal cysteine. A rabbit polyclonal serum against human enthoprotin/epsinR was previously described (17). Monoclonal antibody against CHC used for immunofluorescence was generated from the hybridoma X22 obtained from American Type Culture Collection (Manassas, VA). Mouse monoclonal antibodies against CHC, syntaxin 6, early endosomal antigen 1 (EEA1), Grb2, and AP-1 (γ-adaptin) were purchased from BD Transduction Laboratories. Mouse monoclonal antibodies against the following proteins were from the noted commercial sources: Rab9, Abcam (Cambridge, MA); CI-MPR and AP-2 (α-adaptin), ABR (Golden, CO); Na^+/K^+ ATPase, Upstate Biotechnology (Lake Placid, NY); auxilin 2/cyclin G-associated kinase, MBL International (Woburn, MA); transferrin receptor, Zymed Laboratories Inc. (South San Francisco, CA). Rat monoclonal anti-Hsc70 was from StressGen (Victoria, BC) and rabbit polyclonal antibodies against cathepsin D and EGF receptor were from DAKOCytomation (Mississauga, ON) and Santa Cruz Biotechnology (Santa Cruz, CA), respectively. A pan-cadherin polyclonal antibody was from Sigma (St. Louis, MO). Polyclonal antibodies recognizing VAMP 4 and CI-MPR were generous gifts of Dr. Richard Scheller (Genentech, San Francisco, CA) and Dr. Paul Luzio (University of Cambridge, Cambridge, UK), respectively. Transferrin-Cy3 was from Jackson Laboratories (Mississauga, ON) and transferrin-Alexa Fluor 647, EGF-Texas Red, EGF-Alexa Fluor 488, and cholera toxin B-Alexa 594 were from Molecular Probes Inc. (Eugene, OR).

cDNA Constructs - KIAA0678, encoding a large C-terminal fragment of human RME-8, was produced by and was a generous gift of the Kazusa DNA Research Institute (Chiba, Japan). The RME-8 DnaJ domain (amino acids 1302 to 1366; Fig. 1) was amplified from KIAA0678 by PCR and was subcloned in-frame into pGEX-4T1 vector (Amersham Biosciences) adding an N-terminal GST tag. The terminal domain (TD) of

the CHC fused to GST was previously described (18).

Subcellular Fractionation and GST Affinity Selection Assays - Various rat tissues or cultured cells were homogenized in buffer A (20 mM HEPES, pH 7.4 containing 0.83 mM benzamidine, 0.23 mM phenylmethylsulphonyl fluoride, 0.5 μg/ml aprotinin and 0.5 μg/ml leupeptin) and centrifuged at 800 x *g* for 10 min. Equal protein aliquots of the supernatants were analyzed by SDS-PAGE and Western blot. For some experiments, the supernatant was centrifuged at 12,000 x g for 20 min, the pellet (P2) was resuspended in buffer A, and the supernatant was spun at 205,000 x *g* for 1 h. The resulting pellet (P3) was resuspended in buffer A, and the supernatant was kept (S3). Equal protein aliquots of the fractions were analyzed by SDS-PAGE and Western blot. For extraction experiments, kidney P3 fractions were pelleted at 245,000 x *g* and resuspended in buffer A, buffer A containing 1% Triton X-100 or 150 mM NaCl or 500 mM NaCl or in 50 mM $NaCO_3$, pH 11.0, and incubated on ice for 15 min. Samples were then centrifuged at 245,000 x *g* and equal volume aliquots of the supernatants and pellets were analyzed by SDS-PAGE and Western blot. CCVs were isolated from rat liver as described (19,20). Plasma membrane was isolated from rat liver as described (21) except that the final pellet was resuspended in 1.42 M sucrose, overlaid with 1.0 M sucrose, and centrifuged at 82,000 x g for 1 h in a Beckman SW28 rotor. The pellicle at the 1.0-1.42 M sucrose interface was collected, and the plasma membranes were pelleted by centrifugation at 1000 x *g* after adjusting the sucrose to 0.4 M.

For affinity selection experiments with the CHC TD, soluble fractions resulting from pH 11.0 extraction of P3 pellets, as described above, were neutralized to pH 7.4 by dilution in buffer A and were then centrifuged at 245,000 x *g*. Triton X-100 was added to the supernatant to 1% final and 2-mg aliquots of the extracts were incubated overnight at 4°C with GST or GST-CHC-TD pre-coupled to glutathione-Sepharose beads. After incubation, beads were washed with buffer A containing 1% Triton X-100 and proteins specifically bound to the beads were analyzed by SDS-PAGE and Western blot. In other experiments, adult rat kidneys were homogenized in 10 volumes of buffer B (20 mM HEPES, pH 7.4, 25 mM KCl, 2 mM $MgCl_2$, 10 mM NH_2SO_4, 0.83 mM benzamidine,

0.23 mM phenylmethylsulphonyl fluoride, 0.5 μg/ml aprotinin and 0.5 μg/ml leupeptin) and centrifuged at 800 x *g* for 10 min. The resulting supernatant was centrifuged at 205,000 x *g* for 30 min, and 2-mg aliquots of the resulting supernatant were incubated with 10 mM EDTA or varying concentrations of adenine nucleotides for 10 min at 25°C before incubation for 1 h at 25°C with GST-DnaJ domain fusion protein pre-coupled to glutathione-Sepharose beads. Incubations with ATP were performed in the presence of an ATP regenerating system. After incubation, beads were washed with buffer B with or without 0.1 mM adenine nucleotide and specifically bound proteins were analyzed by SDS-PAGE and Western blot or bands were extracted from Coomassie-stained gels and analyzed by tandem mass spectrometry as described (22).

Immunofluorescence Analysis of RME-8 Localization - Cells grown on poly-L-lysine coated coverslips were washed in PBS (20 mM NaH_2PO_4, 150 mM NaCl, pH 7.4) and then fixed for 20 min in 2% paraformaldehyde, PBS. In some cases, cells were first incubated for 1 h in serum-free DMEM and then incubated with 5 μg/ml Cy3-transferrin or 100 ng/ml Texas Red-EGF for 20 min at 37°C before fixation. After fixation, cells were permeabilized with 0.2% Triton X-100/PBS (or 0.05% saponin/PBS for AP-2 and EGF receptor) and processed for immunofluorescence with the appropriate primary and secondary antibodies. All immunofluorescence images presented in the study were obtained using a Zeiss 510 laser scanning confocal microscope.

siRNA-mediated Knock Down of RME-8 - siRNAs matching selected regions of RME-8 sequence were synthesized by Qiagen with dT overhangs already annealed. The sequences were submitted to BLAST search to ensure specificity of the target. Of the four sequences selected, one (RME-8.3) led to a decrease of RME-8 protein expression superior to 90%. The DNA target sequence of RME-8.3 was 5'-AAGCTGCTCCAGATATGAAAA-3'. For siRNA transfection, COS-7 cells were plated in DMEM without antibiotics. Cells were plated in 6-well plates or coverslips in 24-well plates such that they would be 60% confluent 24 h post-plating. At this time, cells were transfected with siRNAs at a final concentration of 80 nM using Lipofectamine 2000 (Invitrogen) according to the manufacturer's instructions, and transfections were

repeated 24 h later. For the control, cells were transfected with Lipofectamine 2000 only. Experiments were performed 72 h after the first transfection.

Analysis of EGF, Transferrin and Cholera Toxin B Endocytosis - COS-7 cells, mock- transfected or transfected with RME-8.3 siRNA, were serum-starved for 1 h in DMEM and were then incubated for 15 min at 37° with transferrin-Cy3 (5 μg/ml), EGF-Texas Red (10 ng/ml), or cholera toxin B-Alexa 594 (5 μg/ml). Cells were processed for immunofluorescence analysis as described previously. Alternatively, cells were treated the same but were incubated with transferrin-Alexa Fluor 647 (5 μg/ml) or EGF-Alexa Fluor 488 (10 ng/ml). In these cases, one set of cells for each ligand was washed twice in PBS and then fixed in 2% paraformaldehyde,PBS. A second set of cells was washed in acidic buffer (0.2 M acetic acid, pH 2.8 containing 0.5 M NaCl) for 15 min at 4°C to strip cell surface EGF or transferrin, and the cells were then washed twice in PBS and fixed as above. The levels of fluorescent EGF and transferrin were assessed using a FACScan with data analyzed using the CellQuantPro program (BD Biosciences). The percentage of ligand internalized was determined by dividing the amount of ligand in cells (acid washed samples) *versus* total ligand (cells washed with PBS alone) for 10,000 cells.

Cathepsin D Sorting Assay - COS-7 cells mock-transfected or transfected with RME-8.3 siRNA were washed and placed in cysteine/methionine-free DMEM (Invitrogen) for 1 h at 37 °C. Cells were then pulsed for 10 min with 0.25 mCi/ml Pro-Mix [^{35}S] (Amersham Biosciences), washed, and chased in DMEM with 1% fetal bovine serum, 5 mM mannose-6-phosphate and 1 mM methionine. At 1-, 2-, 3-, and 4-h time points, media were collected, cell lysates were prepared, and cathepsin D was immunoprecipitated as described (23). Immunoprecipitated proteins were separated on SDS-PAGE and processed for autoradiography using a STORM Phosphoimager (Amersham Biosciences) followed by exposure to x-ray film. Quantitation was performed using ImageQuant software.

RESULTS

Identification of Mammalian RME-8 - A proteomic analysis of CCVs isolated from rat liver identified proteins that are predicted products of cDNAs and genomic sequence (24). One such protein, identified in the annotated rat genome under gi 27721389, is the rat homolog of RME-8. The rat sequence could be aligned with fly and worm orthologs with the exception of the N-terminal most 448 amino acids. Three overlapping human clones (gi3327169, gi18799409, gi15948602) were aligned to predict a protein (Fig. 3.1) with homology to full-length invertebrate forms. When this sequence was searched against the human genome using the blat algorithm, a series of 56 exons from region q22.1 of chromosome 3 could be annotated to reveal a sequence that was identical to the sequence predicted from the overlapping clones. siRNAs targeting each of the three clones were effective in reducing the expression of the endogenous protein in COS-7 cells as detected with a polyclonal antibody against a C-terminal peptide (Fig. 3.6 and data not shown). The human RME-8 sequence (entered into Genbank under accession number AY779857) encodes a 2243-amino acid protein that is 46, 43, and 28% identical throughout its length to *Drosophila*, *C. elegans,* and *Arabidopsis* RME-8, respectively. As originally described for the *C. elegans* protein (14), human RME-8 has a central DnaJ domain flanked on either side by two IWN repeats of unknown function (Fig. 3.1).

RME-8 is detected as a protein of ~220 kDa in most tissues and cell lines examined (Fig. 3.2, *A* and *B*). A reactive band seen in selective extracts at ~140 kDa may represent a proteolytic fragment or an alternatively spliced form of RME-8 (Fig. 3.2). Subcellular fractionation of kidney extracts reveals that RME-8 is enriched in P3 microsomes with no protein detectable in a cytosolic (S3) fraction whereas the plasma membrane protein cadherin is enriched in P1 and P2 fractions that sediment at lower *g* forces (Fig. 3.2*C*). Purified plasma membrane that is highly enriched for cadherin and EGF receptor has a relatively weak RME-8 signal (Fig. 3.2*D*). RME-8 does not extract from microsomal fractions following treatment with 1% Triton X-100, 150 mM NaCl, or 500 mM NaCl but is partially extracted by sodium carbonate, pH 11.0 (Fig. 3.2*E*). The

integral membrane protein Na^+/K^+ ATPase is resistant to NaCl and pH 11.0 but is extracted with 1% Triton X-100 (Fig. 3.2*E*). Thus, RME-8 appears to be an extrinsic membrane protein tightly associated with a Triton X-100-insoluble microsomal compartment.

RME-8 Binds through Its DnaJ Domain to Hsc70 - To further characterize mammalian RME-8, we sought to identify RME-8-binding partners. We first performed pull-down assays from kidney extracts using a GST-RME-8-DnaJ domain fusion protein in the presence or absence of ATP. Coomassie blue staining revealed a single affinity selected band at ~70 kDa only in the presence of ATP (Fig. 3.3*A*). Tandem mass spectrometry identified Hsc70 with 33 unique peptides, consistent with the observation that Drosophila RME-8 binds to Hsc70 in vitro (15). However, for Drosophila RME-8, binding was dependent on the presence of ADP. This is surprising because proteins bearing DnaJ domains generally bind to heat shock protein 70 family members when the chaperones are in their ATP-bound state (3). We, thus, examined the interaction of human RME-8 with Hsc70 under different nucleotide conditions. Incubation of GST-RME-8-DnaJ domain with kidney extracts in the presence of ATP led to an efficient affinity selection of Hsc70 with less binding observed in the presence of ADP and only weak binding seen in the presence of EDTA, which chelates Mg^{2+} leaving Hsc70 in a nucleotide-free state (Fig. 3.3*B*). This ATP-dependent interaction is direct as it was verified using purified His-tagged Hsc70 (data not shown), and is dose-dependent, with maximal binding observed between 1 and 5 mM (Fig. 3.3*C*), comparable with ATP concentrations required for auxilin interactions with Hsc70 (8). These data demonstrate that mammalian RME-8 interacts with Hsc70 in an ATP-dependent manner. Attempts to identify additional binding partners for RME-8 have been unsuccessful in that the large size of the protein has made it difficult to generate constructs for additional affinity selection experiments, and co-immunoprecipitation experiments are complicated by the fact that the endogenous protein can only be solubilized under conditions that are likely to disrupt protein-protein interactions (Fig. 3.2*E*).

The auxilins, which bind to Hsc70 via a DnaJ domain, also bind to the TD of the

CHC and function in the uncoating of CCVs by recruiting Hsc70 to clathrin coats (4). The identification of mammalian RME-8 on CCVs and the presence within the protein of four potential type II clathrin boxes (LLDFL, LLEMV, LLEFL, LLDYI; Fig. 3.1), interaction motifs for the CHC TD (25-27), suggest that RME-8 could function analogously to auxilins. To address this issue, we first tested if RME-8 binds to the CHC TD. Proteins were extracted from kidney P3 microsomes with $NaCO_3$ buffer, pH 11.0, and the extracts were subsequently adjusted to pH 7.4 and incubated with a GST-CHC-TD. RME-8 failed to bind the TD, whereas enthoprotin/epsinR and the clathrin adaptor protein 1, which bind to the TD through type II clathrin boxes in whole or in part, respectively (28,29), both bound in the same experiment (Fig. 3.4*A*). Moreover, whereas RME-8 is present on CCVs purified from liver, consistent with its identification in this organelle, it was not enriched (Fig. 3.4*B*). Neuron specific auxilin 1 (30) and ubiquitously distributed auxilin 2/GAK (Fig. 3.4*B*) are both highly enriched on CCVs. Thus, RME-8 is unlikely to function analogously to auxilins in the uncoating of CCVs.

Localization of Endogenous RME-8 in Mammalian Cells - Studies in invertebrates demonstrated that GFP-RME-8 was localized to endosomal structures in coelomocytes of *C. elegans* (14) and that RFP-RME-8 partially overlaps with GFP-tagged Rab5 and Rab7 in Garland cells of *Drosophila* (15). Confocal immunofluorescence analysis of COS-7 (Fig. 3.5) and HeLa cells (data not shown) reveals that endogenous mammalian RME-8 has a distributed punctate pattern with accumulation of larger puncta in a perinuclear region. RME-8 puncta are partially co-localized with early endosomal antigen 1 EEA1 (Fig. 3.5*A*) and transferrin that has been endocytosed for 20 min (Fig. 3.5*B*), indicating that pools of the protein are present on early and recycling endosomes. RME-8 also co-localizes with the CI-MPR (Fig. 3.5*C*) and is found in puncta surrounding puncta of Texas Red-EGF following 20 min of endocytic uptake (Fig. 3.5*D*), suggesting that pools of RME-8 are present on late endosomes. That RME-8 puncta surround EGF may reflect the presence of EGF within the lumen of the late endosome with RME-8 on the limiting membrane, and in fact, endocytosed EGF can even be seen in many cases to be adjacent to or surrounded by the EGF receptor (Fig. 3.5*E*). Little co-localization is seen between RME-8 and syntaxin 6,

a TGN marker and no co-localization is seen with LAMP1, a marker of lysosomes (data not shown). Moreover, RME-8 does not co-localize with AP-2, indicating that it is not a component of clathrin-coated pits on the plasma membrane (Supplemental Fig. 3.S1). Together, these results demonstrate that RME-8 is found predominantly on endosomes.

RME-8 Loss of Function Causes Defects in EGF Endocytosis - To explore the functional roles of RME-8, we took a loss of function approach. Four siRNAs were designed to sequences from the coding region of the mRNA of the human protein. Upon transfection into COS-7 and HeLa cells, three of these siRNAs suppressed RME-8 protein expression by greater than 50% (data not shown). The most effective, RME-8.3 reduced RME-8 expression in COS-7 cells to near undetectable levels based on immunofluorescence microscopy (Fig. 3.6*A*) and Western blot (Fig. 3.6*B*). Quantitation of the Western blots revealed that RME-8 expression in RME-8.3 treated cells was 6 ± 0.7% of that seen in mock transfected cells (Fig. 3.6*B*). Depletion of RME-8 did not affect the expression levels of CHC, Hsc70, EEA1, Na^+/K^+-ATPase, syntaxin 6, Rab9, or Grb2 (Fig. 3.6*B*).

We first examined for alterations in clathrin-mediated endocytosis in COS-7 cells depleted of RME-8. RME-8 knock down caused no apparent defect in uptake of fluorescent transferrin as determined by immunofluorescence microscopy, but there was a noticeable decrease in intracellular EGF (Fig. 3.7*A*). To quantify this result, we used fluorescence-activated cell sorting. Control and knock down cells were incubated with fluorescent ligands for 15 minutes to allow internalization and were then fixed after a PBS wash (total ligand) or acid wash (internalized ligand) before fluorescence-activated cell sorting analysis. Interestingly, we noticed a decrease in the total amount of EGF associated with knock-down cells compared to control, whereas transferrin levels were not affected. Western blots revealed that this result reflected a decrease in EGF receptor expression levels (Fig. 3.7*B*). In addition, the percentage of total EGF that was internalized was decreased by ~50%, indicating that the ability of the remaining pool of receptor to undergo endocytosis was compromised (Fig. 3.7*C*). No effect of RME-8 knock down was observed on the endocytosis of cholera toxin B (Fig. 3.7*D*), a marker of

the caveolae-mediated endocytic pathway (31).

We also noticed an effect of RME-8 depletion on the localization of CHC. Specifically, a proportion of RME-8-depleted cells showed less cytosolic CHC staining (Fig. 3.8, *A* and *B*). Cells counts revealed that ~30% of RME-8 knock-down cells display the CHC phenotype (Fig. 3.8*C*). Cells with the strongest changes in CHC distribution often showed the most obvious reduction in EGF endocytosis (Supplemental Fig. 3.S2).

RME-8 Loss of Function Causes Defects in MPR Trafficking - Given the localization of RME-8 to endosomes, we examined for potential defects in endosomal trafficking. MPRs are responsible for the transport of lysosomal hydrolases including pro-cathepsin D from the TGN to endosomes. The enzyme is subsequently targeted to lysosomes where it is cleaved into mature cathepsin D, whereas the MPR escapes degradation by recycling back to the TGN (32-34). Interestingly, RME-8 depleted cells show a striking clustering of the CI-MPR in the perinuclear region whereas mock-transfected cells demonstrate a more distributed pattern of CI-MPR staining (Fig. 3.9*A*). The clustered receptor is co-localized with syntaxin 6 and VAMP 4, markers of the TGN (Fig. 3.9*B*), suggesting that the perinuclear compartment is the TGN or is a compartment that clusters near to the TGN. Pro-cathepsin D trafficking was monitored using an assay that examines processing of pro-cathepsin D to its mature form in pulse-chase experiments (23). Mock-transfected cells show a time-dependent accumulation of mature cathepsin D at 31 kDa, whereas RME-8 knock down cells accumulate less mature form (Fig. 3.9*C*). A portion of pro-cathepsin D normally escapes transport to endosomes and is instead secreted (Fig. 3.9*C* and see, for example, Ref. 35). Interestingly, the secretion of pro-cathepsin D is also reduced after RME-8 knock down (Fig. 3.9*C*). Averaging over multiple experiments reveals that the percentage of cathepsin D that is sorted (released and processed relative to total) is significantly reduced from 52.2 to 34.6% (n=9) at the 3-h time point in mock- *versus* RME-8.3-transfected cells, respectively (Fig. 3.9*D*). The percentage sorted in mock-transfected cells increased to 69.6% at 4 h, where again a significant decrease (to 52.9%, n=11) is

seen after RME-8 knock down (Fig. 3.9*D*). Thus, loss of RME-8 function leads to defects in the trafficking of cathepsin D via the MPR.

DISCUSSION

RME-8 was originally identified as a mutant defective in yolk protein uptake in *C. elegans* (14) and was subsequently shown to function in ligand-stimulated and constitutive endocytosis in *Drosophila* (15). In both invertebrate systems, RME-8 was found to partially co-localize with endosomal vacuoles (14,15). Here we demonstrate that mammalian RME-8 is localized throughout the endosomal system and is enriched on microsomal membranes spinning at 205,000 x *g*. It is not, however co-localized with AP-2, a marker of clathrin-coated structures at the plasma membrane, and its knock down does not affect AP-2 distribution (Supplemental Fig. 3.S1). Moreover, RME-8 is expressed at relatively low levels in highly enriched plasma membrane preparations. Thus, although it is not possible to definitively rule out that a small pool of RME-8 may be present at the plasma membrane, the protein appears to be predominantly endosomal.

Given the seeming discrepancy between the localization of RME-8 to intracellular endosomes and its role in entry of endocytic tracers, we sought to examine for endocytic defects in mammalian systems. Interestingly, we found no effect of RME-8 knock down on endocytosis of transferrin, a cargo of the constitutive endocytic pathway. However, we did observe a reduction in endocytosis of the EGF receptor. EGF receptor can enter cells via clathrin-mediated mechanisms and via caveolae, and the use of these two pathways is very sensitive to the concentration of EGF (36). We thus tested for a potential affect of RME-8 knock down on endocytosis of cholera toxin B, a marker of the caveolae-mediated endocytic pathway (31). Cholera toxin B endocytosis was normal, suggesting that disruption of the caveolae pathway is not responsible for the defect in EGF endocytosis. However, we did make the surprising observation that the level of EGF receptor was significantly reduced in RME-8 knock-down cells. In contrast, the levels of transferrin receptor, as well as those of multiple signaling and vesicle trafficking proteins were unaffected. The EGF receptor displays significant rates of constitutive endocytosis (1-2%/minute) with trafficking through early and late endosomes (37). Enhancing transport from early to late endosomes or decreasing EGF receptor recycling to the plasma membrane from late endosomes can decrease EGF

receptor levels (37). Thus, RME-8 knock down could disrupt the steady state levels of EGF receptor by disrupting endosomal trafficking. The precise mechanism causing loss of EGF receptor remains under investigation.

RME-8 knock down was also seen to alter the distribution of CHC with ~30% of knock-down cells demonstrating reduced cytosolic staining. This is reminiscent of the depletion of cytosolic clathrin that is seen after overexpression of dominant-negative forms of Hsc70 in mammalian cells (12). Moreover, it is consistent with results in Garland cells in *Drosophila* in which RME-8 mutants demonstrate a redistribution of GFP-tagged clathrin light chain from peripheral puncta to larger intracellular puncta, a phenotype mimicked by loss of Hsc70 function (13, 15). Thus, in both mammalian and invertebrate systems, RME-8 and Hsc70 are likely to function in a common pathway. It is unlikely however that RME-8 function is directly analogous to that of auxilins in uncoating CCVs as RME-8 does not bind directly to CHC and is not enriched on CCVs to the same extent as auxilin 1 and 2. This is consistent with the observation in *Drosophila* that overexpressed auxilin and RME-8 exhibit different genetic interactions with Hsc70 (15). Regardless, disruption of CHC distribution following RME-8 knock down may contribute to endocytic defects, as cells with the strongest CHC redistribution phenotype appear to have the most severe impairment of EGF endocytosis. In fact, the selective defect in endocytosis of EGF *versus* transferrin may result from a combination of this clathrin redistribution phenotype and the reduced levels of EGF receptor.

Despite the localization of RME-8 to intracellular membranes, no defect in intracellular trafficking has been described upon loss of RME-8 function. We noticed an accumulation of the CI-MPR in a perinuclear pool after RME-8 knock down. The CI-MPR along with the cation-dependent MPR carry out the delivery of newly synthesized acid hydrolases from the TGN to early and late endosomes for their subsequent transfer to lysosomes (34). To avoid degradation, MPRs recycle back to the TGN before reaching the lysosomal compartment (41). Our data demonstrate that RME-8 is necessary for the normal activity of this trafficking pathway. The receptor accumulates in the vicinity of the TGN based on co-localization studies with TGN markers syntaxin 6 and VAMP 4.

This accumulation may represent trapping of the receptor in the TGN itself or an accumulation in a membrane compartment that accumulates near the TGN. However, when we examined the trafficking of cathepsin D, a lysosomal hydrolase, we noticed a decrease in the processing of cathepsin D to its mature form as well as a decrease in the normal basal rate of cathepsin D secretion. The former observation suggests that the MPR does not reach the lysosome, where processing of the pro form of cathepsin D occurs. However, if the CI-MPR was trapped in the TGN, one might expect to see an increase in pro-cathepsin D that escaped the TGN in constitutive vesicles. Thus, we favor a scenario in which cathepsin D can traffic with the MPR from the TGN but is unable to properly traffic through the endosomal pathway to reach lysosomes. Thus, in addition to providing the first characterization of mammalian RME-8, our data provide the first evidence of a role for the protein in intracellular trafficking. Given its broad tissue distribution and evolutionary conservation, RME-8 is likely to contribute to such trafficking events in the context of many cell types.

REFERENCES

1. Hartl, F. U., and Hayer-Hartl, M. (2002) *Science* **295**, 1852-1858
2. Young, J. C., Barral, J. M., and Hartl, F. U. (2003) *Trends Biochem. Sci.* **28**, 541-547
3. Kelley, W. L. (1999) *Curr. Biol.* **9**, R305-R308
4. Lemmon, S. K. (2001) *Curr. Biol.* **23**, R49-R52
5. Brodsky, F. M., Chen, C. Y., Knuehl, C., Towler, M. C., and Wakeham, D. E. (2001) *Annu. Rev. Cell Dev. Biol.* **17**, 517-568
6. Smythe, E. (2003) *Biochem. Soc. Trans.* **31**, 736-739
7. Umeda, A., Meyerholz, A., and Ungewickell, E. (2000) *Eur. J. Cell Biol.* **79**, 336-342
8. Greener, T., Zhao, X., Nojima, H., Eisenberg, E., and Greene, L. E. (2000) *J. Biol. Chem.* **275**, 1365-1370
9. Scheele, U., Alves, J., Frank, R., Duwel, M., Kalthof, C., and Ungewickell, E. (2003) *J. Biol. Chem.* **278**, 25357-25368
10. Ungewickell, E., Ungewickell, H., Holstein, S. E., Lindner, R., Prasad, K., Barouch, W., Martin, B., Greene, L. E., and Eisenberg, E. (1995) *Nature* **378**, 632-635
11. Fotin, A., Cheng, Y., Grigorieff, N., Walz, T., Harrison, S. C., and Kirchhausen, T. (2004) *Nature* **432**, 649-653
12. Newmyer, S. L., and Schmid, S. L. (2001) *J. Cell Biol.* **152**, 607-620
13. Chang, H. C., Newmyer, S. L., Hull, M. J., Ebersold, M., Schmid, S. L., and Mellman, I. (2002) *J. Cell Biol.* **159**, 477-487
14. Zhang, Y., Grant, B., and Hirsh, D. (2001) *Mol. Biol. Cell* **12**, 2011-2021
15. Chang, H. C., Hull, M., and Mellman, I. (2004) *J. Cell Biol.* **164**, 1055-1064
16. Silady, R. A., Kato, T., Lukowitz, W., Sieber, P., Tasaka, M., and Somerville, C. R. (2004) *Plant Physiol.* **136**, 3095-3103
17. Burman, J. L., Wasiak, S., Ritter, B., de Heuvel, E., and McPherson, P. S. (2005) *FEBS Lett.* **579**, 2177-2184
18. Goodman, O. B. Jr, Krupnick, J. G., Gurevich, V. V., Benovic, J. L., and Keen,

J.H. (1997) *J. Biol. Chem.* **272**, 15017-15022

19. Pilch, P. F., Shia, M. A., Benson, R. J., and Fine, R. E. (1983) *J. Cell Biol.* **96**, 133-138
20. Girard, M., Allaire, P. D., Blondeau, F., and McPherson, P. S. (2005) Isolation of clathrin-coated vesicles by differential and density gradient centrifugation, in "Current Protocols in Cell Biology", Unit 3.13 Subcellular Fractionation and Isolation of Organelles Juan Bonifacino, Jennifer Lippincott-Schwartz, Mary Dasso, Joe Harford and Ken Yamada (Eds): pp 3.13.1-3.13.20. John Wiley and Sons, Inc.
21. Di Guglielmo, G. M., Baass, P. C., Ou, W. J., Posner, B. I., and Bergeron, J. J. (1994) *EMBO J.* **15**, 4269-4277
22. Blondeau, F., Ritter, B., Allaire, P. D., Wasiak, S., Girard, M., Hussain, N. K., Angers, A., Legendre-Guillemin, V., Roy, L., Boismenu, D., Kearney, R. E., Bell, A. W., Bergeron, J. J., and McPherson, P. S. (2004) *Proc Natl Acad Sci USA* **101,** 3833-3838
23. Davidson, H. W. (1995) *J. Cell Biol.* **130**, 797-805
24. Girard, M., Allaire, P. D., McPherson, P.S., and Blondeau, F. (2005) *Mol. Cell Prot.* **4**, 1145-1154
25. Ramjaun, A.R., and McPherson, P. S. (1998) *J. Neurochem.* **70**, 2369-2376
26. ter Haar, E., Harrison, S. C., and Kirchhausen, T. (2000) *Proc. Natl. Acad. Sci. USA* **97**, 1096-1100
27. Drake, M. T., and Traub, L. M. (2001) *J. Biol. Chem.* **276**, 28700-28709
28. Wasiak, S., Legendre-Guillemin, V., Puertollano, R., Blondeau, F., Girard, M., de Heuvel, E., Boismenu, D., Bell, A. W., Bonifacino, J. S., and McPherson, P. S. (2002) *J. Cell Biol.* **158**, 855-862
29. Doray, B., and Kornfeld, S. (2001) *Mol. Biol. Cell* **12**, 1925-1935
30. Ahle S., and Ungewickell, E. (1990) *J Cell Biol* **111,** 19-29
31. Puri, V., Watanabe, R., Singh, R. .D, Dominguez, M., Brown, J. C., Wheatley, C. L., Marks, D. L., and Pagano, R. E. (2001) *J. Cell Biol.* **154**, 535-547
32. Kornfeld, S. (1992) *Annu. Rev. Biochem.* **61**, 307-330
33. Kornfeld, S., and Mellman, I. (1989) *Annu. Rev. Cell Biol.* **5**, 483-525

34. Hille-Rehfeld, A. (1995) *Biochim. Biophys. Acta.* **1241**, 177-194
35. Seaman, M. N. (2004) *J. Cell Biol.* **165**, 111-122
36. Sigismund, S., Woelk, T., Puri, C., Maspero, E., Tacchetti, C., Transidico, P., Di Fiore, P. P., Polo, S. (2005) *Proc. Natl. Acad. Sci. USA* **102**, 2760-2765
37. Wiley, H. S. and Burke, P. M. (2001) *Traffic* **2**, 12-18
38. Hinners, I., and Tooze, S. A. (2003) *J. Cell Sci.* **116**, 763-771

ACKNOWLEDGMENTS

We thank the Kazusa DNA Research Institute, Chiba, Japan, for the gift of KIAA0678, Dave McKay (Stanford University) for Hsc70 cDNA, and Richard Scheller (Genentech) and Paul Luzio (University of Cambridge) for antibodies. We also thank Dr. John Bergeron and Ali Fazel (McGill University) for providing plasma membrane fractions, Elaine de Heuvel for excellent technical assistance, Brigitte Ritter and other members of the laboratory for advice and discussion, and Rob Sladek and Pierre Lepage of Genome Quebec for help with the BLAT program. This work was supported by grant MOP-105863 from the Canadian Institutes of Health Research (CIHR) to PSM. Operating grants from the Genome Quebec/Genome Canada project: Réseau Protéomique de Montréal, Montreal Proteomics Network (RPMPN) also supported this work. MG and VP are recipients of a CIHR studentship and a CIHR fellowship, respectively. PSM is a CIHR Investigator, a Killam Scholar of the Montreal Neurological Institute, and a McGill University William Dawson Scholar.

FIGURE LEGENDS

Figure 3.1. Amino acid sequence of human RME-8. *Dash line* denotes the DnaJ domain, *underlines* denote the IWN repeats, *bold letters* denote sequences that match a consensus for binding to the terminal domain of the CHC, and *double underlines* denotes the peptide sequence used to raise the RME-8 antibody.

Figure 3.2. Tissue distribution and membrane association of RME-8. *A* and *B*, equal protein aliquots of post-nuclear supernatants prepared from different rat tissues (*A*) or cultured cells (*B*) were processed by SDS-PAGE and Western blot with RME-8 antibody. *C*, equal protein aliquots of subcellular fractions prepared from kidney extracts were processed by SDS-PAGE and Western blot with RME-8 and pan-cadherin antibodies. *H*, homogenate; *P*, pellet; *S*, supernatant. *D*, equal protein aliquots of liver homogenate (*H*) and highly enriched plasma membrane (*PM*) were processed by SDS-PAGE and Western blot with RME-8, pan-cadherin and EGF receptor (*EGFR*) antibodies. *E*, equal protein aliquots of kidney P3 fraction were incubated with buffer A (*no extraction*), HEPES buffer containing 1% Triton X-100, 150 mM NaCl, or 500 mM NaCl, or $NaCO_3$ at pH 11.0. After 15 min of incubation, samples were spun for 15 min at 245,000 *g* and the resulting supernatants (*S*) and pellets (*P*) were processed by SDS-PAGE and Western blot with RME-8 and Na^+/K^+ ATPase antibodies.

Figure 3.3. Interaction of RME-8 with Hsc70. *A*, GST and a GST fusion protein encoding the DnaJ domain of RME-8 (GST-DnaJ) were coupled to glutathione-Sepharose and used for affinity selection assay from soluble kidney extracts. Kidney extract or buffer alone was incubated with (+) or without (-) 3 mM ATP for 10 min at 25°C before the addition to the fusion proteins. Proteins specifically bound to the beads along with a 1/10 aliquot of the kidney extract (starting material (*SM*)) were processed by SDS-PAGE and Coomassie Blue staining. The ~70 kDa protein that bound to the GST-DnaJ domain in the presence of ATP was excised and analyzed by tandem mass spectrometry revealing 33 unique peptides for Hsc70. All other bands detected were present when fusion proteins were incubated with buffer alone, indicating that they are

aggregated fusion protein or are proteins co-purifying from bacterial extracts. *B*, GST and GST-DnaJ domain fusion protein were coupled to glutathione-Sepharose and used for affinity selection assay from soluble kidney extracts. Kidney extracts were first incubated for 10 min at 25°C with EDTA (nucleotide-free, NF), 3 mM ADP, or 3 mM ATP. Proteins specifically bound to the beads along with a 1/10 aliquot of the kidney extract (starting material (*SM*)) were processed by SDS-PAGE and Western blot with Hsc70 antibody. *C*, equal protein aliquots of a soluble kidney extract containing no ATP (0) or increasing concentrations of ATP (1 μM to 5 mM in an ATP regenerating system) were incubated with GST-DnaJ domain pre-coupled to glutathione-Sepharose. Proteins specifically bound to the beads were processed by SDS-PAGE and Western blot with Hsc70 antibody.

Figure 3.4. Association of RME-8 with CCVs. *A*, GST and a GST fusion protein encoding the terminal domain of the CHC (GST-TD) were coupled to glutathione-Sepharose and used for affinity selection assay from soluble kidney extracts. Proteins specifically bound to the beads along with a 1/10 aliquot of the kidney extract (starting material (*SM*)) were processed by SDS-PAGE and Western blot with antibodies against RME-8, γ-adaptin (*AP-1*) and enthoprotin. *B*, equal protein aliquots of the various fractions of the subcellular fractionation procedure leading to highly enriched CCVs were processed by SDS-PAGE and Western blot with RME-8, auxilin 2, and CHC antibodies. *H*, homogenate; *P*, pellet; *S*, supernatant.

Figure 3.5. Localization of endogenous RME-8. *A-D*, endogenous RME-8 localization, determined by indirect immunofluorescence was compared to that of EEA1 (*A*), CY3-labeled transferrin that had been endocytosed for 20 min (*B*), CI-MPR (*C*), and Texas Red labeled EGF (*D*) that had been endocytosed for 20 min. A blend of the RME-8 staining (*green*) with the various markers (*red*) is revealed in the *left-most panels* (*blend low mag*). Higher magnification individual images of RME-8 and the respective markers as well as a blend of these images (*blend high mag*) are from the areas indicated by *boxes* in the *lower magnification images*. *E*, panels are presented as in *A-D*, except that localization of endogenous EGF receptor (*EGFR*), determined by indirect

immunofluorescence, was compared to that of Texas Red-labeled EGF that had been endocytosed for 20 min. For *A-C*, *arrows* point to co-localizing punca. In *D* and *E*, *arrows* indicate where RME-8 and EGF receptor is found in punca that surround EGF puncta. *Scale bars* represent 10 and 2 μm for the low and high magnification images, respectively.

Figure 3.6. siRNA-mediated RME-8 knock down. A and B, COS-7 cells were transfected twice at 24-h intervals without (Mock) or with RME-8.3 siRNA. At 72 h past the first transfection cells were processed by indirect immunofluorescence with RME-8 antibody (A) or cell lysates were prepared and equal protein aliquots were processed by SDS-PAGE and Western blot with antibodies for the various proteins indicated (B). Blot signals for RME-8 were quantified using ImageJ software, and the signal in the siRNA-treated cells was plotted in relation to the mock-treated cells, which was set to 100%. The scale bar represents 10 μm.

Figure 3.7. RME-8 knock down cells have reduced EGF endocytosis. *A*, mock or RME-8.3 siRNA transfected COS-7 cells were allowed to endocytose Cy3-transferrin or Texas Red-EGF for 15 min and were then fixed and processed by indirect immunofluorescence with antibody against RME-8. *Scale bars* represent 10 μm. *B*, mock or RME-8.3 transfected cells were lysed, and equal protein aliquots were processed by SDS-PAGE and Western blot with antibodies against EGF receptor (*EGFR*) and transferrin receptor (*TfR*). *C*, cells were treated as in *A* except that transferrin-Alexa Fluor 647 or EGF-Alexa Fluor 488 was used. The percentage of transferrin and EGF internalized by the cells was determined by fluorescence-activated cell sorting analysis as described under "Experimental Procedures". *D*, mock or RME-8.3 siRNA-transfected COS-7 cells were allowed to endocytose Alexa 594-cholera toxin B (*CTB*) and were then fixed and processed by indirect immunofluorecence with antibody against RME-8. The *scale bar* represents 10 μm.

Figure 3.8. Knock down of RME-8 alters CHC distribution. *A*, mock or RME-8.3 siRNA-transfected COS-7 cells were fixed and processed by indirect

immunofluorecence with antibodies against RME-8 and CHC. *B*, cells prepared as described for *A* were scanned in both the *x-y* plane (*top panels*) and with a *z* section (*bottom panels*) from the region indicated by the *blue line*. For *A* and *B*, *scale bars* represent 10 and 5 μm, respectively. *C*, cells were grouped into two categories based on the presence or absence of CHC redistribution.

Figure 3.9. Knock down of RME-8 alters CI-MPR trafficking. *A*, mock or RME-8.3 siRNA-transfected COS-7 cells were processed by indirect immunofluorescence with antibodies for RME-8 and CI-MPR. The *scale bar* represents 10 μm. *B*, RME-8.3-transfected cells were processed by indirect immunofluorescence with antibodies against CI-MPR and either syntaxin 6 or VAMP 4. Blends of the CI-MPR staining (*green*) with syntaxin 6 (*red*) and the CI-MPR (*red*) with VAMP 4 (*green*) are revealed in the *right-most panels*. The *scale bar* represents 2 μm. *C*, COS-7 cells transfected twice at 24 h intervals without (*Mock*) or with RME-8.3 siRNA were pulsed for 10 min with ^{35}S-labeled methione/cysteine followed by a chase with unlabeled methione. At the indicated time points, cathepsin D was immunoprecipitated from cell lysates (C) or culture media (*M*), and the immunoprecipitated samples were analyzed by SDS-PAGE and autoradiography. *D*, the mean ± S.E. of the percentage of sorted cathepsin D is plotted for Mock and RME-8.3 transfected cells for the 3 h (n=9) and 4 h (n=11) time points. Paired t tests reveal a significance of less than 0.01 and 0.001 for the 3- and 4-h time points, respectively. Note that the y axis has been truncated at 30%.

```
   1 MNIIRENKDLACFYTTKHSWRGKYKRVFSVGTHAITTYNPNTLEVTNQWP
  51 YGDICSISPVGKGQGTEFNLTFRKGSGKKSETLKFSTEHRTELLTEALRF
 101 RTDFSEGKITGRRYNCYKHHWSDSRKPVILEVTPGGFDQINPATNRVLCS
 151 YDYRNIEGFVDLSDYQGGFCILYGGFSRLHLFASEQREEIIKSAIDHAGN
 201 YIGISLRIRKEPLEFEQYLNLRFGKYSTDESITSLAEFVVQKISPRHSEP
 251 VKRVLALTETCLVERDPATYNIATLKPLGEVFALVCDSENPQLFTIEFIK
 301 GQVRKYSSTERDSLLASLLDGVRASGNRDVCVKMTPTHKGQRWGLLSMPV
 351 DEEVESLHLRFLATPPNGNFADAVFRFNANISYSGVLHAVTQDGLFSENK
 401 EKLINNAITALLSQEGDVVASNAELESQFQAVRRLVASKAGFLAFTQLPK
 451 FRERLGVKVVKALKRSNNGIIHAAVDMLCALMCPMHDDYDLRQEQLNKAS
 501 LLSSKKFLENLLEKFNSHVDHGTGALVISSLLDFLTFALCAPYSETTEGQ
 551 QFDMLLEMVASNGRTLFKLFQHPSMAIIKGAGLVMKAIIEEGDKEIATKM
 601 QELALSEGALPRHLHTAMFTISSDQRMLTNRQLSRHLVGLWTADNATATN
 651 LLKRILPPGLLAYLESSDLVPEKDADRMHVRDNVKIAMDQYGKFNKVPEW
 701 QRLAGKAAKEVEKFAKEKVDLVLMHWRDRMGIAQKENINQKPVVLRKRRQ
 751 RIKIEANWDLFYYRFGQDHARSNLIWNFKTREELKDTLESEMRAFNIDRE
 801 LGSANVISWNHHEFEVKYECLAEEIKIGDYYLRLLLEEDENEESGSIKRS
 851 YEFFNELYHRFLLTPKVNMKCLCLQALAIVYGRCHEEIGPFTDTRYIIGM
 901 LERCTDKLERDRLILFLNKLILNKKNVKDLMDSNGIRILVDLLTLAHLHV
 951 SRATVPLQSNVIEAAPDMKRESEKEWYFGNADKERSGPYGFHEMQELWTK
1001 GMLNAKTRCWAQGMDGWRPLQSIPQLKWCLLASGQAVLNETDLATLILNM
1051 LITMCGYFPSRDQDNAIIRPLPKVKRLLSDSTCLPHIIQLLLTFDPILVE
1101 KVAILLYHIMQDNPQLPRLYLSGVFFFIMMYTGSNVLPVARFLKYTHTKQ
1151 AFKSEETKGQDIFQRSILGHILPEAMVCYLENYEPEKFSEIFLGEFDTPE
1201 AIWSSEMRRLMIEKIAAHLADFTPRLQSNTRALYQYCPIPIINYPQLENE
1251 LFCNIYYLKQLCDTLRFPDWPIKDPVKLLKDTLDAWKKEVEKKPPMMSID
1301 DAYEVLNLPQGQGPHDESKIRKAYFRLAQKYHPDKNPEGRDMFEKVNKAY
1351 EFLCTKSAKIVDGPDPENIILILKTQSILFNRHKEDLQPYKYAGYPMLIR
1401 TITMETSDDLLFSKESPLLPAATELAFHTVNCSALNAEELRRENGLEVLQ
1451 EAFSRCVAVLTRASKPSDMSVQVCGYISKCYSVAAQFEECREKITEMPSI
1501 IKDLCRVLYFGKSIPRVAALGVECVSSFAVDFWLQTHLFQAGILWYLLGF
1551 LFNYDYTLEESGIQKSEETNQQEVANSLAKLSVHALSRLGGYLAEEQATP
1601 ENPTIRKSLAGMLTPYVARKLAVASVTEILKMLNSNTESPYLIWNNSTRA
1651 ELLEFLESQQENMIKKGDCDKTYGSEFVYSDHAKELIVGEIFVRVYNEVP
1701 TFQLEVPKAFAASLLDYIGSQAQYLHTFMAITHAAKVESEQHGDRLPRVE
1751 MALEALRNVIKYNPGSESECIGHFKLIFSLLRVHGAGQVQQLALEVVNIV
1801 TSNQDCVNNIAESMVLSSLLALLHSLPSSRQLVLETLYALTSSTKIIKEA
1851 MAKGALIYLLDMFCNSTHPQVRAQTAELFAKMTADKLIGPKVRITLMKFL
1901 PSVFMDAMRDNPEAAVHIFEGTHENPELIWNDNSRDKVSTTVREMMLEHF
1951 KNQQDNPEANWKLPEDFAVVFGEAEGELAVGGVFLRIFIAQPAWVLRKPR
2001 EFLIALLEKLTELLEKNNPHGETLETLTMATVCLFSAQPQLADQVPPLGH
2051 LPKVIQAMNHRNNAIPKSAIRVIHALSENELCVRAMASLETIGPLMNGMK
2101 KRADTVGLACEAINRMFQKEQSELVAQALKADLVPYLLKLLEGIGLENLD
2151 SPAATKAQIVKALKAMTRSLQYGEQVNEILCRSSVWSAFKDQKHDLFISE
2201 SQTAGYLTGPGVAGYLTAGTSTSVMSNLPPPVDHEAGDLGYQT*
```

FIGURE 3.1

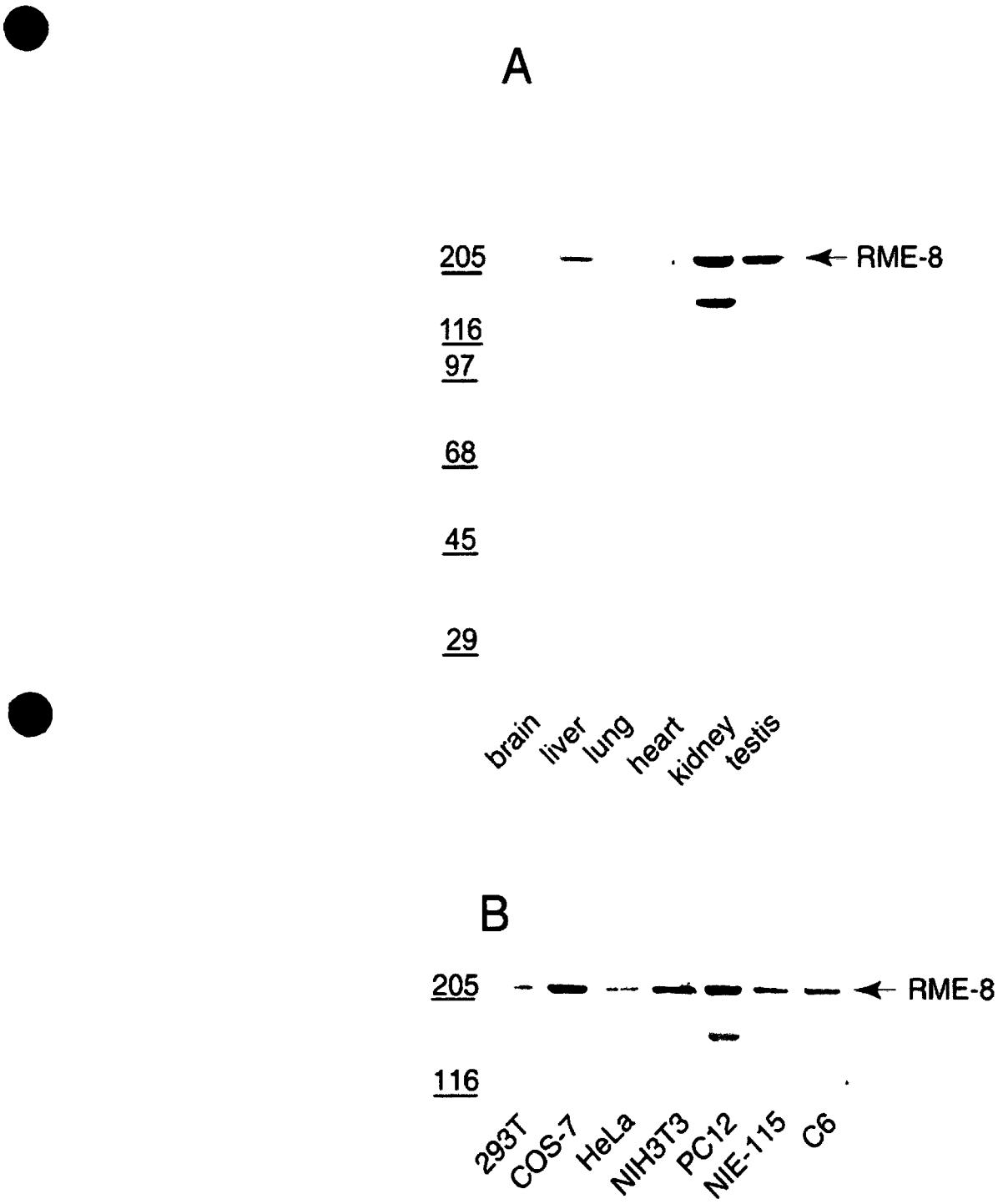
A
205
116
97
68
45
29
RME-8
brain
liver
lung
heart
kidney
testis
B
205
116
RME-8
293T
COS-7
HeLa
NIH3T3
PC12
NIE-115
C6

FIGURE 3.2

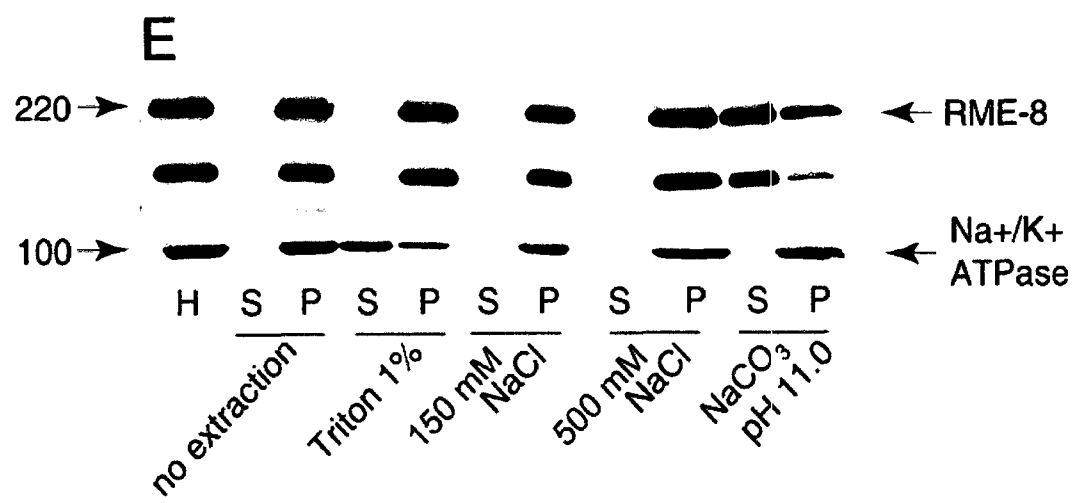

FIGURE 3.2 (next)

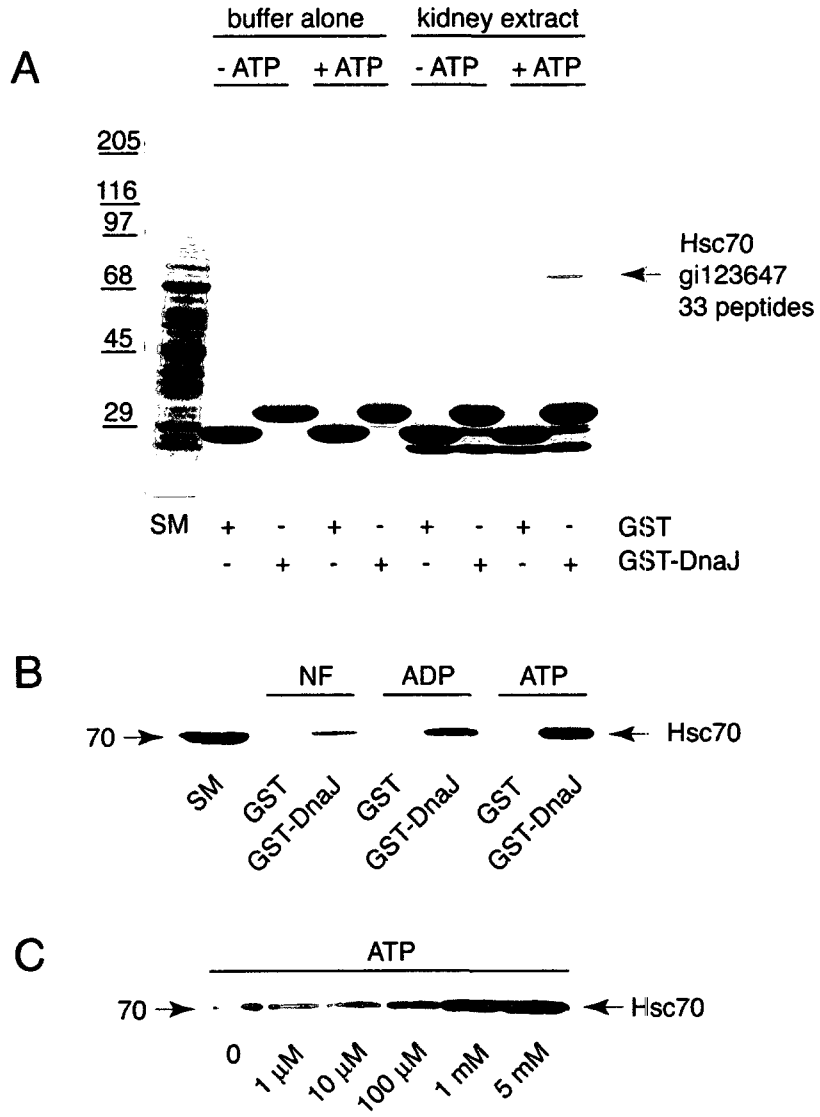
A
buffer alone
kidney extract
- ATP
+ ATP
- ATP
+ ATP
205
116
97
68
45
29
Hsc70
gi123647
33 peptides
SM
+ - + - + - + - GST
- + - + - + - + GST-DnaJ
B
NF
ADP
ATP
70
Hsc70
SM
GST
GST-DnaJ
GST
GST-DnaJ
GST
GST-DnaJ
C
ATP
70
Hsc70
0
1 µM
10 µM
100 µM
1 mM
5 mM

FIGURE 3.3

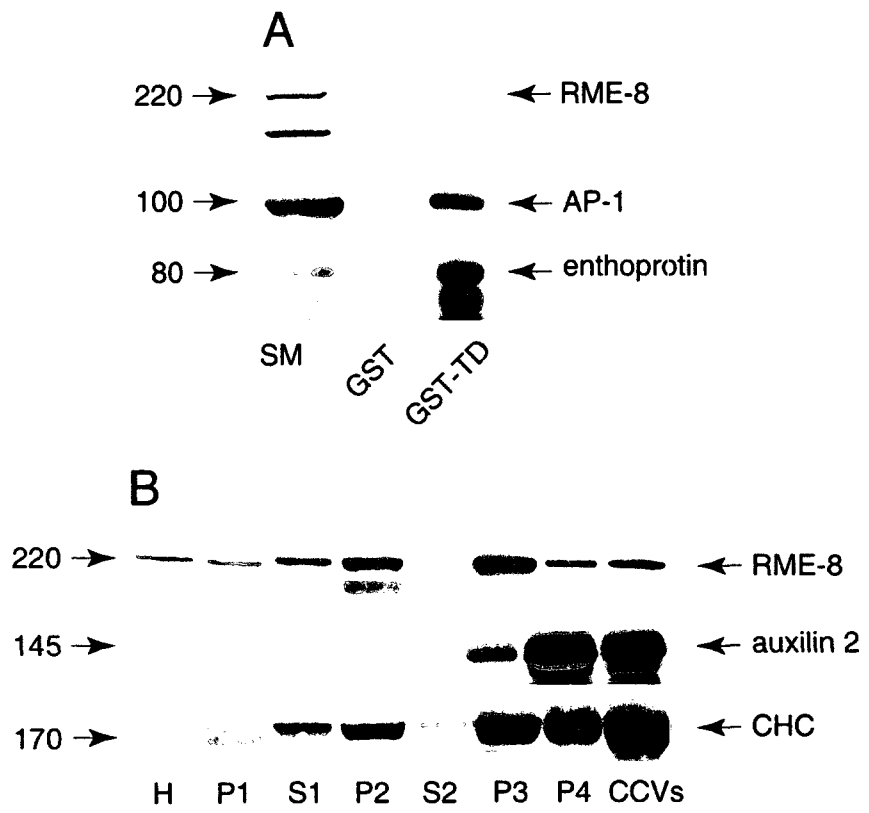
A
220
100
80
RME-8
AP-1
enthoprotin
SM
GST
GST-TD
B
220
145
170
RME-8
auxilin 2
CHC
H
P1
S1
P2
S2
P3
P4
CCVs

FIGURE 3.4

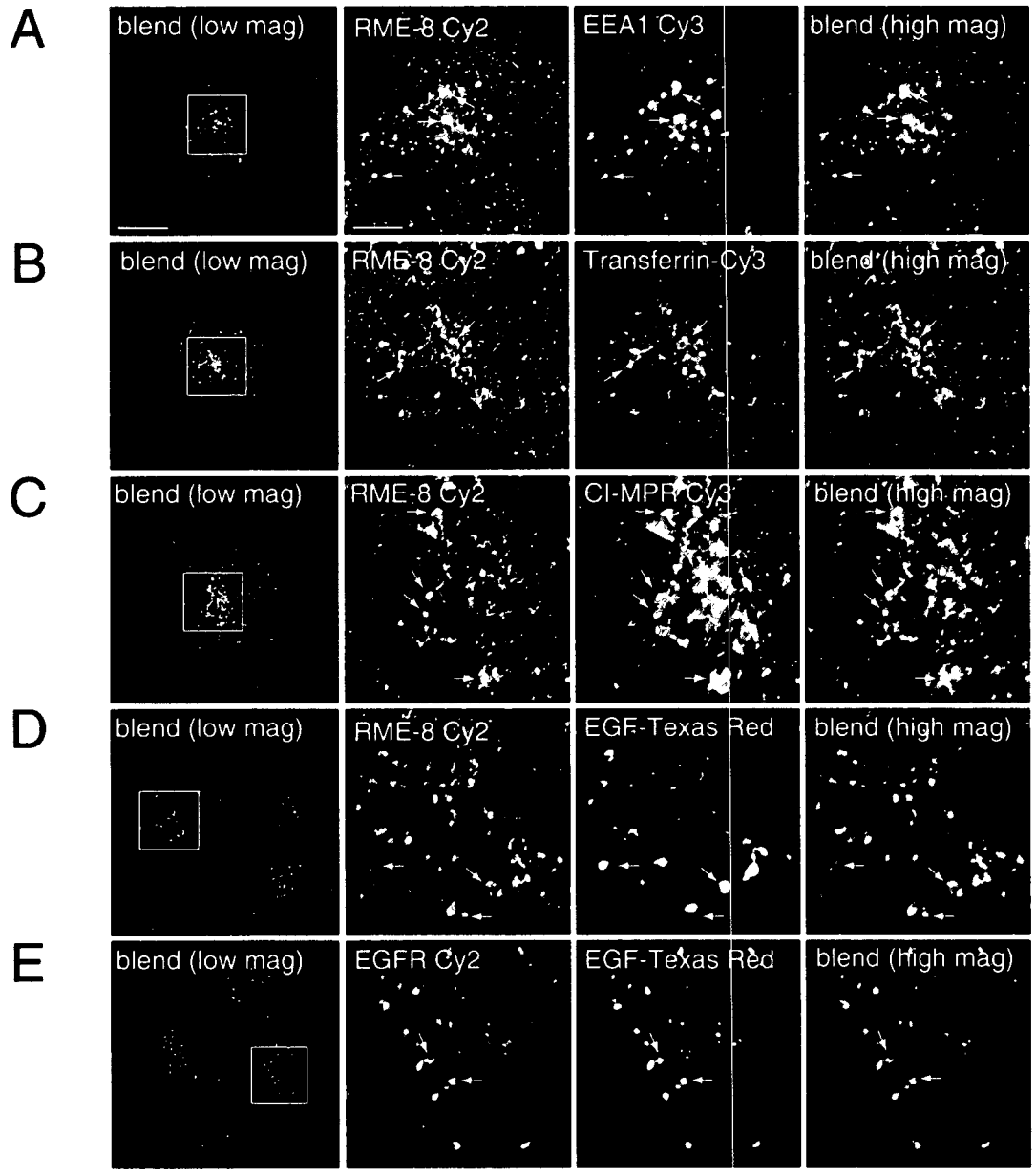
A
blend (low mag)
RME-8 Cy2
EEA1 Cy3
blend (high mag)
B
blend (low mag)
RME-8 Cy2
Transferrin-Cy3
blend (high mag)
C
blend (low mag)
RME-8 Cy2
CI-MPR Cy3
blend (high mag)
D
blend (low mag)
RME-8 Cy2
EGF-Texas Red
blend (high mag)
E
blend (low mag)
EGFR Cy2
EGF-Texas Red
blend (high mag)

FIGURE 3.5

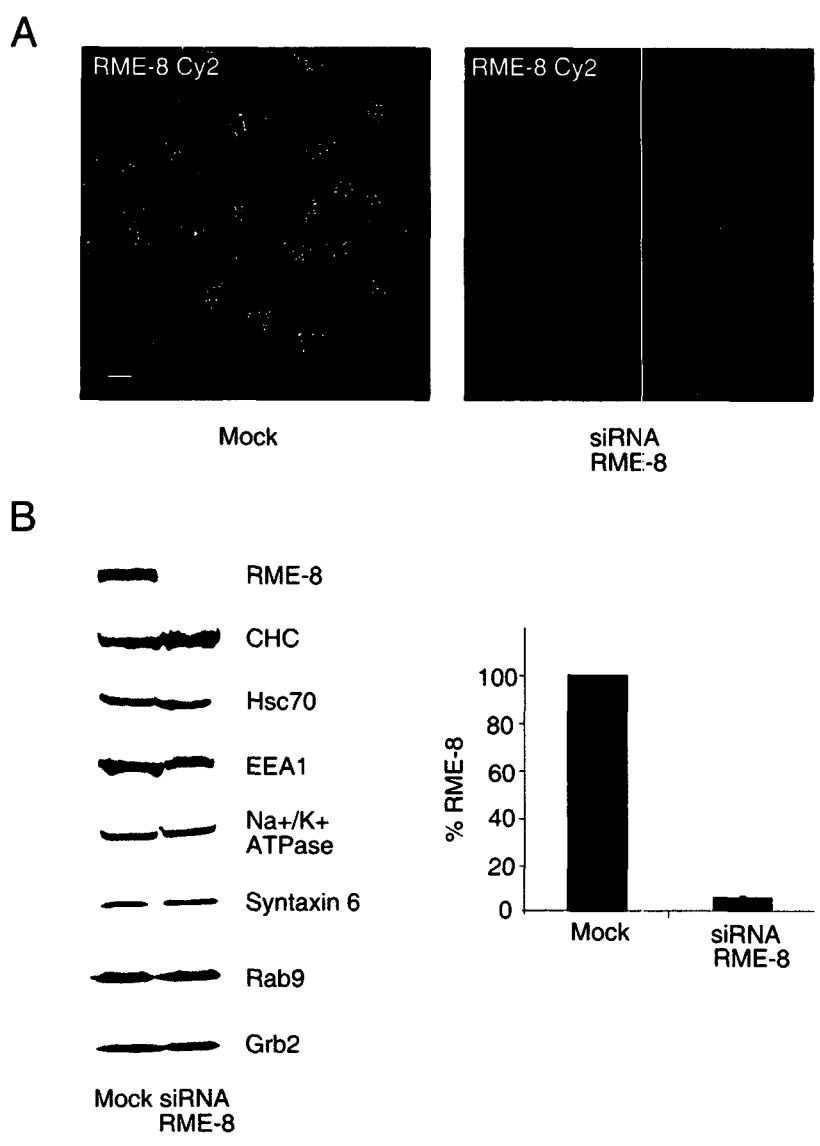
A
RME-8 Cy2
RME-8 Cy2
Mock
siRNA
RME-8
B
RME-8
CHC
Hsc70
EEA1
Na+/K+
ATPase
Syntaxin 6
Rab9
Grb2
Mock siRNA
RME-8
% RME-8
100
80
60
40
20
0
Mock
siRNA
RME-8

FIGURE 3.6

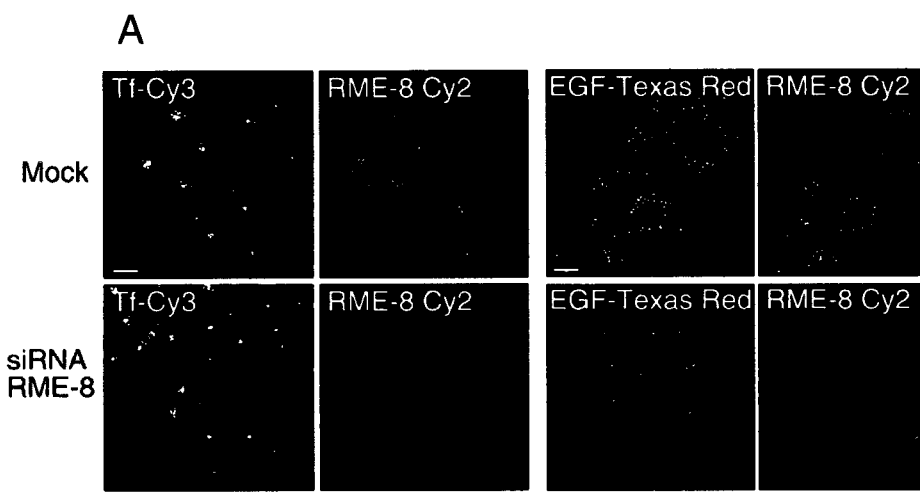
A
Tf-Cy3
RME-8 Cy2
EGF-Texas Red
RME-8 Cy2
Mock
siRNA
RME-8
Tf-Cy3
RME-8 Cy2
EGF-Texas Red
RME-8 Cy2

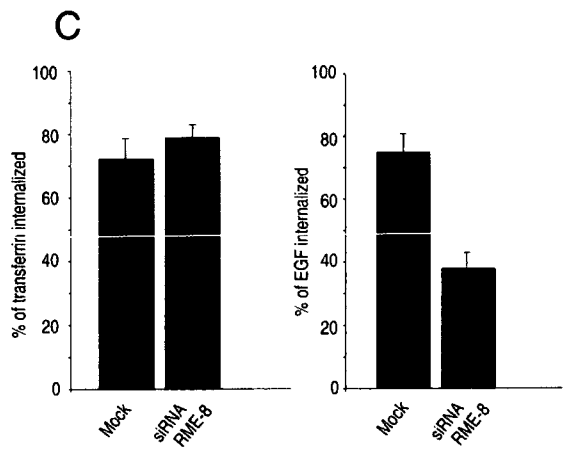
C
% of transferrin internalized
100
80
60
40
20
0
Mock
siRNA RME-8
% of EGF internalized
100
80
60
40
20
0
Mock
siRNA RME-8

FIGURE 3.7

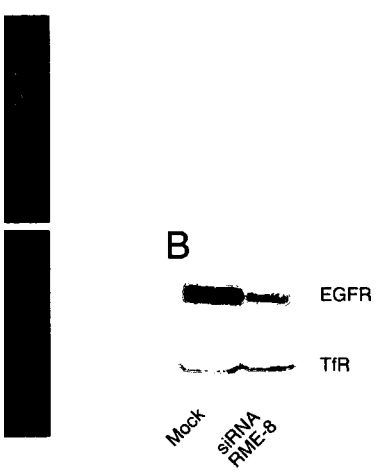
B
EGFR
TfR
Mock
siRNA
RME-8

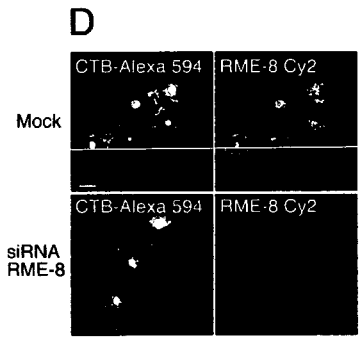
D
CTB-Alexa 594
RME-8 Cy2
Mock
CTB-Alexa 594
RME-8 Cy2
siRNA
RME-8

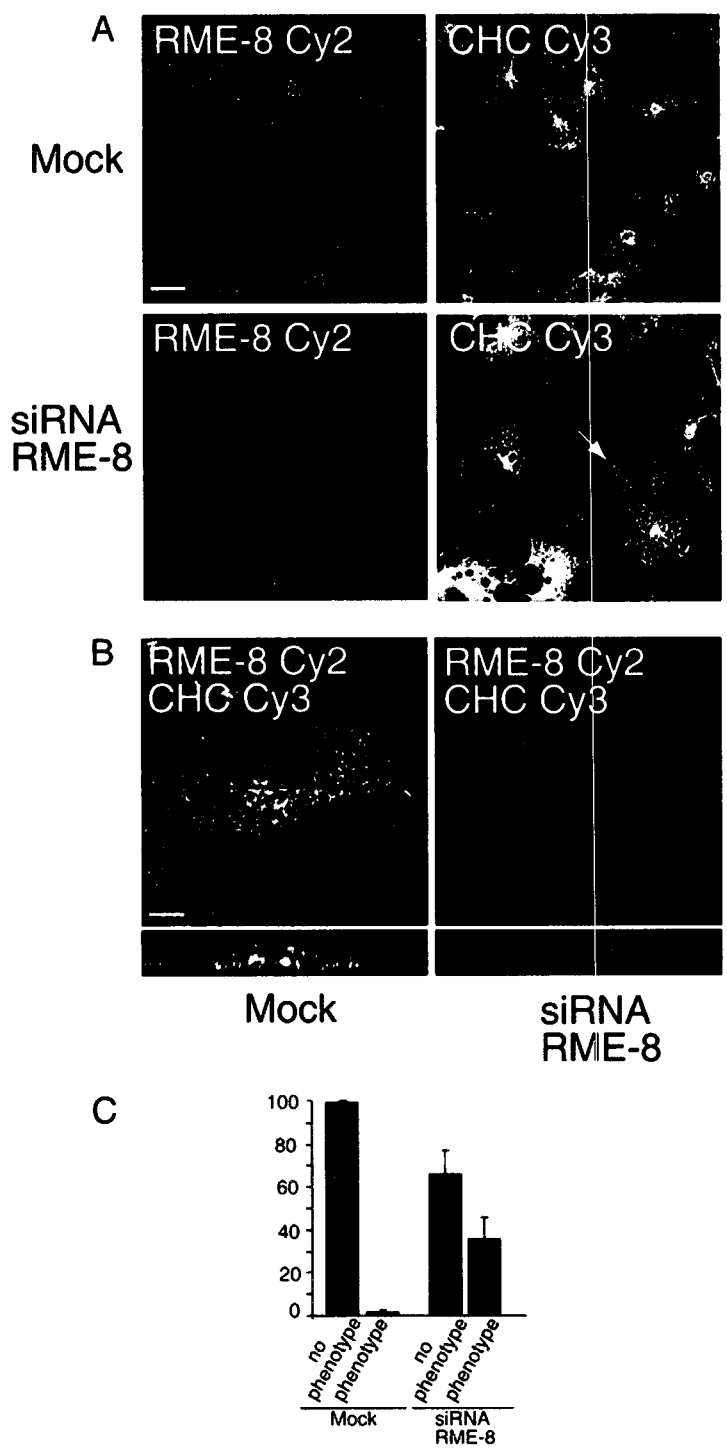
A
RME-8 Cy2
CHC Cy3
Mock
RME-8 Cy2
CHC Cy3
siRNA
RME-8
B
RME-8 Cy2
CHC Cy3
RME-8 Cy2
CHC Cy3
Mock
siRNA
RME-8
C
100
80
60
40
20
0
no phenotype
phenotype
no phenotype
phenotype
Mock
siRNA
RME-8

FIGURE 3.8

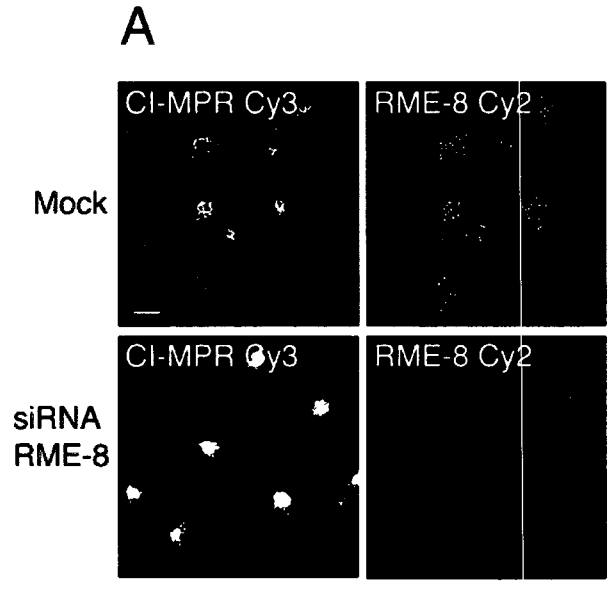
A
CI-MPR Cy3
RME-8 Cy2
Mock
CI-MPR Cy3
RME-8 Cy2
siRNA
RME-8

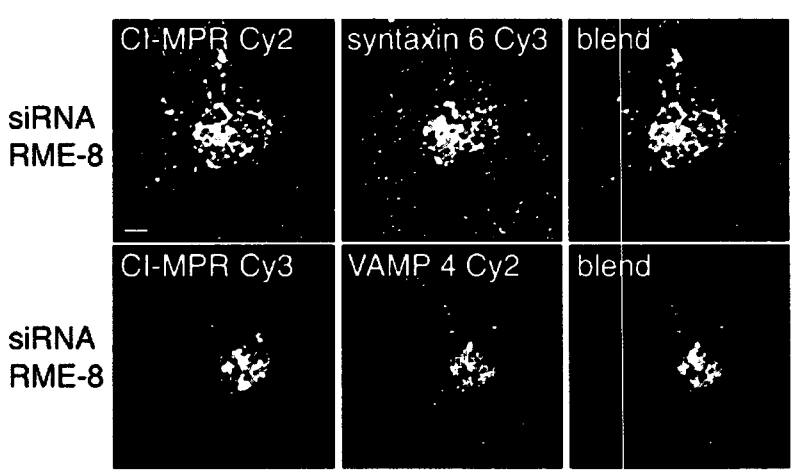
B
CI-MPR Cy2
syntaxin 6 Cy3
blend
siRNA
RME-8
CI-MPR Cy3
VAMP 4 Cy2
blend
siRNA
RME-8

FIGURE 3.9

C

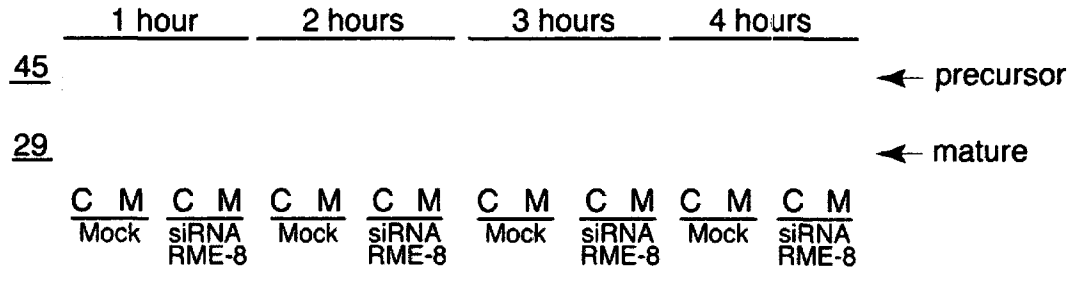

D

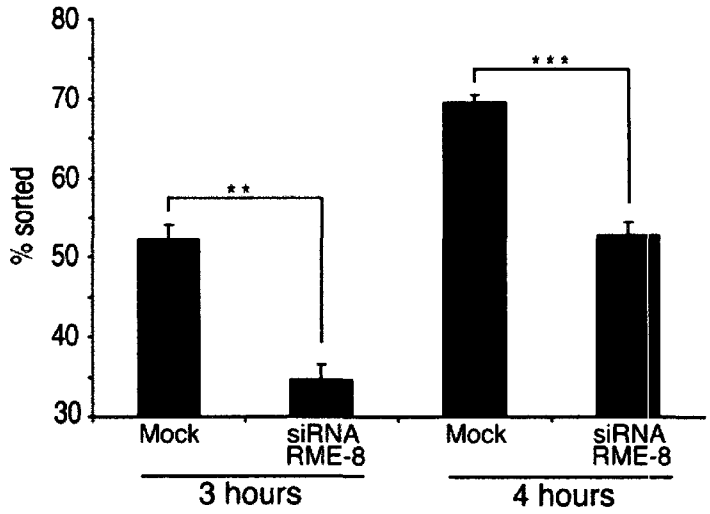

FIGURE 3.9 (next)

SUPPLEMENTAL FIGURE LEGENDS

FIGURE 3.S1. Mock or RME-8.3 siRNA transfected COS-7 cells were processed by indirect immunofluorescence with antibodies for α-adaptin (AP-2) and RME-8. The higher magnification images (bottom panels) are from the areas indicated by boxes. The scale bars represent 10 and 2 μm for the low magnification and high magnification images, respectively.

FIGURE 3.S2. RME-8.3 transfected cells were incubated at 37°C with 10 ng/ml Texas Red-EGF for 15 min and were then fixed and processed by indirect immunofluorecence with antibodies against CHC and RME-8. The higher magnification images in the bottom six panels are from the areas indicated by the boxes in the lower magnification images in the top panel. The images in the middle panels provides an example of a cell in which clathrin depletion from the cytosol correlates to a complete block in EGF endocytosis whereas the images in the bottom panels provides an example of a cell in which a seemingly normal clathrin distribution correlates to detectable EGF internalization. Scale bars represent 10 μm and 2 μm for the low and high magnification images, respectively.

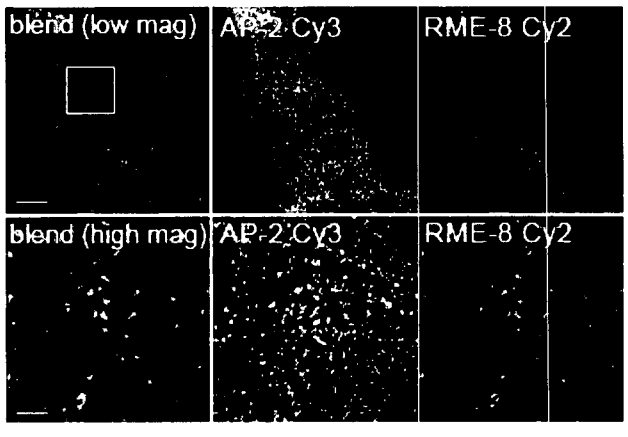

Mock

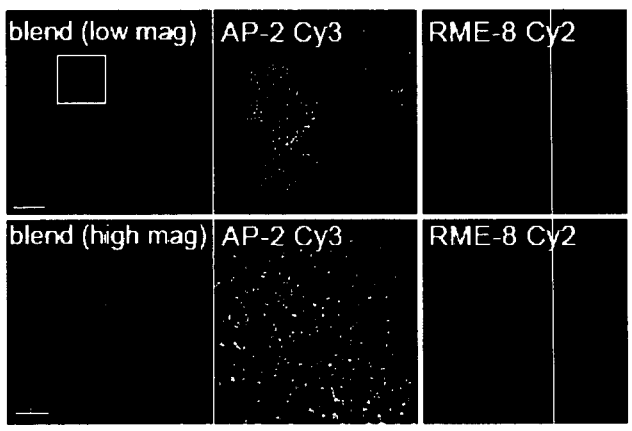

siRNA
RME-8

SUPPLEMENTAL FIGURE 3.S1

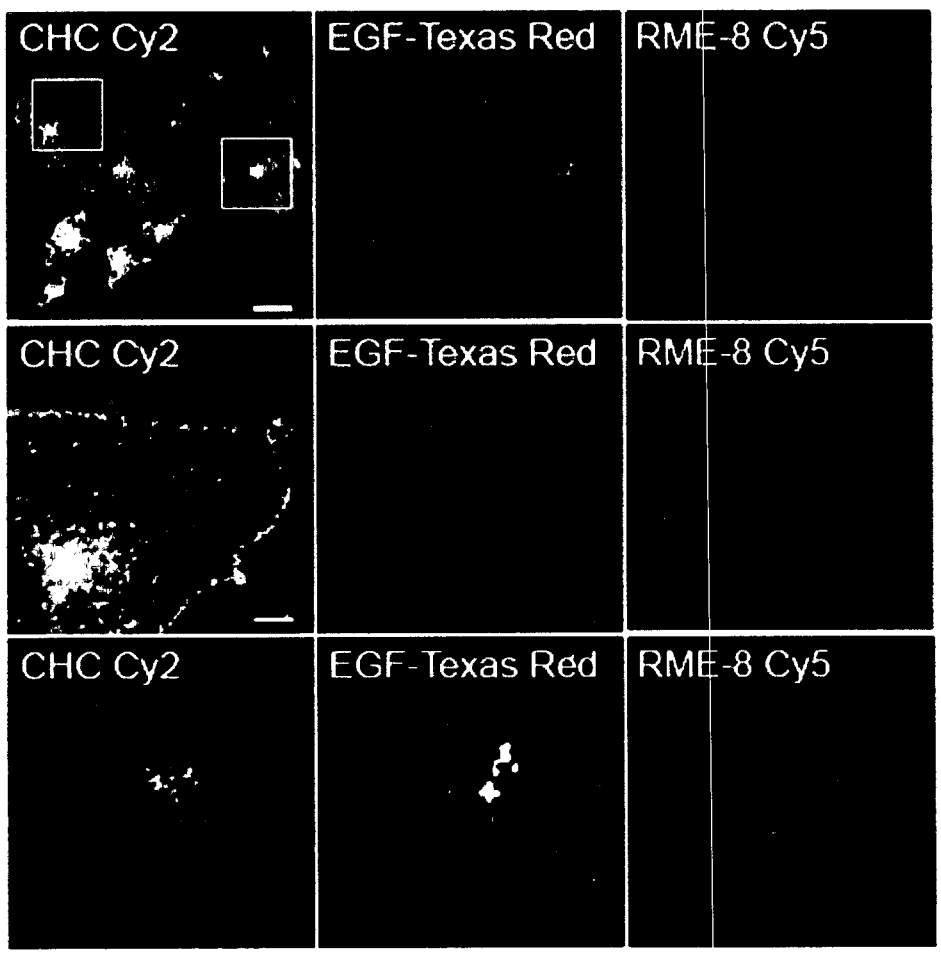

siRNA RME-8

SUPPLEMENTAL FIGURE 3.S2

PREFACE TO CHAPTER 4

Chapter 3 aimed to characterize RME-8 and provide the foundation in understanding its functional role in the intracellular trafficking network. During the course of this study, we observed that the steady-state expression levels of EGFR were decreased upon RME-8 depletion (Girard et al., 2005b).

EGFR is a key player in regulating different cellular processes such as proliferation, migration, tumorigenesis and metastasis (Ullrich and Schlessinger, 1990). It is therefore not surprising that EGFR itself is subjected to tight regulatory control. Upon ligand-induced endocytosis, EGFR is normally degraded in the lysosomes and this downregulation has a major role in its cellular activity (Wang et al., 1999; Ceresa and Schmid, 2000). However, when EGFR heterodimerizes with another member of the EGFR family, ErbB2, the complex is recycled back to the plasma membrane and that situation causes dramatic effects such as an increase in signalling and proliferation that is also seen in many cancers (Wang et al., 1999; Ceresa and Schmid, 2000).

In this chapter, we demonstrate that RME-8 depletion does not affect recycling receptors but increases EGFR degradation rates and consequently decreases its steady-state expression levels. We also show that RME-8 depletion can cause a decrease in EGFR protein levels, even in cancer cell lines that are overexpressing ErbB2. Not only does this paper propose RME-8 as a regulator of EGFR trafficking and degradation but it also suggests that RME-8 could be a valuable target in cancer treatment.

CHAPTER 4

RME-8 REGULATES TRAFFICKING OF THE EPIDERMAL GROWTH FACTOR RECEPTOR

Martine Girard and Peter S. McPherson

Department of Neurology and Neurosurgery, Montreal Neurological Institute, McGill University, Montreal, QC H3A 2B4, Canada

Abstract

We recently identified receptor-mediated endocytosis 8 (RME-8) as a DnaJ domain-bearing protein localized to endosomes. We now demonstrate that siRNA-mediated knock down (KD) of RME-8 leads to a decrease in the steady-state expression level of epidermal growth factor receptor (EGFR) without influencing the levels of receptors that primarily recycle to the plasma membrane. Decreases in EGFR are detected at both surface and intracellular pools. RME-8 KD significantly increases EGFR degradation rates without influencing the rate of synthesis, providing a potential mechanism to explain the alterations in receptor levels. Interestingly, RME-8 KD also leads to a decrease in EGFR levels in breast cancer cell lines in which overexpression of the EGFR family member ErbB2 has been shown to protect EGFR from degradation. These data implicate RME-8 in sorting decisions influencing EGFR at the level of endosomes and point to RME-8 as a potential regulatory target in ErbB2-positive breast cancers.

1. Introduction

Clathrin-coated vesicles (CCVs) are the major carriers for endocytic cargo. Following their fission from the plasma membrane, CCVs uncoat and fuse with early endosomes, the initial sorting station in the endocytic pathway [1]. Cargo such as the transferrin receptor (TfR), which predominantly recycle, segregate into thin membrane tubules that bud off endosomes for transport back to the plasma membrane [1] whereas the remaining early endosome develops into late endosomes, possibly through a series of fusion and fission events coupled with retrograde flow of early endosome resident proteins [2]. Cargo, such as the epidermal growth factor receptor (EGFR), which are predominantly degraded undergo inward invagination into the lumen of the endosome during the maturation process leading to multivesicular bodies (MVBs) that fuse with lysosomes for degradation [1,3].

The process by which cargo is targeted for inward invagination is complex and involves four protein assemblies on endosomal membranes referred to as endosomal sorting complex required for transport (ESCRT) 0 through ESCRT III [4]. Receptors targeted for degradation, such as EGFR are tagged with ubiquitin [5], which is recognized by Hrs within the ESCRT 0 complex [4]. The ubiquitinated cargo is then transferred to the other ESCRT complexes and is eventually coupled to the machinery for inward budding [4]. Hrs binds to phosphatidylinositol-3-P, which is enriched on early endosomes, and also binds clathrin, helping recruit clathrin to early endosome membranes where it forms a poorly defined bilayered clathrin coat that in turn stabilizes Hrs and restricts it to the regions of the endosome where inward invagination occurs [6,7]. Like other clathrin coats [8], the bilayered coat undergoes a dynamic exchange with the cytosol, fluctuating between assembled (membrane associated) and disassembled (cytosolic) states and interestingly, the degree of association of the Hrs-rich coat with the membrane is a critical factor in recruiting ubiquitinated cargo for eventual degradation [7].

We recently identified and characterized the mammalian form of receptor-

mediated endocytosis 8 (RME-8) [9], a DnaJ domain-containing protein originally identified in a screen for endocytic defects in *C. elegans* [10]. As for RME-8 in invertebrates and plants, mammalian RME-8 co-localizes with multiple markers of the endosomal system including internalized transferrin and EGF and the early endosomal marker EEA1 [9-12]. Through its DnaJ domain, RME-8 binds the chaperone Hsc70 [9,11], which regulates uncoating of CCVs [13-15] and which is also involved, in an unknown manner, in regulating receptor trafficking at endosomes [16]. We now use a loss of function approach to demonstrate that RME-8 regulates the cellular levels of EGFR by contributing to the control of EGFR endosomal trafficking and degradation.

2. Materials and methods

2.1. Antibodies

A polyclonal RME-8 antibody was previously described [9]. Mouse monoclonal antibodies against the following proteins were purchased from the indicated commercial sources: Na^+/K^+ ATPase, Upstate Biotechnology (Lake Placid, NY); EGFR, Santa Cruz Biotechnology (Santa Cruz, CA); TfR, Zymed Laboratories Inc. (South San Francisco, CA). Polyclonal antibodies against EGFR, LDLR and ErbB2 were from Santa Cruz Biotechnology (Santa Cruz, CA), Fitzgerald Industries International Inc. (Concord, MA) and Abcam (Cambridge, MA), respectively. Polyclonal antibody against insulin receptor was a gift of Dr. John Bergeron (McGill University, Montreal, Canada). Dr. William Muller (McGill University, Montreal, Canada) kindly provided SKBR3 and BT474 cell lines.

2.2. Analysis of protein levels following siRNA-mediated KD of RME-8

RME-8 siRNA and transfection procedures were previously described [9]. Briefly, COS-7, HeLa, SKBR3 or BT474 cells were plated in DMEM without antibiotics at 60% confluency. At 24 h post-plating, cells were transfected once with 80 nM siRNA using Lipofectamine 2000 (Invitrogen) with the transfection repeated 24 h later. Experiments were performed 72 h after the first transfection for COS-7 and HeLa, and 96 h after the first transfection for SKBR3 and BT474. For Western blot, cells were scrapped in RIPA buffer (10 mM HEPES, pH 7.4, 150 mM NaCl, 1% Triton X-100 and 0.1%SDS supplemented with 0.83 mM benzamidine, 0.23 mM phenylmethylsulfonyl fluoride, 0.5 μg/ml aprotinin and 0.5 μg/ml leupeptin) and centrifuged for 10 min at 800 x g. Proteins from equal protein aliquots of the supernatant were separated by SDS-PAGE, analyzed by Western Blot and blot signals were quantified using NIH ImageJ software.

2.3 EGFR immunofluorescence and FACS analysis

For EGFR immunofluorescence, COS-7 cells were plated on poly-L-lysine coverslips. One set of cells (surface EGFR) was cooled to 4°C, washed in cold PBS, incubated for 3 h on ice with an antibody against EGFR, fixed for 20 min with 3% ice-cold paraformaldehyde (PFA) and incubated with a CY3-conjugated secondary antibody. A second set of cells (total EGFR) was first fixed in 3% PFA, pre-permeabilized for 10 min with 0.05% saponin, incubated for 3 h with EGFR antibody diluted in 0.05% saponin, followed by detection using a CY3-conjugated secondary antibody. Immunofluorescence images were collected using a Zeiss 510 laser scanning confocal microscope and the acquisition settings were kept constant between mock and siRNA treated cells.

Fluorescence activated cell sorting analysis (FACS) was performed using FACScan with data analyzed using the CellQuantPro program (BD Biosciences). COS-7 cells, mock transfected or transfected with RME-8 siRNA were first cooled on ice. One set of cells, used to assess the level of surface EGFR, was incubated with EGFR antibody at 4°C for 3 h, washed with cold PBS, incubated with CY2-conjugated secondary antibody at 4°C for 1 h and resuspended in cold PBS. A second set of cells, used to assess total EGFR level, was pre-permeabilized with 0.05% saponin, incubated with EGFR antibody diluted in 0.05% saponin for 3 h at 4°C, washed with cold PBS, incubated with CY2-conjugated secondary antibody at 4°C for 1 h and resuspended in cold PBS.

2.4. EGFR degradation assay

Mock and RME-8 KD COS-7 cells were serum-starved O/N and then incubated for 1 h at 37°C in cysteine/methionine-free DMEM (Invitrogen). Cells were then pulsed for 2 h at 20°C with 0.1 mCi/ml Pro-Mix [^{35}S] (Amersham Biosciences), washed, and chased at 37°C for 0, 2, 4, and 6 h in DMEM containing methionine (0.06 mg/ml), cysteine (0.1

mg/ml), cycloheximide (25 ug/ml), and EGF (100 ng/ml). At each time point, the cells were washed, lysed (50 mM TRIS pH 7.4, 150 mM NaCl, 10% glycerol, 5mM EDTA, 1% Triton X-100), spun at 20000 x g max and equal protein aliquots of the supernatants were added to 25 µl protein-G beads (Amersham Biosciences) and 10 µl of EGFR monoclonal antibody in order to immunoprecipitate EGFR. Immunoprecipitated proteins were separated on SDS-PAGE and processed for autoradiography using a STORM PhosphorImager (Amersham Biosciences) followed by exposure to x-ray film. Quantification was performed using ImageQuant software.

3. Results and discussion

We previously established conditions using small inhibitory RNA (siRNA) to knock down (KD) RME-8 in cultured cells without influencing the levels of multiple control proteins [9]. During these studies, we noticed that the steady-state level of endogenous EGFR was decreased following loss of RME-8 function in COS-7 cells [9]. We thus sought to further examine this intriguing observation. Importantly, the decrease in EGFR levels resulting from RME-8 KD is not limited to COS-7 cells and is also seen in HeLa cells (Fig. 4.1A). EGFR is decreased by 46.6% and 65.5% of that in control in COS-7 and HeLa, respectively (Fig. 4.1B). The decrease in total level of EGFR was also readily detectable by immunofluorescence when using an EGFR antibody on fixed and permeabilized COS-7 cells (Fig. 4.2A). This decrease appeared to be roughly proportional to a decrease in surface levels as determined by adding the EGFR antibody (which recognizes the extracellular domain) to live cells at 4°C prior to washing and fixation (Fig. 4.2A). To quantify this observation, we performed FACS to measure total versus surface levels of EGFR in control and RME-8 KD conditions. We detected a similar decrease for total and surface pools, 35.5% and 39.3%, respectively (Fig. 4.2B), consistent with the decrease in COS-7 cells measured by Western blot (Fig. 4.1). Thus, the decrease in EGFR levels does not represent a selective loss of the surface pool of receptor.

In contrast to EGFR, the levels of TfR and insulin receptor (InsR) in COS-7 and HeLa cells and the level of low-density lipoprotein receptor (LDLR) in HeLa cells (LDLR is not detected in COS-7 cells with the antibody employed) are unaltered following RME-8 KD (Fig. 1A/B). Na^+/K^+-ATPase is used as a loading control (Fig. 4.1A). Following constitutive clathrin-mediated endocytosis, TfR, InsR and LDLR enter early endosomes and are targeted primarily to recycling pathways for return to the plasma membrane [17-19]. Thus, RME-8 KD does not appear to influence the constitutive recycling pathway but does alter the levels of EGFR, which is targeted from early endosomes to late endosomes/lysosomes [20]. In fact, EGFR undergoes constitutive endocytosis at a rate of 1-2%/min [21]. Thus, it is possible that RME-8

normally plays a negative regulatory role in trafficking of EGFR to the degradative pathway and that loss of RME-8 function allows more EGFR to enter this pathway during the course of the KD leading to decreased steady-state levels. However, it is also conceivable that RME-8 KD leads to decreased EGFR by decreasing mRNA levels or by altering the rate of receptor synthesis.

To examine these possibilities, we performed metabolic labelling experiments. Cells were first pulsed with [^{35}S[cysteine/methionine to label newly synthesized proteins and cell lysates were subjected to immunoprecipitation analysis with an EGFR antibody. Equivalent amounts of newly synthesized EGFR were immunoprecipitated under control and KD conditions (Fig. 3A), strongly suggesting that RME-8 KD does not influence EGFR synthesis. We next chased the metabolically labelled cells for various time points in the presence of 100 ng/ml EGF. Importantly, over a time course of 6 hours, the amount of EGFR decreased more rapidly in RME-8 KD cells than in control (Fig. 4.3B). Quantification of multiple experiments confirmed that RME-8 KD significantly increases the rate of EGFR degradation (Fig. 3C). Thus, we hypothesize that RME-8 is a negative regulator of EGFR trafficking to the degradative pathway and as a consequence, KD of RME-8 increases degradation rates leading to a decrease in receptor steady-state levels. A role for RME-8 in the regulation of degradative trafficking at the level of endosomes is consistent with the recent demonstration that in plants, RME-8 functions in vesicle trafficking from MVBs to the lytic vacuole, the plant equivalent of lysosomes [12].

Trafficking decisions regarding degradation versus recycling have critical pathological implications. For example, although EGFR is normally targeted for degradation following EGF activation, overexpression of the EGFR family member ErbB2 leads to EGFR/ErbB2 heterodimers that are directed towards the recycling pathway [22,23]. This leads to prolonged mitogenic signaling downstream of EGFR and may explain why ErbB2 overexpression is found in many carcinomas and correlates with poor prognosis [23,24]. Since RME-8 KD enhances EGFR degradation we sought to test if it could, at least in part, overcome the ability of ErbB2 to prevent EGFR down

regulation with implications for ErbB2-positive cancers. ErbB2 normally undergoes constitutive endocytosis and recycling. Thus, we examined its steady-state levels in non-overexpressing cells. In this set of experiments, EGFR is decreased by 45.8% and 63.1% in COS-7 and HeLa cells, respectively, following RME-8 KD, whereas in the same experiments there is no significant change in the levels of ErbB2 (Fig. 4.4A/B). Thus, consistent with earlier results, RME-8 KD does not influence the levels of a constitutively recycling receptor.

We next turned to experiments in BT474 and SKBR3 human breast cancer cells lines, which we obtained from Dr. William Muller (McGill University). These cells overexpress ErbB2 and have been used as a model to establish that ErbB2 overexpression leads to increased EGFR recycling [22]. Transfection with RME-8 siRNA led to a large decrease in RME-8 levels (Fig. 4.5A; 73.2% and 74.1% decrease in RME-8 in BT474 and SKBR3 cells, respectively). Although this level of KD is somewhat less than that seen in COS-7 and HeLa (Fig. 4.1B), there was still a significant decrease in the levels of EGFR (37.3% and 32.6% in BT474 and SKBR3, respectively; Fig. 5A/B; note that the EGFR antibody employed in this study cross-reacts with ErbB2 at high levels of ErbB2 expression). As for COS-7 and HeLa cells, RME-8 KD did not influence the steady-state levels of ErbB2 in either breast cancer cell line (Fig. 4.5A/B). Thus, although ErbB2 overexpression may be partially protective of the decrease in EGFR levels caused by RME-8 KD, to the large part, RME-8 KD is an effective method to reduce EGFR levels even in the face of gross ErbB2 overexpression. These data suggest that RME-8 may be a valuable target in the treatment of ErbB2-positive breast cancers.

The mechanism by which RME-8 may function in endosomal trafficking and EGFR degradation is not currently understood. An interesting hypothesis is that RME-8 interacts with Hsc70 on endosomes to regulate the association of bilayered clathrin coats with endosomal membranes. In fact, Hsc70 was previously implicated in trafficking decisions on early endosomes [16]. Normally, RME-8/Hsc70 would disassemble endosomal clathrin coats as part of the normal kinetic equilibrium of clathrin coats and

Hrs between membranes and the cytosol [7]. RME-8 KD would thus lead to increased association of coats and Hrs with membranes. Ubiquitinated cargo would have more binding sites on endosomes, which would increase their targeting to ESCRTs, entry in MVBs and degradation. In fact, RME-8 KD cells have less CHC in the cytosol with no overall change in CHC levels [9]. If this hypothesis is correct, RME-8 could have a general influence on the trafficking of receptors that are targeted via ubiquitination to the degradative pathway and in fact RME-8 KD decreases the levels of the NGF receptor TrkA when transfected in cultured cells (data not shown). Future studies will be directed towards testing this hypothesis.

Acknowledgments

We thank Dr. William Muller (McGill University) for the gift of BT474 and SKBR3 breast cancer cell lines, Dr. John Bergeron (McGill University) for the insulin receptor antibody, Lyne Bourbionnière and Jacynthe Philie for excellent technical assistance, Viviane Poupon for assistance with the FACS analysis and Francois Blondeau and other members of the laboratory for discussion. This work was generously supported by grant MOP-62684 from the Canadian Institutes of Health Research (CIHR) to PSM. PSM is a Fonds de la recherch en santé du Québec Senior Scholar and holds the James McGill Chair.

Figure legends

Fig. 4.1. RME-8 KD decreases steady-state levels of EGFR. (A) COS-7 or HeLa cells were mock transfected or transfected with RME-8 siRNA. At 72 hours following transfection, cell lysates were prepared and processed for Western blot with antibodies against the indicated proteins. (B) Western blots as in A were quantified. The bars represent mean ± s.e.m. (n=between 6 and 8 for the various proteins). Significant differences were detected for RME-8 and EGFR (paired t-test, $p<0.001$).

Fig. 4.2. EGFR is decreased at the surface proportional to the total decrease. (A) COS-7 cells, mock transfected or transfected with RME-8 siRNA, were fixed, permeabilized and stained with an antibody against EGFR (TOTAL EGFR). Alternatively, live cells, held at 4°C, were incubated with the EGFR antibody before washing and fixation (SURFACE EGFR). (B) COS-7 cells, mock transfected or transfected with RME-8 siRNA were incubated with EGFR antibody with (TOTAL) or without (SURFACE) permeabilization as described in Materials and methods and were then resuspended and subjected to a FACS analysis. Significant decreases in EGFR were detected for both total and surface pools following RME-8 KD (paired t-test, $p<0.01$ for total and $p<0.001$ for surface, n=6 for each).

Fig. 4.3. RME-8 KD increases EGFR degradation rates. (A) COS-7 cells, mock transfected or transfected with RME-8 siRNA, were pulsed with [^{35}S]cysteine/methionine to label newly synthesized proteins. Soluble cell lysates were prepared for immunoprecipitation with an EGFR antibody and immunoprecipitated proteins were subject to autoradiography. (B) Cells prepared as in A were subsequently chased for various time points, as indicated, in regular media containing EGF before soluble cell lysates were prepared for immunoprecipitation with EGFR antibody, followed by autoradiography. (C) The levels of EGFR as determined in B were quantified. The points represent mean ± s.e.m., n=4 for each condition.

Fig. 4.4. RME-8 KD does not influence the levels of ErbB2. (A) COS-7 or HeLa cells

were mock transfected or transfected with RME-8 siRNA. At 72 hours following transfection, cell lysates were prepared and processed for Western blot with antibodies against the indicated proteins. (B) The EGFR and ErbB2 Western blots from A were quantified. The bars represent mean ± s.e.m. (n=6 for each blot). Significant differences were detected for EGFR (paired t-test, $p<0.01$).

Fig. 4.5. ErbB2 does not protect EGFR from degradation following RME-8 KD. (A) BT474 or SKBR3 breast cancer cells were mock transfected or transfected with RME-8 siRNA. At 96 hours following transfection, cell lysates were prepared and processed for Western blot with antibodies against the indicated proteins. (B) The EGFR and ErbB2 Western blots from A were quantified. The bars represent mean ± s.e.m. (n=6 for each blot). Significant differences were detected for EGFR (paired t-test, $p<0.05$).

References

[1] Gruenberg, J. (2001). The endocytic pathway: a mosaic of domains. Nat. Rev. Mol. Cell Biol. 2, 721–730.

[2] Rink, J., Ghigo, E., Kalaidzidis, Y. and Zerial, M. (2005) Rab conversion as a mechanism of progression from early to late endosomes. Cell 122, 735-749.

[3] Ebner, R. and Derynck, R. (1991). Epidermal growth factor and transforming growth factor-alpha: differential intracellular routing and processing of ligand-receptor complexes. Cell Regul. 8, 599-612.

[4] Williams, R.L. and Urbe, S. (2007) The emerging shape of the ESCRT machinery. Nat. Rev. Mol. Cell Biol. 8, 355-368.

[5] Clague, M.J. and Urbe, S. (2006) Endocytosis: the DUB version. *Trends Cell Biol.* **16**, 551-559.

[6] Sachse, M., Urbe, S., Oorschot, V., Strous, G.J. and Klumperman, J. (2002) Bilayered clathrin coats on endosomal vacuoles are involved in protein sorting toward lysosomes. Mol. Biol. Cell 13, 1313-1328.

[7] Raiborg, C., Wesche, J., Malerod, L. and Stenmark, H. (2006) Flat clathrin coats on endosomes mediate degradative protein sorting by scaffolding Hrs in dynamic microdomains. J. Cell Sci. 119, 2414-2424.

[8] Wu, X., Zhao, X., Baylor, L., Kaushal, S., Eisenberg, E. and Greene, L.E. (2001) Clathrin exchange during clathrin-mediated endocytosis. J. Cell Biol. 155, 291-300.

[9] Girard, M., Poupon, V., Blondeau, F. and McPherson, P.S. (2005) The DnaJ-

domain protein RME-8 functions in endosomal trafficking. J. Biol. Chem. 280, 40135-40143.

[10] Zhang Y., Grant B. and Hirsh, D. (2001) RME-8, a conserved J-domain protein, is required for endocytosis in Caenorhabditis elegans. Mol. Biol. Cell. 12, 2011-2021.

[11] Chang, H.C., Hull. M. and Mellman, I. (2004) The J-domain protein Rme-8 interacts with Hsc70 to control clathrin-dependent endocytosis in Drosophila. J. Cell Biol. 164, 1055-1064.

[12] Silady, R.A., Ehrhardt, D.W., Jackson, K., Faulkner, C., Oparka, K. and Somerville, C.R. (2008) The GRV2/RME-8 protein of Arabidopsis functions in the late endocytic pathway and is required for vacuolar membrane flow. Plant J. 53, 29-41.

[13] Schmid, S.L. and Rothman, J.E. (1985) Two classes of binding sites for uncoating protein in clathrin triskelions. J. Biol. Chem. 260, 10050-10056.

[14] Ungewickell, E. (1985) The 70-kd mammalian heat shock proteins are structurally and functionally related to the uncoating protein that releases clathrin triskelia from coated vesicles. EMBO J. 16, 3385-3391.

[15] Rapoport, I., Boll, W., Yu, A., Böcking, T. and Kirchhausen, T. (2008) A motif in the clathrin heavy chain required for the hsc70/auxilin uncoating reaction. Mol. Biol. Cell 19, 405-413.

[16] Newmyer, S.L. and Schmid, S.L. (2001) Dominant-interfering Hsc70 mutants disrupt multiple stages of the clathrin-coated vesicle cycle *in vivo*. J. Cell Biol. 152, 607-620.

[17] Knutson, V.P. (1991) Cellular trafficking and processing of the insulin receptor. FASEB J. 5, 2130-2138.

[18] Dautry-Varsat, A., Ciechanover, A. and Lodish, H.F. (1983) pH and the recycling of transferrin during receptor-mediated endocytosis. Proc. Natl. Acad. Sci. U S A 80, 2258-2262.

[19] Basu, S.K., Brown, M.S., Ho, Y.K., Havel, R.J. and Goldstein, J.L. (1981) Mouse macrophages synthesize and secrete a protein resembling apolipoprotein E. Proc. Natl. Acad. Sci. U S A 78, 7545-7549.

[20] Wiley, H.S. (2003). Trafficking of the ErbB receptors and its influence on signaling. Exp. Cell Res. 1, 78-88.

[21] Wiley, H.S. and Burke, P.M. (2001) Regulation of receptor tyrosine kinase signalling by endocytic trafficking. Traffic 2, 12-18.

[22] Wang, Z., Zhang, L., Yeung, T.K. and Chen, X. (1999) Endocytosis deficiency of epidermal growth factor (EGF) receptor-ErbB2 heterodimers in response to EGF stimulation. Mol. Biol. Cell 10, 1621–1636.

[23] Ceresa, B.P. and Schmid, S.L (2000) Regulation of signal transduction by endocytosis. Curr. Opin. Cell Biol. 12, 204-210.

[24] Slamon, D.J., Clark, G.M., Wong, S.G., Levin, W.J., Ullrich, A. and McGuire, W.L. (1987) Human breast cancer: correlation of relapse and survival with amplification of the HER-2/neu oncogene. Science 235, 177-182.

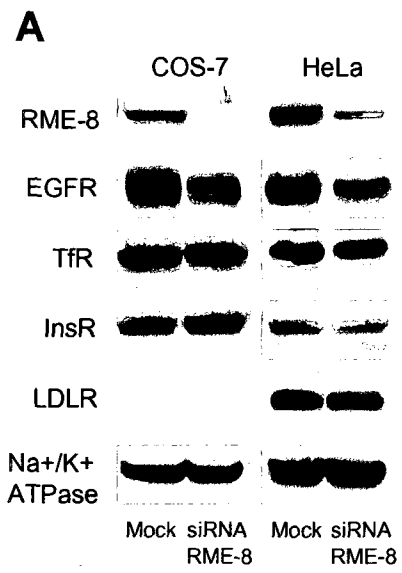
A
COS-7
HeLa
RME-8
EGFR
TfR
InsR
LDLR
Na+/K+
ATPase
Mock
siRNA
RME-8
Mock
siRNA
RME-8

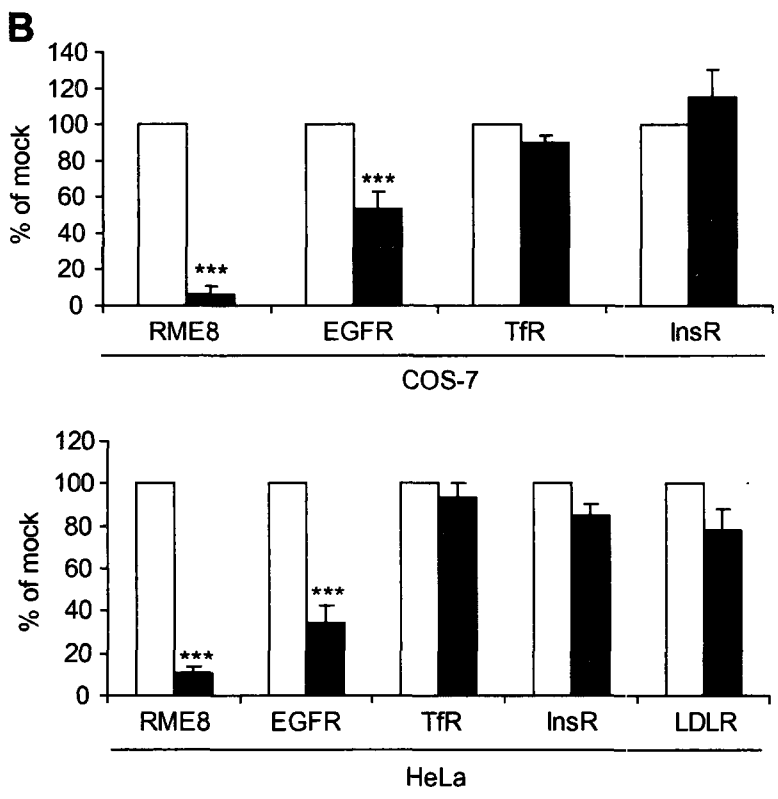
B
% of mock
140
120
100
80
60
40
20
0
***
***
RME8
EGFR
TfR
InsR
COS-7
% of mock
120
100
80
60
40
20
0
***
***
RME8
EGFR
TfR
InsR
LDLR
HeLa

FIGURE 4.1

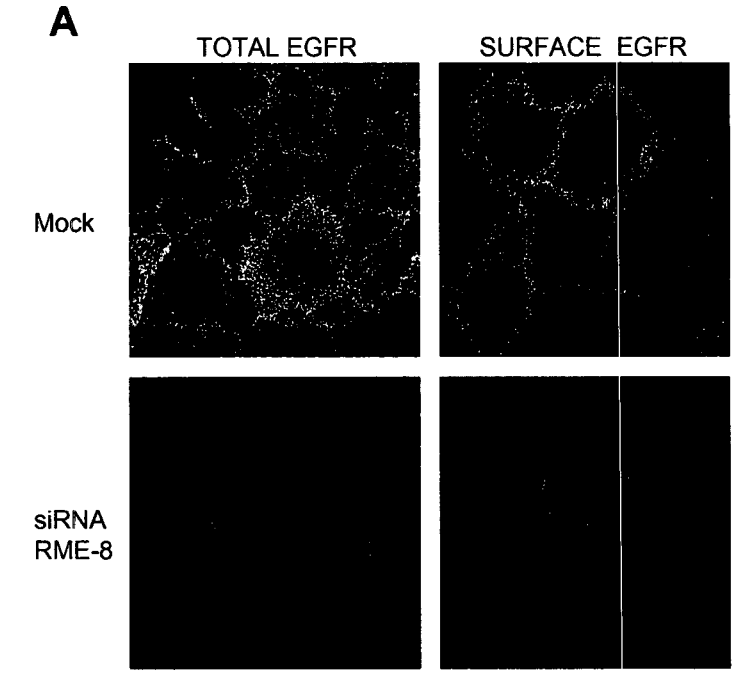
A
TOTAL EGFR
SURFACE EGFR
Mock
siRNA
RME-8

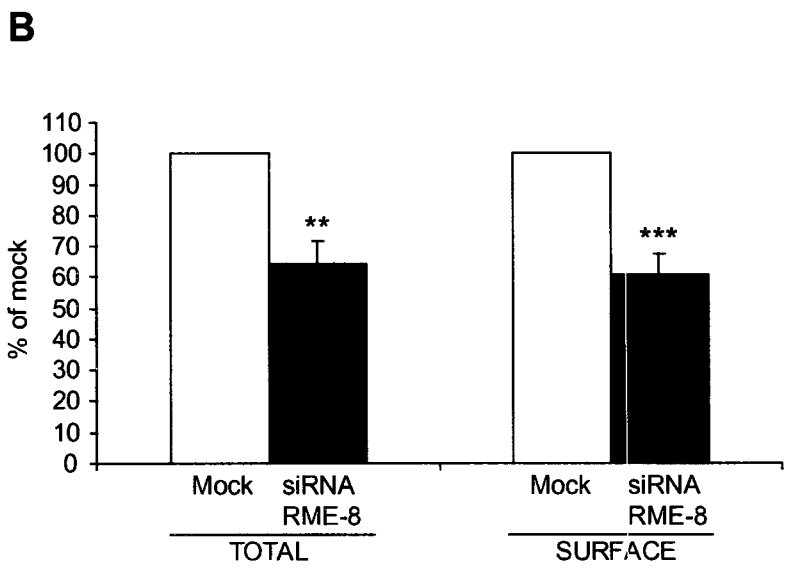
B
% of mock
110
100
90
80
70
60
50
40
30
20
10
0
**
***
Mock
siRNA
RME-8
TOTAL
Mock
siRNA
RME-8
SURFACE

FIGURE 4.2

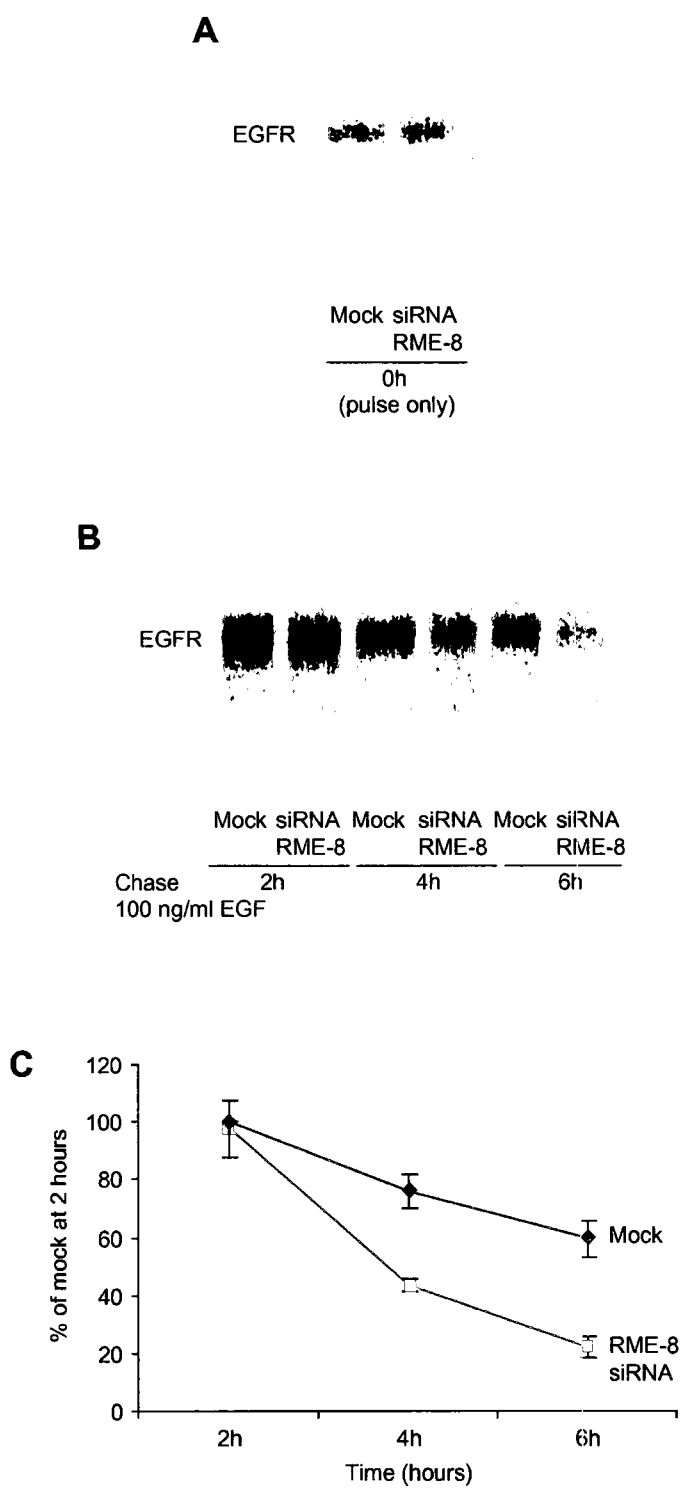
A
EGFR
Mock siRNA
RME-8
0h
(pulse only)
B
EGFR
Mock siRNA Mock siRNA Mock siRNA
RME-8 RME-8 RME-8
Chase 2h 4h 6h
100 ng/ml EGF
C
% of mock at 2 hours
120
100
80
60
40
20
0
2h
4h
6h
Time (hours)
Mock
RME-8
siRNA

FIGURE 4.3

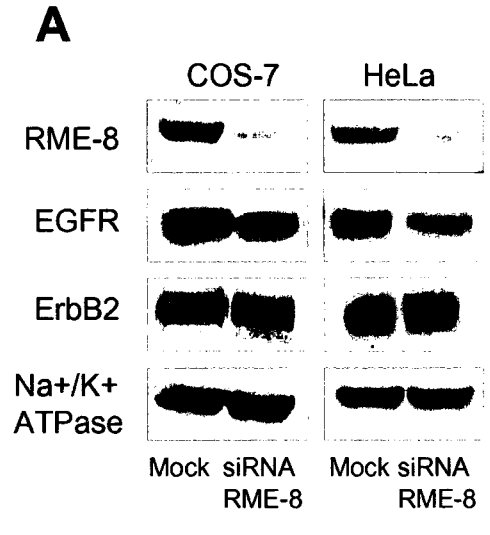
A
COS-7
HeLa
RME-8
EGFR
ErbB2
Na+/K+
ATPase
Mock siRNA
RME-8
Mock siRNA
RME-8

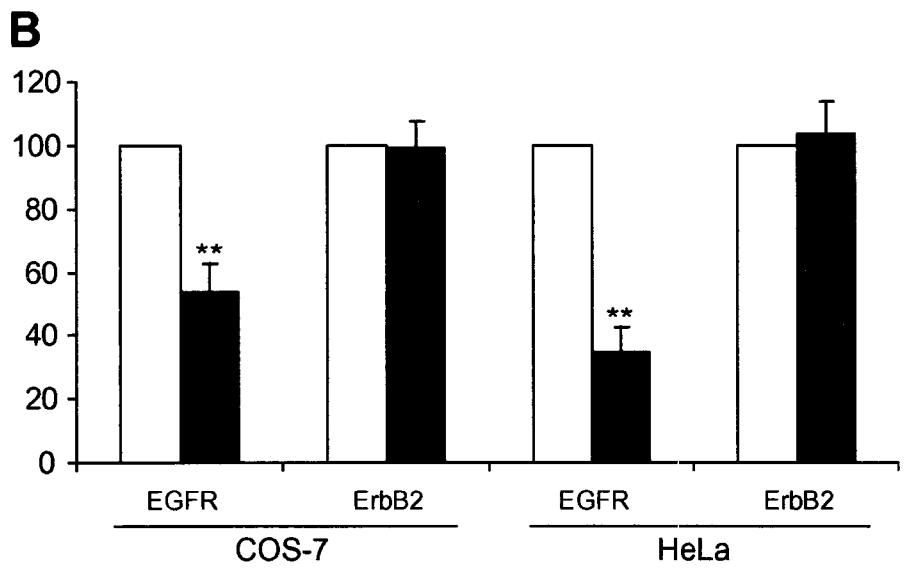
B
120
100
80
60
40
20
0
**
**
EGFR
ErbB2
EGFR
ErbB2
COS-7
HeLa

FIGURE 4.4

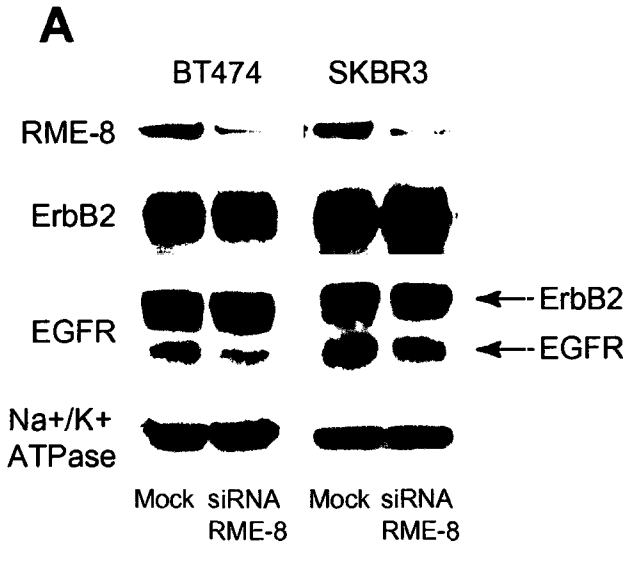
A
BT474
SKBR3
RME-8
ErbB2
EGFR
Na+/K+
ATPase
ErbB2
EGFR
Mock
siRNA
RME-8
Mock
siRNA
RME-8

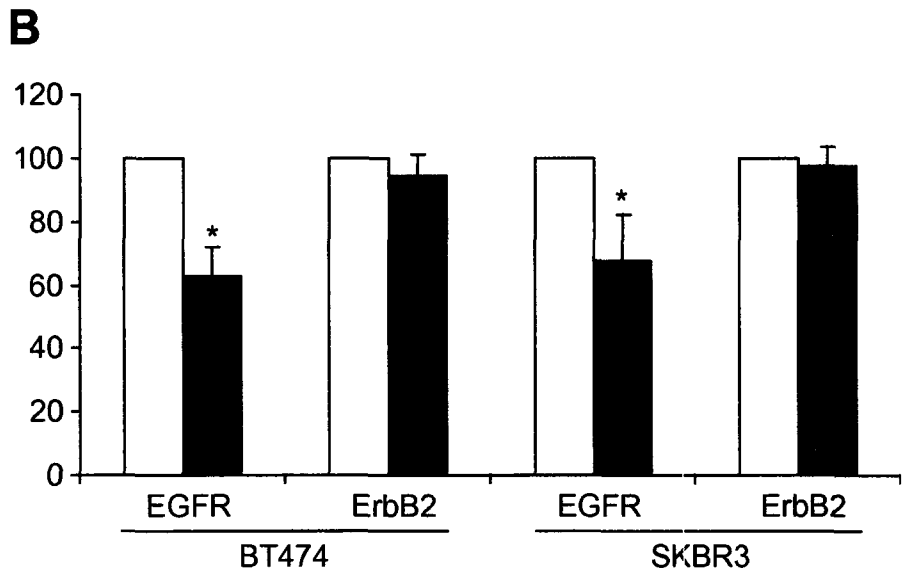
B
120
100
80
60
40
20
0
*
*
EGFR
ErbB2
EGFR
ErbB2
BT474
SKBR3

FIGURE 4.5

CHAPTER 5
ORIGINAL CONTRIBUTION TO SCIENTIFIC KNOWLEDGE

The work presented in chapter 2 provided new insights into the composition of CCVs and their specialized functions in different tissues. Our lab previously developed a label-free quantitative approach applicable to proteomic studies (Blondeau et al., 2003). In the present study we used this approach to quantify and compare abundant CCV components between two different tissues. We were able to confirm quantitatively for the first time that CCVs can exert different specialized functions depending on the tissues. Indeed, we found that in brain, 89% of the plasma membrane-derived CCVs are dedicated to specialized synaptic vesicle recycling and that liver CCVs are performing more general housekeeping endocytic and trafficking tasks. This study also contributed to ending the dogma of the obligatory 1:1 CHC to CLCs ratio and showed that the role of CLCs could be different, at least in non-neuronal tissues, than the one initially proposed. This surprising finding was the basis for other studies on the role of CLCs in both neurons and other cell lines and tissues.

Not only did the work described in chapter 2 provide new information on CCVs but it also allowed us to identify new proteins that are potentially linked to clathrin-mediated trafficking events. Among these novel proteins, we identified and characterized RME-8 and that characterization led to the studies described in chapters 3 and 4. Chapter 3 provides the first characterization of the mammalian RME-8 homolog and demonstrates that RME-8 binds to the chaperone Hsc70 which is known to exert a role in a variety of contexts including assembly and disassembly of protein complexes. In addition to the biochemical characterization of RME-8, this study showed that RME-8 localizes throughout the endosomal system where it functions as a regulator of the endosomal intracellular trafficking. Moreover, this study provided the first evidence of a functional role of a DnaJ domain-containing protein within the endosomal compartment.

While characterizing RME-8 we made the intriguing observation that RME-8 depletion causes a decrease in the expression levels of EGFR. The studies described in chapter 4 investigate the causes of this decrease. RME-8 absence causes an enhanced EGFR degradation and, more importantly, this enhanced degradation does not affect constitutively recycling receptors. This increase in EGFR degradation upon RME-8

depletion can also be observed in cancer cell lines where EGFR is normally protected from degradation due to its association with the overexpressed recycling receptor ErbB2. In addition to providing the mechanism underlying the aberrant EGFR degradation upon RME-8 depletion, this study indicates that RME-8 is a crucial player in EGFR sorting decisions and point to RME-8 as a potential valuable target in the treatment of cancers featuring ErbB2 overexpression.

CHAPTER 6
DISCUSSION AND CONCLUSION

6.1 RATIOS OF CLATHRIN AND ITS ADAPTORS IN BRAIN AND LIVER

A striking evolutionary leap in eukaryotic cells is the appearance of specialized cellular compartments. This compartmentalization provides the proper cellular environment for the plethora of biochemical processes occurring in cells and is accompanied by the compartmentalization of proteins meaning that protein localization is intimately linked to subcellular function. Subcellular proteomics takes advantage of this compartmentalization and can provide a global analysis of the protein components of an organelle. This approach has gradually replaced the two-dimensional gel electrophoresis of whole cell lysates. Using subcellular proteomics, as opposed to "entire homogenate proteomics", has advantages. It reduces the complexity within the sample and therefore proteins that are less abundant are not overwhelmed by more highly expressed proteins. It also allows the localization of the identified proteins. On the other hand, subcellular fractionation methods are giving enrichment and not "pure" organelles, which means that any given preparation will always have some degree of contamination. Moreover, subcellular compartments are dynamic structures and their protein components are in constant exchange. Thus, it can make data interpretation difficult, since it is unlikely that a given organelle will have a definite and static proteome. Protein correlation profiling, which uses MS of marker proteins for an organelle to define their profile through a fractionation step such as sucrose density gradient, compares peptides obtained from consecutive fractions to the reference profile, was aimed to address these issues (Andersen et al., 2003; Foster et al., 2006). Regardless, subcellular proteomics has been widely used for different organelles and has proven to be a useful tool to provide insights of organelle function (for review, see Yates et al., 2005).

The workflow we used in both brain and liver CCV proteomic analysis started with subcellular fractionation protocols that led to highly enriched CCV fractions. The CCV fractions are then separated by one-dimensional SDS-polyacrylamide gel electrophoresis (1D SDS-PAGE). This eliminates problems arising from two-dimensional gel electrophoresis, including the incapacity of many proteins to enter the

first dimension, or to be resolved by their isoelectric points, and the fact that integral-membrane proteins are not well represented. Once the 1D SDS-PAGE-based separation is achieved, the gel lane is cut into even horizontal gel slices that are digested with trypsin in order to generate tryptic peptides and to allow extraction of the peptides from the gel slices. The digested peptide mixture is then analyzed by reversed-phase liquid chromatography quadrupole time-of-flight tandem MS (LC-Q-To F MS/MS) and MS/MS spectra are then assigned to the peptides. Because the proteolytic peptides generated upon digestion exhibit a wide range of physicochemical properties such as charge, size, hydrophobicity, and potential of ionization, MS and, by extension proteomics, is not inherently quantitative.

Many efforts have been made to develop quantitative approaches and most are based on the use of heavy stable isotopes. These quantification methods present several advantages, such as the possibility of combining the samples, of reducing the complexity of the peptide mixture, and performing additional separation steps on labeled samples. However, none of the various methods were suitable in our case. The SILAC method (Ong et al., 2002) is applicable mainly to cells in culture, even though some groups demonstrated the feasibility of the method in other organisms such as *C.elegans*, *Drosophila* (Krijgsveld et al., 2003), plants (Gruhler et al., 2005), and even rats (Wu et al., 2004), but with a cost that increases with the complexity of the organisms. The ICAT method has not been tested in peptide mixtures from tissues and also limits the analysis to proteins bearing cysteine residues. Stable isotope incorporation by enzymatic labeling could have been used in theory, but has not been extensively tested in samples derived from tissues. During our analysis, we realized that the Coomassie blue intensity in the 1D SDS-PAGE run prior to the MS analysis correlated with the number of peptides/spectra found within each band. This suggested a possible quantitative nature of peptide counts. This correlation was observed by Blondeau et al. (Blondeau et al., 2004) using LC-Q-ToF analysis and it was later independently verified by Liu et al. (Liu et al., 2004) using MudPIT (multidimensional protein identification technology) analysis with an LC-Q ion trap mass spectrometer. This indicates that peptide counting is valuable for quantification independently of the nature of the MS apparatus used. In

our case, because of a) the low complexity in the number of proteins, b) the elution profile of abundant peptides, and c) the sensitivity of the MS apparatus used for the analysis, the more abundant a protein, the more redundant peptide identifications that were seen in a given band. For example, in Girard et al. (Girard et al., 2005b), in preparation 1 there were 309 MS/MS spectra that were assigned to 77 CHC peptides. Because of their abundance, these peptides have broad peaks of elution off the LC column and are therefore sampled multiple times. However, the fact that some peptides are detected with multiple spectra is also due to low resolution in the LC, which can be explained by their hydrophobicity or other intrinsic physico-chemical properties. This illustrates one of the limitations of the technique, as it would ideally require proteins that have a "homogenous" peptide composition to cover all physico-chemical properties, and average for changes from one peptide to another for a given protein. Another limitation concerns the transmembrane proteins that contain highly hydrophobic residues and that won't optimally resolve in the C18 liquid chromatography column used, or may never elute, depending on the conditions used. That could explain why in Blondeau et al. (2004), the peptides corresponding to the small transmembrane domain proteins of the ATPase subcomplex were not found in the expected ratios. Another limitation can come from the trypsin digestion profile. For example, the γ subunit of the adaptor protein AP-1 in the brain CCVs analysis has an uneven distribution of lysine and arginine and therefore shows a deficit in the number of peptide/spectra relative to other AP-1 subunits (Blondeau et al., 2004). Despite its limitations, the peptide/spectral count approach is a valuable and versatile tool for determining relative protein abundance. Indeed, Liu et al. (2004) have spiked a yeast protein mixture with known concentrations of sample proteins and have demonstrated that spectral count is accurate as they obtained an almost perfect linear correlation with a R^2 value of more than 0.99 for the six proteins studied (Liu et al., 2004).

We used peptide counting together with Western blot analysis to compare ratios of CHC, CLC, and AP subunits in CCVs enriched from brain and liver and then to examine how these ratios compared between the two samples. Several studies in brain, including the brain CCV proteomics analysis, suggest that CHC and CLCs are stably

associated in a 1:1 molar ratio and, with time, this notion had been extended to all tissues (Kirchhausen and Harrison, 1981; Ungewickell and Branton, 1981; Blondeau et al., 2004). We were thus surprised to find that, in liver CCVs, the CLCs to CHC ratio was 0.2:1 ratio. Western blot analysis showed a decreased amount of CLCs in liver compared to brain for an equivalent amount of CHC. Moreover, these differences were seen when using two different CCV isolation protocols. In fact, the 1:1 ratio might be a unique characteristic of brain CCVs since no other tissues or commonly used cell lines taht we tested exhibit this equimolar ratio. At a lower than 1:1 ratio, according to the model that CLCs function as stoichiometric negative regulators of CHC assembly, CHC should be over assembled and non functional. In fact, loss of function experiments are not consistent with this model. In non-neuronal cells, CLC knock-down (KD) has no effect on endocytosis (Yang et al., 2002; Huang et al., 2004; Poupon et al., 2008). Moreover, a recent study showed that the role of CLCs is to regulate actin assembly and membrane trafficking at the TGN (Poupon et al., 2008). In this model of function, CLC can readily work at substoichiometric levels. In the case of brain, it was previously demonstrated that the major role of CCVs is recycling of SVs (Blondeau et al., 2004). Thus, it is possible that the 1:1 ratio of CLCs to CHC in brain is specific in an unknown manner to regulation of SVs.

We also found differences in the ratios of AP-1 to AP-2 between the two tissues. In liver, there was more AP-1 than AP-2, and in brain, these ratios were inverted. This strongly reinforces the idea that brain is specialized in endocytosis as a way to retrieve SVs. This notion is also supported by our calculations demonstrating that approximately 90% of the AP-2 positive CCVs are dedicated to SV recycling. It was, thus, not surprising to find some endocytic cargoes such as TfR and EGFR that were detected in liver CCVs were not detected in brain, likely because they were present but overwhelmed with the abundant SV protein cargo. It is of interest to note that the composition of AP-2 subunits differs in brain compared to liver. In brain, AP-2αA isoform is more present, whereas in liver AP-2αC predominates. Since brain CCVs are highly specialized and biased toward SV recycling, this opens a field of investigation in which the brain specific isoform AP-2αA may have a specialized function in SV

recycling. Taken together, the CHC to CLC and the AP2 to AP1 ratios validate the approach of spectral counting as a quantitative feature of MS. It is likely that such an approach would not be limited to the two examples we described in this thesis.

In agreement with the above biological findings, and with the feasibility of protein quantification by MS/MS after subcellular fractionation, new areas of investigation are now open. For example, it would be possible to follow individual proteins, as well as protein complexes, over a complete fractionation protocol. The brain CCV isolation protocol generates 8 different fractions with increasing CCV enrichment. They could be analyzed for CHC enrichment. For any given protein, its distribution across fractions could be compared to other proteins and to CCV markers. By analyzing the complete set of fractions derived from the CCV protocol (Girard et al, 2005a), we should be able to assign individual proteins to protein complexes, and possibly give insights regarding their function.

Even though the peptide/spectral counting approach does not measure any physical properties of a peptide, and is therefore not as accurate as quantitative approaches that factor in those properties (Old et al., 2005), it has gained in popularity in the field and was validated by several groups, who used this easy and relatively reliable technique together with traditional biochemical experimental approaches, in order to get insights on biological systems. For example, Gilchrist et al., used the technique to assign subcellular localization of new proteins and confirm the role of COPI vesicles in recycling and cisternal maturation (Gilchrist et al. 2006). Despite its limitations, the label-free approach has to be considered when choosing a quantification method. It is less time-consuming since the biochemical workflow is simplified, and is also less expensive than the labeling approaches, especially if the sample to analyze is from an animal tissue. The number of experiments that can be compared is, in theory, unlimited (so multiple states can be analyzed), as compared to labeling techniques, which can only accommodate a comparison of 2-8 experiments. Moreover, the peptide accounting approach allows a more dynamic range of quantification which is certainly an advantage if the goal is to perform a global proteomic analysis. In addition, and as shown

previously, to compare the ratios between two proteins (CHC and CLCs), or two stable protein complexes (AP-2 and AP-1), the peptide/spectral counting approach is proven to be accurate and will certainly be a method of choice for new biological discoveries.

6.2 IDENTIFICATION OF NEW COMPONENTS OF THE TRAFFICKING MACHINERY

Proteomics analysis of brain CCVs led to the identification of 8 novel proteins that, at the time, were hypothetical gene products not yet detected at the protein level (Wasiak et al., 2002; Blondeau et al., 2004). Since then, 7 of them have been linked to vesicle trafficking. FENS-1 localizes to early endosomes and is implicated in vesicular trafficking (Ridley et al., 2001). AAK1 localizes to the plasma membrane and is a kinase that phosphorylates AP-2 and regulates cargo recruitment (Conner and Schmid, 2002). CVAK104 is a kinase that phosphorylates AP-2 but that has also been proposed to function in clathrin-dependent pathways between the TGN and the endosomes as well as in SNARE sorting (Conner and Schmid, 2005; Düwel and Ungewickell, 2006; Borner et al., 2007). NECAP1 and NECAP2 are enriched on the coats of CCVs and partially localize with CCPs at the cell surface. NECAPs are binding partners for both AP-1 and AP-2, although AP-2 is the major interactor (Ritter et al., 2003). Enthoprotin colocalizes with AP-1 and Arf at the TGN and stimulates clathrin assembly (Wasiak et al., 2002). Clavesin (gi 12855458 in the analysis) contains a Sec14 domain, enriches in CCV fractions, and is mainly localized to the TGN (Yohei Katoh, personal communication). The protein corresponding to gi 12859193 has not been characterized yet, but contains a putative GTP-binding domain.

The proteomics analysis of liver CCVs validated the peptide accounting approach and revealed new insights on the properties and trafficking specialization of CCVs. In terms of novel proteins, 21 were identified including NECAP1, enthoprotin and FENS-1, which were also identified in the brain CCVs analysis. Many of the remaining proteins have been characterized since the publication of the table and, among

them, many have been linked to membrane trafficking. Connecdenn (RIKEN cDNA 6030446I19) is a binding partner for AP-2 and is thought to function in SV endocytosis (Allaire et al., 2006). Atlastin-3 (RIKEN cDNA 5730596K20) localizes to endosomal structures (Viviane Poupon, personal communication). The protein p200 (similar to KIAA1414 protein) binds to AP-1 (Lui et al., 2003). Vac14 protein interacts with nNOS through a new PDZ motif (Lemaire and McPherson, 2006). RME-8 localizes throughout the endosomal system and regulates endosomal trafficking (Girard et al., 2005c; Fujibayashi et al., 2008; Girard and McPherson, 2008). SEC14-related protein C is implicated in the selective export of membrane proteins from the endoplasmic reticulum (Wendeler et al., 2007). EHD4 (EH domain containing-4) is found at the early endosomes and regulates transport from the early endosome to the recycling endosome (George et al., 2007). TB2 like-1 (similar to deleted in polyposis 1-like 1) shows a cytoplasmic punctate pattern and is thought to be implicated in membrane trafficking regulation (Sato et al., 2005). All other ten proteins in the category of novel proteins (Girard et al., 2005b) remain uncharacterized gene products.

Many proteomics analysis have been published over the last ten years, but the challenge for scientists now is to integrate these data into biological systems. The ideal way to achieve that goal would be to combine and integrate several approaches. The first approach will use MS and proteomics to identify and quantify new proteins in different tissues and subcellular fractions. The second approach will aim to generate antibodies for each protein identified, in order to assess the biochemical properties and localization of these proteins within tissues and cells. This will provide biological studies as well as a validation of the proteomics findings. Validation is an important step since high-throughput approaches, such as large scale protein identification in "semi-pure" enriched subcellular fractions, may lead to some misidentifications and false positives. The third approach will be to identify the binding partners of each previously identified protein in order to build up the protein machineries necessary for organelle homeostasis. The fourth approach, but not the least, will be to manipulate the levels of each of the different proteins identified in order to evaluate how it will influence the proper function of the organelle under investigation. So far, this was achieved by

overexpression of full length proteins, or truncated dominant-negative and positive constructs for proteins that have an already known activity such as phosphatidyl-inositol-3 kinase (PI3K) (Krasilnikov et al., 2003). Less popular, because of technical costs and time spent for validation, was the use of knock-out in cell lines (mainly embryonic stem cells), and in laboratory animals (Ibarra-Sanchez et al., 2001; Qiu et al., 2004). With the recent increased knowledge in RNA metabolism, it is now possible to cause the destruction of an mRNA, and to inhibit the production of its corresponding protein (Filipowicz, 2005). Techniques such siRNA, shRNA and microRNA, where the silencing RNA is introduced in cells either by simple transfection, or by viral infection, are now widely used, and are very powerful tools to investigate endogenous function of a single protein (Huang et al., 2004; Girard et al., 2005c; Poupon et al., 2008). This ambitious project represents an enormous amount of work, and that will necessitate collaboration from many scientific teams around the world to generate the data, develop bioinformatics tools, and integrate all the information so high-resolution models of cell function can emerged.

6.3 RME-8, A NEW PLAYER IN ENDOSOMAL TRAFFICKING

6.3.1 IDENTIFICATION AND BIOCHEMICAL PROPERTIES OF MAMMALIAN RME-8

The mammalian form of RME-8 was identified in the proteomics analysis of liver CCVs as the rat homolog of RME-8 that was first found in a genetic screen for endocytic defects in *C. elegans* (Zhang et al., 2001). RME-8 was subsequently found in *Drosophila* (Chang et al., 2004) and *Arabidopsis* (Silady et al., 2004) but there is no known RME-8 in yeast. Mammalian RME-8 sequence was predicted by aligning three partial human EST (expressed sequence tag) cloned sequences. Even though RME-8 sequence was *in silico* assembled from three different clones, we are confident that the predicted sequence is accurate since, when searched against the human genome, the RME-8 sequence mapped to a series of 56 exons from chromosome 3 that reveals a

sequence identical to the one predicted from the overlapping clones. Moreover, the predicted sequence aligns from the beginning to the end to its *C.elegans* and *Drosophila* counterparts, and its predicted molecular weight agrees with the RME-8 endogenous signal seen by Western blots.

The RME-8 sequence encodes for a 2243 amino acids protein that possesses a central DnaJ domain, flanked on either side by two IWN repeats of unknown function, as well as four putative type II clathrin boxes. The highest degree of homology between RME-8 forms is found for the DnaJ domain and IWN repeats, which are also well conserved between species. This high degree of homology for both the DnaJ domain and the IWN repeats suggest they are critical for RME-8 function.

RME-8 protein is detectable in a variety of tissues as a ~220 kDa band with the highest expression levels being in kidney, liver and testis, as well as in many routinely used cell lines, including COS-7 and HeLa cells. At the subcellular level, RME-8 is enriched in a microsomal P3 fraction, inexistent in the cytosolic fraction, and only present as traces in an plasma membrane-enriched fraction. So even though we can not totally rule out the possibility that a small pool of RME-8 might be present at the plasma membrane, we can certainly say that RME-8 is predominantly a microsomal "resident" protein. RME-8 can not be extracted from the microsomal fraction with Triton X-100, which is efficient in extracting integral plasma membrane proteins. Instead, RME-8 can be extracted only by using sodium carbonate at pH 11.0, which is characteristic of extrinsic membrane-associated proteins. This unique biochemical property of RME-8, together with the almost absence of RME-8 from plasma membrane-enriched fractions, indicates that RME-8 is not an integral plasma membrane protein, but instead a peripheral membrane protein that is tightly associated with microsomal compartment.

The expression pattern we observed for RME-8 is consistent with previous reports on RME-8 in invertebrates and confirms that RME-8 has a ubiquitous expression pattern. In *C.elegans*, RME-8 is also present in multiple cell types including oocytes, gut, gonads, coloemocytes (macrophage-like structures), and muscle cells, and is

essential for the worm development and viability (Zhang et al., 2001). The study done in *Drosophila* showed that RME-8 is expressed in Garland cells (nephrocyte-like cells) and photoreceptors, but the authors focused their study on these cell types only and did not investigate the expression of RME-8 in other cells (Chang et al., 2004). However, given the ubiquitous distribution of RME-8 in other organisms, it is reasonable to think that RME-8 would be ubiquitously expressed in *Drosophila* as well.

Mammalian RME-8 biochemical properties may differ from those of other species. Like its mammalian orthologue, the plant RME-8 is found in microsomal fractions. However, it can be solubilized from the microsomal fraction using denaturing agents such as urea as well as with the detergent Triton X-100 but can not be extracted with high basic pH 11.0 (Silady et al., 2008). This suggests that, in *Arabidopsis*, RME-8 is an integral membrane protein, or a protein that shares hydrophobic interactions with other integral membrane protein(s). This result is surprising, especially since the RME-8 sequence does not contain any known or putative membrane spanning domains, but we can not rule out that the sequence may contain new domain(s) responsible for that different characteristic. Moreover, it is possible that this different biochemical property reflects a different function of RME-8 in non-mammalian organisms.

Another study of mammalian RME-8 later confirmed its resistance to Triton X-100 and high salt, but sensitivity to $NaCO_3$ pH 11.0 (Fujibayashi et al., 2008), thus confirming our study in COS-7 cells. This study also determined that RME-8 was not a typical raft-associated protein. In addition, Fujibayashi et al. (2008) found that the N-terminal region spanning amino acids 1-453 of RME-8 is responsible for its membrane association, but more extensive mutagenesis studies will be necessary to determine if there are any specific motifs or residues implicated in RME-8 membrane association.

The function of the IWN repeats are unknown and further investigations will be required to assess their biochemical properties. Indeed, preliminary results demonstrate that they are mostly insoluble when individually expressed in bacteria. Unfortunately, the small portion that is soluble might not be sufficient for resolving their crystal

structure, which would be the ideal method to determine their tertiary structure, as well as their electrostatic and hydrophobic patches. Alternatively, IWN repeats could be expressed in SF9 insect cells as these eukaryotic cells may contain the machinery necessary for proper folding and solubility that maybe is not present in bacteria. How IWN repeats influence RME-8 localization and membrane association still has to be determined.

RME-8 possesses a central DnaJ domain, which is known in other proteins to bind to heat shock proteins in an ATP-dependent manner. Interestingly, two other DnaJ domain-containing proteins, GAK (auxilin-2) and auxilin-1 are implicated in clathrin-mediated trafficking events. GAK and auxilin are responsible for CCV uncoating at the plasma membrane and at the TGN. GAK and auxilin-1 bind to the terminal domain of CHC, and the ATP-dependent interaction of their DnaJ domain with the molecular chaperone Hsc70 mediates the uncoating of CCVs (Lemmon, 2001; Eisenberg and Greene, 2007). Since RME-8 was found in the proteomics analysis of CCVs and, given the presence in its sequence of four potential type II clathrin boxes, which are consensus sequences for binding to the terminal domain of clathrin heavy chain, one hypothesis was that RME-8 function is similar to that of auxilins. Moreover, genetic interactions between RME-8 and Hsc70 were observed in *Drosophila*, thus suggesting that RME-8 could also be a co-chaperone for Hsc70. Our studies demonstrated that the RME-8 DnaJ domain binds to Hsc70 in an ATP-dependent manner. Interestingly, *Drosophila* RME-8 also binds to Hsc70 but, in this case, the binding is ADP dependent, which is surprising since to date, all DnaJ domain containing-proteins usually bind Hsc70 in an ATP-dependent manner (Kelley, 1999). As stated previously, *Drosophila* RME-8 was found to be predominantly a cytosolic protein and not a microsomal protein as is the case in the other species. Therefore, it is possible that the difference seen in the nucleotide binding is responsible for the difference seen in RME-8 association to the microsomal compartment. Thus far, Hsc70 is the only binding partner that has been identified for mammalian RME-8 as well as for *Drosophila* and *C.elegans* RME-8. It has been difficult to identify more binding partners due to the large size of the protein which complicates the generation of constructs, and also because RME-8 can only be extracted

using sodium carbonate pH 11.0, which disrupts protein interactions and is therefore not suitable for any co-immunoprecipitation experiments. Since the affinity selection assays that identify Hsc70 as a binding partner for RME-8 were done using only a RME-8 DnaJ domain construct, it is likely that the use of a full-lenght RME-8 construct would be successful in identifying other RME-8 binding partners. Surprisingly, despite the presence of four potential consensus sequences for clathrin binding, RME-8 does not bind to clathrin. One possible explanation is that, even though RME-8 was found in a CCV proteomics analysis, it is not dramatically enriched in the CCV fraction, especially when compared to auxilin-2 (GAK). In contrast, Hsc70 which is ubiquitously expressed and has many different cellular functions, is present in all fractions. This raises the possibility that a pool of RME-8 could be present in a CCV positive compartment, and/or in another compartment close to the CCVs compartment, where its role might not need direct binding to clathrin, and where it could exert a function different than auxilins.

6.3.2 ENDOGENOUS LOCALIZATION OF RME-8

Studies done in non-mammalian species showed that RME-8 is localized throughout the entire endosomal system. In *C.elegans*, RME-8 is present in many cell types and is localized to the limiting membrane of large endosomes that are likely to be late endosomes (Zhang et al., 2001). In *Drosophila*, although predominantly cytosolic, RME-8 is also found associated with multiple endocytic compartments, including the early and late endosomal compartments (Chang et al., 2004). In *Arabidopsis*, RME-8 localizes to late endosomal structures as well (Silady et al., 2008). Thus it is likely that RME-8 would exert a role in the endosomal pathway, either at early or late endosome levels, or at both.

When characterizing the role of a protein, it is important to assess where it resides within the cell, since this localization can be indicative of the protein function. Immunofluorescence is a way to assess the localization of a protein. By staining cells

with an antibody that recognizes endogenous RME-8, together with antibodies that are labeling different compartments within the cell, we can have clues regarding the localization of RME-8. RME-8 staining showed a punctate staining pattern that was found throughout the cell. RME-8 staining also presents an accumulation on large punctate structures within the perinuclear area of the different cell lines we examined. RME-8 staining did not show any cytosolic component, which is consistent with the fact that RME-8 was clearly not found in the cytosolic fraction of a subcellular fractionation preparation. The staining pattern observed for RME-8 is reminiscent of an endosomal staining pattern. Indeed, RME-8 partially colocalizes with different markers of the endosomal population. EEA1 and 20 minutes endocytosed Tf are markers of the early and recycling endosomes respectively, and these markers have been extensively used and characterized in the literature (Mu et al., 1995; Trischler et al., 1995; Raiborg et al., 2001; Lawe et al., 2002). Endogenous RME-8 partially colocalizes with both EEA1 and Tf which indicates that RME-8 is present in both early and recycling structures. However, the colocalization is partial and there are RME-8-positive structures not found labeled with EEA1 or Tf. Staining with other markers showed that RME-8 is also partially colocalized with MPR and with 20 minutes endocytosed EGF, which are both markers of late endosomes. RME-8 would therefore be present in the late endosomal structures as well. Moreover, the fact that RME-8, punctate structures surround or are adjacent to the endocytosed EGF may indicate that RME-8 is localized to the limiting membrane of the late endosomes. This is consistent with the observation that mammalian RME-8 is probably an extrinsic membrane protein due to the fact that it can only be extracted under pH 11.0 treatment. Given that particular feature of RME-8 it is reasonable to think that RME-8 would also be associated with the membrane of early and recycling endosomes. However, whether or not RME-8 has the same or different function at the different endosomal compartments can not be deciphered by immunofluorescence. Another study characterizing mammalian RME-8 found it to be colocalized with EEA1 and Tf but also with Hrs, another marker of early endosomes (Fujibayashi et al., 2008). This helps confirm our observations regarding the presence of RME-8 at early and recycling endosomes. However, there were some discrepancies regarding the presence of RME-8 at the late endosomes between our results and theirs.

As stated previously, our colocalization studies demonstrated that a pool of RME-8 was localized to late endosomes. In their study, Fujibayashi et al. (2008), did not observe any colocalization with late endosomals markers LBPA and GFP-Rab7. This difference could be due to the fact they were using the A549 cell line, which is a human lung adenocarcinoma epithelial cell line, as our studies were done in COS-7, which is a kidney fibroblast cell line from the African Green monkey. They also found partial colocalization of RME-8 with labeled EGF after 15 minutes of chase, which for them indicated the presence of RME-8 at the early endosomes. This kinetic may be particular to that specific A549 cell line, since EGFR was shown to be associated with late endosomal structures after 15-20 minutes in a variety of other cell lines (Haglund et al., 2003; Schmidt and Dikic, 2006).

Little colocalization of RME-8 is seen with syntaxin 6, which is a marker of the TGN, and with the lysosomal marker LAMP1, thus indicating that RME-8 is probably not associated with either of these structures. RME-8 does not colocalize with either AP-2 or AP-1, which is somewhat surprising given the fact that RME-8 was first identified in a proteomics analysis of CCVs. On the other hand, this can be explained by the fact that, although RME-8 is present in the CCV enriched fraction of the CCV preparation, it is not enriched. In addition, RME-8 does not contain any known AP-2 binding motif, such as DPW, DPF, FXDXF and WXXF, which are features of accessory proteins that are binding to AP-2. However, studies have shown the presence of clathrin lattices that are assembling at the membrane of the early endosomes (Raiborg et al., 2001; Raiborg et al., 2002; Raiborg et al., 2006). Although the protocol for enrichment of CCVs leads to a degree of purity close to 90%, the preparation does not allow to differentially isolate vesicles that are budding at the plasma membrane, from the ones budding at the TGN or at the endosomal compartments. This may explain the lack of colocalization of RME-8 with classical markers of the CCV pathway such as AP-2, since the presence of RME-8 within the CCV preparation could be due to its partial association with the endosomal system, or to its presence with an AP-1 derived endosomal cargo. If it is the case, that would explain why RME-8 is not enriched in CCVs, but was still detected by MS. Furthermore, we are confident about the lack of

colocalization with AP-2 at the plasma membrane or with AP-1 at the TGN, since the endosomal punctate immunofluorescence signal disappeared upon RME-8 knock-down, implying that the endogenous RME-8 localization is real as seen in different cell lines and by others (Girard et al., 2005c; Fujibayashi et al., 2008)

6.3.3 RME-8 LOSS-OF-FUNCTION PERTURBS ENDOSOMAL TRAFFICKING

Immunofluorescence studies are useful to assess the localization of a protein and to get an indication as to where it could function, but it does not provide direct information regarding its functional role. We thus turned to small interfering RNA (siRNA)-mediated KD as a means to study the function of RME-8.

Among four selected siRNA sequences for mammalian RME-8, two were efficient in knocking down the protein levels at the concentrations and conditions tested. The absence of RME-8 did not affect the expression levels of many other proteins, including EEA1 and CHC. The omnipresence of RME-8 throughout the endosomal system prompted us to study the effect of RME-8 depletion on endosomal trafficking. We observed that RME-8 depletion causes MPR to cluster in the vicinity of the TGN. However, we did not see any obvious change in the total amount of MPR staining between mock and siRNA treated cells. One of the disadvantages of siRNA is the possibility of off-target effects and, therefore, of phenotypes that would not be caused by the depletion of the protein. We can be confident that the MPR clustering observed upon RME-8 KD is not an off-target effect of the siRNA, since the same phenotype was observed in two different cell lines and with two different siRNA sequences. As introduced previously, MPR transports the lysosomal enzymes, including cathepsin D, from the TGN to late endosomes, and then to lysosomes. This transport allows maturation of cathepsin D, as the pro-cathepsin D that exits the TGN gets cleaved into a mature product once in the lysosome. However, a portion of cathepsin D will escape transport and maturation and will be instead secreted. The cathepsin D assay takes

advantage of that maturation route and monitors the trafficking through the maturation of the enzyme. In this assay, newly synthesized proteins, including cathepsin D, are metabolically labeled with ^{35}S-methionine/cysteine and cathepsin D maturation status is then immunoprecipitated at different time points. We observed that RME-8 depleted cells accumulate less mature cathepsin D over time when compared to their mock transfected counterparts. Moreover, RME-8 KD cells also have reduced secretion of cathepsin D. Since there is a decrease in the maturation of cathepsin D in RME-8 depleted cells, it suggests that MPR is not able to reach the lysosome. It is thus possible that MPR is trapped within the TGN in the absence of RME-8. However, it is probably not the case because if MPR would accumulate at the TGN, the amount of secreted cathepsin D would be expected to increase, as demonstrated by other studies showing that when the TGN exit is blocked, MPR enters the default secretory pathway from the Golgi (Davidson, 1995). Moreover, RME-8 is not localized to the TGN so it is unlikely that TGN is the site of function of RME-8. Thus it seems most likely that MPR is able to leave the TGN but is incapable of reaching the lysosome. RME-8 could be responsible for completing the uncoating of the VAMP4- and syntaxin 6-positive vesicles that are leaving the TGN. In the absence of RME-8, the uncoating process would be impaired, and the VAMP4- and syntaxin 6-positive vesicles would accumulate between the TGN and the endosomal/lysosomal compartment. Interestingly, CLCs do not function in budding but instead in actin organization and trafficking of vesicles towards lysosomes (Poupon et al., 2008). Thus, RME-8, through Hsc70, could regulate the association of CLC with the transport vesicle and RME-8 KD could then alter the trafficking of the TGN-derived vesicles. A third possibility is that RME-8 in late endosomes works on the retrograde pathway from endosomes to TGN. Disruption of RME-8 would thus disrupt the delivery back to the TGN of a factor needed for cathepsin D transport and maturation.

It would be interesting to see what happens to the cathepsin D phenotype in rescue experiments in which we reintroduce wild-type RME-8 and mutant DnaJ RME-8 constructs in RME-8 KD cells. We predict that wt RME-8 would rescue the cathepsin D phenotype but mutant DnaJ RME-8 would not, which would mean that RME-8

interaction with Hsc70 is crucial for the proper trafficking of the lysosomal enzymes. What could be happening in this case is that RME-8 interacts with Hsc70 to uncoat TGN-derived vesicles so they can correctly fuse with endosomes or to otherwise regulate a protein complex needed for transport or fusion. In the first model, when RME-8 is absent from the cell, the uncoating is impaired, the vesicles accumulate because they can not properly fuse with endosomes, and the delivery of lysosomal enzymes is perturbed. This would explain the cathepsin D phenotype we see upon RME-8 KD. This scenario also predicts that RME-8 acts downstream of the TGN CHC/AP-1-mediated budding machinery. This would explain the lack of colocalization between AP-1 and RME-8 as well as the accumulation of immature cathepsin D and MPR in syntaxin-6 and VAMP4 positive structures, but AP-1 and LAMP1 negative structures.

6.3.4 RME-8 DEPLETION AFFECTS EGFR, A RECEPTOR DESTINED TO DEGRADATION, BUT DOES NOT AFFECT RECYCLING RECEPTORS

In non-mammalian organisms, RME-8 was identified in genetic screens for endocytic defects (Zhang et al., 2001; Chang et al., 2004) and gravitroprism defects (Silady et al., 2004). In *C.elegans*, RME-8 is essential for both receptor-mediated endocytosis and fluid-phase endocytosis (Zhang et al., 2001). In *Drosophila*, RME-8 mutants show defects in internalization of Boss (Bride of sevenless), which is the ligand for the receptor tyrosine kinase sevenless, as well as defects in fluid-phase endocytosis. Moreover, RME-8 mutant flies have disorganized endosomal compartments, as well as mislocalized clathrin, two phenotypes that are also observed in *Drosophila* Hsc70 mutants. In *Arabidopsis*, RME-8 mutants did not show any defect in endocytosis but traffic between the pre-vacuolar compartment (PVC; the equivalent of MVB) and the lytic vacuole was perturbed (Silady et al., 2008), which is consistent with the predominant late endosomal localization of RME-8 in plants.

We thus sought to examine the effects of RME-8 depletion on CME. We first studied TfR which is constitutively internalized via CME and then recycles back to the plasma membrane. We did not see any changes in the internalization of Tf either qualitatively by immunofluorescence or quantitatively by fluorescence-activated cell sorting (FACS). Moreover, Western blot for TfR of lysates from mock and RME-8 KD cells did not reveal any difference in the expression levels between control and siRNA treated cells. We then studied EGFR, which is also internalized through CME but then goes for degradation in lysosomes. RME-8 depletion causes a decrease in intracellular EGF as observed by both immunofluorescence and FACS. Unlike TfR, which is a cargo of the constitutive endocytosis pathway, EGFR receptor can enter the cells via CME but also via caveolae (Sigismund et al., 2005; Xiao et al., 2008). It is thus possible that the effect seen in RME-8 depleted cells regarding the EGF decrease is due to defects in the caveolae internalization pathway, instead of the clathrin-mediated pathway. However, this is most likely not the case since the uptake of cholera toxin B, which uses the caveolae pathway, is not affected by RME-8 depletion, and especially since the caveolae internalization pathway is not the main one utilized for the low concentration of EGF we used (Sigismund et al., 2005). Surprisingly, we noticed by Western blot that the expression levels of EGFR were decreased in the absence of RME-8. Therefore, it is most likely that the decrease in intracellular EGF observed in RME-8 KD cells is due to the fact that there is less EGFR expression in these cells, with the consequence that less EGF gets into the cells. This is in agreement with Fujibayashi et al. (2008) who did not observe any endocytosis phenotype or decrease for EGFR upon RME-8 depletion. This other study regarding mammalian RME-8 also used an siRNA approach to assess the RME-8 functional role and Fujibayashi et al. (2008) were successful in decreasing the expression levels of RME-8 by more than 95% using this technique. Since they found that RME-8 was predominantly colocalized with early endocytic markers, they first tested the implication of RME-8 in the early endocytic pathway. No significant effect could be observed on EEA1 and CHC subcellular localization in RME-8 depleted cells. There were also no differences in Tf and EGF uptake as well as in TfR and EGFR endogenous expression levels upon RME-8 KD, which they claimed might be due to lower endogenous levels in A549 compare to COS-7 cells. Their RME-8 KD did not

seem to have any effect on endocytosis. This does not disagree with our study since the effect we found on EGF endocytosis was an indirect effect coming from the decrease in expression levels of EGFR. Moreover, as they mention, it is still possible that in their particular cell line other proteins are compensating for the RME-8 knock-down and that therefore no effect would be seen on EGFR expression levels. Given the absence of phenotype in their siRNA treated cells, they studied the effect of overexpression of RME-8 truncated constructs on early endosome-mediated membrane trafficking. Fujibayashi et al. (2008) found that overexpression of an artificial RME-8 construct comprising the DnaJ domain and the first three N-terminus IWN repeats and lacking the last IWN repeat, caused the formation of large early endosomes as well as a delay in the transport of EGF and transferrin from early endosomal structures. They thus concluded that the trafficking through the early endosomes is compromised in these overexpressing cells. Although very interesting, that phenotype was obtained in the context of an overexpressed truncated protein, which does not always reflect physiological conditions. Nevertheless, this trafficking defect, although different and more pronounced than our observation in knock-down cells, is still in agreement with RME-8 being involved in endosomal sorting.

As seen previously, Western blot analysis of control and siRNA treated cells showed that RME-8 depletion causes a decrease in EGFR expression levels in COS-7 and HeLa cells. Moreover, immunoflorescence staining for total EGFR versus cell surface EGFR did not reveal any striking differences, thus suggesting that the decrease in EGFR receptor is a global generalized decrease, and not a compartment specific decrease. This qualitative observation was confirmed by FACS analysis that quantitatively showed a similar decrease for both the total and the surface EGFR pools compared to control cells. Since RME-8 depletion causes a decrease in EGFR expression levels but has no effect on TfR, it is possible that only receptors destined for degradation are affected by RME-8 absence and that was confirmed in four different cell types (HeLa, COS-7, SKBR3 and BT474). In fact, we demonstrated that other receptors that recycle, such as InsR and LDLR, were also not affected by RME-8 KD, thus reinforcing the possibility that RME-8 depletion does not affect the recycling pathway.

Other RTKs such as TGFβR, HGFR or Met, PDGFR and NGF or TrkA, are clearly destined to degradation (Zerial, 2004; Miranda and Sorkin, 2007). It would be of relevance to decipher if RME-8 function is specific to EGFR or is general for all RTKs destined for degradation. One way to confirm if RME-8 absence affects only receptors that are destined for degradation would be to transfect such receptors (EGFR, TGFβR, HGFR and TrkA), as well as recycling receptors (TfR, LDLR and InsR), in HEK293T cells already KD for RME-8. This experiment would allow a direct comparison between both recycling and targeted for degradation receptors. However, it is possible that the transfection efficiency of the receptors will be different between mock and siRNA-treated cells (thus affecting their expression in the cells) which would complicate the comparison. Moreover, the main disadvantage of the transfection system is that it could self-activate RTKs and make the interpretation for basal levels complicated. RTK family members share common signaling pathways as well as some endocytic accessory proteins even though they have specific binding partners. This is the case for EGFR which signals through Erk/Ras/MAPK pathway and requires specific adaptors such as Eps15 and Grb2. Whether or not RME-8 will be specific to EGFR among the RTK family still remains to be investigated.

6.3.5 RME-8 KD AFFECTS EGFR DEGRADATION RATES

Two reasons can explain the decrease in EGFR steady-state levels in RME-8 KD cells. First, RME-8 depletion could affect the synthesis rate of EGFR, meaning that RME-8 acts upstream of translation. Second, RME-8 depletion could increase the degradation rate of EGFR protein, and consequently decrease its steady-state levels. Metabolic labeling with ^{35}S-methionine/cysteine of newly synthesized proteins in both mock and RME-8 KD cells, followed by immunoprecipitation of EGFR, allowed us to rule out the first option since in both conditions the same amount of EGFR was immunoprecipitated (before stimulation with EGF), which implies that there is no difference in protein synthesis. Previous studies have shown that degradation of EGFR can be monitored simply by treating cells with EGF for different time periods, in the

presence of translation inhibitors, and blotting for EGFR on equal amounts of cell lysates (Huang et al., 2006). However, in our case this approach was far from being ideal, since EGFR expression levels are already decreased at steady-state levels in RME-8 depleted cells. That problem was overcome by doing metabolic labeling of newly synthesized proteins (including EGFR), and by chasing with cold media for different periods of time with EGF in a so-called pulse-chase assay. Using that technique, we found that EGFR degrades faster in RME-8 KD cells, thus confirming the increase degradation rate hypothesis. EGFR degradation can occur through the lysosome and/or through the proteasome (Alwan et al., 2003). Even though we already found that RME-8 was causing an increase in EGFR degradation rate, we still don't know if this is the result of an increase in lysosomal or proteasomal degradation. We should be able to decipher between these two possibilities by doing pulse-chase assays using mock and RME-8 KD cells treated with lysosomal and/or proteosomal inhibitors. If the increased degradation of EGFR in RME-8 knock-down cells is lysosomal dependent, treating these cells with lysosomal inhibitors (Werner et al., 1984) should bring back the EGFR expression levels to those seen in mock cells. More explicitly, if the increased degradation of EGFR in RME-8 KD cells is lysosomal dependent, here is what should happen in theory: 1) mock cells non-treated with lysosomal inhibitors will have a normal EGFR degradation rate; 2) mock cells treated with lysosomal inhibitors will not degrade over time or may degrade slower if the proteasome compensates for the inactivity of the lysosome; 3) RME-8 KD cells not treated with lysosomal inhibitors will degrade EGFR faster than the mock untreated cells, as observed previously; and 4) RME-8 KD cells treated with lysosomal inhibitors will not be able to degrade EGFR as fast anymore, and therefore the EGFR degradation rate should be similar to the one seen in mock cells also treated with lysosomal inhibitors. The same scenario should occur using proteasome inhibitors (Lee and Goldberg, 1998), providing the increased degradation is proteasome dependent. However, this is the perfect situation and it is still possible that both the lysosome and the proteasome are contributing to increased EGFR degradation rate upon RME-8 knock-down, especially given that it has already been shown that both the lysosome and the proteasome are necessary for EGFR degradation (Alwan et al., 2003). Lysosomal and proteasomal inhibitors will also have to be used in pulse-chase assays for

the other RTKs if these also show an increased degradation rate, although it is reasonable to think that if they have the same fate as EGFR upon RME-8 knock down, they will also be degraded in the same pathway. In this case, RME-8 will act as a chaperone which slows down the EGFR degradation pathway by preventing or delaying its targeting to either to the proteasome or the lysosome.

EGFR can accommodate different ligands and depending on which ligand is bound, the signaling generated by its activation, as well as its fate, will differ. Indeed, EGFR processing differs whether the ligand is EGF or TGFα, with EGF favouring proteolytic degradation, and TGFα favoring the recycling of the receptor to the cell surface (Ebner and Derynck, 1991). It would therefore be interesting to look at the degradation of EGFR in TGFα stimulated cells. In mock cells, TGFα is not expected to promote degradation of EGFR. However, in RME-8 depleted cells two scenarios are possible. In the first scenario, the amount of EGFR is comparable, indicating that RME-8 acts downstream of the recycling pathway. In the second scenario, degradation is increased, thus indicating that RME-8 functions at early endosomes in sorting EGFR out of the degradation pathway, to favor its recycling, or to delay its degradation and modulating its signaling. Even though the majority of EGFR gets internalized and degraded upon activation, some studies suggest that still 25-30% of the EGFR recycles back to the plasma membrane (Wiley, 2003; Sorkin et al., 2001). It is thus possible that RME-8 depletion increases the degradation rate by redirecting EGFR recycling pool to the degradative pathway. One way to address that possibility is to perform an ^{125}I-EGF recycling/degradation assay, which is also a pulse-chase assay but with a radioligand, with both EGF and TGFα ligands. Since this assay monitors both recycling and degradation of EGFR, it would allow us to monitor recycling and confirm the degradation rate observed with the ^{35}S-methionine/cysteine pulse-chase assay. Moreover, it would also determine the effect of RME-8 knock down on binding of a ligand that promotes exclusively the recycling of EGFR.

Another factor that influences EGFR trafficking fate is the composition of the EGFR dimer. When EGFR is a homodimer it is targeted to the degradation pathway and

the receptor can terminate its signaling. However, when EGFR heterodimerizes with ErbB2, it is redirected to the recycling pathway, and the major consequence is sustained signaling, and that sustained signaling has a positive impact on cell proliferation (Ceresa and Schmid, 2000; Wang et al., 1999). Indeed, ErbB2 overexpression is a common feature in many types of cancer including breast cancer where it strongly correlates with poor prognosis for the patients (Slamon et al., 1987). Since RME-8 depletion enhances degradation of EGFR, we sought to examine if this KD could overcome the effect of the presence of ErbB2, and therefore have potential implication for mitogenesis and cancer. In order to test that hypothesis, we used two human breast cancer cell lines, BT474 and SKBR3, which are known to overexpress ErbB2, and in which it is established that ErbB2 overexpression increases EGFR signaling (Wang et al., 1999). We first verified the endogenous expression levels of ErbB2 in COS-7 and HeLa cells, and found no difference between mock and siRNA-treated cells, thus indicating again that RME-8 depletion does not affect the expression levels of receptors that are primarily recycling back to the plasma membrane. In both BT474 and SKBR3 cancer lines we were able to significantly KD RME-8 and we did not find any difference in ErbB2 expression levels between mock and RME-8 depleted cells. However, we did observe a significant decrease in EGFR steady-state levels in the siRNA-treated cells. So even in a context where ErbB2 is overexpressed, and therefore a large part of EGFR receptor is recycling, RME-8 knock down still causes an increase in EGFR degradation. This finding could have some clinical value in treatment of ErbB2 positive cancers since decreasing RME-8 expression in neoplastic cells could increase degradation of EGFR and attenuate mitogenic signaling. It would be crucial to test if the increase in EGFR degradation in RME-8 knock down cancer cells also correlates with attenuation in signaling, by testing the activation and the fate in response to EGF, of key signaling components, such as Ras, Erk1 and Akt. Since signaling is intimately linked to cells viability, the effect of RME-8 KD on growth rates of cancer cells will also have to be investigated, and that could be done using MTT assays. Another interesting feature of the SKBR3 and BT474 breast cancer cell lines is their anchorage-independent growth, which is thought to be mediated by overexpression of ErbB2 and activation of Erk1/2 and Akt (Lin et al., 2007). We could assess if RME-8 knock-down interferes with that property by using soft agar

assays in which cells in suspension from both mock and siRNA-treated cells would be resuspended, supplemented with soft agarose, and plated on solidified media where they will grow colonies (Lin et al., 2007). Signaling and growth rate could also be tested using these same assays, but this time in the context of an overexpressing system where 293T cells mock and siRNA-treated will be transfected with EGFR with or without ErbB2 constructs. Since RME-8 KD downregulates EGFR expression by increasing its degradation, and that this kind of downregulation is a well described mechanism to turn off signaling (Wiley, 2003), we predict that RME-8 KD would decrease signaling, slow down growth rate, and disrupt the anchorage-independent growth of cancer cells.

6.3.6 MECHANISTIC FUNCTION OF RME-8 AND CLATHRIN REGULATION ON ENDOSOMES

We established that RME-8 localizes throughout the endosomal system, interacts with Hsc70 through its DnaJ domain, and regulates EGFR degradation rate. We propose that RME-8, together with Hsc70, functions as a negative regulator of clathrin coat assembly on endosomes. Previous studies revealed the presence of clathrin coat on endosomes (Raiborg et al., 2006) and Hsc70 has already been described as a key molecule in sorting decisions on early endosomes (Newmyer and Schmid, 2001). Normally, RME-8 and Hsc70 would disassemble clathrin coats on endosomes in order to maintain equilibrium of clathrin coats and Hrs between the endosomal membranes and the cytosol (Raiborg et al., 2006). In the absence of RME-8, the equilibrium is perturbed and more clathrin coats and Hrs are associating with the endosomal membrane. This creates more sites for ubiquitinated cargoes on the endosomal membrane and thus more cargo can be targeted to ESCRT complexes, enter the MVBs, and reach the lysosome for degradation. This would explain why EGFR degrades more in RME-8 depleted cells. In addition, this hypothesis is even more plausible given the fact that RME-8 KD cells have less clathrin in their cytosol even though their total clathrin levels are not changed. Moreover, this model has the advantage of being readily testable. We could first assess the degree of colocalization of endogenous RME-8 with Hrs. According to our model, RME-8 may regulate the assembly of clathrin by keeping a balanced kinetic between

clathrin coats and Hrs at the endosomal membrane. Therefore it is likely that RME-8 and Hrs would colocalize. Colocalization of CHC with Hrs and Tgs101 would have to be examined in mock and KD cells. Following our hypothesis, CHC should colocalize more with Hrs upon RME-8 depletion compared to mock cells, since RME-8 absence would favor assembly of clathrin coats on endosomal membranes. Ubiquitin is also an important molecule implicated in intracellular transport that can act as a sorting signal to target proteins, including EGFR, for degradation (Haglund et al., 2003; Mosesson et al., 2003). Moreover, clathrin coats and Hrs association are critical for recruitment of ubiquitinated cargoes such as EGFR (Raiborg et al., 2003). It is thus very important, in the light of our model, to test for the ubiquitination status of EGFR: we expect to see an increase in EGFR ubiquitination in knock down cells.

We could transfect wt RME-8 and DnaJ mutant RME-8 constructs into RME-8 depleted cells and see if we can rescue the different phenotypes we observed in RME-8 KD cells. Constructs where the DnaJ-domain critical tripeptide HPD was mutated into QPN have already been described to block the binding of DnaJ to Hsc70 (Genevaux et al., 2002; Walsh et al. 2004), and we will have to confirm by pull-down assay that our RME-8 mutant construct disrupts the interaction of RME-8 DnaJ domain with Hsc70. If RME-8 depletion causes more clathrin to assemble at the endosomal membrane, putting back wt RME-8 into KD cells should bring back the equilibrium between the assembled and disassembled pools of clathrin, whereas the DnaJ mutant RME-8 should not have any effect, thus proving the crucial role of RME-8 and Hsc70 interaction. These constructs could also be used to check if we can rescue the EGFR degradation phenotype, and if it is possible to bring back the EGFR expression levels close to the ones seen in control cells. If the model is accurate, EGFR phenotypes should be rescued with wt RME-8 construct and no effect should be seen with the DnaJ mutant construct. Moreover, if the prediction that RME-8 depletion causes a decrease in mitogenic signaling and proliferation in ErbB2 cancer cells is true, reintroducing RME-8 should reinstate the signaling and increase the proliferation rate. Not only will these rescue experiments allow us to assess the functional role of RME-8 and but they will also introduce RME-8 as a potential therapeutic tool in ErbB2 positive cancers.

6.4 GENERAL CONCLUSION

The liver CCVs allowed us to use the peptide/spectral accounting approach for the first time in order to compare abundant proteins between two different proteomes. To our surprise, we found that CLCs are not stoichiometrically associated with CHC and, as such, are unlikely the universal regulator of clathrin assembly, at least in non-neuronal tissues. The proteomics also revealed differences in CHC adaptor proteins between brain and liver and confirm that the brain possesses a very specialized form of endocytosis compared to liver which exhibits more general housekeeping endocytic tasks. New proteins that will give insights into different protein complexes and subcellular compartments were identified. Among these novel proteins, RME-8 was characterized and we found that it was localized throughout the endosomal system where it is thought to function in the intracellular trafficking of cargoes such as MPR. In the context of MPR, RME-8 might be involved in late stages of TGN sorting towards the lysosomes to render vesicles competent for fusion with the late endosome/lysosome compartment. RME-8 is also a new regulator of EGFR downregulation processes and may therefore play an important role in regulation of cell signaling. RME-8 function on RTKs regulation is still elusive, but in light of this first set of data, it may be implicated in the sorting and/or timing as an Hsc70 co-chaperone of EGFR from the endosome to the Hrs/ESCRT-0 complex toward its ultimate fate of signaling downregulation and degradation.

REFERENCES LIST

Acton SL, Brodsky FM. Predominance of clathrin light chain LCb correlates with the presence of a regulated secretory pathway. J Cell Biol. 1990 Oct;111(4):1419-26.

Aebersold R, Mann M. Mass spectrometry-based proteomics. Nature. 2003 Mar 13;422(6928):198-207.

Ahle S, Ungewickell E. Auxilin, a newly identified clathrin-associated protein in coated vesicles from bovine brain. J Cell Biol. 1990 Jul;111(1):19-29.

Allaire PD, Ritter B, Thomas S, Burman JL, Denisov AY, Legendre-Guillemin V, Harper SQ, Davidson BL, Gehring K, McPherson PS. Connecdenn, a novel DENN domain-containing protein of neuronal clathrin-coated vesicles functioning in synaptic vesicle endocytosis. J Neurosci. 2006 Dec 20;26(51):13202-12.

Alwan HA, van Zoelen EJ, van Leeuwen JE. Ligand-induced lysosomal epidermal growth factor receptor (EGFR) degradation is preceded by proteasome-dependent EGFR de-ubiquitination. J Biol Chem. 2003 Sep 12;278(37):35781-90.

Andersen JS, Wilkinson CJ, Mayor T, Mortensen P, Nigg EA, Mann M. Proteomic characterization of the human centrosome by protein correlation profiling. Nature. 2003 Dec 4;426(6966):570-4.

Aniento F, Emans N, Griffiths G, Gruenberg J. Cytoplasmic dynein-dependent vesicular transport from early to late endosomes. J Cell Biol. 1993 Dec;123(6 Pt 1):1373-87.

Arévalo JC, Waite J, Rajagopal R, Beyna M, Chen ZY, Lee FS, Chao MV. Cell survival through Trk neurotrophin receptors is differentially regulated by ubiquitination. Neuron. 2006 May 18;50(4):549-59.

Babst M. A protein's final ESCRT. Traffic. 2005 Jan;6(1):2-9.

Bache KG, Raiborg C, Mehlum A, Stenmark H. STAM and Hrs are subunits of a multivalent ubiquitin-binding complex on early endosomes. J Biol Chem. 2003 Apr 4;278(14):12513-21.

Bache KG, Slagsvold T, Stenmark H. Defective downregulation of receptor tyrosine kinases in cancer. EMBO J. 2004 Jul 21;23(14):2707-12.

Bai H, Doray B, Kornfeld S. GGA1 interacts with the adaptor protein AP-1 through a WNSF sequence in its hinge region. J Biol Chem. 2004 Apr 23;279(17):17411-7.

Bar-Sagi D, Hall A. Ras and Rho GTPases: a family reunion. Cell. 2000 Oct 13;103(2):227-38.

Baulida J, Kraus MH, Alimandi M, Di Fiore PP, Carpenter G. All ErbB receptors other than the epidermal growth factor receptor are endocytosis impaired. J Biol Chem. 1996 Mar 1;271(9):5251-7.

Beck KA, Keen JH. Interaction of phosphoinositide cycle intermediates with the plasma membrane-associated clathrin assembly protein AP-2. J Biol Chem. 1991 Mar 5;266(7):4442-7.

Beguinot L, Lyall RM, Willingham MC, Pastan I. Down-regulation of the epidermal growth factor receptor in KB cells is due to receptor internalization and subsequent degradation in lysosomes. Proc Natl Acad Sci U S A. 1984 Apr;81(8):2384-8.

Bell AW, Ward MA, Blackstock WP, Freeman HN, Choudhary JS, Lewis AP, Chotai D, Fazel A, Gushue JN, Paiement J, Palcy S, Chevet E, Lafrenière-Roula M, Solari R, Thomas DY, Rowley A, Bergeron JJ. Proteomics characterization of abundant Golgi membrane proteins. J Biol Chem. 2001 Feb 16;276(7):5152-65.

Benmerah A, Gagnon J, Bègue B, Mégarbané B, Dautry-Varsat A, Cerf-Bensussan N. The tyrosine kinase substrate eps15 is constitutively associated with the plasma membrane adaptor AP-2. J Cell Biol. 1995 Dec;131(6 Pt 2):1831-8.

Blondeau F, Ritter B, Allaire PD, Wasiak S, Girard M, Hussain NK, Angers A, Legendre-Guillemin V, Roy L, Boismenu D, Kearney RE, Bell AW, Bergeron JJ, McPherson PS. Tandem MS analysis of brain clathrin-coated vesicles reveals their critical involvement in synaptic vesicle recycling. Proc Natl Acad Sci U S A. 2004 Mar 16;101(11):3833-8.

Borner GH, Rana AA, Forster R, Harbour M, Smith JC, Robinson MS. CVAK104 is a novel regulator of clathrin-mediated SNARE sorting. Traffic. 2007 Jul;8(7):893-903.

Bomsel M, Parton R, Kuznetsov SA, Schroer TA, Gruenberg J. Microtubule- and motor-dependent fusion in vitro between apical and basolateral endocytic vesicles from MDCK cells. Cell. 1990 Aug 24;62(4):719-31.

Bonifacino JS. The GGA proteins: adaptors on the move. Nat Rev Mol Cell Biol. 2004 Jan;5(1):23-32.

Bonifacino JS, Traub LM. Signals for sorting of transmembrane proteins to endosomes and lysosomes. Annu Rev Biochem. 2003;72:395-447.

Brett TJ, Traub LM, Fremont DH. Accessory protein recruitment motifs in clathrin-mediated endocytosis. Structure. 2002 Jun;10(6):797-809.

Brodsky FM. Living with clathrin: its role in intracellular membrane traffic. Science. 1988 Dec 9;242(4884):1396-402.

Brodsky FM, Hill BL, Acton SL, Näthke I, Wong DH, Ponnambalam S, Parham P. Clathrin light chains: arrays of protein motifs that regulate coated-vesicle dynamics. Trends Biochem Sci. 1991 Jun;16(6):208-13.

Brown MS, Goldstein JL (1979). "Receptor-mediated endocytosis: insights from the lipoprotein receptor system.". Proc. Natl. Acad. Sci. U.S.A. 76 (7): 3330–7.

Cajo GC, Horne BE, Kelley WL, Schwager F, Georgopoulos C, Genevaux P. The role of the DIF motif of the DnaJ (Hsp40) co-chaperone in the regulation of the DnaK (Hsp70) chaperone cycle. J Biol Chem. 2006 May 5;281(18):12436-44.

Cao H, Thompson HM, Krueger EW, McNiven MA. Disruption of Golgi structure and function in mammalian cells expressing a mutant dynamin. J Cell Sci. 2000 Jun;113 (Pt 11):1993-2002.

Cao Z, Wu X, Yen L, Sweeney C, Carraway KL 3rd. Neuregulin-induced ErbB3 downregulation is mediated by a protein stability cascade involving the E3 ubiquitin ligase Nrdp1. Mol Cell Biol. 2007 Mar;27(6):2180-8.

Carpenter G. Receptors for epidermal growth factor and other polypeptide mitogens. Annu Rev Biochem. 1987;56:881-914.

Carpenter G, Cohen S. Epidermal growth factor. Annu Rev Biochem. 1979;48:193-216.

Carpentier JL, Gorden P, Anderson RG, Goldstein JL, Brown MS, Cohen S, Orci L. Co-localization of 125I-epidermal growth factor and ferritin-low density lipoprotein in coated pits: a quantitative electron microscopic study in normal and mutant human fibroblasts. J Cell Biol. 1982 Oct;95(1):73-7.

Carreno S, Engqvist-Goldstein AE, Zhang CX, McDonald KL, Drubin DG. Actin dynamics coupled to clathrin-coated vesicle formation at the trans-Golgi network. J Cell Biol. 2004 Jun 21;165(6):781-8.

Carroll RC, Beattie EC, von Zastrow M, Malenka RC. Role of AMPA receptor endocytosis in synaptic plasticity. Nat Rev Neurosci. 2001 May;2(5):315-24.

Ceresa BP, Schmid SL. Regulation of signal transduction by endocytosis. Curr Opin Cell Biol. 2000 Apr;12(2):204-210.

Chang HC, Hull M, Mellman I. The J-domain protein Rme-8 interacts with Hsc70 to control clathrin-dependent endocytosis in Drosophila. J Cell Biol. 2004 Mar 29;164(7):1055-64.

Cheetham ME, Caplan AJ. Structure, function and evolution of DnaJ: conservation and adaptation of chaperone function. Cell Stress Chaperones. 1998 Mar;3(1):28-36.

Chen CY, Brodsky FM. Huntingtin-interacting protein 1 (Hip1) and Hip1-related protein (Hip1R) bind the conserved sequence of clathrin light chains and thereby influence clathrin assembly in vitro and actin distribution in vivo. J Biol Chem. 2005 Feb 18;280(7):6109-17.

Chen YG, Wang Z, Ma J, Zhang L, Lu Z. Endofin, a FYVE domain protein, interacts with Smad4 and facilitates transforming growth factor-beta signaling. J Biol Chem. 2007 Mar 30;282(13):9688-95.

Cho JY, Guo C, Torello M, Lunstrum GP, Iwata T, Deng C, Horton WA. Defective lysosomal targeting of activated fibroblast growth factor receptor 3 in achondroplasia. Proc Natl Acad Sci U S A. 2004 Jan 13;101(2):609-14.

Citri A, Yarden Y. EGF-ERBB signalling: towards the systems level. Nat Rev Mol Cell Biol. 2006 Jul;7(7):505-16.

Clague MJ, Urbé S. Endocytosis: the DUB version. Trends Cell Biol. 2006 Nov;16(11):551-9.

Collins BM, McCoy AJ, Kent HM, Evans PR, Owen DJ. Molecular architecture and functional model of the endocytic AP2 complex. Cell. 2002 May 17;109(4):523-535.

Conner SD, Schmid SL. Identification of an adaptor-associated kinase, AAK1, as a regulator of clathrin-mediated endocytosis. J Cell Biol. 2002 Mar 4;156(5):921-929.

Conner SD, Schmid SL. Regulated portals of entry into the cell. Nature. 2003 Mar 6;422(6927):37-44.

Conner SD, Schmid SL. CVAK104 is a novel poly-L-lysine-stimulated kinase that targets the beta2-subunit of AP2. J Biol Chem. 2005 Jun 3;280(22):21539-44.

Cox B, Kislinger T, Emili A. Integrating gene and protein expression data: pattern analysis and profile mining. Methods. 2005 Mar;35(3):303-14.

Cravatt BF, Simon GM, Yates JR 3rd. The biological impact of mass-spectrometry-based proteomics. Nature. 2007 Dec 13;450(7172):991-1000.

Cronshaw JM, Krutchinsky AN, Zhang W, Chait BT, Matunis MJ. Proteomic analysis of the mammalian nuclear pore complex. J Cell Biol. 2002 Sep 2;158(5):915-27.

Damke, H., Baba, T., Warnock, D. E. and Schmid, S. L. (1994) Induction of mutant dynamin specifically blocks endocytic coated vesicle formation. J. Cell Biol. 127, 915–934.

Davidson HW. Wortmannin causes mistargeting of procathepsin D. evidence for the involvement of a phosphatidylinositol 3-kinase in vesicular transport to lysosomes. J Cell Biol. 1995 Aug;130(4):797-805.

Decker SJ. Epidermal growth factor and transforming growth factor-alpha induce differential processing of the epidermal growth factor receptor. Biochem Biophys Res Commun. 1990 Jan 30;166(2):615-21.

Delcroix JD, Valletta JS, Wu C, Hunt SJ, Kowal AS, Mobley WC. NGF signaling in sensory neurons: evidence that early endosomes carry NGF retrograde signals. Neuron. 2003 Jul 3;39(1):69-84.

Di Fiore PP, De Camilli P. Endocytosis and signaling. an inseparable partnership. Cell. 2001 Jul 13;106(1):1-4.

Di Fiore PP, Gill GN. Endocytosis and mitogenic signaling. Curr Opin Cell Biol. 1999 Aug;11(4):483-8.

Di Guglielmo GM, Baass PC, Ou WJ, Posner BI, Bergeron JJ. Compartmentalization of SHC, GRB2 and mSOS, and hyperphosphorylation of Raf-1 by EGF but not insulin in liver parenchyma. EMBO J. 1994 Sep 15;13(18):4269-77.

Di Guglielmo GM, Le Roy C, Goodfellow AF, Wrana JL. Distinct endocytic pathways regulate TGF-beta receptor signalling and turnover. Nat Cell Biol. 2003 May;5(5):410-21.

Dikic I. Mechanisms controlling EGF receptor endocytosis and degradation. Biochem Soc Trans. 2003 Dec;31(Pt 6):1178-81.

Donaldson JG, Jackson CL. Regulators and effectors of the ARF GTPases. Curr Opin Cell Biol. 2000 Aug;12(4):475-82.

Doray B, Bruns K, Ghosh P, Kornfeld S. Interaction of the cation-dependent mannose 6-phosphate receptor with GGA proteins. J Biol Chem. 2002a May 24;277(21):18477-82.

Doray B, Ghosh P, Griffith J, Geuze HJ, Kornfeld S. Cooperation of GGAs and AP-1 in packaging MPRs at the trans-Golgi network. Science. 2002b Sep 6;297(5587):1700-3.

Doyotte A, Russell MR, Hopkins CR, Woodman PG. Depletion of TSG101 forms a mammalian "Class E" compartment: a multicisternal early endosome with multiple sorting defects. J Cell Sci. 2005 Jul 15;118(Pt 14):3003-17.

Dreger M. Emerging strategies in mass-spectrometry based proteomics. Eur J Biochem. 2003 Feb;270(4):569.

Dunn KW, McGraw TE, Maxfield FR. Iterative fractionation of recycling receptors from lysosomally destined ligands in an early sorting endosome. J Cell Biol. 1989 Dec;109(6 Pt 2):3303-14.

Duval M, Bédard-Goulet S, Delisle C, Gratton JP. Vascular endothelial growth factor-dependent down-regulation of Flk-1/KDR involves Cbl-mediated ubiquitination. Consequences on nitric oxide production from endothelial cells. J Biol Chem. 2003 May 30;278(22):20091-7.

Ebner R, Derynck R. Epidermal growth factor and transforming growth factor-alpha: differential intracellular routing and processing of ligand-receptor complexes. Cell Regul. 1991 Aug;2(8):599-612.

Ehrlich M, Boll W, Van Oijen A, Hariharan R, Chandran K, Nibert ML, Kirchhausen T. Endocytosis by random initiation and stabilization of clathrin-coated pits. Cell. 2004 Sep 3;118(5):591-605.

Eisenberg E, Greene LE. Multiple roles of auxilin and hsc70 in clathrin-mediated endocytosis. Traffic. 2007 Jun;8(6):640-6.

Evergren E, Tomilin N, Vasylieva E, Sergeeva V, Bloom O, Gad H, Capani F, Shupliakov O. A pre-embedding immunogold approach for detection of synaptic endocytic proteins in situ. J Neurosci Methods. 2004 May 30;135(1-2):169-74.

Farsad K, Ringstad N, Takei K, Floyd SR, Rose K, De Camilli P. Generation of high curvature membranes mediated by direct endophilin bilayer interactions. J Cell Biol. 2001 Oct 15;155(2):193-200.

Felder S, Miller K, Moehren G, Ullrich A, Schlessinger J, Hopkins CR. Kinase activity controls the sorting of the epidermal growth factor receptor within the multivesicular body. Cell. 1990 May 18;61(4):623-34.

Filipowicz W. RNAi: the nuts and bolts of the RISC machine. Cell. 2005 Jul 15;122(1):17-20.

Flynn GC, Pohl J, Flocco MT, Rothman JE. Peptide-binding specificity of the molecular chaperone BiP. Nature. 1991 Oct 24;353(6346):726-30.

Ford AC, Grandis JR. Targeting epidermal growth factor receptor in head and neck cancer. Head Neck. 2003 Jan;25(1):67-73.

Ford MG, Mills IG, Peter BJ, Vallis Y, Praefcke GJ, Evans PR, McMahon HT. Curvature of clathrin-coated pits driven by epsin. Nature. 2002 Sep 26;419(6905):361-6.

Foster LJ, de Hoog CL, Zhang Y, Zhang Y, Xie X, Mootha VK, Mann M. A mammalian organelle map by protein correlation profiling. Cell. 2006 Apr 7;125(1):187-99.

Frederick L, Wang XY, Eley G, James CD. Diversity and frequency of epidermal growth factor receptor mutations in human glioblastomas. Cancer Res. 2000 Mar 1;60(5):1383-7.

Fujibayashi A, Taguchi T, Misaki R, Ohtani M, Dohmae N, Takio K, Yamada M, Gu J, Yamakami M, Fukuda M, Waguri S, Uchiyama Y, Yoshimori T, Sekiguchi K. Human RME-8 is involved in membrane trafficking through early endosomes. Cell Struct Funct. 2008;33(1):35-50.

Fukuda R, McNew JA, Weber T, Parlati F, Engel T, Nickel W, Rothman JE, Söllner TH. Functional architecture of an intracellular membrane t-SNARE. Nature. 2000 Sep 14;407(6801):198-202.

Futter CE, Felder S, Schlessinger J, Ullrich A, Hopkins CR. Annexin I is phosphorylated in the multivesicular body during the processing of the epidermal growth factor receptor. J Cell Biol. 1993 Jan;120(1):77-83.

Gaidarov I, Chen Q, Falck JR, Reddy KK, Keen JH. A functional phosphatidylinositol 3,4,5-trisphosphate/phosphoinositide binding domain in the clathrin adaptor AP-2 alpha subunit. Implications for the endocytic pathway. J Biol Chem. 1996 Aug 23;271(34):20922-9.

Gall WE, Higginbotham MA, Chen C, Ingram MF, Cyr DM, Graham TR. The auxilin-like phosphoprotein Swa2p is required for clathrin function in yeast. Curr Biol. 2000 Nov 2;10(21):1349-58.

Gao J, Friedrichs MS, Dongre AR, Opiteck GJ. Guidelines for the routine application of the peptide hits technique. J Am Soc Mass Spectrom. 2005 Aug;16(8):1231-8.

Garin J, Diez R, Kieffer S, Dermine JF, Duclos S, Gagnon E, Sadoul R, Rondeau C, Desjardins M. The phagosome proteome: insight into phagosome functions. J Cell Biol. 2001 Jan 8;152(1):165-80.

Garrett TP, McKern NM, Lou M, Elleman TC, Adams TE, Lovrecz GO, Kofler M, Jorissen RN, Nice EC, Burgess AW, Ward CW. The crystal structure of a truncated ErbB2 ectodomain reveals an active conformation, poised to interact with other ErbB receptors. Mol Cell. 2003 Feb;11(2):495-505.

Geetha T, Jiang J, Wooten MW. Lysine 63 polyubiquitination of the nerve growth factor receptor TrkA directs internalization and signaling. Mol Cell. 2005 Oct 28;20(2):301-12.

Geetha T, Wooten MW. TrkA receptor endolysosomal degradation is both ubiquitin and proteasome dependent. Traffic. 2008 Jul;9(7):1146-56.

Genevaux P, Schwager F, Georgopoulos C, Kelley WL. Scanning mutagenesis identifies amino acid residues essential for the in vivo activity of the Escherichia coli DnaJ (Hsp40) J-domain. Genetics. 2002 Nov;162(3):1045-53.

George M, Ying G, Rainey MA, Solomon A, Parikh PT, Gao Q, Band V, Band H. Shared as well as distinct roles of EHD proteins revealed by biochemical and functional comparisons in mammalian cells and C. elegans. BMC Cell Biol. 2007 Jan 18;8:3.

Gerber SA, Rush J, Stemman O, Kirschner MW, Gygi SP. Absolute quantification of proteins and phosphoproteins from cell lysates by tandem MS. Proc Natl Acad Sci U S A. 2003 Jun 10;100(12):6940-5.

Ghosh P, Dahms NM, Kornfeld S. Mannose 6-phosphate receptors: new twists in the tale. Nat Rev Mol Cell Biol. 2003a Mar;4(3):202-12.

Ghosh P, Griffith J, Geuze HJ, Kornfeld S. Mammalian GGAs act together to sort mannose 6-phosphate receptors. J Cell Biol. 2003b Nov 24;163(4):755-66.

Gilchrist A, Au CE, Hiding J, Bell AW, Fernandez-Rodriguez J, Lesimple S, Nagaya H, Roy L, Gosline SJ, Hallett M, Paiement J, Kearney RE, Nilsson T, Bergeron JJ. Quantitative proteomics analysis of the secretory pathway. Cell. 2006 Dec 15;127(6):1265-81.

Gillingham AK, Munro S. Long coiled-coil proteins and membrane traffic. Biochim Biophys Acta. 2003 Aug 18;1641(2-3):71-85.

Girard M, Allaire PD, Blondeau F, McPherson PS. Isolation of clathrin-coated vesicles by differential and density gradient centrifugation. Curr Protoc Cell Biol. 2005a Apr;Chapter 3:Unit 3.13.

Girard M, Allaire PD, McPherson PS, Blondeau F. Non-stoichiometric relationship between clathrin heavy and light chains revealed by quantitative comparative proteomics of clathrin-coated vesicles from brain and liver. Mol Cell Proteomics. 2005b Aug;4(8):1145-54.

Girard M, Poupon V, Blondeau F, McPherson PS. The DnaJ-domain protein RME-8 functions in endosomal trafficking. J Biol Chem. 2005c Dec 2;280(48):40135-43.

Graus-Porta D, Beerli RR, Daly JM, Hynes NE. ErbB-2, the preferred heterodimerization partner of all ErbB receptors, is a mediator of lateral signaling. EMBO J. 1997 Apr 1;16(7):1647-55.

Greener T, Grant B, Zhang Y, Wu X, Greene LE, Hirsh D, Eisenberg E. Caenorhabditis elegans auxilin: a J-domain protein essential for clathrin-mediated endocytosis in vivo. Nat Cell Biol. 2001 Feb;3(2):215-9.

Greener T, Zhao X, Nojima H, Eisenberg E, Greene LE. Role of cyclin G-associated kinase in uncoating clathrin-coated vesicles from non-neuronal cells. J Biol Chem. 2000 Jan 14;275(2):1365-70.

Griffiths G, Hoflack B, Simons K, Mellman I, Kornfeld S. The mannose 6-phosphate receptor and the biogenesis of lysosomes. Cell. 1988 Feb 12;52(3):329-41.

Gruenberg J. The endocytic pathway: a mosaic of domains. Nat Rev Mol Cell Biol. 2001 Oct;2(10):721-30.

Gruenberg J, Maxfield FR. Membrane transport in the endocytic pathway. Curr Opin Cell Biol. 1995 Aug;7(4):552-63.

Gruenberg J, Stenmark H. The biogenesis of multivesicular endosomes. Nat Rev Mol Cell Biol. 2004 Apr;5(4):317-23.

Gruhler A, Schulze WX, Matthiesen R, Mann M, Jensen ON. Stable isotope labeling of Arabidopsis thaliana cells and quantitative proteomics by mass spectrometry. Mol Cell Proteomics. 2005 Nov;4(11):1697-709.

Guy PM, Platko JV, Cantley LC, Cerione RA, Carraway KL 3rd. Insect cell-expressed p180erbB3 possesses an impaired tyrosine kinase activity. Proc Natl Acad Sci U S A. 1994 Aug 16;91(17):8132-6.

Hagedorn EJ, Bayraktar JL, Kandachar VR, Bai T, Englert DM, Chang HC. Drosophila melanogaster auxilin regulates the internalization of Delta to control activity of the Notch signaling pathway. J Cell Biol. 2006 May 8;173(3):443-52.

Haglund K, Sigismund S, Polo S, Szymkiewicz I, Di Fiore PP, Dikic I. Multiple monoubiquitination of RTKs is sufficient for their endocytosis and degradation. Nat Cell Biol. 2003 May;5(5):461-6.

Hanover JA, Willingham MC, Pastan I. Kinetics of transit of transferrin and epidermal growth factor through clathrin-coated membranes. Cell. 1984 Dec;39(2 Pt 1):283-93.

Hartl FU, Hayer-Hartl M. Molecular chaperones in the cytosol: from nascent chain to folded protein. Science. 2002 Mar 8;295(5561):1852-8.

Hartl FU, Martin J, Neupert W. Protein folding in the cell: the role of molecular chaperones Hsp70 and Hsp60. Annu Rev Biophys Biomol Struct. 1992;21:293-322.

Haslekås C, Breen K, Pedersen KW, Johannessen LE, Stang E, Madshus IH. The inhibitory effect of ErbB2 on epidermal growth factor-induced formation of clathrin-coated pits correlates with retention of epidermal growth factor receptor-ErbB2 oligomeric complexes at the plasma membrane. Mol Biol Cell. 2005 Dec;16(12):5832-42.

Haucke V, Wenk MR, Chapman ER, Farsad K, De Camilli P. Dual interaction of synaptotagmin with mu2- and alpha-adaptin facilitates clathrin-coated pit nucleation. EMBO J. 2000 Nov 15;19(22):6011-9.

Hayashi T, Sakamoto S. Radioimmunoassay of human epidermal growth factor--hEGF levels in human body fluids. J Pharmacobiodyn. 1988 Mar;11(3):146-51.

Heath CM, Stahl PD, Barbieri MA. Lipid kinases play crucial and multiple roles in membrane trafficking and signaling. Histol Histopathol. 2003 Jul;18(3):989-98.

Heuser JE, Keen J. Deep-etch visualization of proteins involved in clathrin assembly. J Cell Biol. 1988 Sep;107(3):877-86.

Heuser JE, Reese TS. Evidence for recycling of synaptic vesicle membrane during transmitter release at the frog neuromuscular junction. J Cell Biol. 1973 May;57(2):315-44.

Hicke L, Dunn R. Regulation of membrane protein transport by ubiquitin and ubiquitin-binding proteins. Annu Rev Cell Dev Biol. 2003;19:141-72.

Hicke L, Riezman H. Ubiquitination of a yeast plasma membrane receptor signals its ligand-stimulated endocytosis. Cell. 1996 Jan 26;84(2):277-87.

Hinshaw JE, Schmid SL. Dynamin self-assembles into rings suggesting a mechanism for coated vesicle budding. Nature. 1995 Mar 9;374(6518):190-2.

Holstein SE, Ungewickell H, Ungewickell E. Mechanism of clathrin basket dissociation: separate functions of protein domains of the DnaJ homologue auxilin. J Cell Biol. 1996 Nov;135(4):925-37.

Honda A, Nogami M, Yokozeki T, Yamazaki M, Nakamura H, Watanabe H, Kawamoto K, Nakayama K, Morris AJ, Frohman MA, Kanaho Y. Phosphatidylinositol 4-phosphate 5-kinase alpha is a downstream effector of the small G protein ARF6 in membrane ruffle formation. Cell. 1999 Nov 24;99(5):521-32.

Hong W. SNAREs and traffic. Biochim Biophys Acta. 2005 Jul 10;1744(3):493-517.

Hopkins CR. Intracellular routing of transferrin and transferrin receptors in epidermoid carcinoma A431 cells. Cell. 1983 Nov;35(1):321-30.

Hu Y, Zhou Z, Huang X, Xu M, Lu L, Xu Z, Li J, Sha J. Expression of a novel DnaJA1 alternative splicing in human testis and sperm. Int J Androl. 2004 Dec;27(6):343-9.

Huang F, Goh LK, Sorkin A. EGF receptor ubiquitination is not necessary for its internalization. Proc Natl Acad Sci U S A. 2007 Oct 23;104(43):16904-9.

Huang F, Khvorova A, Marshall W, Sorkin A. Analysis of clathrin-mediated endocytosis of epidermal growth factor receptor by RNA interference. J Biol Chem. 2004 Apr 16;279(16):16657-61.

Huang F, Kirkpatrick D, Jiang X, Gygi S, Sorkin A. Differential regulation of EGF receptor internalization and degradation by multiubiquitination within the kinase domain. Mol Cell. 2006 Mar 17;21(6):737-48.

Hurley JH, Emr SD. The ESCRT complexes: structure and mechanism of a membrane-trafficking network. Annu Rev Biophys Biomol Struct. 2006;35:277-98.

Hynes NE, Lane HA. ERBB receptors and cancer: the complexity of targeted inhibitors. Nat Rev Cancer. 2005 May;5(5):341-54.

Ibarra-Sánchez MJ, Wagner J, Ong MT, Lampron C, Tremblay ML. Murine embryonic fibroblasts lacking TC-PTP display delayed G1 phase through defective NF-kappaB activation. Oncogene. 2001 Aug 2;20(34):4728-39.

Ishikawa K, Nagase T, Suyama M, Miyajima N, Tanaka A, Kotani H, Nomura N, Ohara O. Prediction of the coding sequences of unidentified human genes. X. The complete sequences of 100 new cDNA clones from brain which can code for large proteins in vitro. DNA Res. 1998 Jun 30;5(3):169-76.

Jahn R, Scheller RH. SNAREs--engines for membrane fusion. Nat Rev Mol Cell Biol. 2006 Sep;7(9):631-43. Epub 2006 Aug 16.

Jahraus A, Storrie B, Griffiths G, Desjardins M. Evidence for retrograde traffic between terminal lysosomes and the prelysosomal/late endosome compartment. J Cell Sci. 1994 Jan;107 (Pt 1):145-57.

Jiang RF, Greener T, Barouch W, Greene L, Eisenberg E. Interaction of auxilin with the molecular chaperone, Hsc70. J Biol Chem. 1997 Mar 7;272(10):6141-5.

Jones RB, Gordus A, Krall JA, MacBeath G. A quantitative protein interaction network for the ErbB receptors using protein microarrays. Nature. 2006 Jan 12;439(7073):168-74.

Keen JH. Clathrin assembly proteins: affinity purification and a model for coat assembly. J Cell Biol. 1987 Nov;105(5):1989-98.

Kelley WL. Molecular chaperones: How J domains turn on Hsp70s. Curr Biol. 1999 Apr 22;9(8):R305-8.

Klapper LN, Glathe S, Vaisman N, Hynes NE, Andrews GC, Sela M, Yarden Y. The ErbB-2/HER2 oncoprotein of human carcinomas may function solely as a shared coreceptor for multiple stroma-derived growth factors. Proc Natl Acad Sci U S A. 1999 Apr 27;96(9):4995-5000.

Kolch W. Meaningful relationships: the regulation of the Ras/Raf/MEK/ERK pathway by protein interactions. Biochem J. 2000 Oct 15;351 Pt 2:289-305.

Kraus MH, Issing W, Miki T, Popescu NC, Aaronson SA. Isolation and characterization of ERBB3, a third member of the ERBB/epidermal growth factor receptor family: evidence for overexpression in a subset of human mammary tumors. Proc Natl Acad Sci U S A. 1989 Dec;86(23):9193-7.

Krendel M, Osterweil EK, Mooseker MS. Myosin 1E interacts with synaptojanin-1 and dynamin and is involved in endocytosis. FEBS Lett. 2007 Feb 20;581(4):644-50.

Le Borgne R, Bardin A, Schweisguth F. The roles of receptor and ligand endocytosis in regulating Notch signaling. Development. 2005 Apr;132(8):1751-62.

Lemaire JF, McPherson PS. Binding of Vac14 to neuronal nitric oxide synthase: Characterisation of a new internal PDZ-recognition motif. FEBS Lett. 2006 Dec 22;580(30):6948-54.

Lemmon SK. Clathrin uncoating: Auxilin comes to life. Curr Biol. 2001 Jan 23;11(2):R49-52.

Longva KE, Blystad FD, Stang E, Larsen AM, Johannessen LE, Madshus IH. Ubiquitination and proteasomal activity is required for transport of the EGF receptor to inner membranes of multivesicular bodies. J Cell Biol. 2002 Mar 4;156(5):843-54.

Lopez MF. Better approaches to finding the needle in a haystack: optimizing proteome analysis through automation. Electrophoresis. 2000 Apr;21(6):1082-93.

Lu P, Vogel C, Wang R, Yao X, Marcotte EM. Absolute protein expression profiling estimates the relative contributions of transcriptional and translational regulation. Nat Biotechnol. 2007 Jan;25(1):117-24.

Lui WW, Collins BM, Hirst J, Motley A, Millar C, Schu P, Owen DJ, Robinson MS. Binding partners for the COOH-terminal appendage domains of the GGAs and gamma-adaptin. Mol Biol Cell. 2003 Jun;14(6):2385-98.

Kazazic M, Roepstorff K, Johannessen LE, Pedersen NM, van Deurs B, Stang E, Madshus IH. EGF-induced activation of the EGF receptor does not trigger mobilization of caveolae. Traffic. 2006 Nov;7(11):1518-27.

Kelley WL. Molecular chaperones: How J domains turn on Hsp70s. Curr Biol. 1999 Apr 22;9(8):R305-8.

Kirchhausen T. Three ways to make a vesicle. Nat Rev Mol Cell Biol. 2000 Dec;1(3):187-98.

Kirchhausen T, Harrison SC. Protein organization in clathrin trimers. Cell. 1981 Mar;23(3):755-61.

Klumperman J, Hille A, Veenendaal T, Oorschot V, Stoorvogel W, von Figura K, Geuze HJ. Differences in the endosomal distributions of the two mannose 6-phosphate receptors. J Cell Biol. 1993 Jun;121(5):997-1010.

Klumperman J, Kuliawat R, Griffith JM, Geuze HJ, Arvan P. Mannose 6-phosphate receptors are sorted from immature secretory granules via adaptor protein AP-1, clathrin, and syntaxin 6-positive vesicles. J Cell Biol. 1998 Apr 20;141(2):359-71.

Knutson VP. Cellular trafficking and processing of the insulin receptor. FASEB J. 1991 May;5(8):2130-8.

Kobayashi T, Stang E, Fang KS, de Moerloose P, Parton RG, Gruenberg J. A lipid associated with the antiphospholipid syndrome regulates endosome structure and function. Nature. 1998 Mar 12;392(6672):193-7.

Komada M, Soriano P. Hrs, a FYVE finger protein localized to early endosomes, is implicated in vesicular traffic and required for ventral folding morphogenesis. Genes Dev. 1999 Jun 1;13(11):1475-85.

Krasilnikov M, Ivanov VN, Dong J, Ronai Z. ERK and PI3K negatively regulate STAT-transcriptional activities in human melanoma cells: implications towards sensitization to apoptosis. Oncogene. 2003 Jun 26;22(26):4092-101.

Krauss M, Kinuta M, Wenk MR, De Camilli P, Takei K, Haucke V. ARF6 stimulates clathrin/AP-2 recruitment to synaptic membranes by activating phosphatidylinositol phosphate kinase type Igamma. J Cell Biol. 2003 Jul 7;162(1):113-24.

Krijgsveld J, Ketting RF, Mahmoudi T, Johansen J, Artal-Sanz M, Verrijzer CP, Plasterk RH, Heck AJ. Metabolic labeling of C. elegans and D. melanogaster for quantitative proteomics. Nat Biotechnol. 2003 Aug;21(8):927-31.

Kuliawat R, Kalinina E, Bock J, Fricker L, McGraw TE, Kim SR, Zhong J, Scheller R, Arvan P. Syntaxin-6 SNARE involvement in secretory and endocytic pathways of cultured pancreatic beta-cells. Mol Biol Cell. 2004 Apr;15(4):1690-701.

Lamaze C, Schmid SL. Recruitment of epidermal growth factor receptors into coated pits requires their activated tyrosine kinase. J Cell Biol. 1995 Apr;129(1):47-54.

Lawe DC, Chawla A, Merithew E, Dumas J, Carrington W, Fogarty K, Lifshitz L, Tuft R, Lambright D, Corvera S. Sequential roles for phosphatidylinositol 3-phosphate and Rab5 in tethering and fusion of early endosomes via their interaction with EEA1. J Biol Chem. 2002 Mar 8;277(10):8611-7.

Lax I, Wong A, Lamothe B, Lee A, Frost A, Hawes J, Schlessinger J. The docking protein FRS2alpha controls a MAP kinase-mediated negative feedback mechanism for signaling by FGF receptors. Mol Cell. 2002 Oct;10(4):709-19.

Le Borgne R, Griffiths G, Hoflack B. Mannose 6-phosphate receptors and ADP-ribosylation factors cooperate for high affinity interaction of the AP-1 Golgi assembly proteins with membranes. J Biol Chem. 1996 Jan 26;271(4):2162-70.

Le Borgne R, Hoflack B. Protein transport from the secretory to the endocytic pathway in mammalian cells. Biochim Biophys Acta. 1998 Aug 14;1404(1-2):195-209.

Lee DH, Goldberg AL. Proteasome inhibitors: valuable new tools for cell biologists. Trends Cell Biol. 1998 Oct;8(10):397-403.

Lee DW, Zhao X, Yim YI, Eisenberg E, Greene LE. Essential Role of Cyclin-G-associated Kinase (Auxilin-2) in Developing and Mature Mice. Mol Biol Cell. 2008 Jul;19(7):2766-76.

Lee JC, Wang ST, Chow NH, Yang HB. Investigation of the prognostic value of coexpressed erbB family members for the survival of colorectal cancer patients after curative surgery. Eur J Cancer. 2002 May;38(8):1065-71.

Lee PS, Wang Y, Dominguez MG, Yeung YG, Murphy MA, Bowtell DD, Stanley ER. The Cbl protooncoprotein stimulates CSF-1 receptor multiubiquitination and endocytosis, and attenuates macrophage proliferation. EMBO J. 1999 Jul 1;18(13):3616-28.

Legendre-Guillemin V, Metzler M, Lemaire JF, Philie J, Gan L, Hayden MR, McPherson PS. Huntingtin interacting protein 1 (HIP1) regulates clathrin assembly through direct binding to the regulatory region of the clathrin light chain. J Biol Chem. 2005 Feb 18;280(7):6101-8.

Lenferink AE, Pinkas-Kramarski R, van de Poll ML, van Vugt MJ, Klapper LN, Tzahar E, Waterman H, Sela M, van Zoelen EJ, Yarden Y. Differential endocytic routing of homo- and hetero-dimeric ErbB tyrosine kinases confers signaling superiority to receptor heterodimers. EMBO J. 1998 Jun 15;17(12):3385-97.

Levkowitz G, Waterman H, Ettenberg SA, Katz M, Tsygankov AY, Alroy I, Lavi S, Iwai K, Reiss Y, Ciechanover A, Lipkowitz S, Yarden Y. Ubiquitin ligase activity and tyrosine phosphorylation underlie suppression of growth factor signaling by c-Cbl/Sli-1. Mol Cell. 1999 Dec;4(6):1029-40.

Liberek K, Georgopoulos C, Zylicz M. Role of the Escherichia coli DnaK and DnaJ heat shock proteins in the initiation of bacteriophage lambda DNA replication. Proc Natl Acad Sci U S A. 1988 Sep;85(18):6632-6.

Lin JH, Tsai CH, Chu JS, Chen JY, Takada K, Shew JY. Dysregulation of HER2/HER3 signaling axis in Epstein-Barr virus-infected breast carcinoma cells. J Virol. 2007 Jun;81(11):5705-13.

Liu H, Sadygov RG, Yates JR 3rd. A model for random sampling and estimation of relative protein abundance in shotgun proteomics. Anal Chem. 2004 Jul 15;76(14):4193-201.

Liu SH, Wong ML, Craik CS, Brodsky FM. Regulation of clathrin assembly and trimerization defined using recombinant triskelion hubs. Cell. 1995 Oct 20;83(2):257-67.

Lui WW, Collins BM, Hirst J, Motley A, Millar C, Schu P, Owen DJ, Robinson MS. Binding partners for the COOH-terminal appendage domains of the GGAs and gamma-adaptin. Mol Biol Cell. 2003 Jun;14(6):2385-98.

Mallick P, Schirle M, Chen SS, Flory MR, Lee H, Martin D, Ranish J, Raught B, Schmitt R, Werner T, Kuster B, Aebersold R. Computational prediction of proteotypic peptides for quantitative proteomics. Nat Biotechnol. 2007 Jan;25(1):125-31.

Marquèze B, Berton F, Seagar M. Synaptotagmins in membrane traffic: which vesicles do the tagmins tag? Biochimie. 2000 May;82(5):409-20.

Marsh M, McMahon HT. The structural era of endocytosis. Science. 1999 Jul 9;285(5425):215-20.

Masson K, Heiss E, Band H, Rönnstrand L. Direct binding of Cbl to Tyr568 and Tyr936 of the stem cell factor receptor/c-Kit is required for ligand-induced ubiquitination, internalization and degradation. Biochem J. 2006 Oct 1;399(1):59-67.

Maxfield FR, McGraw TE. Endocytic recycling. Nat Rev Mol Cell Biol. 2004 Feb;5(2):121-32.

Mayor S, Presley JF, Maxfield FR. Sorting of membrane components from endosomes and subsequent recycling to the cell surface occurs by a bulk flow process. J Cell Biol. 1993 Jun;121(6):1257-69.

McCullough J, Row PE, Lorenzo O, Doherty M, Beynon R, Clague MJ, Urbé S. Activation of the endosome-associated ubiquitin isopeptidase AMSH by STAM, a component of the multivesicular body-sorting machinery. Curr Biol. 2006 Jan 24;16(2):160-5.

McNiven MA, Cao H, Pitts KR, Yoon Y. The dynamin family of mechanoenzymes: pinching in new places. Trends Biochem Sci. 2000 Mar;25(3):115-20.

McNiven MA, Thompson HM. Vesicle formation at the plasma membrane and trans-Golgi network: the same but different. Science. 2006 Sep 15;313(5793):1591-4.
McPherson PS, Kay BK, Hussain NK. Signaling on the endocytic pathway. Traffic. 2001 Jun;2(6):375-84.

Mellman I. Endocytosis and molecular sorting. Annu Rev Cell Dev Biol. 1996;12:575-625.

Mello CC, Conte D Jr. Revealing the world of RNA interference. Nature. 2004 Sep 16;431(7006):338-42.

Merrifield CJ, Feldman ME, Wan L, Almers W. Imaging actin and dynamin recruitment during invagination of single clathrin-coated pits. Nat Cell Biol. 2002 Sep;4(9):691-8.

Miaczynska M, Pelkmans L, Zerial M. Not just a sink: endosomes in control of signal transduction. Curr Opin Cell Biol. 2004 Aug;16(4):400-6.

Michalopoulos GK, Khan Z. Liver regeneration, growth factors, and amphiregulin. Gastroenterology. 2005 Feb;128(2):503-6.

Miranda M, Sorkin A. Regulation of receptors and transporters by ubiquitination: new insights into surprisingly similar mechanisms. Mol Interv. 2007 Jun;7(3):157-67.

Morgan JR, Prasad K, Jin S, Augustine GJ, Lafer EM. Uncoating of clathrin-coated vesicles in presynaptic terminals: roles for Hsc70 and auxilin. Neuron. 2001 Oct 25;32(2):289-300.

Mori S, Heldin CH, Claesson-Welsh L. Ligand-induced polyubiquitination of the platelet-derived growth factor beta-receptor. J Biol Chem. 1992 Mar 25;267(9):6429-34.

Mosesson Y, Shtiegman K, Katz M, Zwang Y, Vereb G, Szollosi J, Yarden Y. Endocytosis of receptor tyrosine kinases is driven by monoubiquitylation, not polyubiquitylation. J Biol Chem. 2003 Jun 13;278(24):21323-6.

Mu FT, Callaghan JM, Steele-Mortimer O, Stenmark H, Parton RG, Campbell PL, McCluskey J, Yeo JP, Tock EP, Toh BH. EEA1, an early endosome-associated protein. EEA1 is a conserved alpha-helical peripheral membrane protein flanked by cysteine "fingers" and contains a calmodulin-binding IQ motif. J Biol Chem. 1995 Jun 2;270(22):13503-11.

Mullin JM. Epithelial barriers, compartmentation, and cancer. Sci STKE. 2004 Jan 13;2004(216):pe2.

Mullock BM, Bright NA, Fearon CW, Gray SR, Luzio JP. Fusion of lysosomes with late endosomes produces a hybrid organelle of intermediate density and is NSF dependent. J Cell Biol. 1998 Feb 9;140(3):591-601

Murthy VN, De Camilli P. Cell biology of the presynaptic terminal. Annu Rev Neurosci. 2003;26:701-28.

Muthuswamy SK, Gilman M, Brugge JS. Controlled dimerization of ErbB receptors provides evidence for differential signaling by homo- and heterodimers. Mol Cell Biol. 1999 Oct;19(10):6845-57.

Newmyer SL, Schmid SL. Dominant-interfering Hsc70 mutants disrupt multiple stages of the clathrin-coated vesicle cycle in vivo. J Cell Biol. 2001 Feb 5;152(3):607-20

Nicholson RI, Gee JM, Harper ME. EGFR and cancer prognosis. Eur J Cancer. 2001 Sep;37 Suppl 4:S9-15.

Normanno N, Bianco C, Strizzi L, Mancino M, Maiello MR, De Luca A, Caponigro F, Salomon DS. The ErbB receptors and their ligands in cancer: an overview. Curr Drug Targets. 2005 May;6(3):243-57.

Old WM, Meyer-Arendt K, Aveline-Wolf L, Pierce KG, Mendoza A, Sevinsky JR, Resing KA, Ahn NG. Comparison of label-free methods for quantifying human proteins by shotgun proteomics. Mol Cell Proteomics. 2005 Oct;4(10):1487-502.

Omerovic J, Santangelo L, Puggioni EM, Marrocco J, Dall'Armi C, Palumbo C, Belleudi F, Di Marcotullio L, Frati L, Torrisi MR, Cesareni G, Gulino A, Alimandi M. The E3 ligase Aip4/Itch ubiquitinates and targets ErbB-4 for degradation. FASEB J. 2007 Sep;21(11):2849-62.

Ong SE, Blagoev B, Kratchmarova I, Kristensen DB, Steen H, Pandey A, Mann M. Stable isotope labeling by amino acids in cell culture, SILAC, as a simple and accurate approach to expression proteomics. Mol Cell Proteomics. 2002 May;1(5):376-86.

Orci L, Glick BS, Rothman JE. A new type of coated vesicular carrier that appears not to contain clathrin: its possible role in protein transport within the Golgi stack. Cell. 1986 Jul 18;46(2):171-84.

Orenes-Piñero E, Cortón M, González-Peramato P, Algaba F, Casal I, Serrano A, Sánchez-Carbayo M. Searching urinary tumor markers for bladder cancer using a two-dimensional differential gel electrophoresis (2D-DIGE) approach. J Proteome Res. 2007 Nov;6(11):4440-8.

Orlichenko L, Huang B, Krueger E, McNiven MA. Epithelial growth factor-induced phosphorylation of caveolin 1 at tyrosine 14 stimulates caveolae formation in epithelial cells. J Biol Chem. 2006 Feb 24;281(8):4570-9.

Orth JD, Krueger EW, Weller SG, McNiven MA. A novel endocytic mechanism of epidermal growth factor receptor sequestration and internalization. Cancer Res. 2006 Apr 1;66(7):3603-10.

Owen DJ, Evans PR. A structural explanation for the recognition of tyrosine-based endocytotic signals. Science. 1998 Nov 13;282(5392):1327-32

Owen DJ, Vallis Y, Noble ME, Hunter JB, Dafforn TR, Evans PR, McMahon HT. A structural explanation for the binding of multiple ligands by the alpha-adaptin appendage domain. Cell. 1999 Jun 11;97(6):805-15.

Paleotti O, Macia E, Luton F, Klein S, Partisani M, Chardin P, Kirchhausen T, Franco M. The small G-protein Arf6GTP recruits the AP-2 adaptor complex to membranes. J Biol Chem. 2005 Jun 3;280(22):21661-6.

Pawson T, Gish GD. SH2 and SH3 domains: from structure to function. Cell. 1992 Oct 30;71(3):359-62.

Pearse BM. Clathrin: a unique protein associated with intracellular transfer of membrane by coated vesicles. Proc Natl Acad Sci U S A. 1976 Apr;73(4):1255-9.

Peden AA, Park GY, Scheller RH. The Di-leucine motif of vesicle-associated membrane protein 4 is required for its localization and AP-1 binding. J Biol Chem. 2001 Dec 28;276(52):49183-7.

Peschard P, Fournier TM, Lamorte L, Naujokas MA, Band H, Langdon WY, Park M. Mutation of the c-Cbl TKB domain binding site on the Met receptor tyrosine kinase converts it into a transforming protein. Mol Cell. 2001 Nov;8(5):995-1004.

Peschard P, Park M. Escape from Cbl-mediated downregulation: a recurrent theme for oncogenic deregulation of receptor tyrosine kinases. Cancer Cell. 2003 Jun;3(6):519-23.

Pfeffer S. Membrane domains in the secretory and endocytic pathways. Cell. 2003 Feb 21;112(4):507-17.

Pickart CM, Eddins MJ. Ubiquitin: structures, functions, mechanisms. Biochim Biophys Acta. 2004 Nov 29;1695(1-3):55-72.

Pilch PF, Shia MA, Benson RJ, Fine RE. Coated vesicles participate in the receptor-mediated endocytosis of insulin. J Cell Biol. 1983 Jan;96(1):133-8.

Pinkas-Kramarski R, Shelly M, Guarino BC, Wang LM, Lyass L, Alroy I, Alimandi M, Kuo A, Moyer JD, Lavi S, Eisenstein M, Ratzkin BJ, Seger R, Bacus SS, Pierce JH, Andrews GC, Yarden Y. ErbB tyrosine kinases and the two neuregulin families constitute a ligand-receptor network. Mol Cell Biol. 1998 Oct;18(10):6090-101

Pinkas-Kramarski R, Soussan L, Waterman H, Levkowitz G, Alroy I, Klapper L, Lavi S, Seger R, Ratzkin BJ, Sela M, Yarden Y. Diversification of Neu differentiation factor and epidermal growth factor signaling by combinatorial receptor interactions. EMBO J. 1996 May 15;15(10):2452-67.

Pishvaee B, Costaguta G, Yeung BG, Ryazantsev S, Greener T, Greene LE, Eisenberg E, McCaffery JM, Payne GS. A yeast DNA J protein required for uncoating of clathrin-coated vesicles in vivo. Nat Cell Biol. 2000 Dec;2(12):958-63.

Plowman GD, Green JM, Culouscou JM, Carlton GW, Rothwell VM, Buckley S. Heregulin induces tyrosine phosphorylation of HER4/p180erbB4. Nature. 1993 Dec 2;366(6454):473-5.

Poupon V, Girard M, Legendre-Guillemin V, Thomas S, Bourbonniere L, Philie J, Bright NA, McPherson PS. Clathrin light chains function in mannose phosphate receptor trafficking via regulation of actin assembly. Proc Natl Acad Sci U S A. 2008 Jan 8;105(1):168-73.

Praefcke GJ, McMahon HT. The dynamin superfamily: universal membrane tubulation and fission molecules? Nat Rev Mol Cell Biol. 2004 Feb;5(2):133-47.

Prywes R, Livneh E, Ullrich A, Schlessinger J. Mutations in the cytoplasmic domain of EGF receptor affect EGF binding and receptor internalization. EMBO J. 1986 Sep;5(9):2179-90.

Puertollano R, Aguilar RC, Gorshkova I, Crouch RJ, Bonifacino JS. Sorting of mannose 6-phosphate receptors mediated by the GGAs. Science. 2001 Jun 1;292(5522):1712-6.

Puertollano R, Bonifacino JS. Interactions of GGA3 with the ubiquitin sorting machinery. Nat Cell Biol. 2004 Mar;6(3):244-51.

Qiu XB, Goldberg AL. Nrdp1/FLRF is a ubiquitin ligase promoting ubiquitination and degradation of the epidermal growth factor receptor family member, ErbB3. Proc Natl Acad Sci U S A. 2002 Nov 12;99(23):14843-8.

Qiu XB, Shao YM, Miao S, Wang L. The diversity of the DnaJ/Hsp40 family, the crucial partners for Hsp70 chaperones. Cell Mol Life Sci. 2006 Nov;63(22):2560-70.

Qiu W, Avramoglu RK, Dubé N, Chong TM, Naples M, Au C, Sidiropoulos KG, Lewis GF, Cohn JS, Tremblay ML, Adeli K. Hepatic PTP-1B expression regulates the assembly and secretion of apolipoprotein B-containing lipoproteins: evidence from protein tyrosine phosphatase-1B overexpression, knockout, and RNAi studies. Diabetes. 2004 Dec;53(12):3057-66.

Qualmann B, Kessels MM, Kelly RB. Molecular links between endocytosis and the actin cytoskeleton. J Cell Biol. 2000 Sep 4;150(5):F111-6.

Raiborg C, Bache KG, Gillooly DJ, Madshus IH, Stang E, Stenmark H. Hrs sorts ubiquitinated proteins into clathrin-coated microdomains of early endosomes. Nat Cell Biol. 2002 May;4(5):394-8.

Raiborg C, Bache KG, Mehlum A, Stang E, Stenmark H. Hrs recruits clathrin to early endosomes. EMBO J. 2001 Sep 3;20(17):5008-21.

Raiborg C, Malerød L, Pedersen NM, Stenmark H. Differential functions of Hrs and ESCRT proteins in endocytic membrane trafficking. Exp Cell Res. 2008 Feb 15;314(4):801-13.

Raiborg C, Wesche J, Malerød L, Stenmark H. Flat clathrin coats on endosomes mediate degradative protein sorting by scaffolding Hrs in dynamic microdomains. J Cell Sci. 2006 Jun 15;119(Pt 12):2414-24.

Rappoport JZ, Simon SM. Real-time analysis of clathrin-mediated endocytosis during cell migration. J Cell Sci. 2003 Mar 1;116(Pt 5):847-55.

Razi M, Futter CE. Distinct roles for Tsg101 and Hrs in multivesicular body formation and inward vesiculation. Mol Biol Cell. 2006 Aug;17(8):3469-83.

Ridley SH, Ktistakis N, Davidson K, Anderson KE, Manifava M, Ellson CD, Lipp P, Bootman M, Coadwell J, Nazarian A, Erdjument-Bromage H, Tempst P, Cooper MA, Thuring JW, Lim ZY, Holmes AB, Stephens LR, Hawkins PT. FENS-1 and DFCP1 are FYVE domain-containing proteins with distinct functions in the endosomal and Golgi compartments. J Cell Sci. 2001 Nov;114(Pt 22):3991-4000.

Rink J, Ghigo E, Kalaidzidis Y, Zerial M. Rab conversion as a mechanism of progression from early to late endosomes. Cell. 2005 Sep 9;122(5):735-49.

Ritter B, Philie J, Girard M, Tung EC, Blondeau F, McPherson PS. Identification of a family of endocytic proteins that define a new alpha-adaptin ear-binding motif. EMBO Rep. 2003 Nov;4(11):1089-95.

Robinson MS, Bonifacino JS. Adaptor-related proteins. Curr Opin Cell Biol. 2001 Aug;13(4):444-53.

Roepstorff K, Grøvdal L, Grandal M, Lerdrup M, van Deurs B. Endocytic downregulation of ErbB receptors: mechanisms and relevance in cancer. Histochem Cell Biol. 2008 May;129(5):563-78.

Ross JS, Fletcher JA, Linette GP, Stec J, Clark E, Ayers M, Symmans WF, Pusztai L, Bloom KJ. The Her-2/neu gene and protein in breast cancer 2003: biomarker and target of therapy. Oncologist. 2003;8(4):307-25.

Roth TF, Porter KR. Yolk protein uptake in the oocyte of the mosquito Aedes aegypti. J Cell Biol. 1964 Feb;20:313-32.

Rout MP, Aitchison JD, Suprapto A, Hjertaas K, Zhao Y, Chait BT. The yeast nuclear pore complex: composition, architecture, and transport mechanism. J Cell Biol. 2000 Feb 21;148(4):635-51.

Royle SJ, Murrell-Lagnado RD. Constitutive cycling: a general mechanism to regulate cell surface proteins. Bioessays. 2003 Jan;25(1):39-46.

Russell MR, Nickerson DP, Odorizzi G. Molecular mechanisms of late endosome morphology, identity and sorting. Curr Opin Cell Biol. 2006 Aug;18(4):422-8.

Sachse M, Strous GJ, Klumperman J. ATPase-deficient hVPS4 impairs formation of internal endosomal vesicles and stabilizes bilayered clathrin coats on endosomal vacuoles. J Cell Sci. 2004 Apr 1;117(Pt 9):1699-708.

Sachse M, Urbé S, Oorschot V, Strous GJ, Klumperman J. Bilayered clathrin coats on endosomal vacuoles are involved in protein sorting toward lysosomes. Mol Biol Cell. 2002 Apr;13(4):1313-28.

Salcini AE, Confalonieri S, Doria M, Santolini E, Tassi E, Minenkova O, Cesareni G, Pelicci PG, Di Fiore PP. Binding specificity and in vivo targets of the EH domain, a novel protein-protein interaction module. Genes Dev. 1997 Sep 1;11(17):2239-49.

Sato H, Tomita H, Nakazawa T, Wakana S, Tamai M. Deleted in polyposis 1-like 1 gene (Dp1l1): a novel gene richly expressed in retinal ganglion cells. Invest Ophthalmol Vis Sci. 2005 Mar;46(3):791-6.

Schlessinger J. Signal transduction by allosteric receptor oligomerization. Trends Biochem Sci. 1988 Nov;13(11):443-7.

Schlessinger J. Cell signaling by receptor tyrosine kinases. Cell. 2000 Oct 13;103(2):211-25.

Schlessinger J. Ligand-induced, receptor-mediated dimerization and activation of EGF receptor. Cell. 2002 Sep 20;110(6):669-72.

Schmidt A, Wolde M, Thiele C, Fest W, Kratzin H, Podtelejnikov AV, Witke W, Huttner WB, Söling HD. Endophilin I mediates synaptic vesicle formation by transfer of arachidonate to lysophosphatidic acid. Nature. 1999 Sep 9;401(6749):133-41.

Schmidt MH, Dikic I. Assays to monitor degradation of the EGF receptor. Methods Mol Biol. 2006;327:131-8.

Schoeberl B, Eichler-Jonsson C, Gilles ED, Müller G. Computational modeling of the dynamics of the MAP kinase cascade activated by surface and internalized EGF receptors. Nat Biotechnol. 2002 Apr;20(4):370-5.

Scott JD, Pawson T. Cell communication: the inside story. Sci Am. 2000 Jun;282(6):72-9.

Seaman MN, Ball CL, Robinson MS. Targeting and mistargeting of plasma membrane adaptors in vitro. J Cell Biol. 1993 Dec;123(5):1093-105.

Seto ES, Bellen HJ, Lloyd TE. When cell biology meets development: endocytic regulation of signaling pathways. Genes Dev. 2002 Jun 1;16(11):1314-36.

Shih W, Gallusser A, Kirchhausen T. A clathrin-binding site in the hinge of the beta 2 chain of mammalian AP-2 complexes. J Biol Chem. 1995 Dec 29;270(52):31083-90.

Sigismund S, Woelk T, Puri C, Maspero E, Tacchetti C, Transidico P, Di Fiore PP, Polo S. Clathrin-independent endocytosis of ubiquitinated cargos. Proc Natl Acad Sci U S A. 2005 Feb 22;102(8):2760-5.

Silady RA, Ehrhardt DW, Jackson K, Faulkner C, Oparka K, Somerville CR. The GRV2/RME-8 protein of Arabidopsis functions in the late endocytic pathway and is required for vacuolar membrane flow. Plant J. 2008 Jan;53(1):29-41.

Silady RA, Kato T, Lukowitz W, Sieber P, Tasaka M, Somerville CR. The gravitropism defective 2 mutants of Arabidopsis are deficient in a protein implicated in endocytosis in Caenorhabditis elegans. Plant Physiol. 2004 Oct;136(2):3095-103.

Simonsen A, Gaullier JM, D'Arrigo A, Stenmark H. The Rab5 effector EEA1 interacts directly with syntaxin-6. J Biol Chem. 1999 Oct 8;274(41):28857-60.

Slagsvold T, Pattni K, Malerød L, Stenmark H. Endosomal and non-endosomal functions of ESCRT proteins. Trends Cell Biol. 2006 Jun;16(6):317-26.

Slamon DJ, Clark GM, Wong SG, Levin WJ, Ullrich A, McGuire WL. Human breast cancer: correlation of relapse and survival with amplification of the HER-2/neu oncogene. Science. 1987 Jan 9;235(4785):177-82.

Slamon DJ, Godolphin W, Jones LA, Holt JA, Wong SG, Keith DE, Levin WJ, Stuart SG, Udove J, Ullrich A, et al. Studies of the HER-2/neu proto-oncogene in human breast and ovarian cancer. Science. 1989 May 12;244(4905):707-12.

Smith CJ, Pearse BM. Clathrin: anatomy of a coat protein. Trends Cell Biol. 1999 Sep;9(9):335-8.

Smolka MB, Zhou H, Purkayastha S, Aebersold R. Optimization of the isotope-coded affinity tag-labeling procedure for quantitative proteome analysis. Anal Biochem. 2001 Oct 1;297(1):25-31.

Söllner T, Bennett MK, Whiteheart SW, Scheller RH, Rothman JE. A protein assembly-disassembly pathway in vitro that may correspond to sequential steps of synaptic vesicle docking, activation, and fusion. Cell. 1993 Nov 5;75(3):409-18.

Sorkin A, Krolenko S, Kudrjavtceva N, Lazebnik J, Teslenko L, Soderquist AM, Nikolsky N. Recycling of epidermal growth factor-receptor complexes in A431 cells: identification of dual pathways. J Cell Biol. 1991 Jan;112(1):55-63.

Sorkin A, McClure M, Huang F, Carter R. Interaction of EGF receptor and grb2 in living cells visualized by fluorescence resonance energy transfer (FRET) microscopy. Curr Biol. 2000 Nov 2;10(21):1395-8.

Sorkin A, Von Zastrow M. Signal transduction and endocytosis: close encounters of many kinds. Nat Rev Mol Cell Biol. 2002 Aug;3(8):600-14.

Sorkin A, Waters CM. Endocytosis of growth factor receptors. Bioessays. 1993 Jun;15(6):375-82.

Sorkina T, Huang F, Beguinot L, Sorkin A. Effect of tyrosine kinase inhibitors on clathrin-coated pit recruitment and internalization of epidermal growth factor receptor. J Biol Chem. 2002 Jul 26;277(30):27433-41.

Spudich G, Chibalina MV, Au JS, Arden SD, Buss F, Kendrick-Jones J. Myosin VI targeting to clathrin-coated structures and dimerization is mediated by binding to Disabled-2 and PtdIns(4,5)P2. Nat Cell Biol. 2007 Feb;9(2):176-83.

Stang E, Blystad FD, Kazazic M, Bertelsen V, Brodahl T, Raiborg C, Stenmark H, Madshus IH. Cbl-dependent ubiquitination is required for progression of EGF receptors into clathrin-coated pits. Mol Biol Cell. 2004 Aug;15(8):3591-604.

Steegmaier M, Klumperman J, Foletti DL, Yoo JS, Scheller RH. Vesicle-associated membrane protein 4 is implicated in trans-Golgi network vesicle trafficking. Mol Biol Cell. 1999 Jun;10(6):1957-72.

Stern KA, Place TL, Lill NL. EGF and amphiregulin differentially regulate Cbl recruitment to endosomes and EGF receptor fate. Biochem J. 2008 Mar 15;410(3):585-94.

Stoscheck CM, Carpenter G. Characteristics of antibodies to the epidermal growth factor receptor-kinase. Arch Biochem Biophys. 1983 Dec;227(2):457-68.

Sundquist WI, Schubert HL, Kelly BN, Hill GC, Holton JM, Hill CP. Ubiquitin recognition by the human TSG101 protein. Mol Cell. 2004 Mar 26;13(6):783-9.

Taylor CM, Pfeiffer SE. Enhanced resolution of glycosylphosphatidylinositol-anchored and transmembrane proteins from the lipid-rich myelin membrane by two-dimensional gel electrophoresis. Proteomics. 2003 Jul;3(7):1303-12.

Terada K, Yomogida K, Imai T, Kiyonari H, Takeda N, Kadomatsu T, Yano M, Aizawa S, Mori M. A type I DnaJ homolog, DjA1, regulates androgen receptor signaling and spermatogenesis. EMBO J. 2005 Feb 9;24(3):611-22.

ter Haar E, Musacchio A, Harrison SC, Kirchhausen T. Atomic structure of clathrin: a beta propeller terminal domain joins an alpha zigzag linker. Cell. 1998 Nov 13;95(4):563-73.

Thiele C, Gerdes HH, Huttner WB. Protein secretion: puzzling receptors. Curr Biol. 1997 Aug 1;7(8):R496-500.

Thuring JW, Lim ZY, Holmes AB, Stephens LR, Hawkins PT. FENS-1 and DFCP1 are FYVE domain-containing proteins with distinct functions in the endosomal and Golgi compartments. J Cell Sci. 2001 Nov;114(Pt 22):3991-4000.

Traub LM, Bannykh SI, Rodel JE, Aridor M, Balch WE, Kornfeld S. AP-2-containing clathrin coats assemble on mature lysosomes. J Cell Biol. 1996 Dec;135(6 Pt 2):1801-14.

Traub LM, Downs MA, Westrich JL, Fremont DH. Crystal structure of the alpha appendage of AP-2 reveals a recruitment platform for clathrin-coat assembly. Proc Natl Acad Sci U S A. 1999 Aug 3;96(16):8907-12.

Trischler M, Stoorvogel W, Ullrich O. Biochemical analysis of distinct Rab5- and Rab11-positive endosomes along the transferrin pathway. J Cell Sci. 1999 Dec;112 (Pt 24):4773-83.

Tsai J, Douglas MG.A conserved HPD sequence of the J-domain is necessary for YDJ1 stimulation of Hsp70 ATPase activity at a site distinct from substrate binding. J Biol Chem. 1996 Apr 19;271(16):9347-54.

Ullrich A, Schlessinger J. Signal transduction by receptors with tyrosine kinase activity. Cell. 1990 Apr 20;61(2):203-12.

Umeda A, Meyerholz A, Ungewickell E. Identification of the universal cofactor (auxilin 2) in clathrin coat dissociation. Eur J Cell Biol. 2000 May;79(5):336-42.

Ungewickell E, Branton D. Assembly units of clathrin coats. Nature. 1981 Jan 29;289(5796):420-2.

Ungewickell E, Ungewickell H. Bovine brain clathrin light chains impede heavy chain assembly in vitro. J Biol Chem. 1991 Jul 5;266(19):12710-4.

Ungewickell E, Ungewickell H, Holstein SE, Lindner R, Prasad K, Barouch W, Martin B, Greene LE, Eisenberg E. Role of auxilin in uncoating clathrin-coated vesicles. Nature. 1995 Dec 7;378(6557):632-5.

Urbé S, Sachse M, Row PE, Preisinger C, Barr FA, Strous G, Klumperman J, Clague MJ. The UIM domain of Hrs couples receptor sorting to vesicle formation. J Cell Sci. 2003 Oct 15;116(Pt 20):4169-79.

van Delft S, Schumacher C, Hage W, Verkleij AJ, van Bergen en Henegouwen PM. Association and colocalization of Eps15 with adaptor protein-2 and clathrin. J Cell Biol. 1997 Feb 24;136(4):811-21.

van der Geer P, Pawson T. The PTB domain: a new protein module implicated in signal transduction. Trends Biochem Sci. 1995 Jul;20(7):277-80.

van der Goot FG, Gruenberg J. Intra-endosomal membrane traffic. Trends Cell Biol. 2006 Oct;16(10):514-21.

van Vliet C, Thomas EC, Merino-Trigo A, Teasdale RD, Gleeson PA. Intracellular sorting and transport of proteins. Prog Biophys Mol Biol. 2003 Sep;83(1):1-45.

Vecchione A, Marchese A, Henry P, Rotin D, Morrione A. The Grb10/Nedd4 complex regulates ligand-induced ubiquitination and stability of the insulin-like growth factor I receptor. Mol Cell Biol. 2003 May;23(9):3363-72.

von Zastrow M, Sorkin A. Signaling on the endocytic pathway. Curr Opin Cell Biol. 2007 Aug;19(4):436-45.

Walsh P, Bursać D, Law YC, Cyr D, Lithgow T. The J-protein family: modulating protein assembly, disassembly and translocation. EMBO Rep. 2004 Jun;5(6):567-71.

Wan L, Molloy SS, Thomas L, Liu G, Xiang Y, Rybak SL, Thomas G. PACS-1 defines a novel gene family of cytosolic sorting proteins required for trans-Golgi network localization. Cell. 1998 Jul 24;94(2):205-16.

Wang G, Wu WW, Zeng W, Chou CL, Shen RF. Label-free protein quantification using LC-coupled ion trap or FT mass spectrometry: Reproducibility, linearity, and application with complex proteomes. J Proteome Res. 2006 May;5(5):1214-23.

Wang J, Virta VC, Riddelle-Spencer K, O'Halloran TJ. Compromise of clathrin function and membrane association by clathrin light chain deletion. Traffic. 2003 Dec;4(12):891-901.

Wang Z, Zhang L, Yeung TK, Chen X. Endocytosis deficiency of epidermal growth factor (EGF) receptor-ErbB2 heterodimers in response to EGF stimulation. Mol Biol Cell. 1999 May;10(5):1621-36.

Warren RA, Green FA, Stenberg PE, Enns CA. Distinct saturable pathways for the endocytosis of different tyrosine motifs. J Biol Chem. 1998 Jul 3;273(27):17056-63.

Warren CM, Landgraf R. Signaling through ERBB receptors: multiple layers of diversity and control. Cell Signal. 2006 Jul;18(7):923-33.

Wasiak S, Legendre-Guillemin V, Puertollano R, Blondeau F, Girard M, de Heuvel E, Boismenu D, Bell AW, Bonifacino JS, McPherson PS. Enthoprotin: a novel clathrin-associated protein identified through subcellular proteomics. J Cell Biol. 2002 Sep 2;158(5):855-62.

Waterman H, Sabanai I, Geiger B, Yarden Y. Alternative intracellular routing of ErbB receptors may determine signaling potency. J Biol Chem. 1998 May 29;273(22):13819-27.

Waterman H, Yarden Y. Molecular mechanisms underlying endocytosis and sorting of ErbB receptor tyrosine kinases. FEBS Lett. 2001 Feb 16;490(3):142-52.

Wendeler MW, Paccaud JP, Hauri HP. Role of Sec24 isoforms in selective export of membrane proteins from the endoplasmic reticulum. EMBO Rep. 2007 Mar;8(3):258-64.

Werner G, Hagenmaier H, Drautz H, Baumgartner A, Zähner H. Metabolic products of microorganisms. 224. Bafilomycins, a new group of macrolide antibiotics. Production, isolation, chemical structure and biological activity. J Antibiot (Tokyo). 1984 Feb;37(2):110-7.

Wilde A, Beattie EC, Lem L, Riethof DA, Liu SH, Mobley WC, Soriano P, Brodsky FM. EGF receptor signaling stimulates SRC kinase phosphorylation of clathrin, influencing clathrin redistribution and EGF uptake. Cell. 1999 Mar 5;96(5):677-87.

Wiley HS. Anomalous binding of epidermal growth factor to A431 cells is due to the effect of high receptor densities and a saturable endocytic system. J Cell Biol. 1988 Aug;107(2):801-10.

Wiley HS. Trafficking of the ErbB receptors and its influence on signaling. Exp Cell Res. 2003 Mar 10;284(1):78-88.

Wiley HS, Burke PM. Regulation of receptor tyrosine kinase signaling by endocytic trafficking. Traffic. 2001 Jan;2(1):12-8.

Williams RL, Urbé S. The emerging shape of the ESCRT machinery. Nat Rev Mol Cell Biol. 2007 May;8(5):355-68.

Wong A, Lamothe B, Lee A, Schlessinger J, Lax I. FRS2 alpha attenuates FGF receptor signaling by Grb2-mediated recruitment of the ubiquitin ligase Cbl. Proc Natl Acad Sci U S A. 2002 May 14;99(10):6684-9.

Woodman PG. Biogenesis of the sorting endosome: the role of Rab5. Traffic. 2000 Sep;1(9):695-701.

Worthylake R, Opresko LK, Wiley HS. ErbB-2 amplification inhibits down-regulation and induces constitutive activation of both ErbB-2 and epidermal growth factor receptors. J Biol Chem. 1999 Mar 26;274(13):8865-74.

Wu CC, MacCoss MJ, Howell KE, Matthews DE, Yates JR 3rd. Metabolic labeling of mammalian organisms with stable isotopes for quantitative proteomic analysis. Anal Chem. 2004 Sep 1;76(17):4951-9.

Xiao Z, Zhang W, Yang Y, Xu L, Fang X. Single-molecule diffusion study of activated EGFR implicates its endocytic pathway. Biochem Biophys Res Commun. 2008 May 2;369(2):730-4.

Xu W, Marcu M, Yuan X, Mimnaugh E, Patterson C, Neckers L. Chaperone-dependent E3 ubiquitin ligase CHIP mediates a degradative pathway for c-ErbB2/Neu. Proc Natl Acad Sci U S A. 2002 Oct 1;99(20):12847-52.

Yamashiro DJ, Tycko B, Fluss SR, Maxfield FR. Segregation of transferrin to a mildly acidic (pH 6.5) para-Golgi compartment in the recycling pathway. Cell. 1984 Jul;37(3):789-800.

Yang D, Buchholz F, Huang Z, Goga A, Chen CY, Brodsky FM, Bishop JM. Short RNA duplexes produced by hydrolysis with Escherichia coli RNase III mediate effective RNA interference in mammalian cells. Proc Natl Acad Sci U S A. 2002 Jul 23;99(15):9942-7.

Yates JR 3rd, Gilchrist A, Howell KE, Bergeron JJ. Proteomics of organelles and large cellular structures. Nat Rev Mol Cell Biol. 2005 Sep;6(9):702-14.

Ybe JA, Brodsky FM, Hofmann K, Lin K, Liu SH, Chen L, Earnest TN, Fletterick RJ, Hwang PK. Clathrin self-assembly is mediated by a tandemly repeated superhelix. Nature. 1999 May 27;399(6734):371-5.

Yochem J, Uchida H, Sunshine M, Saito H, Georgopoulos CP, Feiss M. Genetic analysis of two genes, dnaJ and dnaK, necessary for Escherichia coli and bacteriophage lambda DNA replication. Mol Gen Genet. 1978 Aug 4;164(1):9-14.

Young JC, Barral JM, Ulrich Hartl F. More than folding: localized functions of cytosolic chaperones. Trends Biochem Sci. 2003 Oct;28(10):541-7.

Young JC, Agashe VR, Siegers K, Hartl FU. Pathways of chaperone-mediated protein folding in the cytosol. Nat Rev Mol Cell Biol. 2004 Oct;5(10):781-91.

Zandi R, Larsen AB, Andersen P, Stockhausen MT, Poulsen HS. Mechanisms for oncogenic activation of the epidermal growth factor receptor. Cell Signal. 2007 Oct;19(10):2013-23.

Zaremba S, Keen JH. Assembly polypeptides from coated vesicles mediate reassembly of unique clathrin coats. J Cell Biol. 1983 Nov;97(5 Pt 1):1339-47.

Zerial M, McBride H. Rab proteins as membrane organizers. Nat Rev Mol Cell Biol. 2001 Feb;2(2):107-17.

Zhang B, VerBerkmoes NC, Langston MA, Uberbacher E, Hettich RL, Samatova NF. Detecting differential and correlated protein expression in label-free shotgun proteomics. J Proteome Res. 2006 Nov;5(11):2909-18.

Zhang CX, Engqvist-Goldstein AE, Carreno S, Owen DJ, Smythe E, Drubin DG. Multiple roles for cyclin G-associated kinase in clathrin-mediated sorting events. Traffic. 2005 Dec;6(12):1103-13.

Zhang Y, Grant B, Hirsh D. RME-8, a conserved J-domain protein, is required for endocytosis in Caenorhabditis elegans. Mol Biol Cell. 2001 Jul;12(7):2011-21.

Zhou P, Fernandes N, Dodge IL, Reddi AL, Rao N, Safran H, DiPetrillo TA, Wazer DE, Band V, Band H. ErbB2 degradation mediated by the co-chaperone protein CHIP.

Zhou Z, Licklider LJ, Gygi SP, Reed R. Comprehensive proteomic analysis of the human spliceosome. Nature. 2002 Sep 12;419(6903):182-5.

Zhu Y, Traub LM, Kornfeld S. ADP-ribosylation factor 1 transiently activates high-affinity adaptor protein complex AP-1 binding sites on Golgi membranes. Mol Biol Cell. 1998 Jun;9(6):1323-37.

Zybailov B, Coleman MK, Florens L, Washburn MP. Correlation of relative abundance ratios derived from peptide ion chromatograms and spectrum counting for quantitative proteomic analysis using stable isotope labeling. Anal Chem. 2005 Oct 1;77(19):6218-24.

ANNEXE 1

SUPPLEMENTAL TABLE 2.S1

PROTEINS IDENTIFIED IN RAT LIVER CCV PREPARATIONS

Supplemental Table 2.S1 - Proteins identified in rat liver CCV preparations
The peak gel band number represents the band in which the peak number of peptides were identified for each protein within each preparation.
The range of gel bands from which peptide matches were obtained is also indicated.
The number of specific and shared peptides is indicated for the corresponding protein.
Proteins with like lower case letters share peptides.

group	protein		group name protein name peak gel band, range of gel bands	mass
1			COAT PROTEINS	
	1		clathrin, heavy polypeptide	193187
		prep1	52, 40-66	
		prep2	48, 18-65	
		prep3	51, 38-62	
	2		Clathrin heavy chain 2	189020
		prep2	46,	
		prep3	50, 38-62	
	3		clathrin light chain A	23608
		prep1	21;20, 8-21	
		prep2	16, 16-17	
		prep3	20,	
	4		clathrin light chain B	26013
		prep1	17, 3-18	
		prep2	14,	
		prep3	18;19, 18-19	
	5		AP-1 beta 1	104768
		prep1	47, 39-60	
		prep2	40;41, 29-45	
		prep3	43, 34-45	
	6		AP-1 gamma 1	92147
		prep1	44, 37-48	
		prep2	38, 31-39	
		prep3	40, 39-43	
	7		AP-1 gamma 2	88607
		prep1	42, 38-43	
		prep2	36, 36-37	
		prep3	39, 36-39	

specific peptides	shared peptides	NCBI GIs				
1638	172	9506497	25072051	33438248		
386	0 a					
857	36					
395	136					
5	172	2506298	4502903	7441348	9257202	1335854
1	36 a					
4	136					
31	0	203278				
20	0					
6	0					
5	0					
17	0	71563	203361	116505	4502901	12844891
12	0					
1	0					
4	0					
377	128	6671553	8392872	1703167		
128	48 b					
119	53					
130	27					
208	0	6753070	2765190	7512448	12643391	18104998
67	0					
63	0					
78	0					
31	0	6671555	4503843	27700033		
14	0					
11	0					
6	0					

group	protein		group name protein name peak gel band, range of gel bands	mass
	8		AP-1 mu 1	48727
		prep1	29, 28-29	
		prep2	24, 23-24	
		prep3	27, 27-28	
	9		AP-1sigma 1	18949
		prep1	7, 7-9	
		prep2	5, 5-6	
		prep3	9, 8-9	
	10		AP-2 alpha 1	108679
		prep1	45, 35-46	
		prep2	40, 39-41	
		prep3	42, 41-43	
	11		AP-2 alpha C	104863
		prep1	44, 35-46	
		prep2	39, 13-42	
		prep3	41, 18-42	
	12		AP-2 beta 2	105398
		prep1	45, 41-60	
		prep2	39, 35-45	
		prep3	41, 37-42	
	13		AP-2 mu 1 or mu 2	49965
		prep1	30, 29-31	
		prep2	25, 24-26	
		prep3	29, 29-30	
	14		AP-2 sigma 1 or 2	17178
		prep1	4, 3-4	
		prep2	4,	
		prep3	5, 4-6	
	15		CALM	71108
		prep1	36, 32-39	
		prep2	30, 29-33	
		prep3	33;34, 25-36	
	16		cyclin G-associated kinase	144981
		prep1	55, 48-56	
		prep2	49, 44-55	
		prep3	51, 51-52	

SUPPLEMENTAL TABLE

specific peptides	shared peptides	NCBI GIs				
122	0	14210504	6671557			
53	0					
33	0					
36	0					
28	0	4557471	5630084	27664100		
11	0					
11	0					
6	0					
53	26	6671561	27731549	90292	2246667	4314340
12	6 c					
18	11					
23	9					
181	26	90292	6671563	13591908	14042895	14714884
46	6 c					
80	11					
55	9					
121	128	4557469	1703167	18034787		
26	48 b					
54	53					
41	27					
68	0	6729920	6730004	7448827	6753074	7448828
27	0					
25	0					
16	0					
11	0	231553	4757996	12621128	23595927	30851514
6	0					
1	0					
4	0					
145	0	16758324	18204423	2792500	6005733	18204423
49	0					
48	0					
48	0					
43	0	13591947	28519095			
11	0					
25	0					
7	0					

group	protein		group name protein name peak gel band, range of gel bands	mass
	17		Hsc70	70989
		prep1	38, 38-39	
		prep2	32,	
		prep3	36,	
	18		huntingtin interacting protein 1	112648
		prep1	48, 48-49	
		prep2	42,	
		prep3	45,	
	19		huntingtin interacting protein 12	120163
		prep1	49, 49-50	
		prep2	43,	
		prep3	46,	
2			ACCESSORY PROTEINS	
	20		Epsin 1	60235
		prep1	42, 42-43	
		prep2	36,	
		prep3	39, 39-40	
	21		*m-Numb*	64980
		prep1	38,	
		prep2	35, 32-35	
		prep3	36, 36-38	
	22		epidermal growth factor receptor pathway substrate 15	98924
		prep2	42;44;45, 42-45	
		prep3	46;47, 46-47	
3			VESICLE TRAFFICKING-SNARE *SNARE proteins*	
	23		NSF	83811
		prep1	25, 24-40	
		prep2	34,	
		prep3	23,22-37	

specific peptides	shared peptides	*NCBI GIs*				
59	0	123647	347019	476850	5729877	13242237
17	0					
26	0					
16	0					
24	0	3510693	22122461	23831094		
13	0					
4	0					
7	0					
33	0	12718814	27665094			
15	0					
4	0					
14	0					
17	0	16923990	28422275			
4	0					
7	0					
6	0					
9	0	1575756	4050088	4102705	4691549	5713183
2	0					
4	0					
3	0					
5	0	6679671	28981402	27715647		
3	0					
2	0					
16	0	90219	4505331	134267	1171774	7435752
7	0					
1	0					
8	0					

group	protein		group name protein name peak gel band, range of gel bands	mass
	24		SPNAP alpha	33549
		prep1	19, 18-200	
		prep2	15, 15-16	
		prep3	20, 19-20	
	25		SNARE Vti1a-beta protein	25145
		prep1	15,	
		prep2	12,	
		prep3	15,	
	26		syntaxin7	29888
		prep1	22,	
		prep2	17,	
		prep3	21;22, 21-22	
	27		syntaxin 8	27122
		prep1	14, 13-14	
		prep2	10,	
		prep3	14,	
	28		syntaxin 12	31318
		prep1	22, 21-22	
		prep2	18,	
		prep3	21,	
	29		syntaxin 13	30563
		prep1	22, 21-22	
		prep2	17,	
		prep3	22,	
	30		VAMP-2	3547
		prep1	4, 2-5	
		prep3	6,	
	31		GES30	26465
		prep1	16, 16-26	
		prep3	16,	
			VESICLE TRAFFICKING-Rab and others	
	32		RAB1A	22891
		prep1	13,	
		prep2	10,	
		prep3	12;13, 12-13	

SUPPLEMENTAL TABLE

specific peptides	shared peptides	NCBI GIs				
42	0	12851441	18034791	13385392	2143586	12851441
17	0					
16	0					
9	0					
5	0	12831221	13928668			
2	0					
2	0					
1	0					
5	0	11177920				
2	0					
1	0					
2	0					
10	0	13928908	9055356	4433649	4759188	
5	0					
1	0					
4	0					
6	7	14715019	19527102			
0	7 d					
2	0					
4	0					
5	7	3184552	12621104			
0	7 d					
3	0					
2	0					
9	0	479872	2253399	4759300	4894188	6678551
5	0					
4	0					
5	0	4104432	13124606	31980617		
3	0					
2	0					
8	6	4758988	13592035	27692431	32527715	
2	1 e					
2	1					
4	4					

group	protein		group name protein name peak gel band, range of gel bands	mass
	33		Rab1B	22347
		prep1	13,	
		prep2	10,	
		prep3	13, 12-13	
	34		Rab2	23688
		prep1	11, 11-12	
		prep2	9,	
		prep3	12,	
	35		Rab4B	23899
		prep1	12, 12-13	
		prep2	10, 9-10	
		prep3	13, 13-14	
	36		RAB5C	23626
		prep1	14,	
		prep2	11,	
		prep3	14,	
	37		Rab6	23692
		prep1	13,	
		prep2	10,	
		prep3	14,	
	38		Rab14	24078
		prep1	13,	
		prep2	10,	
		prep3	13, 13-14	
	39		ARF1	20610
		prep1	8, 7-9	
		prep2	6, 6-7	
		prep3	9, 8-9	
	40		CD-mannose-6-phosphate receptor	31589
		prep1	26, 23-28	
		prep2	22, 19-24	
		prep3	25, 23-26	
	41		CI-mannose-6-phosphate receptor	280179
		prep1	61, 62-64	
		prep2	58, 57-58	
		prep3	59, 58-60	

SUPPLEMENTAL TABLE

specific peptides	shared peptides	NCBI GIs				
5	6	92339	131803	131804	234746	420269
1	1 e					
1	1					
3	4					
11	0	266878	106185	4506365	10946940	12837642
4	0					
4	0					
3	0					
19	0	15986733	131791	21361509	33150586	
6	0					
6	0					
7	0					
9	0	18606182	20072723	27689503	28514415	
4	0					
2	0					
3	0					
9	2	131796	13195674	17512290	19923231	
4	1 e					
3	1					
2	0					
12	3	420272	16758368	18390323		
4	1 e					
2	1					
6	1					
20	0	1065361	4502201	4502203	4502209	6671571
9	0					
4	0					
7	0					
48	0	27713160	4505061	16877746	14916479	27706250
19	0					
13	0					
16	0					
51	0	6981078	1709091	52979	23956054	14647149
28	0					
12	0					
11	0					

group	protein		group name protein name peak gel band, range of gel bands	mass
	42		SCAMP-1	38222
		prep1	20;19, 19-20	
		prep2	16, 15-16	
		prep3	19;20, 19-20	
	43		SCAMP-3	38743
		prep1	23, 23-24	
		prep2	18, 18-19	
		prep3	22, 12-23	
	44		SEC23A	87019
		prep1	41,	
		prep2	36, 35-36	
		prep3	38, 38-39	
	45		VPS35	92349
		prep1	41, 41-42	
		prep2	35, 35-36	
		prep3	39,	
	46		VPS45	65310
		prep1	36,	
		prep2	30,	
		prep3	34, 34-35	
	47		Transmembrane protein Tmp21	25033
		prep1	9;8, 9-8	
		prep2	6;7, 6-7	
		prep3	9, 9-10	
	48		similar to pantophysin; Pan I	18392
		prep1	21,	
		prep2	16;18;20, 16-20	
		prep3	16,	
	49		ERS-24	24824
		prep2	10,	
		prep3	14, 13-14	
	50		phosphatidylinositol 3-kinase, C2 domain containing, alpha polypeptide	172381
		prep1	56,	
		prep2	50, 50-51	
		prep3	52,	

SUPPLEMENTAL TABLE

specific peptides	shared peptides	NCBI GIs				
8	0	2232239	2791682	3395572	3914958	12854143
2	0					
4	0					
2	0					
23	0	27692941	2232243	6755404	10764629	10764631
8	0					
6	0					
9	0					
25	0	25052355	26389719	6677901	5454042	22477159
2	0					
15	0					
8	0					
14	0	7022978	9622850	10435637	12053275	13928670
8	0					
5	0					
1	0					
22	0	7447775	25742604	4583679	7305631	18105063
8	0					
7	0					
7	0					
12	0	3915123	3915137	16758214	20894167	21312062
2	0					
6	0					
4	0					
5	0	27717207				
1	0					
3	0					
1	0					
6	0	1927215	4759086	14290512		
2	0					
4	0					
16	0	6755058	11259849			
3	0					
7	0					
6	0					

group	protein		group name protein name peak gel band, range of gel bands	mass
	51		phosphatidylinositol 4-kinase type II	54388
		prep1	32,	
		prep2	27,	
		prep3	30,	
4			INTEGRAL PLASMA MEMBRANE AND CARGO RECEPTORS	
	52		Sodium/potassium-transporting ATPase alpha-1 chain	113936
		prep1	44,	
		prep2	39,	
		prep3	40,	
	53		Porin 31HM [human, skeletal muscle membranes]	30737
		prep1	18;19, 18-19	
		prep2	16,	
		prep3	19,	
	54		Vesicular integral-membrane protein VIP36 precursor	40530
		prep1	21,	
		prep2	17,	
		prep3	21,20-21	
	55		CD36 antigen (collagen type I receptor)	54513
		prep2	36, 36-37	
		prep3	39, 38-39	
	56		lysosomal membrane glycoprotein-type B precursor	43556
		prep1	45,	
		prep2	39;40, 39-40	
		prep3	41, 41-43	
	57		rat CD1 antigen precursor	38993
		prep1	32,	
		prep2	27, 27-28	
		prep3	30,	
	58		similar to NSE1	34769
		prep1	23;24, 23-24	
		prep2	19,	
		prep3	22;23, 22-23	

SUPPLEMENTAL TABLE

specific peptides	shared peptides	NCBI GIs				
7	0	13559514	16758554	21703986		
2	0					
2	0					
3	0					
5	0	114373	114375	114377	164382	179212
1	0					
3	0					
1	0					
8	0	238427	4507879	6063691	8745552	6755963
2	0					
5	0					
1	0					
9	0	1353234	27682691	13385300	21264125	26350553
1	0					
3	0					
5	0					
7	0	16758914				
4	0					
3	0					
7	0	205169	1346462	8393690		
1	0					
2	0					
4	0					
6	0	2118857	5420461	8393070		
1	0					
3	0					
2	0					
8	0	27719075				
2	0					
4	0					
2	0					

group	protein		group name protein name peak gel band, range of gel bands	mass
	59		36 kDa beta-galactoside binding lectin	36692
		prep1	20;21, 20-21	
		prep2	17, 17-19	
		prep3	21, 20-24	
	60		lipoprotein receptor-related protein	523309
		prep1	63, 43-64	
		prep2	60, 39-61	
		prep3	61, 39-62	
	61		mannose receptor precursor, macrophage	167666
		prep1	56, 56-57	
		prep2	51, 51-52	
		prep3	53, 52-54	
	62		asialoglycoprotein receptor 1 (hepatic lectin)	33398
		prep1	27, 26-28	
		prep2	21;22;23, 20-23	
		prep3	25, 24-27	
	63		asialoglycoprotein receptor R2/3	35548
		prep1	30;34, 30-37	
		prep2	29;30, 25-31	
		prep3	31, 29-35	
	64		107 kDa sialoglycoprotein	42275
		prep1	48;47, 47-48	
		prep2	28,	
		prep3	31;32;33;44, 31-44	
	65		transferrin	78090
		prep1	40, 40-41	
		prep2	35, 34-36	
		prep3	46, 39-46	
	66		transferrin receptor 2	92146
		prep1	44, 44-45	
		prep2	38, 38-39	
		prep3	40, 40-42	
	67		polymeric immunoglobulin receptor	86057
		prep1	48, 47-48	
		prep2	42, 41-42	
		prep3	45, 44-45	

SUPPLEMENTAL TABLE

specific peptides	shared peptides	NCBI GIs				
18	0	1916610	2851467	6981156		
4	0					
3	0					
11	0					
113	0	6678720	15825005	15825096	4758686	
20	0					
27	0					
66	0					
69	0	477362	6678932	27688835	4505245	
7	0					
21	0					
41	0					
58	0	7705290	202988			
10	0					
19	0					
27	0					
45	0	126136	206649	6680734	7110516	8392926
12	0					
10	0					
23	0					
7	0	56578	91900	6981144		
2	0					
1	0					
4	0					
59	0	8394439	33086606	33187764	6175089	202176
16	0					
24	0					
19	0					
43	0	27663630	7141286	15718463	20140821	31982728
11	0					
12	0					
20	0					
34	0	27151742	458422	8099665	31981570	
6	0					
10	0					
18	0					

group	protein		group name protein name peak gel band, range of gel bands	mass
	68		hyaluronan receptor for endocytosis HARE precursor	161856
		prep2	52;53;58, 52-58	
		prep3	54, 53-59	
	69		Fc Receptor (Neonatal) Complexed With Fc (Igg) (FcFCRN Complex)	11743
		prep2	2,	
		prep3	2, 2-3	
	70		gp250 precursor	232635
		prep1	61,	
		prep3	59,	
	71		ApoE	38359
		prep1	19,	
		prep3	20, 19-20	
	72		glucose transport protein, hepatic	57448
		prep1	33;35, 32-35	
		prep2	29,	
		prep3	32;33, 31-33	
	73		solute carrier family 25, member 13	74819
		prep1	37,	
		prep2	31,	
	74		ferritin heavy chain	21257
		prep1	62, 10-66	
		prep2	57;58, 7-60	
		prep3	58, 10-60	
	75		Ferritin light chain (Ferritin L subunit)	20827
		prep1	62, 10-65	
		prep2	58, 8-59	
		prep3	59, 10-62	
5			CYTOSKELETON	
	76		beta actin	42066
		prep1	27, 15-27	
		prep2	22,	
		prep3	26,	

SUPPLEMENTAL TABLE

specific peptides	shared peptides	NCBI GIs				
17	0	24285893				
3	0					
14	0					
5	0	999862	7549746	27573700		
2	0					
3	0					
6	0	2654025	7513715	8928391		
3	0					
3	0					
9	0	913986	202959	1703338	114041	20301954
3	0					
6	0					
16	0	6981548	90518	111669	535722	1911419
7	0					
4	0					
5	0					
14	0	7657583	12833101	12849571		
6	0					
8	0					
48	0	6978859	111625	120519	15076951	27703550
13	0					
16	0					
19	0					
148	0	2119695	120527	2119695	6679873	6753914
79	0					
39	0					
30	0					
41	0	71620	71621	71625	576368	809561
18	0					
8	0					
15	0					

group	protein		group name protein name peak gel band, range of gel bands	mass
	77		tubulin alpha	50748
		prep1	32, 31-34	
		prep2	27, 26-28	
		prep3	30, 29-31,	
	78		tubulin beta	50361
		prep1	31, 31-32	
		prep2	27, 26-28	
		prep3	30,	
	79		radixin	68523
		prep2	35,	
		prep3	38,	
	80		myosin, heavy polypeptide 9, non-muscle	227646
		prep1	58,	
		prep3	56,	
	81		Moesin (Membrane-organizing extension spike protein)	67733
		prep1	40,	
		prep2	34, 33-34	
6			SIGNALING GTPases	
	82		G protein beta subunit like	35453
		prep1	18, 17-18	
		prep2	15, 14-15	
		prep3	19,	
	83		GTP-binding protein (G-alpha-i2)	41007
		prep1	25,	
		prep2	19;20, 19-20	
		prep3	24, 23-24	
	84		GTP-binding protein, 23K	23075
		prep2	10,	
		prep3	13;14, 13-14	
	85		RAP1A, member of RAS oncogene family	21316
		prep2	8,8-9	
		prep3	11, 11-12	

SUPPLEMENTAL TABLE

specific peptides	shared peptides	NCBI GIs				
60	0	90217	135412	5174477	6678469	37492
40	0					
11	0					
9	0					
100	0	92930	135451	5174735	13542680	23958133
56	0					
25	0					
19	0					
18	0	91254	6677699	131821	4506467	28436809
10	0					
8	0					
7	0	12667788	553596	625305	20137006	29436380
1	0					
6	0					
5	0	127236	462608	4505257	6754750	13540689
1	0					
4	0					
32	0	475012	5174447	12848861	18543331	30025862
3	0					
23	0					
6	0					
13	0	183182	348273	1730227	4504041	13591955
2	0					
2	0					
9	0					
5	0	92022	131797	1174149	1709999	4105819
3	0					
2	0					
8	0	4506413	5821936	14595132	539995	1942609
4	0					
4	0					

group	protein		*group name* *protein name* peak gel band, range of gel bands	mass
7			CALCIUM & PHOSPHATE	
	86		annexin VI	76106
		prep1	37, 37-38	
		prep2	32, 31-32	
		prep3	35;36, 21-36	
	87		Annexin V	35458
		prep1	18,	
		prep2	14;15, 14-15	
	88		nucleobindin CALNUC	53698
		prep2	29;30, 29-30	
		prep3	33, 32-33	
8			RNA GRANULES AND NUCLEUS	
	89		elongation factor 1-alpha	50437
		prep1	29, 28-30	
		prep2	22,	
		prep3	26, 22-29	
	90		heterogeneous nuclear ribonucleoprotein A2/B1 isoform A2	36041
		prep1	21, 21-28	
		prep2	17;18, 14-19	
		prep3	21, 20-22	
	91		heterogeneous nuclear ribonucleoprotein C	33721
		prep1	25;26, 19-26	
		prep2	16, 15-16	
		prep3	21;24, 20-24	
	92		heterogeneous nuclear ribonucleoprotein L	60712
		prep1	35, 35-41	
		prep2	30, 29-30	
		prep3	33,	
	93		M4 protein	77940
		prep1	38, 33-39	
		prep2	32, 31-33	
		prep3	31;37, 31-37	

SUPPLEMENTAL TABLE

specific peptides	shared peptides	NCBI GIs				
12	0	13994159	35218	113962	2914360	3121751
7	0					
4	0					
7	0					
6	0	1421099	2981437	3318923	4139938	999926
2	0					
4	0					
5	0	189308	2506255	6679158	12841873	16758210
2	0					
3	0					
46	0	1169475	72870	1169475	2119924	31092
8	0					
1	0					
37	0					
32	0	4504447	14043072	133262	7949053	21071091
14	0					
12	0					
6	0					
26	0	8393544	3660678	4758544	8393544	12847394
16	0					
5	0					
5	0					
21	0	20824058	12832989	27729903	29165751	32363497
11	0					
4	0					
6	0					
50	0	21313308	16124253	479852	1710636	14141152
39	0					
8	0					
3	0					

group	protein		group name protein name peak gel band, range of gel bands	mass
	94		laminin-binding protein	31888
		prep1	18,	
		prep2	22, 19-22	
	95		ribosomal protein S2	28403
		prep1	18,17-18	
		prep2	14, 14-15	
		prep3	18;19, 17-19	
	96		ribosomal protein S3, cytosolic [validated]	26814
		prep1	17,17-18	
		prep2	13, 13-14	
		prep3	18, 17-19	
	97		ribosomal protein S8; 40S ribosomal protein S8	24475
		prep1	15,	
		prep2	1;12, 11-12	
		prep3	15, 15-16	
	98		Major vault protein	99982
		prep1	46, 44-49	
		prep2	40, 37-42	
		prep3	43, 40-44	
	99		splicing factor 3a, subunit 1, 120kDa	88888
		prep1	49,	
		prep2	43,	
		prep3	46,	
	100		eukaryotic translation initiation factor 3, subunit 6 interacting protein	66912
		prep1	36, 35-36	
		prep2	30, 30-31	
		prep3	24, 33-35	
	101		ATP-binding cassette sub-family E member 1 (RNase L inhibitor)	68240
		prep1	35, 35-36	
		prep2	30, 30-31	
		prep3	34, 33-35	
	102		polypyrimidine tract-binding protein PTB-1	56918
		prep1	32, 31	
		prep2	28, 27-28	
		prep3	30;31, 30-31	

SUPPLEMENTAL TABLE

specific peptides	shared peptides	NCBI GIs				
18	0	34234	34272	91035	226005	250127
4	0					
14	0					
24	0	2920825	25032791	2920833	18087805	27681907
3	0					
12	0					
9	0					
42	0	70850	6755372	7765076	12848978	13097759
4	0					
13	0					
25	0					
16	0	4506743	20838041	20859553	20892859	26353710
4	0					
6	0					
6	0					
394	0	12083689	28515979	2498602	26352970	18079351
127	0					
92	0					
175	0					
5	0	5032087	20988230	26324776	26325080	26326219
2	0					
1	0					
2	0					
61	0	7705433	6572154	18700307	21553089	21758474
10	0					
25	0					
26	0					
36	0	22001498	7657518	4506559		
7	0					
11	0					
18	0					
28	0	110819	266862	480289	6679515	13487910
7	0					
7	0					
14	0					

group	protein		group name *protein name* peak gel band, range of gel bands	mass
	103		heterogeneous nuclear ribonucleoprotein H1	49484
		prep1	31, 27-31	
		prep2	22;26, 22-26	
		prep3	28,	
	104		eukaryotic translation initiation factor 3, subunit 5 epsilon, 47kDa	37654
		prep1	30, 27-30	
		prep2	25, 21-25	
		prep3	29, 25-29	
	105		translation initiation factor eIF-4A2 homolog	47088
		prep1	28,	
		prep2	23,	
		prep3	27,	
	106		eIF3-p44	35682
		prep1	28,	
		prep2	23, 22-23	
		prep3	27, 26-27	
	107		Splicing factor, arginine/serine-rich 5 (Pre-mRNA splicing factor SRP40)	30987
		prep1	26, 25-27	
		prep3	24, 23-24	
	108		heterogeneous nuclear ribonucleoprotein A3	37291
		prep1	23, 23-26	
		prep2	20, 19-21	
		prep3	23;24, 22-24	
	109		translation initiation factor eIF3 p40 subunit; eIF3p40	40075
		prep1	26,	
		prep2	20,	
		prep3	24,	
	110		eukaryotic translation initiation factor 3, subunit 2 beta, 36kDa	36878
		prep1	24,	
		prep2	19,	
		prep3	23, 22-23	
	111		eukaryotic translation initiation factor 3, subunit 1 alpha, 35kDa	29087
		prep1	22,	
		prep2	18,	
		prep3	21, 21-22	

SUPPLEMENTAL TABLE

specific peptides	shared peptides	NCBI GIs				
9	0	5031753	10946928	26353116	27769212	9624998
6	0					
2	0					
1	0					
31	0	4503519	17426420	21313620	21754858	26353564
6	0					
13	0					
12	0					
20	0	631472	7661920	20149756	26344810	
6	0					
6	0					
8	0					
16	0	4097873	4503517	23503064	31980808	27663624
1	0					
7	0					
8	0					
7	0	1168968	2435501	3929378	6677919	12841460
4	0					
3	0					
28	0	31559916	23274114	20849702	20849702	23274114
16	0					
5	0					
7	0					
19	0	3986482	4503515	18079341	26353442	27718783
2	0					
6	0					
11	0					
17	0	4503513	9055370	27664176		
2	0					
6	0					
9	0					
9	0	4503511	10435304	20878026	23503065	26349519
3	0					
1	0					
5	0					

group	protein		group name protein name peak gel band, range of gel bands	mass
	112		TAR DNA binding protein	44918
		prep1	27,	
		prep3	26,	
	113		splicing factor, arginine/serine-rich 1 (splicing factor 2)	27842
		prep1	21, 17-21	
		prep2	17,	
		prep3	21, 20-21	
	114		Splicing factor, arginine/serine-rich 7 (Splicing factor 9G8)	27578
		prep1	19;20, 19-20	
		prep3	20,	
	115		ribonucleoprotein	36217
		prep1	19, 18-20	
		prep2	*15;16, 15-16*	
	116		ribosomal protein S3a, cytosolic	30168
		prep1	18,	
		prep2	15, 14-15	
	117		ribosomal protein S6	28842
		prep1	17,	
		prep2	14,	
		prep3	19,	
	118		ribosomal protein S7; 40S ribosomal protein S7	21835
		prep1	11,	
		prep2	9, 8-9	
		prep3	11, 11-12	
	119		ribosomal protein S9; 40S ribosomal protein S9	22635
		prep1	11,	
		prep2	9, 8-9	
		prep3	11;12, 11-12	
	120		ribosomal protein S11; 40S ribosomal protein S11	18590
		prep1	8,	
		prep2	6,	
		prep3	1;8;9, 1-9	

SUPPLEMENTAL TABLE

specific peptides	shared peptides	NCBI GIs				
5	0	21704096	26350443			
2	0					
3	0					
22	0	5902076	105294	105295	284701	5902076
11	0					
4	0					
7	0					
5	0	3929380	15928796	20071765	22122585	26328639
4	0					
1	0					
8	0	13124196	26330019	26344670	26347149	2137740
6	0					
2	0					
12	0	7441114	8394221	20872608	27675360	31980669
1	0					
11	0					
8	0	337514	6677809	15342049	20381196	26389925
3	0					
4	0					
1	0					
12	0	4506741	337518	20887033	20985952	
1	0					
5	0					
6	0					
15	0	14141193	27665858			
1	0					
8	0					
6	0					
7	0	4506681	12836870	5441535	12847180	25046185
2	0					
2	0					
3	0					

group	protein		group name protein name peak gel band, range of gel bands	mass
	121		ribosomal protein S13; 40S ribosomal protein S13	17212
		prep1	6;7, 6-7	
		prep2	4;5, 4-5	
		prep3	8;7, 7-8	
	122		ribosomal protein S25; 40S ribosomal protein S25	13791
		prep1	6, 5-6	
		prep2	4,	
		prep3	7, 6-7	
	123		ribosomal protein S18	17730
		prep1	6,	
		prep2	4;5, 4-5	
		prep3	7, 7-8	
	124		ribosomal protein S17	15395
		prep1	6,	
		prep2	4;5, 4-5	
		prep3	6;7, 6-7	
	125		ribosomal protein S16; 40S ribosomal protein S16	16549
		prep1	5,	
		prep2	3,	
		prep3	6;7, 6-7	
	126		ribosomal protein S20; 40S ribosomal protein S20	13478
		prep1	4;5, 4-5	
		prep2	3,	
		prep3	6,	
	127		ribosomal protein S14	16462
		prep1	5,	
		prep2	4,	
		prep3	6, 6-7	
	128		ribosomal protein S21	9236
		prep1	1,	
		prep2	2,	
		prep3	2,	
	129		40S ribosomal protein S27; metallopanstimulin 1	9797
		prep1	1,	
		prep2	2, 1-2	
		prep3	2, 2-3	

SUPPLEMENTAL TABLE

specific peptides	shared peptides	NCBI GIs				
12	0	4506685	4633275	15029927	20881046	20887059
2	0					
4	0					
6	0					
10	0	4506707	20836444	20846986	23633141	27484941
5	0					
2	0					
3	0					
16	0	6755368	27715307	28189422	28189549	198578
2	0					
6	0					
8	0					
5	0	950111	2119133	4506693	6677801	26377673
1	0					
2	0					
9	0	4506691	7305445	27721735	70920	18591367
2	0					
1	0					
6	0					
6	0	4506697	20875700	27659246	27715719	27720981
2	0					
2	0					
2	0					
9	0	3097244	5032051	5441523	7440317	12083607
1	0					
2	0					
6	0					
5	0	13592073	21536222	26369983	3088341	4506699
2	0					
1	0					
2	0					
10	0	4506711	7705706	13277528	13559175	27479204
1	0					
4	0					
5	0					

group	protein		group name *protein name* peak gel band, range of gel bands	mass
	130		splicing factor 3b, subunit 1, 155kDa	146464
		prep1	52,	
		prep3	48,	
	131		splicing factor 3b, subunit 3, 130kDa	136575
		prep1	51,	
		prep2	44;45, 44-45	
		prep3	47,	
	132		U5 snRNP-specific protein, 116 kD	110336
		prep1	49,	
		prep2	43,	
		prep3	45, 45-46	
	133		Eukaryotic translation initiation factor 3 subunit 9 (eIF-3 eta)	75275
		prep1	48, 42-48	
		prep2	42, 36-42	
		prep3	44, 44-45	
	134		eukaryotic translation initiation factor 3, subunit 7 (zeta)	64202
		prep1	36;37, 36-37	
		prep2	31,	
		prep3	35, 34-35	
	135		*heterogeneous ribonuclear particle protein U*	88492
		prep2	37, 35-37	
		prep3	39,	
	136		*eukaryotic translation initiation factor 3 subunit k*	25329
		prep1	12,	
		prep2	9,	
		prep3	13, 12-13	
	137		eIF-3 p110 subunit	106163
		prep1	48, 41-48	
		prep2	35, 32-37	
		prep3	38, 38-45	

SUPPLEMENTAL TABLE

specific peptides	shared peptides	NCBI GIs				
5	0	6912654	14042921			
1	0					
4	0					
16	0	11034823	19527174	19863446		
2	0					
4	0					
10	0					
14	0	4759280	6755594	12803113	24474791	30851704
3	0					
3	0					
8	0					
51	0	13938120	20847610	23271707	3123230	7513399
11	0					
17	0					
23	0					
36	0	9055214	26337171	26340494		
6	0					
13	0					
17	0					
13	0	16923996	17390825	26354194	284156	14044052
8	0					
5	0					
8	0	10801345	5114051	21312044	27730981	
1	0					
1	0					
6	0					
37	0	19263839	22203755	1931584	4503525	27679942
5	0					
15	0					
17	0					

group	protein		group name protein name peak gel band, range of gel bands	mass
	138		U5 small nuclear ribonucleoprotein 200 kDa helicase	233221
		prep1	60,	
		prep2	54, 54-55	
		prep3	56,	
	139		DEAD (Asp-Glu-Ala-Asp) box polypeptide 5; DEAD box-5	67394
		prep1	34;37, 34-37	
		prep2	28,	
		prep3	34, 32-35	
	140		eukaryotic translation initiation factor 2, subunit 1 alpha, 35kDa	36374
		prep2	18,	
		prep3	22,	
	141		Eukaryotic translation initiation factor 3 subunit 10 (eIF-3 theta)	162251
		prep2	46, 42-4	
		prep3	47, 47-49	
	142		Eif4g1 protein	176076
		prep2	55,	
		prep3	56,	
	143		Ribosome-binding protein 1 (Ribosome receptor protein) (mRRp)	143890
		prep2	42,	
		prep3	40, 40-45	
	144		*acidic ribosomal protein P0*	34365
		prep2	16, 15-18	
		prep3	21, 19-22	
	145		ribosomal protein S4	29892
		prep2	12, 12-13	
		prep3	16, 16-17	
	146		ribosomal protein S5, cytosolic	22934
		prep2	8;9, 8-9	
		prep3	11,	
	147		ribosomal protein S10; 40S ribosomal protein S10	18886
		prep2	5, 5-6	
		prep3	8;9, 8-9	

SUPPLEMENTAL TABLE

specific peptides	shared peptides	NCBI GIs				
22	0	20521660	12643640	24307975	28893243	
1	0					
8	0					
13	0					
18	0	4758138	226021	6681157	25029528	27690065
8	0					
2	0					
8	0					
8	0	4758256	9506571	27671772		
1	0					
7	0					
30	0	6686292	4503509	32449796		
17	0					
13	0					
6	0	20892055				
2	0					
4	0					
15	0	27703664				
2	0					
13	0					
19	0	11693176	71138	2293577	3041728	4506667
9	0					
10	0					
22	0	227229	337930	1350996	2119059	4506725
4	0					
18	0					
7	0	1362935	3717978	13904870	27675812	
4	0					
3	0					
11	0	13399310	27669179	4506679		
5	0					
6	0					

group	protein		group name *protein name* peak gel band, range of gel bands	mass
	148		ribosomal protein S12; 40S ribosomal protein S12	14859
		prep2	3, 2-3	
		prep3	5,	
	149		ribosomal protein S19; 40S ribosomal protein S19	16051
		prep2	4, 3-4	
		prep3	6, 6-7	
	150		ribosomal protein L4, cytosolic [validated]	47565
		prep2	24, 21-24	
		prep3	27, 26-28	
	151		ribosomal protein L5	34534
		prep2	*16;17, 16-17*	
		prep3	20, 20-21	
	152		ribosomal protein L6	33663
		prep2	17, 17-21	
		prep3	20,	
	153		ribosomal protein L7, cytosolic	30367
		prep2	13,	
		prep3	17, 16-17	
	154		60S ribosomal protein L7a; surfeit 3	30148
		prep2	13, 13-14	
		prep3	18, 16-18	
	155		60S ribosomal protein L9	21694
		prep2	10,	
		prep3	*13,12-13*	
	156		ribosomal protein L11, cytosolic	19062
		prep2	7, 6-7	
		prep3	9, 1-10	
	157		ribosomal protein L14	23438
		prep2	11,	
		prep3	14;15, 14-15	
	158		60S ribosomal protein L24; ribosomal protein L30	17882
		prep2	7, 6-7	
		prep3	9, 1-10	

SUPPLEMENTAL TABLE

specific peptides	shared peptides	NCBI GIs				
6	0	133742	6755366	13928992	14277700	27485488
5	0					
1	0					
9	0	4506695	12963511	16924231	27676006	2500494
3	0					
6	0					
9	0	1363989	11968086	132958	337580	347964
3	0					
6	0					
10	0	206734	1173054	13592051	14591909	21483852
4	0					
6	0					
6	0	16758864	27668585	6755354	9488975	14210106
3	0					
12	0	11383729	27660180	133023	206736	11383729
5	0					
7	0					
17	0	4506661	7305443	25025731	25051544	27729543
5	0					
12	0					
8	0	15431303	27676004	27717985	687604	2136121
3	0					
5	0					
8	0	3914659	14719845	13385408	18204109	631361
3	0					
5	0					
6	0	12621122	12841593	12846159	13385472	27781339
2	0					
4	0					
9	0	4506619	26346504	28189765	28174943	28189314
4	0					
5	0					

group	protein		group name protein name peak gel band, range of gel bands	mass
	159		60S ribosomal protein L26	17267
		prep2	6,	
		prep3	9,	
	160		nucleolin	77059
		prep2	27,	
		prep3	30,	
	161		SYNCRIP	62733
		prep2	31,	
		prep3	33,	
	162		histone H1d	21832
		prep2	15,	
		prep3	17, 16-19	
	163		60S ribosomal protein L17 (L23)	21637
		prep2	8,	
		prep3	10;11, 10-11	
	164		ribosomal protein L23a	17692
		prep2	6,	
		prep3	9,1-9	
	165		regulator of nonsense transcript stability	124351
		prep2	44;45, 44-45	
		prep3	47, 45-47	
	166		40S ribosomal protein SA (P40) (34/67 kDa laminin receptor)	31888
		prep2	14,	
		prep3	26, 16-26	
	167		Tho2	171128
		prep1	51, 50-51,	
		prep2	44;45, 44-45	
		prep3	47, 46-47	
	168		matrin 3	95085
		prep1	49, 40-50	
		prep2	35, 34-35	
		prep3	46, 45-46	

SUPPLEMENTAL TABLE

specific peptides	shared peptides	NCBI GIs				
5	0	132827	292435	4506621	27729769	28189641
1	0					
4	0					
7	0	92559	6981248			
3	0					
4	0					
9	0	6576815	15809588	15809590	21619168	23397427
2	0					
7	0					
10	0	92378	109973	121903	121915	356168
1	0					
9	0					
9	0	22001904	23682842	27679110	27730945	202990
4	0					
5	0					
13	0	404015	16741485	20071865	17105394	306549
2	0					
11	0					
8	0	1575536	1885356	13507601	1944407	17380291
2	0					
6	0					
21	0	34234	34272	91035	730679	226005
1	0					
20	0					
19	0	20799318	22055158	27692565	27714887	
2	0					
4	0					
13	0					
29	0	25141233	6563246	111944	9506881	6497041
17	0					
6	0					
6	0					

group	protein		group name protein name peak gel band, range of gel bands	mass
	169		telomerase associated protein 1; telomerase protein component 1	295173
		prep1	59, 59-61	
		prep2	56, 54-59	
		prep3	57, 56-58	
	170		EBNA-2 co-activator (100kD)	100313
		prep1	47,	
		prep2	41, 41-42	
		prep3	44, 34-44	
	171		DEA/H (Asp-Glu-Ala-His) box polypeptide 15; DEAD/H box-15	93568
		prep1	43,	
		prep2	37,	
		prep3	40,	
	172		DEAD/H (Asp-Glu-Ala-Asp/His) box polypeptide 1	83587
		prep1	43,	
		prep2	37, 36-37	
		prep3	39,	
	173		acinusS	67754
		prep1	43,	
		prep2	37, 37-61	
		prep3	55,	
	174		nuclear pore-targeting complex protein, 97K	98377
		prep1	43,	
		prep2	37,	
		prep3	40,	
	175		THO complex 1	76130
		prep1	42,	
		prep2	36,	
		prep3	38, 38-39	
	176		DEAD-box protein 3 (Helicase-like protein 2) (HLP2)	69793
		prep1	40, 36-40	
		prep3	38, 32-38	
	177		Polyadenylate-binding protein 1 (Poly(A)-binding protein 1) (PABP 1)	70826
		prep1	39,	
		prep2	33, 27-34	
		prep3	36, 30-37	

SUPPLEMENTAL TABLE

specific peptides	shared peptides	NCBI GIs				
66	0	12018250				
15	0					
27	0					
24	0					
23	0	7657431	9790067	12083649	13938020	100313
1	0					
10	0					
12	0					
7	0	4557517	6681155	13124667	31563436	4557517
3	0					
3	0					
1	0					
23	0	14250287	19527256			
2	0					
12	0					
9	0					
6	0	5931961	5931963	5931965	7513059	7662238
2	0					
3	0					
1	0					
6	0	2137601	5107666	8393610	19923142	30931411
1	0					
2	0					
3	0					
10	0	23956332	26343023			
1	0					
4	0					
5	0					
26	0	27707738	3023628	6753620	13514813	14861844
12	0					
14	0					
50	0	129535	3183544	4505575	12229876	19705459
1	0					
25	0					
24	0					

group	protein		group name protein name peak gel band, range of gel bands	mass
	178		Apobec-1 complementation factor	65864
		prep1	36, 36-37	
		prep2	31,	
		prep3	35, 34-35	
	179		transformation upregulated nuclear protein	51325
		prep1	35, 34-35	
		prep2	30, 22-30	
	180		nuclear matrix protein NMP200 related to splicing factor PRP19	55603
		prep1	32,	
		prep2	27;28, 27-28	
		prep3	31,	
	181		mammary tumor integration site 6 oncogene protein	46815
		prep1	29,	
		prep2	24, 23-24	
		prep3	27, 27-28	
	182		protein synthesis initiation factor 4A	46688
		prep1	28,	
		prep2	23,	
		prep3	27,	
	183		interferon response element-binding factor IREBF-2	30785
		prep1	19;20, 19-24	
		prep3	20,	
	184		repressor of estrogen receptor activity; B-cell associated protein	33276
		prep1	20,	
		prep2	16,	
	185		14.5 kDa translational inhibitor protein (Perchloric acid soluble protein)	14352
		prep1	2,	
		prep2	2,	
		prep3	3;4, 3-4	
	186		splicing factor Prp8	274922
		prep1	60,	
		prep2	55, 55-56	
		prep3	57,	

specific peptides	shared peptides	NCBI GIs				
14	0	15072439	19173760	6996658	8515877	8515879
7	0					
2	0					
5	0					
12	0	460789	473912	1083569	12230546	13384620
6	0					
6	0					
5	0	7657381	19527358	21326455	26338912	26345812
1	0					
2	0					
2	0					
27	0	7513720	4503521	17389740	12847562	20902039
6	0					
10	0					
11	0					
24	0	673433	4503531	7305019	7582292	50815
3	0					
14	0					
7	0					
9	0	423485	1405747	4506899	6755478	26345390
7	0					
2	0					
5	0	6005854	28526501			
4	0					
1	0					
5	0	1709863	14269572	631868		
1	0					
2	0					
2	0					
22	0	3661610	20149742	17999537	2463577	21961512
5	0					
8	0					
9	0					

group	protein		group name protein name peak gel band, range of gel bands	mass
	187		Srp20	14422
		prep1	10,	
		prep2	8, 8-16	
		prep3	11;12, 11-12	
	188		heterogeneous nuclear ribonucleoprotein G	47419
		prep1	27,	
		prep2	22,	
		prep3	26,	
9			METABOLIC ENZYMES	
	189		phosphofructokinase, liver, B-type	86083
		prep1	40,	
		prep2	35,	
		prep3	38,	
	190		Fructose-bisphosphate aldolase B	39961
		prep1	25,	
		prep2	20, 19-20	
		prep3	24, 23-24	
	191		Glyceraldehyde 3-phosphate dehydrogenase (GAPDH)	36098
		prep1	23, 22-23	
		prep2	19;18, 18-19	
		prep3	21, 21-22	
	192		Glycogen synthase 2 (liver)	81424
		prep1	41, 38-43	
		prep2	32;33;36, 32-36	
		prep3	38, 36-38	
	193		3-phosphoglycerate dehydrogenase	57344
		prep1	32,	
		prep2	27,	
		prep3	31,	
	194		lactate dehydrogenase A	36712
		prep1	21;20, 20-21	
		prep2	17, 16-17	

specific peptides	shared peptides	NCBI GIs				
10	0	2125864	4506901	5441529	12844972	26351845
2	0					
4	0					
4	0					
6	0	542850	15030328	4504451	20930284	6755296
1	0					
3	0					
2	0					
5	0	6981352	31560653			
1	0					
2	0					
2	0					
32	0	113611	178357	359734	1619606	2160383
9	0					
7	0					
16	0					
24	0	120707	6679937	8393418	20820032	20821496
12	0					
4	0					
8	0					
50	0	13242186	6981002	517112	7595922	11496237
43	0					
3	0					
4	0					
8	0	29789074	13928850	20877520	20894859	23308577
5	0					
2	0					
1	0					
5	0	8393706	27719855	5031857	13786849	17368677
2	0					
3	0					

group	protein		group name protein name peak gel band, range of gel bands	mass
	195		glutamine synthetase (glutamate-ammonia ligase)	42982
		prep2	21;22, 21-22	
		prep3	25, 25-26	
10			OTHER ENZYMES	
	196		serine/threonine kinase 16	34843
		prep1	18,	
		prep2	15, 14-16	
		prep3	19,	
	197		tripeptidylpeptidase II	139688
		prep1	51,	
		prep2	44, 44-46	
		prep3	48, 47-48	
	198		carboxypeptidase D	153546
		prep1	58, 57-58	
		prep2	52, 52-53	
		prep3	54, 53-54	
	199		ATP citrate lyase	121471
		prep1	48, 48-49	
		prep2	42, 42-43	
		prep3	45,	
	200		dipeptidyl-peptidase IV	91610
		prep1	46;48, 46-48	
		prep2	41, 30-41	
		prep3	44, 33-44	
	201		fatty acid Coenzyme A ligase, long chain 2	79155
		prep1	39, 38-40	
		prep2	33, 32-35,	
		prep3	37, 36-37	
	202		enoyl-Coenzyme A, hydratase	79179
		prep1	40, 39-40	
		prep2	34, 33-34	
		prep3	37,	

SUPPLEMENTAL TABLE

specific peptides	shared peptides	NCBI GIs				
8	0	121376	228136	8393456		
2	0					
6	0					
7	0	27465615	4106342	13124556	26327983	4106342
1	0					
5	0					
1	0					
51	0	13592121	6678419			
20	0					
19	0					
12	0					
36	0	6978699	6681001	9652339		
14	0					
13	0					
9	0					
39	0	8392839	17028103	18204829	21754275	28514402
26	0					
3	0					
10	0					
15	0	111948	6978773	109788	111948	6753674
2	0					
4	0					
9	0					
85	0	25742739	729927	31560705		
17	0					
52	0					
16	0					
33	0	19424318				
9	0					
9	0					
15	0					

group	protein		group name protein name peak gel band, range of gel bands	mass
	203		hydroxyacyl-Coenzyme A dehydrogenase/3-ketoacyl-Coenzyme A hiolase	83202
		prep1	39,	
		prep2	34,	
		prep3	37,	
	204		acyl-Coenzyme A oxidase 2, branched chain	77548
		prep1	38,	
		prep2	32, 32-33	
		prep3	36,35-36	
	205		acyl-Coenzyme A oxidase 3, pristanoyl	79080
		prep1	37, 37-38	
		prep2	32,	
		prep3	35;36, 35-36	
	206		Amine oxidase [flavin-containing] A (Monoamine oxidase) (MAO-A)	60097
		prep1	35,	
		prep2	29,	
		prep3	32,	
	207		aldehyde dehydrogenase family 3; aldehyde dehydrogenase 4	54503
		prep1	34,	
		prep2	27, 27-29	
		prep3	30, 30-31	
	208		choline dehydrogenase	49193
		prep1	34,	
		prep2	29,	
		prep3	32,	
	209		flavin containing monooxygenase	60530
		prep1	33,	
		prep2	29,	
		prep3	32,	
	210		Catalase	60013
		prep1	33,	
		prep2	29,	
		prep3	32, 32-33	
	211		formiminotransferase cyclodeaminase	59504
		prep1	32,	
		prep2	27,	
		prep3	30;31, 30-31	

SUPPLEMENTAL TABLE

specific peptides	shared peptides	NCBI GIs				
12	0	18677763	20824845			
6	0					
5	0					
1	0					
26	0	21955130				
9	0					
10	0					
7	0					
15	0	16758056	26324764	28703869		
7	0					
6	0					
2	0					
6	0	113979	220810	383383	8170739	27707494
1	0					
4	0					
1	0					
22	0	6680678	27679356	13929028	12698456	12698457
3	0					
13	0					
6	0					
5	0	1154950	27667200			
1	0					
3	0					
1	0					
7	0	21426797				
1	0					
1	0					
5	0					
40	0	115704	6978607	15004258	26344712	
1	0					
2	0					
37	0					
10	0	16758338	18252784			
2	0					
4	0					
4	0					

group	protein		group name protein name peak gel band, range of gel bands	mass
	212		ATP synthase alpha chain, mitochondrial precursor	58904
		prep1	31,	
		prep2	27, 26-27,	
		prep3	30,	
	213		Dihydrolipoamide succinyltransferase	47668
		prep1	31,	
		prep2	26,	
		prep3	30,	
	214		phosphoribosylaminoimidazole carboxylase	47807
		prep1	27,	
		prep2	22,	
		prep3	26,	
	215		paraoxonase	38660
		prep1	27,	
		prep2	22, 20-22	
		prep3	23;25, 23-25	
	216		Arginase 1 (Liver-type arginase)	35122
		prep1	25;26, 25-26	
		prep2	20,	
		prep3	24, 23-24	
	217		fumarylacetoacetase (AA 1-349)	46231
		prep1	26,	
		prep2	21,	
		prep3	25,	
	218		alcohol dehydrogenase	40532
		prep1	25, 23-25	
		prep2	19;20, 19-20	
		prep3	24;23, 23-24	
	219		phosphoribosyl pyrophosphate synthetase-associated protein 2	41299
		prep1	25,	
		prep2	20,	
		prep3	23;24, 23-24	
	220		phosphoribosylpyrophosphate synthetase-associated protein	39753
		prep1	24,	
		prep2	19,	
		prep3	23,	

SUPPLEMENTAL TABLE

specific peptides	shared peptides	NCBI GIs				
30	0	114523	6729934			
17	0					
10	0					
3	0					
5	0	266684	21313536	22775474	27667044	643589
1	0					
1	0					
3	0					
8	0	18266726	13385434	15214218	5453539	27671151
4	0					
1	0					
3	0					
10	0	1945471	2829441	27708566		
1	0					
5	0					
4	0					
16	0	114146	3212816	8392920	13786702	14488500
4	0					
5	0					
7	0					
7	0	4557587	31291	8393349		
1	0					
3	0					
3	0					
15	0	91930	113392	1168349	31982384	28404
6	0					
4	0					
5	0					
6	1	4506133	16923984	20837615	21450169	26346208
1	0 f					
1	0					
4	1					
8	1	11968140	23623796	24418495	26346302	
2	0 f					
1	0					
5	1					

group	protein		group name protein name peak gel band, range of gel bands	mass
	221		*hydroxysteroid 11-beta dehydrogenase 1*	31977
		prep1	20,	
		prep2	16,	
		prep3	20, 19-20	
	222		3-hydroxybutyrate dehydrogenase	38721
		prep1	17, 17-18	
		prep2	14;15, 14-15	
		prep3	18;19, 18-19	
	223		Retinol dehydrogenase type I or III	35982
		prep1	16;17, 16-17	
		prep2	15, 12-15	
		prep3	18, 17-19	
	224		RETINOL DEHYDROGENASE TYPE II (RODH II)	35973
		prep1	17,	
		prep2	13;14, 12-14	
		prep3	18, 18-19	
	225		Epoxide hydrolase 1 (Microsomal epoxide hydrolase)	52719
		prep1	28,	
		prep2	23, 23-24	
		prep3	27,	
	226		arginosuccinate synthetase; arginosuccinate synthetase 1	46752
		prep1	27,	
		prep2	22,	
		prep3	26,	
	227		bile acid CoA ligase	77129
		prep2	32,	
		prep3	35,	
	228		mannosidase 1, alpha	73458
		prep2	32, 31-32	
		prep3	35,	
	229		Dihydrolipoamide acetyltransferase	59126
		prep2	31,	
		prep3	34, 34-35	

SUPPLEMENTAL TABLE

specific peptides	shared peptides	NCBI GIs				
10	0	8393570	23830928	1583519	1706408	23477364
1	0					
5	0					
4	0					
12	0	16758902	26345604	20071589	31982169	
4	0					
6	0					
2	0					
19	8	1710629	1710631	31377477	27545384	27680727
2	4 g					
1	1					
16	3					
23	8	1710630	27671254	27671310		
1	4 g					
20	1					
2	3					
21	0	123928	6978813			
5	0					
12	0					
4	0					
11	0	25453414	20860648			
2	0					
3	0					
6	0					
10	0	13162326				
7	0					
3	0					
8	0	6678788	27705330	631290	1083160	1170852
5	0					
3	0					
6	0	266685	220838	2117706	27681529	27720121
3	0					
3	0					

group	protein		group name protein name peak gel band, range of gel bands	mass
	230		fatty acid amide hydrolase	64228
		prep2	29, 28-29	
		prep3	31;32, 31-32	
	231		Protein disulfide isomerase precursor (PDI)	57315
		prep2	28, 27-28	
		prep3	31,	
	232		carboxylesterase (EC 3.1.1.1) ES-10 precursor, microsoma	62376
		prep2	28,	
		prep3	31,	
	233		Liver carboxylesterase 4 precursor (Carboxyesterase ES-4)	62634
		prep2	28,	
		prep3	32, 31-32	
	234		UDP-glucuronosyltransferase 1 family, member 1	60422
		prep2	27,	
		prep3	30,	
	235		flavin-containing monooxygenase 1	60427
		prep2	27,	
		prep3	30,	
	236		L-gulonolactone oxidase (EC 1.1.3.8)	51295
		prep2	24,	
		prep3	28, 27-28	
	237		glucuronosyltransferase (EC 2.4.1.17) 3 precursor	61131
		prep2	24,	
		prep3	28, 298-30	
	238		betaine-homocysteine methyltransferase	45404
		prep2	22,	
		prep3	26, 25-26	
	239		hydroxy-delta-5-steroid dehydrogenase	42465
		prep2	21,	
		prep3	25, 25-26	
	240		Peptidyl-prolyl cis-trans isomerase B precursor (PPIase) (Cyclophilin B)	22785
		prep2	7, 6-7	
		prep3	9, 10-9	

SUPPLEMENTAL TABLE

specific peptides	shared peptides	NCBI GIs				
5	0	13162304	27573966			
3	0					
2	0					
24	0	129731	202549	6981324	129729	129729
15	0					
9	0					
14	0	92053	119596	1162964	420265	807109
7	0					
7	0					
11	0	2494386				
4	0					
7	0					
6	0	28849913				
3	0					
7	0	6978847				
1	0					
6	0					
6	0	625202	11560006			
2	0					
4	0					
9	0	92287	31543923	136733	27677480	57449
2	0					
7	0					
8	0	13540663	7709990	28525627		
4	0					
4	0					
13	0	6981050				
6	0					
7	0					
6	0	118090	118092	181250	2118329	2143900
3	0					
3	0					

group	protein	group name protein name peak gel band, range of gel bands	mass
	241	fatty acid Coenzyme A ligase, long chain 5	77211
	prep2	32,	
	prep3	36,	
	242	cystathionine gamma-lyase	44236
	prep2	21,	
	prep3	24, 24-25	
	243	UDP-N-acetylglucosamine-2-epimerase/N-acetylmannosamine kinase	80193
	prep1	39,	
	prep2	33,	
	244	multifunctional protein 2	79654
	prep1	41,	
	prep2	35,	
	prep3	38,	
	245	Fms interacting protein / serum/glucocorticoid regulated kinase 2	79347
	prep1	41,	
	prep2	36, 35-36	
	prep3	38,	
	246	Mammalian 2-Cys Peroxiredoxin, Hbp23	22250
	prep1	12,	
	prep2	9,	
	prep3	12,	
	247	electron transffering flavoprotein, dehydrogenase	68903
	prep1	35, 35-36	
	prep2	30,	
	248	methylenetetrahydrofolate dehydrogenase (NADP)	101662
	prep2	40,	
	prep3	42, 42-43	
	249	UDP glycosyltransferase 2 family, polypeptide B	61459
	prep2	25,	
	prep3	29,	

SUPPLEMENTAL TABLE

specific peptides	shared peptides	NCBI GIs				
14	0	16758398	7437838			
4	0					
10	0					
7	0	13699175	8393215			
3	0					
4	0					
5	0	4885285	16758602	25048862	4456673	32352100
2	0					
3	0					
6	0	1620451	2492741	4504505	7514017	13242303
1	0					
4	0					
1	0					
9	0	24980875	27369587	27696878		
5	0					
3	0					
9	0	6435547	6754976	6942233	12846314	
2	0					
4	0					
3	0					
7	0	15214778	21313290	26344475	27691916	
5	0					
2	0					
12	0	111430	26335437	11968082	19850913	20270275
1	0					
11	0					
7	0	13928718	57453			
5	0					
2	0					

group	protein		group name protein name peak gel band, range of gel bands	mass
11			COATOMER	
	250		Coatomer gamma subunit (Gamma-coat protein) (Gamma-COP)	98635
		prep1	43;44, 43-44	
		prep2	37;38, 37-38	
		prep3	40, 39-40	
	251		coatomer protein complex, subunit beta; beta coat protein	108214
		prep1	44,	
		prep3	41, 41-42	
	252		Coatomer delta subunit (Delta-coat protein) (Delta-COP)	57694
		prep1	35,	
		prep2	30,	
		prep3	33,	
	253		Coatomer alpha subunit (Alpha-coat protein)	140832
		prep2	46,	
		prep3	48, 47-48	
	254		Cop-coated vesicle membrane protein p24 precursor	22289
		prep2	8,	
		prep3	11, 11-12	
	255		beta prime COP	103342
		prep2	39,	
		prep3	41, 40-41	
12			ENDOPLASMIC RETICULUM	
	256		ribophorin II; ribophorin	66375
		prep2	30,	
		prep3	33,	
	257		BIP ER dnaK-type molecular chaperone HSPA5 precursor	72185
		prep1	40,	
		prep2	34,	
		prep3	27, 37-38	
	258		thioredoxin domain containing 4; endoplasmic reticulum resident protein	47222
		prep2	23,	
		prep3	27,	

specific peptides	shared peptides	NCBI GIs				
9	0	1706000	11559929	6912320	8567340	14198159
3	0					
2	0					
4	0					
19	0	7705369	12644310	15426055	18158449	
1	0					
18	0					
17	0	1705999	11863154	22122433		
3	0					
1	0					
13	0					
14	0	23512328	23620060	23958509	31981828	
3	0					
11	0					
8	0	1352660	5803149	9790015	13929014	26354785
3	0					
5	0					
16	0	11120716	20893607	486784	4758032	27805865
4	0					
12	0					
6	0	9790203	12836555	14714733	13928974	
3	0					
3	0					
18	0	87528	109893	121570	627823	1304157
1	0					
11	0					
6	0					
5	0	19072792	3043670			
3	0					
2	0					

group	protein		group name protein name peak gel band, range of gel bands	mass
	259		protein disulfide-isomerase (EC 5.3.4.1) ER60 precursor	57044
		prep1	34,	
		prep2	28,	
		prep3	31,	
13			CHAPERON PROTEIN FOLDING	
	260		chaperonin subunit 5 (epsilon)	60654
		prep2	29,	
		prep3	32, 31	
	261		chaperonin	58598
		prep2	28,	
		prep3	31,	
	262		chaperonin subunit 6a (zeta); chaperonin containing TCP-1	58424
		prep2	29;30, 29-30	
		prep3	33;32, 32-33	
	263		matricin	61021
		prep2	30,	
		prep3	33,	
	264		T-complex protein 1, alpha subunit (TCP-1-alpha)	60814
		prep1	35,	
		prep2	30,	
		prep3	33,	
	265		T-complex protein 1, theta subunit (TCP-1-theta)	60008
		prep1	33,	
		prep2	29,	
		prep3	32,	
	266		chaperonin subunit 2 (beta)	57753
		prep1	31,	
		prep2	27,	
		prep3	30,	
	267		T-complex protein 1, eta subunit (TCP-1-eta)	60127
		prep2	28,	
		prep3	31,	

SUPPLEMENTAL TABLE

specific peptides	shared peptides	*NCBI GIs*				
31	0	91897	1083311	1352384	1583929	545439
1	0					
18	0					
12	0					
5	0	6671702	603955	12804225	14495685	24307939
1	0					
4	0					
6	0	460317	2559008	6753322	13358930	33414505
2	0					
4	0					
9	0	6753324	184462	4502643	6094438	14517632
2	0					
7	0					
6	0	631730	2136253	6753320	27692905	31542292
2	0					
4	0					
9	0	135536	135538	201725	228954	1729865
1	0					
5	0					
3	0					
11	0	1174621	5295992	31560613		
2	0					
3	0					
6	0					
6	0	6671700	7670405	22654291	26376306	
1	0					
2	0					
3	0					
8	0	549060	27712178	31982472		
4	0					
4	0					

group	protein		group name protein name peak gel band, range of gel bands	mass
14			OTHERS	
	268		ubiquitin	8446
		prep1	24;35;42;64, 24-64	
		prep2	37;28, 23-57	
		prep3	24-56	
	269		Alpha-1-inhibitor III precursor	165038
		prep1	58,	
		prep2	53,	
		prep3	54, 54-55	
	270		arsenite-resistance protein	25823
		prep1	50,	
		prep3	46, 33-46	
	271		Ig mu chain C region	38189
		prep1	39,	
		prep2	33;34;35, 33-35	
		prep3	38, 37-38	
	272		*hemopexin*	52000
		prep1	38,	
		prep2	32, 32-33	
		prep3	36, 35-37	
	273		albumin	70670
		prep1	36, 33-38	
		prep2	31, 30-32	
		prep3	35, 33-36	
	274		Serum albumin precursor	70700
		prep1	35, 33-37	
		prep2	30;31;32, 30-32	
		prep3	35, 33-36	
	275		Transthyretin precursor (Prealbumin) (TBPA)	15824
		prep1	26,	
		prep3	25,	
	276		complement component 3	187828
		prep1	37, 36-37	
		prep2	31;50, 31-50	
		prep3	34;35;45, 34-45	

SUPPLEMENTAL TABLE

specific peptides	shared peptides	NCBI GIs				
30	0	70637	91870	91871	136670	1050930
4	0					
15	0					
11	0					
11	0	112893	202577	12831225		
1	0					
2	0					
8	0					
5	0	1127863	4336349	12652667	13492031	13492032
1	0					
4	0					
7	0	111977	70047	1346606	27717429	
1	0					
3	0					
3	0					
31	0	16758014	1881768	22022646	23956086	
4	0					
8	0					
19	0					
75	86	19705431				
20	23 h					
29	29					
26	34					
12	86	5915682	26340966	26341396		
5	23 h					
3	29					
4	34					
5	0	136467	3212532	6981684	20663827	
1	0					
4	0					
8	0	8393024	1352102	23956044	28175786	
3	0					
2	0					
3	0					

group	protein		group name protein name peak gel band, range of gel bands	*mass*
	277		serine proteinase inhibitor 1	45881
		prep1	36, 35-36	
		prep2	30, 27-31	
		prep3	33, 31-34	
	278		Tum-P91A antigen	60726
		prep1	35,	
		prep3	32,	
	279		ADP-ribosylation-like factor 6 interacting protein 2	65114
		prep1	35, 33-35	
		prep2	29, 29-30	
		prep3	32;33, 32-33	
	280		fetuin beta	42361
		prep1	32;34, 32-34	
		prep2	28, 27-28	
		prep3	31,	
	281		lectin, mannose-binding, 1	58206
		prep1	34,	
		prep2	28, 28-29	
		prep3	31, 31-32	
	282		ALPHA-1-ANTIPROTEINASE PRECURSOR (ALPHA-1-ANTITRYPSIN)	46278
		prep1	32,	
		prep2	27, 27-28	
		prep3	30, 31-30	
	283		Cathepsin L precursor (Major excreted protein) (MEP) (Cyclic protein-2)	38206
		prep1	22;23, 21-23	
		prep3	22,	
	284		preprohaptoglobin	30428
		prep1	22, 3-23	
		prep2	18, 16-18	
		prep3	22, 4-22	
	285		*major beta-hemoglobin*	16097
		prep1	3,2-3	
		prep3	4, 3-4	

SUPPLEMENTAL TABLE

specific peptides	shared peptides	NCBI GIs				
23	0	57233	92335	92880	266407	6981576
7	0					
7	0					
9	0					
6	0	2137840	2656092	15126760	19705424	19856169
5	0					
1	0					
25	0	16041114	22476866	31565344	11641303	22476865
3	0					
7	0					
15	0					
7	0	17865327	10947006	26331904		
2	0					
3	0					
2	0					
21	0	16758758	21312570			
1	0					
8	0					
12	0					
12	0	112889	203063	11968100		
2	0					
6	0					
4	0					
6	0	115743	6978723	67650	246148	
5	0					
1	0					
21	0	204657	484201	6016254	123513	33086640
4	0					
5	0					
12	0					
18	0	204570	546056	984679	17985949	
5	0					
13	0					

group	protein		group name protein name peak gel band, range of gel bands	mass
	286		fatty acid-binding protein, hepatic	14249
		prep1	2, 2-3	
		prep2	2,	
		prep3	4;3, 3-4	
	287		hemoglobin alpha chain	15446
		prep1	2,	
		prep3	4,	
	288		Aa1064	537740
		prep2	55, 54-55	
		prep3	56,	
	289		fibrinogen, B beta polypeptide	54828
		prep2	28,	
		prep3	31,	
	290		DnaJ protein homolog	45590
		prep2	23,	
		prep3	27,	
	291		RER1 protein	23057
		prep2	8,	
		prep3	11, 11-12	
	292		alpha-2u globulin precursor()	20454
		prep2	5, 5-6	
		prep3	8,	
	293		similar to Microsomal triglyceride transfer protein, large subunit precursor	130787
		prep2	37;38, 37-38	
		prep3	40,48,	
	294		fibroblast growth factor 2-interacting factor	49800
		prep2	30,	
		prep3	32, 22-33	
	295		ATP-binding cassette, sub-family A (ABC1), member 6	184864
		prep2	51,51-53	
		prep3	53, 54-58	
	296		ATP-binding cassette, sub-family A (ABC1), member 8a	185760
		prep2	52,51-52	
		prep3	53,	

SUPPLEMENTAL TABLE

specific peptides	shared peptides	NCBI GIs				
20	0	71857	204074	2392417	6978825	
4	0					
8	0					
8	0					
15	0	1304381	6981010	552374		
2	0					
13	0					
14	0	32492562				
7	0					
7	0					
6	0	27692042	29789106	32527707		
2	0					
4	0					
9	0	219588	4504511	6680297	20830104	219588
4	0					
5	0					
5	0	6226763	7688699	13385882	19923787	
2	0					
3	0					
9	0	204261	22219450	8307686	27714645	204264
7	0					
2	0					
6	0	27697569				
2	0					
4	0					
16	0	12656083	5729730	6671567	20839855	2623761
2	0					
14	0					
7	2	22267462				
3	0 i					
4	2					
6	0	23346593	27690222			
3	0					
3	0					

group	protein		group name protein name peak gel band, range of gel bands	mass
	297		MAL2A	36044
		prep1	10;14, 10-14	
		prep2	9,	
		prep3	10;15, 10-15	
	298		stromal membrane-associated protein SMAP1A	48313
		prep2	25, 23-28	
		prep3	29, 28-29	
15			ATPases	
	299		bB206I21.1 (ATPase, Class VI, type 11C)	95006
		prep1	48,48-50	
		prep2	43, 41-56	
		prep3	46, 45-47	
	300		H+-exporting ATPase	31814
		prep1	23;24, 23-24	
		prep2	19,	
		prep3	22;23, 22-23	
	301		Transitional endoplasmic reticulum ATPase (TER ATPase)	89936
		prep1	44,	
		prep2	38,	
		prep3	40,	
	302		H+-transporting two-sector ATPase (EC 3.6.3.14) beta chain	50738
		prep1	30, 30-31	
		prep2	26, 25-26	
	303		ATP synthase, H+ transporting, mitochondrial F0 complex, subunit b	28965
		prep1	13, 12-13	
		prep2	10,	
	304		ATPase 7B	122242
		prep1	65, 55-66	
		prep2	46,	
		prep3	48;49, 48-49	

SUPPLEMENTAL TABLE

specific peptides	shared peptides	NCBI GIs				
5	0	32693285	27718963			
2	0					
1	0					
2	0					
12	0	16303736	10435055	13561010	21264558	23273590
9	0					
3	0					
38	0	27709974	17644260	28528317	30315929	
11	0					
11	0					
16	0					
15	0	89602	542837	3955100	15029719	19913432
4	0					
3	0					
8	0					
6	0	400712	6005942	17865351	26350783	1174636
1	0					
4	0					
1	0					
24	0	92350	114562	1374715	1827812	3660251
16	0					
8	0					
5	0	19705465	87611	114617	13543618	20875157
3	0					
2	0					
8	0	6680758	6006291	6006293	6978561	631354
4	0					
2	0					
2	0					

group	protein		group name protein name peak gel band, range of gel bands	mass
16			CYTOCHROME	
	305		Cytochrome P450 2D1 (CYPIID1) (P450-DB1) (P450-CMF1A)	57595
		prep1	30, 29-31	
		prep2	24;25, 24-25	
		prep3	29, 28-29	
	306		cytochrome P450, subfamily IID3	57061
		prep1	30, 30-31	
		prep2	25,	
		prep3	29,	
	307		Cytochrome P450 2D2 (CYPIID2) (P450-DB2) (P450-CMF2)	56876
		prep1	30, 30-31	
		prep2	25, 24-26	
		prep3	29, 28-29	
	308		cytochrome P450 2D9-like	56988
		prep1	30,	
		prep2	25,	
	309		Cytochrome P450 2C11 (CYPIIC11) (P-450(M-1)) (P450H) (P450-UT-A)	57658
		prep1	30,	
		prep2	25,	
		prep3	29,	
	310		Cytochrome P450 2C6 (CYPIIC6) (P450 PB1) (PTF2)	56708
		prep1	30,	
		prep2	25,	
		prep3	29,30	
	311		Cytochrome P450 4A2 precursor (CYPIVA2)	58274
		prep1	30,	
		prep2	26,	
		prep3	29,	
	312		Cytochrome P450 2C13, male-specific (CYPIIC13) (P450-G) (UT-5)	56337
		prep1	29,	
		prep2	24,	
		prep3	28,	

specific peptides	shared peptides	NCBI GIs				
62	20	117241	203803	203807	23463315	27545374
10	3 j					
23	8					
29	9					
14	17	27465519	92147			
2	4 j					
4	8					
8	5					
40	21	117242	6978747	92145		
7	3 j					
16	9					
17	9					
3	3	21728384				
1	0 j					
2	3					
24	0	117228	203695	226036		
2	0					
13	0					
9	0					
13	0	117223	203875	27684019		
1	0					
5	0					
7	0					
8	0	117164	27715769	27715855	28461155	27715857
1	0					
2	0					
5	0					
14	0	117230	2117406	25453406		
1	0					
7	0					
6	0					

group	protein		group name protein name peak gel band, range of gel bands	mass
	313		cytochrome b5 [mice, D2, liver microsomes]	11203
		prep1	6,	
		prep2	4;5, 4-5	
		prep3	7, 6-7	
	314		NADPH-cytochrome P-450 oxidoreductase	77285
		prep1	40,	
		prep2	34,	
		prep3	38, 37-38	
	315		cytochrome P450, family 4, subfamily a, polypeptide 3	58530
		prep1	31,	
		prep3	30,	
	316		cytochrome P450 2B3	37388
		prep2	25, 24-25	
		prep3	28, 29	
	317		Cytochrome P450 2E1 (CYPIIE1) (P450-J) (P450RLM6)	56990
		prep2	25,	
		prep3	29,	
	318		Cytochrome P450 2C23 (CYPIIC23) (Arachidonic acid epoxygenase)	57024
		prep2	25,	
		prep3	30,	
	319		cytochrome P450 2C7	56777
		prep2	25,	
		prep3	29,	
	320		cytochrome P450, subfamily 2A, polypeptide 1; Cytochrome P450 IIA2	56480
		prep2	24,	
		prep3	27;28, 27-28	
	321		cytochrome-b5 reductase (EC 1.6.2.2), microsomal form	34347
		prep2	15, 15-16	
		prep3	19,	
	322		Cytochrome P450 2C22 (CYPIIC22) (P450 MD) (P450 P49)	56690
		prep2	24,	
		prep3	28,	

SUPPLEMENTAL TABLE

specific peptides	shared peptides	NCBI GIs				
11	0	251978	2098349	2914179	2554670	3660010
3	0					
4	0					
4	0					
17	0	205660	3318958	13928780	15826744	15826748
2	0					
8	0					
7	0					
7	0	28461155	27715769			
4	0					
3	0					
10	0	562164	27676490			
7	0					
3	0					
12	0	1352193	13928734	259785		
7	0					
5	0					
10	0	6166042				
5	0					
5	0					
6	0	482947	8393233			
4	0					
2	0					
8	0	6978741				
4	0					
4	0					
7	0	1070444	20302049			
6	0					
1	0					
6	0	117236	19924039			
2	0					
4	0					

group	protein		group name protein name peak gel band, range of gel bands	mass
17			GLUTATHIONE TRANSFERASE	
	323		glutathione S-transferase Yb-1 subunit (EC 2.5.1.18)	26127
		prep1	14,	
		prep2	11, 10-11	
		prep3	14,	
	324		glutathione transferase (EC 2.5.1.18) class alpha chain Ya1	25737
		prep1	13,	
		prep2	10,	
		prep3	14, 13-14	
	325		microsomal glutathione S-transferase 1	17517
		prep2	4,	
		prep3	6, 5-6	
18			NOVEL	
	326		NECAP 1	37228
		prep1	27,	
		prep2	19, 19-20	
		prep3	24;25, 24-25	
	327		enthoprotin; epsin 4	68273
		prep1	40;39, 22-42	
		prep2	34, 36-36	
		prep3	37, 28-39	
	328		RIKEN cDNA 6030446I19 gene	112066
		prep1	50,	
		prep2	44;45, 44-45	
		prep3	46,	
	329		RIKEN cDNA 5730596K20, homology to ARF-Like 6 interacting protein 2	60993
		prep2	27;28, 27-28	
		prep3	31,	
	330		similar to hypothetical protein MGC12103 [Homo sapiens]	46194
		prep2	27,	
		prep3	31,	

specific peptides	shared peptides	NCBI GIs				
12	0	204503	442967	1943431	1943433	90534
8	0					
3	0					
1	0					
9	0	66611	121712	6680119	7110611	11514499
4	0					
2	0					
3	0					
7	0	19705453				
3	0					
4	0					
8	0	37945074	27229051	27713302	15079260	
1	0					
5	0					
2	0					
319	0	7661968	13278582	20345123	21751443	26006105
116	0					
112	0					
91	0					
7	0	31542027	13449265	24980923		
1	0					
2	0					
4	0					
12	0	16877810	26326645	31559920	10435296	13477255
7	0					
5	0					
5	0	27679620	27532965			
1	0					
4	0					

group	protein		group name protein name peak gel band, range of gel bands	mass
	331		similar to hypothetical protein KIAA0678 (RME-8)	306705
		prep1	58,	
		prep2	54,	
		prep3	55, 55-56	
	332		KIAA0255 gene product	73235
		prep1	34,	
		prep2	28, 27-28	
		prep3	31,	
	333		KIAA0183	116963
		prep1	50,	
		prep2	44;45;, 37-45	
	334		similar to KIAA1414 protein	226839
		prep1	58,	
		prep3	55,	
	335		similar to mKIAA0219 protein	316133
		prep2	56,	
		prep3	57,	
	336		FENS-1	47904
		prep2	21,	
		prep3	25, 25-26	
	337		unknown [Homo sapiens]	24209
		prep1	12, 10-14	
		prep2	9;10, 9-10	
		prep3	13, 12-14	
	338		hypothetical protein D10Wsu52e	55631
		prep2	28, 27-28	
		prep3	31,	
	339		similar to Protein transport protein Sec24C (SEC24-related protein C)	112455
		prep2	42;43, 42-43	
		prep3	45, 45-46	
	340		EH domain containing 4	60888
		prep1	35, 33-35	
		prep3	32, 32-33	

SUPPLEMENTAL TABLE

specific peptides	shared peptides	NCBI GIs				
59	0	27721389	26006199	28546047	26328693	26350527
5	0					
28	0					
26	0					
6	0	7662028	26352305	31542095	26339180	
1	0					
3	0					
2	0					
8	0	1136426	3005744	8922114	16307515	28524994
1	0					
7	0					
16	0	27478091	26348058			
13	0					
3	0					
6	0	27666086				
1	0					
5	0					
5	0	18482373	7243268	19484187	30795186	
1	0					
4	0					
17	0	3005742	12857585	12857927	18490304	20531765
7	0					
4	0					
6	0					
15	0	21703842	6841456	7657015	7688673	21703842
4	0					
11	0					
6	0	27673609	20072091	27722283	28477301	28916673
2	0					
4	0					
16	0	10181214	7212811	7657056	10181214	20302075
4	0					
12	0					

group	protein		group name protein name peak gel band, range of gel bands	mass
	341		similar to Vault poly(ADP-ribose) polymerase (VPARP)	126096
		prep1	60;58, 57-60	
		prep2	53,	
		prep3	55, 54-55	
	342		similar to ATP-binding cassette, sub-family A (ABC1), member 6	65888
		prep2	51, 51-54	
		prep3	53, 53-55	
	343		dendritic cell protein GA17	42946
		prep1	25,	
		prep2	20, 19-20	
		prep3	24, 23-25	
	344		similar to deleted in polyposis 1-like 1	39229
		prep1	7;6, 6-7	
		prep2	4;5, 4-5	
		prep3	8,	
	345		macrophage expressed gene 1	74478
		prep2	38;39, 38-39	
		prep3	40, 40-41	
	346		vacuole 14 protein; Vac14 protein; hydin	89095
		prep1	43,	
		prep2	37,	

SUPPLEMENTAL TABLE

specific peptides	shared peptides	NCBI GIs				
28	0	28479540				
4	0					
8	0					
16	0					
16	2	27690422	34875258			
9	0 i					
7	2					
21	0	21703762	23397429	27702767	3152660	12751096
1	0					
6	0					
14	0					
7	0	27717621				
4	0					
2	0					
1	0					
5	0	12018298	2137564	18676680	20482397	
2	0					
3	0					
5	0	29293817	26327751	26338430	31542488	
1	0					
4	0					

ANNEXE 2

ETHIC CERTIFICATES

5. RESEARCH PERSONNEL: (attach additional sheets if preferred)

Name	Department	Job Title/Classification	Trained in the safe use of biological safety cabinets within the last 3 years? If yes, indicate training date.
Peter McPherson	Neurology & Neurosurgery	PI	No
Lyne Bourbonniere	Neurology & Neurosurgery	Technician	No
Jacynthe Philie	Neurology & Neurosurgery	Technician	No
Martine Girard	Neurology & Neurosurgery	Graduate Student	No
Patrick Allaire	Neurology & Neurosurgery	Graduate Student	No
Brigitte Ritter	Neurology & Neurosurgery	Research Associate	No
Francois Blondeau	Neurology & Neurosurgery	Post-doctoral fellow	No
Jonathon Burman	Neurology & Neurosurgery	Graduate Student	No
Andrea Marat	Neurology & Neurosurgery	Graduate Student	No

6. Briefly describe:

i) the biohazardous material involved (e.g. bacteria, viruses, human tissues, toxins of biological origin) & designated biosafety risk group

Containement level 1: We are using complementary DNA fragments and plasmids and cell lines that express specific human and rat ...es. We are also maintaining cell culture lines of non-human origin (rat). Manipulations of DNA are performed in a designated laboratory area which is properly cleaned after use. The DNA samples are kept in a specific freezer. The cell lines are cultured in a tissue culture hood and grown in a tissue culture incubator.
- Containment level 2: In addition to our previous protocols at a containment level of 1, we will now begin to produce and use adenovirus. The adenoviruses will encode for rat and frog proteins that function in endocytosis. The adenovirus does not replicate. It is used routinely by many laboratories at McGill University

ii) the procedures involving biohazards

- The plasmids contain gene fragments for sequencing on expression of fusion proteins in bacteria.
- Cell lines (PC-12, A431, COS) are used for biochemical studies or are transfected with plasmid to express a specific rat protein.
- Adenovirus will be produced in 239-A cells in culture. The adenovirus will be used to infect mammalian cells in culture

iii) the protocol for decontaminating spills

- All laboratory personnel are aware that there is no eating, drinking, or smoking in the laboratory. The laboratory is equipped with a fume hood and two sinks. Research personnel will wash their hands following manipulation of biohazards.
- In the event of a spill, any contaminated surface or tool will be identified and decontaminated with bleach.
- In case of a large spill, the McGill Safety Office will be contacted.
- All manipulations involving adenovirus will be performed in a LabConco Purifier Class II biosafety cabinet. Samples will only be removed from the safety cabinet in sealed containers. Liquid waste will be treated with mild bleach before disposal. Dry waste will be sealed in a biohazard bag in the safety cabinet and will then be placed in biohazard boxes for disposal. All surfaces in contact with the adenovirus will be decontaminated with bleach or ETOH

7. Does the protocol present conditions (e.g. handling of large volumes or high concentrations of pathogens) that could increase the hazards?

No

8. Do the specific procedures to be employed involving genetically engineered organisms have a history of safe use?

Yes

9. What precautions will be taken to reduce production of infectious droplets and aerosols?

N/A

10. Will the biohazardous materials in this project expose members of the research team to any risks that might require special training, vaccination or other protective measures? If yes, please explain.

No

11. Will this project produce combined hazardous waste – i.e. radioactive biohazardous waste, biohazardous animal carcasses contaminated with toxic chemicals, etc.? If yes, please explain how disposal will be handled.

No

12. List the biological safety cabinets to be used.

Building	Room No.	Manufacturer	Model No.	Serial No.	Date Certified
MNI	BT206A	Forma Scientific	Purifier Class IIA/B3	19727-302	August 21, 2006

Include here ALL procedures described in the original protocol. New and changed procedures in CAPS *(was section 10a in main protocol); Please only attach SOPs related to new and changed procedures to this renewal form.*

7. Endpoints

a) For B and C level of invasiveness,

The procedures are the same as the original protocol: YES☒ NO☐

IF NO, supply new endpoints that are different from the original protocol:

Experimental endpoints:

Clinical endpoints:

b) For D level of invasiveness,

Include here ALL endpoints, including the ones described in the original protocol as well as new and changed endpoints in CAPS:

Experimental endpoints:

Clinical endpoints:

8. Hazards (check here if none are used: ☒)

a) Are the hazards different from original protocol? (infectious, radioactive, toxic, carcinogen, tumours)

YES☐ NO☐ if yes, supply details (material, risks, precautions):

b) Have the cell lines been tested for human and animal pathogens? YES:☐ NO:☐ None used:☒

9. Description of Animals to be used in the coming year (only):

Quality Control Assurance: To prevent introduction of infectious diseases into animal facilities, a health status report or veterinary inspection certificate may be required prior to receiving animals from all non-commercial sources or from commercial sources whose animal health status is unknown or questionable. Quarantine and further testing may be required for these animals. *If more than 6 columns are needed, please attach another page*

	Sp/strain 1	Sp/strain 2	Sp/strain 3	Sp/strain 4	Sp/strain 5	Sp/strain 6
Species	Rat	Timed pregnant rat	Mice			
Supplier/Source	Charles River	Charles River	Charles River			
Strain	Sprague-Dawley	Sprague-Dawley	CD1			
Sex	M/F	F	M/F			

Age/Wt	150g	300-400g	30-50g			
# To be purchased	480	50	10			
# Produced by in-house breeding	0	0	0			
# Other (e.g. field studies)	0	0	0			
TOTAL# /YEAR	**480**	**50**	**10**			

10. Explanation of Animal Numbers:

BASED ON THE EXPERIMENTAL OBJECTIVES OF THE PROJECT, describe the number of animals required for one year. Include information on experimental and control groups, # per group, and failure rates.

For breeding, specify how many adults are used, number of offspring produced, and how many offspring are used in experimental procedures. The arithmetic explaining how the total of animals for each column in the table above is calculated should be made clear.

- Rats (SD) are used for protein purification. Each protein prep. requires 10 rats. For the studies in this grant, we do approximately 4 prep/month. This number of rats allows for one years worth of preps (10 rats x 4 prep/mth x 12 months = 480).

- Timed pregnant rats (SD) are used for neuronal cultures. Each pregnant rat yields enough material for one culture. We need to prepare 1 culture/week = 50 rats.
- Mice (CD1) are used for tissue extraction. Each mouse yields approximately 200mg of brain tissue. We require approximately 1g of tissue for RNA production. We anticipate isolating RNA 2 times/year (1000/200 x 2 = 10).

Submit to your local Facility Animal Care Committee. Please note that after two renewals, a full protocol needs to be submitted.

This approval does not imply that space will be made available. If a major increase of space needs is anticipated, please contact the appropriate animal facility manager.

4. RESEARCH PERSONNEL: (attach additional sheets if preferred)

Name	Department	Check appropriate classification				Fellow
		Investigator	Technician & Research Assistant	Student		
				Undergraduate	Graduate	
Peter McPherson	Neurology & Neurosurgery	X				
Elain DeHeuvel	Neurology & Neurosurgery		X			
Jacynthe Philie	Neurology & Neurosurgery		X			
Annie Angers	Neurology & Neurosurgery					X
Valerie Legendre-Guillemin	Neurology & Neurosurgery					X
Brigitte Ritter	Neurology & Neurosurgery					X
Francois Blondeau	Neurology & Neurosurgery					X
Sylwia Wasiak	Neurology & Neurosurgery				X	
Martine Girard	Neurology & Neurosurgery				X	
Patrick Allaire	Neurology & Neurosurgery				X	

5. EMERGENCY: Person(s) designated to handle emergencies

Name: Peter McPherson Phone No: work: 398-7355 home: 639-1249

Name: Elaine DeHeuvel Phone No: work: 398-6644 Ext: 00209 home: 630-4167

6. Briefly describe:

i) the biohazardous material involved (e.g. bacteria, viruses, human tissues) & designated biosafety risk group

- Containement level 1: We are using complementary DNA fragments and plasmids and cell lines that express specific human and rat genes. We are also maintaining cell culture lines of human and non-human origin. Manipulations of DNA are performed in a designated laboratory area which is properly cleaned after use. The DNA samples are kept in specific freezers. The cell lines are cultured in a tissue culture hood and grown in a tissue culture incubator.

- Containment level 2: In addition to our previous protocols at a containment level of 1, we will produce and use adenovirus. The adenoviruses will encode for proteins that function in endocytosis. The adenovirus does not replicate. It is used routinely by many laboratories at McGill University

ii) the procedures involving biohazards

- The plasmids contain gene fragments for sequencing an expression of fusion proteins in bacteria and mammalian cells.

- Cell lines (PC-12, A431, COS, HEF293, C6 glioma, HER14) are used for biochemical studies or are transfected with plasmid to express a specific rat protein.

- Adenovirus will be produced in 239-A cells in culture. The adenovirus will be used to infect mammalian cells in culture

iii) the protocol for decontaminating spills

- All laboratory personnel are aware that there is no eating, drinking, or smoking in the laboratory. The laboratory is equipped with a fume hood and two sinks. Research personnel will wash their hands following manipulation of biohazards.

- In the event of a spill, any contaminated surface or tool will be identified and decontaminated with bleach.

- In case of a large spill, the McGill Safety Office will be contacted.

- All manipulations involving adenovirus will be performed in a Forma Scientific Purifier Class II biosafety cabinet. Samples will only be removed from the safety cabinet in sealed containers. Liquid waste will be treated with mild bleach before disposal. Dry waste will be sealed in a biohazard bag in the safety cabinet and will then be placed in biohazard boxes for disposal. All surfaces in contact with the adenovirus will be decontaminated with bleach or ETOH

---

7. Does the protocol present conditions (e.g. handling of large volumes or high concentrations of pathogens) which could increase the hazards of the infectious agent(s)? NO

8. Do the specific procedures to be employed involving genetically engineered organisms have a history of safe use? YES

9. What precautions are being taken to reduce production of infectious droplets and aerosols? N/A

---

10. List the biological safety cabinets to be used.

Building	Room No.	Manufacturer	Model No.	Serial No.	Date Certified
Montreal Neurological Institute	BT206A	Forma Scientific	Purifier Class IIA/B3	19727-302	2002/07/10

☐ **Renewal requires submission of full Animal Use Protocol form**

Form version July 2007

3. Summary (in language that will be understood by members of the general public)
AIMS AND BENEFITS: Describe, in a short paragraph, the overall aim of the study and its potential benefit to human/animal health or to the advancement of scientific knowledge *(was section 5a in main protocol).*

We study proteins that are involved in neuronal communication. It is important to understand how these proteins function as neuronal communication forms the basis of important abilities such as the ability to learn and remember. Abnormal changes in neuronal communication can lead to diseases such as Alzheimer's disease and Schizophenia.
We study proteins that are involved in endocytosis. Alterations in this process are associated with many psychiatric and neurological diseases.

4. Has there been any animal care issues? YES ☐ NO ☒ **if yes, supply details:**

5. If creating genetically modified animals or new combinations of genetic modifications, complete and attach a *Phenotype Disclosure form.*
If mice expressing new phenotype have been produced, submit a *Phenotype Disclosure form.*
Blank forms at *http://www.mcgill.ca/researchoffice/compliance/animal/forms/*

6. Procedures

a) For B and C level of invasiveness,

The procedures are the same as the original protocol: YES☒ NO ☐

IF NO, complete the following:
Detail new procedures that are different from section 10a of the original protocol, including amendments *(include a copy of the entire revised procedure section 10a of the original protocol with the changes and/or new procedures in CAPS):*

b) For D level of invasiveness,

Include here ALL procedures described in the original protocol. New and changed procedures in CAPS *(was section 10a in main protocol); Please only attach SOPs related to new and changed procedures to this renewal form.*

7. Endpoints

a) For B and C level of invasiveness,

The procedures are the same as the original protocol: YES☒ NO ☐

IF NO, supply new endpoints that are different from the original protocol:

Experimental endpoints:

Clinical endpoints:

b) For D level of invasiveness,

Include here ALL endpoints, including the ones described in the original protocol as well as new and changed endpoints in CAPS:

Experimental endpoints:

Clinical endpoints:

8. Hazards (check here if none are used: ☒)

a) Are the hazards different from original protocol? (infectious, radioactive, toxic, carcinogen, tumours)

YES ☐ **NO** ☐ **if yes, supply details (material, risks, precautions):**

b) Have the cell lines been tested for human and animal pathogens? YES: ☐ **NO:** ☐ **None used:** ☒

9. Description of Animals to be used in the coming year (only):

Quality Control Assurance: To prevent introduction of infectious diseases into animal facilities, a health status report or veterinary inspection certificate may be required prior to receiving animals from all non-commercial sources or from commercial sources whose animal health status is unknown or questionable. Quarantine and further testing may be required for these animals. *If more than 6 columns are needed, please attach another page*

	Sp/strain 1	Sp/strain 2	Sp/strain 3	Sp/strain 4	Sp/strain 5	Sp/strain 6
Species	Rat	Timed pregnant rat	Frogs (Rana pipiens)			
Supplier/Source	Charles River	Charles River	Carolina Biological Supply Co.			
Strain	Sprague-Dawley	Sprague-Dawley				
Sex	M/F	F				
Age/Wt	150g	300-400g	2 inches			
# To be purchased	240	100	150			
# Produced by in-house breeding						
#Other (e.g.field studies)						
TOTAL# /YEAR	240	100	150			

10. Explanation of Animal Numbers:

BASED ON THE EXPERIMENTAL OBJECTIVES OF THE PROJECT, describe the number of animals required for one year. Include information on experimental and control groups, # per group, and failure rates.

For breeding, specify how many adults are used, number of offspring produced, and how many offspring are used in experimental procedures. The arithmetic explaining how the total of animals for each column in the table above is calculated should be made clear.

- Rats are used for protein purification. Each protein prep. requires 10 rats. For the studies in this grant, we do approximately 2 prep/month. This number of rats allows for one years worth of preps (10 rats x 2 prep/mth x 12 months = 240).
- Timed pregnant rats are used for biochemical studies. Each pregnant rat yeilds approximately 2g of embryonic brain tissue. We need approximately 200g of tissue/year (200g/2g/rat = 100)
- Frogs: This model will provide us the opportunity to study our novel clathrin-coated vesicle protiens in an intact, isolated and well characterized synapse. In addition, frogs maintain their vital functions for many hours after being pithed. This feature will allow us to administer very specifically compunds to the nerve terminals using axonal transport. The neuromuscular junction preparations prepared from the sacrificed frogs are stable for only one day of experimentation. Thus, each experiment requires 1 frog. We will do 3 experiments per week x 50 weeks per year = 150 frogs.

Submit to your local Facility Animal Care Committee. Please note that after two renewals, a full protocol needs to be submitted.

This approval does not imply that space will be made available. If a major increase of space needs is anticipated, please contact the appropriate animal facility manager.